

Self-assembly and Gelation Properties of Novel Peptides for Biomedical Applications

A thesis submitted to the University of Manchester
for the degree of Doctor of Philosophy
in the Faculty of Engineering and Physical Sciences

2013

Jie Gao

School of Materials

Contents

Contents	1
List of tables	6
List of figures	7
List of abbreviations.....	18
Abstract	20
Declaration	21
Copyright	21
Acknowledgements	22
Chapter 1 Introduction	23
1.1 Overview	23
1.2 ECM and cells	24
1.2.1 ECM.....	24
1.2.2 Cell adhesion to ECM.....	27
1.2.3 Human dermal fibroblast cells.....	28
1.3 Scaffold design to mimic ECM.....	29
1.4 Hydrogel as scaffold in tissue engineering	35
1.4.1 Natural materials.....	36
1.4.2 Synthetic polymers	37
1.4.3 Designed peptides	38
1.5 Self-assembling peptides.....	39

1.5.1 Amino acids	39
1.5.2 Peptide formation.....	41
1.5.3 Self-assembling peptides systems.....	43
1.6 References	51
Chapter 2 Materials and methodology	64
2.1 Introduction	64
2.2 Peptide synthesis and characterisation:	64
2.2.1 Materials	64
2.2.2 Solid phase peptide synthesis (SPPS).....	64
2.2.3 Matrix-assisted laser desorption ionization-time of flight (MALDI-TOF) mass spectroscopy	70
2.2.4 Reversed phase high performance liquid chromatography (RP-HPLC)	70
2.3 Gel preparation and characterisation:.....	71
2.3.1 Gel preparation and phase diagram	71
2.3.2 Transmission electron microscopy (TEM)	73
2.3.3 Small angle scattering (SAS).....	73
2.3.4 Fourier transform infrared spectroscopy (FTIR)	75
2.3.5 Rheology.....	75
2.4 Cell culture and assays	78
2.4.1 Materials	78
2.4.2 Cell culture.....	79
2.4.3 Fluorescence microscopy:	79

2.4.4 F-actin staining	80
2.4.5 Cell counting.....	80
2.4.6 Live/Dead assay	80
2.4.7 Immunostaining assay	81
2.5 References	82
Chapter 3 Self-assembly and gelation properties of FEFEFKFK peptide	83
3.1 FEFEFKFK peptide	83
3.1.1 Self-assembly of FEFEFKFK peptide	83
3.1.2 Gel properties	87
3.1.3 Rheological properties of peptide hydrogels.....	92
3.1.3.1 Amplitude sweep	92
3.1.3.2 Frequency sweep	93
3.1.3.3 Temperature sweep	99
3.1.3.4 Time sweep (recovery)	101
3.2 pH and ionic strength effect on FEFEFKFK gel properties.....	103
3.2.1 Introduction	103
3.2.2 pH effect.....	103
3.2.2.1 Results.....	103
3.2.2.2 Discussion.....	112
3.2.3 Ionic strength effect.....	115
3.2.3.1 Results.....	115
3.2.3.2 Discussion.....	123

3.3 2D cell culture protocol development on FEFEFKFK peptide gel.....	124
3.3.1 Introduction.....	124
3.3.2 Gel preparation protocol development for 2D cell culture	124
3.3.3 2D cell culture protocol development.....	128
3.3.3.1 NaOH effect.....	128
3.3.3.2 Gel concentration effect.....	129
3.3.3.3 2D cell culture protocol development for HDF cell	132
3.4 Summary	133
3.5 References	135
Chapter 4 Functionalized peptide and HDF cell culture.....	138
4.1 Introduction.....	138
4.2 Functionalised peptide hydrogel	139
4.2.1 Peptide synthesis.....	139
4.2.2 Functionalised peptide hydrogel properties.....	140
4.2.3 Fibre morphology and network structure	144
4.3 2D HDF cell culture	149
4.3.1 2D HDF cell culture protocol development.....	149
4.3.2 Long term 2D cell culture.....	156
4.4 3D HDF cell culture	166
4.4.1 Gel preparation protocol development for 3D HDF cell culture.....	166
4.4.2 3D HDF cell culture protocol development.....	168
4.4.3 3D HDF cell culture.....	171

4.5 Summary	174
4.6 References	173
Chapter 5 Conclusion and future work	177

Word count: 54,499

List of tables

Table 1.1 20 Natural amino acids and their structures.	39
Table 3.1 The exponent values of the scattering intensity curves for FEFKFK peptide at 10 mg ml ⁻¹ at different pH.	106
Table 3.2 The value of $R\sigma$ of scattered fibres of 10 mg ml ⁻¹ FEFKFK peptide at different pH.	108
Table 3.3 The value of the radius of the scattered fibres of 10 mg ml ⁻¹ FEFKFK peptide at different pH.	109
Table 3.4 The value of the radius of the scattered fibres of 10 mg ml ⁻¹ FEFKFK peptide at different pH.	110
Table 3.5 The pK _a values of amino groups and carboxyl groups of FEFKFK peptide from CRC Handbook of Chemistry and Physics. ²⁷	113
Table 3.6 The average diameter d of peptide fibres at different salt concentrations at pH 2.8.	119
Table 3.7 The exponent values of scattering intensity curves for FEFKFK peptide at different NaCl salt concentrations at pH 2.8.	120
Table 3.8 The value of $R\sigma$ of scattered fibres of 10 mg ml ⁻¹ FEFKFK peptide at different salt concentrations.	122
Table 3.9 The value of radius of scattered fibres of 10 mg ml ⁻¹ FEFKFK peptide at different salt concentrations at pH 2.8.	123

List of figures

- Figure 1.1 The general structure of the fibronectin polypeptide, location of its binding sites, and the alternatively spliced fibronectin variants.⁷25
- Figure 1.2 Ribbon representation of the 10th FnIII unit, highlighting secondary structure elements and the RGD motif.⁹26
- Figure 1.3 An illustration of cell adhesion to ECM through ligand-integrin interaction.¹⁹ .28
- Figure 1.4 Fibroblasts in culture. Left: sub-confluent culture at 5th passage in which the cells are amoeboid and migratory. Middle: confluent culture at 5th passage showing characteristic swirling pattern. Right: culture at 12th passage showing senescent phenotype. Original magnification, 120X.²²29
- Figure 1.5 A) The common structure of amino acid; B) the structure of proline.39
- Figure 1.6 The illustration of the formation of one peptide bond.42
- Figure 1.7 The illustration of the structure of A) α -helix;¹²¹ B) parallel β -sheet and C) anti-parallel β -sheet.42
- Figure 1.8 Images of (A) a dimeric coiled coil illustrating the left-handed supercoil, (B) the knobs-into-holes interactions, ‘hole’ residues are shown in grey and labelled with their positions in the heptad repeat, the ‘knob’ residue is shown in black. (C) heptad repeat.¹³⁵ 45
- Figure 1.9 MAX1 folding and self-assembly¹³⁹46
- Figure 1.10 β -Sheet forming short peptides with alternating ionic complementary properties: peptide sequences of 4 β -sheet 16-mer peptides, including the commercially available RADA16-I (PuraMatrixTM). Structure and assembly of RADA16-1 peptide into fibres and nanofibrous scaffolds (electron microscopy image of RADA16-I is shown).¹⁴⁴ 47
- Figure 1.11 Molecular modelling and simulation of a left-handed double helical β -sheet.¹⁴⁹48
- Figure 1.12 Short amphiphilic β -sheet peptides that self-assemble into anti-parallel nanotapes and further aggregate into ribbons and higher order structures. In a recent paper,

shorter sequences (P9-6 and P7-6) with aliphatic hydrophobic residues (in green) were demonstrated to form fibrillar structures. (C) Trans-mission electron micrograph of a P11-4 gel in water (6.3 mM, pH 3) showing semi-rigid fibrils and fibers. ¹⁴⁴	51
Figure 2.1 The multi-step process of peptide synthesis. Y^1 = amino-protecting group; Y^2 = carboxyl protecting group; R^1 , R^2 = amino acid side chains. ¹	65
Figure 2.2 Structure of A) C-terminal amino acid linked to the resin; B) Wang resin	65
Figure 2.3 The mechanism of the Fmoc deprotection. ¹	66
Figure 2.4 The mechanism of the activation and coupling reaction. ²	66
Figure 2.5 MALDI-TOF mass spectrum of FEFEFKFK in positive reflectron mode. The number beside each peak represents the molecular weight of $[M-H]^+$	68
Figure 2.6 HPLC graph of FEFEFKFK.	69
Figure 2.7 Illustration of a SAS experiment.	73
Figure 2.8 Rheometer with a parallel geometry	77
Figure 3.1 The molecular structure of FEFEFKFK peptide at neutral pH.....	83
Figure 3.2 Schemes of an anti-parallel β -sheet structure formed by FEFEFKFK peptide (A—top view; B—side view); ⁵ Schemes of the formation of the fibres by FEFEFKFK peptide (C). ⁸	84
Figure 3.3 FTIR spectra of peptide hydrogels at concentrations of 10, 30 and 40 mg ml ⁻¹ all at pH 2.8.	85
Figure 3.4 (A) Peak fitted FTIR spectra of FEFEFKFK peptide at concentration of 40 mg ml ⁻¹ at pH 2.8. (B) The percentage peak area of the peak at ~ 1625 cm ⁻¹ in the amide I region area as a function of peptide concentration.	85
Figure 3.5 TEM micrographs of the diluted FEFEFKFK peptide hydrogel at pH 2.8. Boxes	

- were used to indicate the presence of branched fibres; while circles were used to point out the entanglement of the fibres. The scale bar represents 50 nm.86
- Figure 3.6 Schematic presentation of the fibrillar model suggested by Guenet. C_{gel} stands for the critical gelation concentration. ξ stands for the mesh size.¹³87
- Figure 3.7 The phase diagram of FEFEFKFK peptide, where samples in the form of solution (empty circle), weak gel/viscous liquid (light filled circle) and gel (dark filled circle) were recorded. All samples were prepared at pH 2.8 (A), FEEFFKFK at 40 mg ml⁻¹ forms a self-supporting transparent hydrogel at pH 2.8 (B).88
- Figure 3.8 (A) SANS spectra of the FEFEFKFK peptide. The plot of I_A against q at 40 mg ml⁻¹ (Δ), 20 mg ml⁻¹ (\bullet) 10 mg ml⁻¹ (\circ) and 5 mg ml⁻¹ (\blacktriangle); (B) SAXS spectra of FEFEFKFK peptide. Plot of I_A against q at 30 mg ml⁻¹ ($|$) and 50 mg ml⁻¹ ($—$); (C) SANS spectra of the FEFEFKFK peptide. The plot of I_N against q in the logarithmic scale at 40 mg ml⁻¹ (Δ), 20 mg ml⁻¹ (\bullet) 10 mg ml⁻¹ (\circ) and 5 mg ml⁻¹ (\blacktriangle);(D) SAXS spectra of FEFEFKFK peptide. The plot of I_N against q in the logarithmic scale at 30 mg ml⁻¹ ($|$) and 50 mg ml⁻¹ ($—$). All the experiments were taken at pH 2.8.90
- Figure 3.9 Plot of the q^* value (circle) and the mesh size d (triangle) against peptide concentration from SANS (solid) and SAXS (empty) scattering curves. Error bars are the standard deviation. All the experiments were taken at pH 2.8.91
- Figure 3.10 Plot of elastic modulus (G' , \bullet), viscous modulus (G'' , \circ) and $\tan\delta$ (\times) of FEFEFKFK peptide at 20 (red), 30 (blue) and 40 (green) mg ml⁻¹ as a function of strain from 0.1 % to 100 % at 1 Hz at 20 °C in the logarithmic scale. All the experiments were taken at pH 2.8.93
- Figure 3.11 Plot of elastic modulus (G' , solid), viscous modulus (G'' , empty) and $\tan\delta$ (\times) of FEFEFKFK peptide at 25 (black), 30(red), 35 (green), 40(blue), 45(cyan), 50(purple), 55(navy) and 60 mg ml⁻¹ (olive) as a function of frequency from 0.1 to 10 Hz at 1 % strain at 20 °C in the logarithmic scale. All the experiments were taken at pH 2.8.94
- Figure 3.12 Plot of the stress relaxation modulus $G(t)$ as a function of t for peptide at concentrations of 30, 40, 50 and 60 mg ml⁻¹ at 20 °C in the logarithmic scale. All the experiments were taken at pH 2.8. The value of $G(t)$ at the beginning of the plateau is

called the plateau shear modulus (G_N). In the long time range, $G(t)$ was approaching the equilibrium state, which is called the equilibrium shear modulus (G_e).	95
Figure 3.13 A) The plot of G_N against gel concentration; B) The plot of G_N against gel mesh size d . All the experiments were taken at pH 2.8.....	96
Figure 3.14 Plot of elastic modulus (G' , ●) and viscous modulus (G'' , ○) of FEFEFKFK peptide as a function of concentration (C) in the logarithm scale. n represents the slope of the fitted line. The solid line (—) represents a fitting of G' against concentration. The dash line (— —) represents a fitting of G'' against concentration. All the experiments were taken at pH 2.8.	98
Figure 3.15 The plot of elastic modulus (G' , solid) and viscous modulus (G'' , empty) of the FEFEFKFK peptide at 25 (A), 30 (B) and 40 (C) mg ml^{-1} as a function of temperature in the logarithmic scale. All the experiments were taken at pH 2.8. G' was marked red when the gels were heated up and blue when the gels were cooled down. The squares (■/□) represent the 1st heating and cooling cycle; the circles (●/○) represent the 2nd heating and cooling cycle; the triangles (▲/△) represent the 3rd heating and cooling cycle.	100
Figure 3.16 Plot of elastic modulus (G' , ○) of FEFEFKFK peptide at 25 mg ml^{-1} as a function of time at 20 °C at pH 2.8 in logarithmic scale. The inset is the magnified form of data from 280 to 360 seconds to give a closer look of the initial recovery process.....	102
Figure 3.17 (A) The pH phase diagram of FEFEFKFK where samples in the form of solution (empty circle), transparent gel (dark filled circle) and cloudy gel (black dot) were recorded at 25 °C. (B) Plot of G' (○) of FEFEFKFK peptide at 30 mg ml^{-1} against pH.	104
Figure 3.18 FTIR spectra of FEFEFKFK peptide at 30 mg ml^{-1} at pH 2.8 (blue), pH 10.8 (red), pH 11.3 (purple) and pH 11.5 (green).	105
Figure 3.19 Plots of lgI_A against lgq . (A) SAXS results of FEFEFKFK peptide at 10 mg ml^{-1} at pH 2.8 (blue), pH 4 (red), pH 5 (green), pH 7 (purple) and pH 10 (orange); (B) SANS results of FEFEFKFK peptide at 10 mg ml^{-1} at pH 2.8 (blue), pH 4 (red), pH 5 (green), pH 7 (purple) and pH 10 (orange).	106

Figure 3.20 Porod plot ($lnqIA$ against q^2) of FEFEFKFK peptide at 10 mg ml^{-1} at pH 2.8 (blue), pH 4 (red), pH 5 (green) and pH 10 (purple) tested by SAXS (A) and SANS (B). The solid lines represent the best fit using Equation 3.6.....	108
Figure 3.21 Kratky plot (q^2IA against q) of FEFEFKFK peptide at 10 mg ml^{-1} at pH 2.8 (blue), pH 4 (red), pH 5 (green) and pH 10 (purple) tested by SAXS. The solid lines represent the best fit using Equation 3.7.	109
Figure 3.22 Kratky plot (q^2IA against q) of FEFEFKFK peptide at 10 mg ml^{-1} at pH 2.8 (blue), pH 4 (red), pH 5 (green) and pH 10 (purple) tested by SANS. The solid lines represent the best fit by using Equation 3.8.	110
Figure 3.23 Illustration of patterns that could be taken by the association of fibres.	111
Figure 3.24 TEM images of FEFEFKFK peptide at different pH. Scale bars represent 50 nm. ¹²	112
Figure 3.25 Plot of the net charge against pH of FEFEFKFK peptide. ²⁸	113
Figure 3.26 The phase diagram of FEFEFKFK peptide where samples in the form of solution (empty circle), transparent gel (dark filled circle) and cloudy gel (black dot) were recorded at $25 \text{ }^\circ\text{C}$ at different salt concentrations. All the samples were at pH 2.8.....	116
Figure 3.27 Plot of elastic modulus (G' , solid), viscous modulus (G'' , empty) and $\tan\delta$ (\times) of FEFEFKFK peptide at 10 (left) and 20(right) mg ml^{-1} at NaCl concentration of 20 (red), 50 (green), 100 (blue), 500 (cyan) and 1000 mM (purple) as a function of strain from 0.05% to 100% at 1 Hz at $20 \text{ }^\circ\text{C}$ in the logarithmic scale. All the experiments were taken at pH 2.8.	117
Figure 3.28 Plot of elastic modulus (G' , solid), viscous modulus (G'' , empty) and $\tan\delta$ (\times) of FEFEFKFK peptide at 10 (left) and 20(right) mg ml^{-1} at NaCl concentration of 20 (red), 50 (green), 100 (blue), 500 (cyan) and 1000 mM (purple) as a function of frequency from 0.1 to 100 Hz at 1% strain at $20 \text{ }^\circ\text{C}$ in logarithmic scale. All the experiments were taken at pH 2.8.....	117
Figure 3.29 Plot of G' (solid), G'' (empty), $\tan\delta$ (\times) and yield strain (+) of FEFEFKFK peptide at 10 mg ml^{-1} (red) and 20 mg ml^{-1} (blue) against the salt concentration. All the experiments were taken at 1% strain at $20 \text{ }^\circ\text{C}$ at pH 2.8.....	118

Figure 3.30 TEM images of FEFEFKFK peptide at different salt concentrations. Scale bars represent 50 nm. All the samples were at pH 2.8.....	119
Figure 3.31 Plot of $\lg I_A$ against $\lg q$ of FEFEFKFK peptide at 10 mg ml^{-1} with the salt concentration at 0 M (blue), 0.1 M (red), 0.5 M (green) and 1M (purple) tested by SANS. All the experiments were taken at pH 2.8.....	121
Figure 3.32 Porod plot ($\ln qIA$ against q^2) of FEFEFKFK peptide at 10 mg ml^{-1} with the salt concentration at 0 M (blue), 0.1 M (red), 0.5 M (green) and 1M (purple) tested by SANS. Solid lines represent the best fit by using Equation 3.6. All the experiments were taken at pH 2.8.	121
Figure 3.33 Kratky plot (q^2IA against q) of FEFEFKFK peptide at 10 mg ml^{-1} with the salt concentration at 0 M (blue), 0.1 M (red), 0.5 M (green) and 1M (purple) tested by SANS. Solid lines represent the best fit by using Equation 3.7. All the experiments were taken at pH 2.8.....	122
Figure 3.34 Scheme of the gel preparation for 2D cell culture.....	126
Figure 3.35 Plot of elastic modulus (G') against gel concentrations for the peptide gel prepared by Method 2 (empty) and Method 1 (solid) in the logarithmic scale. All the samples were at physiological conditions.....	127
Figure 3.36 (A) Optical micrograph of chondrocyte cell morphology 7 days post cell culture on 10 mg ml^{-1} gels prepared by Method 2; (B) Optical micrograph of chondrocyte cell morphology 7 days post cell culture on 10 mg ml^{-1} gels prepared by Method 1; (C) Fluorescence micrograph of chondrocyte cell viability 7 days post cell culture on 10 mg ml^{-1} gels prepared by Method 2 and (D) Fluorescence micrograph of chondrocyte cell viability 7 days post cell culture on 10 mg ml^{-1} gels prepared by Method 1. Scale bars represent $50 \mu\text{m}$. 5×10^4 cells were seeded on top of the gel surface in each well.	128
Figure 3.37 Optical micrographs of chondrocyte cell morphology at day0, day1 and day3 of cell culture on the gels prepared by Method 2 at the concentration of 5 mg ml^{-1} (A0, A1, A3), 10 mg ml^{-1} (B0, B1, B3) and 15 mg ml^{-1} (C0, C1, C3). Optical micrographs were overlapped with the rheological tests results of all three types of gels before cell seeding. All the samples were at physiological conditions. Scale bars represent $50 \mu\text{m}$. 5×10^4 cells were seeded on top of the gel surface in each well.	130

- Figure 3.38 Optical micrographs of chondrocyte cell morphology at day0, day1 and day3 of cell culture on the gels prepared by Method 1 at the concentration of 5 mg ml⁻¹ (A0, A1, A3), 10 mg ml⁻¹ (B0, B1, B3) and 15 mg ml⁻¹ (C0, C1, C3). Optical micrographs were overlapped with the rheological tests results of all three types of gels before cell seeding. All the samples were at physiological conditions. Scale bars represent 50 μm. 5×10⁴ cells were seeded on top of the gel surface in each well.130
- Figure 3.39 Fluorescence micrograph of chondrocyte cell viability 7 days post cell culture on the gels prepared by Method 1 (A5, A10, A15) and Method 2 (B5, B10, B15) at concentrations of 5 mg ml⁻¹ (A5, B5), 10 mg ml⁻¹ (A10, B10) and 15 mg ml⁻¹ (A15, B15). Scale bars represent 50 μm. 5×10⁴ cells were seeded on top of the gel surface in each well.131
- Figure 3.40 Optical micrographs of HDF cell morphology at day0, day1 and day3 of cell culture on the gels prepared by Method 2 (A0, A1, A3) and Method 1 (B0, B1, B3) at a concentration of 20 mg ml⁻¹. Fluorescence micrographs were also presented for HDF cell viability at day7 on the gels prepared by Method 2 (A7) and Method 1 (B7). Scale bars represent 50 μm. 5×10⁴ cells were seeded on top of the gel surface in each well.132
- Figure 4.1 The structure of Mpr-hRGDWP.....139
- Figure 4.2 A, B) MALDI-TOF MS spectra of two HPLC elution solutions corresponding to the two major peak 1 and 2 in HPLC spectra respectively; The number beside each peak represents the molecular weight of [M-H]⁺. C) HPLC spectrum of the product after the first coupling to link Mpr-hRGDWP on FEFEFKFK; D) HPLC spectrum of the product after repeating the coupling.140
- Figure 4.3 The phase diagram of ``hRGD`` peptide shows the variation of gel (dark solid circle), viscous liquid (light solid circle) and solution (empty circle) as a function of temperature. All the samples were at pH 2.8.141
- Figure 4.4 Plot of elastic modulus (G', solid), viscous modulus (G'', empty) and tanδ (×) of ``hRGD`` peptide at 10 (black), 20 (red), 30 (green), 40 (blue) and 50 (cyan) on the left while 15 (black), 25 (red), 35 (green), 45 (blue) on the right as a function of strain from 0.01% to 100% at 1 Hz at 20 °C in the logarithmic scale. All the samples were at pH 2.8.

.....	142
Figure 4.5 Plot of elastic modulus (G' , solid), viscous modulus (G'' , empty) and $\tan\delta$ (\times) of ``hRGD`` peptide at 10 (black), 20 (red), 30 (green), 40 (blue) and 50 (cyan) on the left while 15 (black), 25 (red), 35 (green), 45 (blue) on the right as a function of frequency from 1 to 100 Hz at 1% strain at 20 °C in the logarithmic scale. All the samples were at pH 2.8.....	142
Figure 4.6 A) Plot of elastic modulus (G' , \bullet), viscous modulus (G'' , \circ) of ``hRGD`` peptide as a function of concentration in the logarithmic scale. B) Plot of $\tan\delta$ (\times) and yield strain ($+$) of ``hRGD`` peptide as a function of concentration. G' , G'' and $\tan\delta$ are the average values in the frequency independent region in Figure 4.5 and were tested at 1 % strain; the yield strain is from Figure 4.4 and was tested at 1 Hz; n represents the slope of the fitted line which is also the power law exponent. The solid line (—) represents a fitting of G' against concentration. The large/small dash line (- — -) represents a fitting of G'' against concentration. The small dash line (----) represents a fitting of $\tan\delta$ against concentration. All the samples were at pH 2.8.....	142
Figure 4.7 Plot of G' of the ``hRGD`` (empty circle) and FEFKFK gels (solid circle) as a function of peptide concentrations. The solid line (—) represents a fitting of G' of the ``hRGD`` gels against concentration. The dash line (— — —) represents a fitting of G' of the FEFKFK gels against concentration. All the samples were at pH 2.8.....	143
Figure 4.8 FTIR spectra of ``hRGD`` peptide at different concentrations. All the samples were at pH 2.8.	145
Figure 4.9 TEM image of 5 mg ml ⁻¹ ``hRGD`` peptide solution at pH 2.8 shows a dense fibrillar network. Scale bar presents 50 nm.	146
Figure 4.10 Plot of $\lg I_A$ against $\lg q$ of ``hRGD`` peptide at concentrations of 3 mg ml ⁻¹ (blue), 5 mg ml ⁻¹ (red) and 10 mg ml ⁻¹ (green) and 20 mg ml ⁻¹ (purple) tested by SANS. All the samples were at pH 2.8.	147
Figure 4.11 Porod plot ($\ln q I_A$ against q^2) of FEFKFK peptide at concentrations of 3 mg ml ⁻¹ (blue), 5 mg ml ⁻¹ (red) and 10 mg ml ⁻¹ (green) tested by SANS. Solid lines represent the best fit by using Equation 3.6. All the samples were at pH 2.8.....	147

- Figure 4.12 Kratky plot (q^2IA against q) of peptide ``hRGD`` at concentrations of 3 mg ml^{-1} (blue), 5 mg ml^{-1} (red) and 10 mg ml^{-1} (green) tested by SANS. Solid lines represent the best fit by using Equation 3.7. All the samples were at pH 2.8.....148
- Figure 4.13 Optical micrographs of HDF on ``hRGD`` gel surfaces during 7 days of cell culture show the cells adopt a spindle shape. Fluorescence micrograph shows the living (green) and dead (red) cells on gel surfaces 7 days post cell culture. Scale bars represent $50 \mu\text{m}$. 5×10^4 cells were seeded on top of the gel surface in each well.....149
- Figure 4.14 Plot of elastic modulus (G' , solid), viscous modulus (G'' , empty) and $\tan\delta$ (\times) of FEFEFKFK (A) at cell culture day0 (black), day1 (red), day3 (green) and day7 (blue); FEFEFKFK+NaOH (B) at cell culture day0 (black), day1 (red), day3 (green) and day7 (blue) and ``hRGD`` (C) at cell culture day0 (black), day1 (red), day3 (green) and day7 (blue) as a function of strain from 0.01% to 100% at 1 Hz at $37 \text{ }^\circ\text{C}$ in the logarithmic scale. All the samples were at physiological conditions.....150
- Figure 4.15 Plot of elastic modulus (G' , solid), viscous modulus (G'' , empty) and $\tan\delta$ (\times) of FEFEFKFK (A) at cell culture day0 (black), day1 (red), day3 (green) and day7 (blue); FEFEFKFK+NaOH (B) at cell culture day0 (black), day1 (red), day3 (green) and day7 (blue) and ``hRGD`` (C) at cell culture day0 (black), day1 (red), day3 (green) and day7 (blue) as a function of frequency from 1 to 100 Hz at 1% strain at $37 \text{ }^\circ\text{C}$ in the logarithmic scale. All the samples were at physiological conditions.....151
- Figure 4.16 Plot of elastic modulus (G' , \bullet), viscous modulus (G'' , \circ), $\tan\delta$ (\times) and yield strain (+) of FEFEFKFK (A), FEFEFKFK+NaOH (B) and ``hRGD`` (C) gel as a function of cell culture time at $37 \text{ }^\circ\text{C}$ in the logarithmic scale. G' , G'' and $\tan\delta$ are the average values in the frequency independent region in Figure 4.15 and tested at 1 % strain; the yield strain is from Figure 4.14 and tested at 1 Hz. All the samples were at physiological conditions.....152
- Figure 4.17 The change of mechanical strength of the gels during the 7 day cell culture; \circ represents the FEFEFKFK gels prepared by Method 2 (Section 3.3.2); \times represents the FEFEFKFK gels prepared by Method 1 (Section 3.3.2); | represents the ``hRGD`` gels prepared by Method 2 (Section 3.3.2). All the samples were at physiological conditions.....153

- Figure 4.18 Optical micrographs of HDF on the ``hRGD`` gel surfaces with different loading ratios of ``hRGD`` peptide show cell morphologies during 3 days of cell culture. The fluorescence micrographs show the living (green) and dead (red) cells on the gel surfaces 7 days post cell culture. 5×10^4 cells were seeded on top of the gel surface in each well.....154
- Figure 4.19 Optical micrographs of the HDF cells grow on the FEFEFKFK gels and the ``hRGD`` gels show cell morphologies during the 15 days of cell culture. Scale bars represent 100 μm . 5×10^4 cells were seeded on top of the gel surface in each well.157
- Figure 4.20 Fluorescence micrographs show phalloidin-stained F-actin (green) of cells on gel surfaces during 14 days of cell culture. Scale bars represent 100 μm . 5×10^4 cells were seeded on top of the gel surface in each well.....158
- Figure 4.21 The aspect ratios (circle), average lengths (square) and average widths (diamond) of the cells in 14 days of cell culture; the ``hRGD`` gels are presented by solid symbols; the FEFEFKFK gels are presented by empty symbols. 5×10^4 cells were seeded on top of the gel surface in each well.....159
- Figure 4.22 A) Plot of cell numbers against cell culture days in the 14 days of cell culture; \circ represents FEFEFKFK; \bullet represents ``hRGD``; B) Plot of cell numbers against cell culture days in integrin blocking tests; circles represent the normal cells; triangles represent the blocked cells; empty symbols represent FEFEFKFK; solid symbol represent ``hRGD``; C,D) optical micrograph of normal cells (C) and integrin blocked cells (D) on fibronectin coated glass surface 4 hours post cell culture; Scale bars represent 100 μm . 5×10^4 cells were seeded on top of the gel surface in each well.162
- Figure 4.23 Fluorescence micrographs of fibronectin secreted on the FEFEFKFK and the ``hRGD`` gels in 14 days of cell culture. Scale bars represent 100 μm . 5×10^4 cells were seeded on top of the gel surface in each well.....165
- Figure 4.24 Fluorescence micrographs of HDF cells in the FEFEFKFK gels at 3D cell culture day 3 (left) and day 7(right). Scale bars represent 500 μm . Cell density was $10^6 \text{ cell ml}^{-1}$ gel.167
- Figure 4.25 The ratio of living cells using different cell culture protocols. Left column is the results of cell counting. Right column is the results of image analysis of Live/dead

assay results. Empty symbols represent the FEFEFKFK gels; solid symbols represent the ``hRGD`` gels.....	169
Figure 4.26 Fluorescence micrographs of 3D HDF cell culture in the FEFEFKFK and ``hRGD`` gels during 7 days of cell culture. Scale bars represent 100 μm . Cell density was 10^6 cell ml^{-1} gel.	172
Figure 4.27 Fluorescence micrographs of stained F-actin of HDF cells in the FEFEFKFK (A) and ``hRGD`` (B) gels at day 7 post cell culture. Scale bars represent 100 μm . Cell density was 10^6 cell ml^{-1} gel.....	173
Figure 4.28 Fluorescence micrographs of F-actin assay result (green) and collagen I assay result (red) at day 7 post cell culture. Scale bars represent 100 μm . Cell density was 10^6 cell ml^{-1} gel.	173

List of abbreviations

2D	2-dimensional
3D	3-dimensional
AAc	acrylic acid
AEAK16-I	AEAKAEAKAEAKAEAK
AEAK16-II	AEAEAKAKAEAEAKAK
BSA	bovine serum albumin
BDDA	1,4-butanediol diacrylate
C_{gel}	critical gelation concentration
DCM	dichloro methane
D_F	fractal dimension
DGR	DGRGDSVAYG
DIPEA	N, N'-Diisopropylethylamine
D_m	mass fractal dimension
DMAEMA	N,N-dimethylaminoethylmethacrylate
DMEM	Dulbecco's modified Eagle's medium
DMF	N, N-dimethylformamide
DMSO	dimethyl sulfoxide
DPBS	Dulbecco's phosphate buffered saline
EA	ethylacrylate
ECM	extracellular matrix
EGD	ethyleneglycol dimethacrylate
EthD-1	ethidium homodimer-1
FBS	fetal bovine serum
FITC	fluorescein isothiocyanate
FnIII	type III unit of fibronectin
FTIR	Fourier transform infrared spectroscopy
G	L-guluronic acid
G'	elastic modulus
G''	viscous modulus
HA	hyaluronic acid
HCTU	2-(6-Chloro-1H-benzotriazole-1-yl)-1,1,3,3-tetramethylaminium hexafluorophosphate
HDF	human dermal fibroblasts
HPLC	high performance liquid chromatography
``hRGD``	functionalised Mpr-hRGDWPFEFEFKFK peptide
hSAF	hydrogelating self-assembling fibre
LCST	lower critical solution temperature
LVR	linear visco-elastic region
M	D-mannuronic acid
MA	maleic anhydride
MAAc	methacrylic acid
MALDI-TOF	matrix-assisted laser desorption ionization-time of flight
MAPTAC	methacrylamidopropyltrimethylammonium chloride
Mpr-hRGDWP	3-mercaptopropionyl-homoarginine-glycine-aspartic acid-tryptophan- proline
MS	mass spectroscopy
NMP	N-methylpyrrolidone

P11-4	QQRFEWEFEQQ
PA	peptide-amphiphile
PAA	poly(acrylic acid)
PDMA+	poly(N,N-dimethylaminoethylmethacrylate)
PEG	poly(ethylene glycol)
PEGD	poly(ethylene glycol) dimethacrylate
PEO	poly(ethylene oxide)
PNIPAAm	poly(N-isopropylacrylamide)
PPO	poly(propylene oxide)
PRG	PRGDSGYRGDS
PVA	poly(vinyl alcohol)
RAD16-I	RADARADARADARADA
RAD16-II	RARADADARARADADA
RGD	arginine-glycine-aspartate
RGDS	arginine-glycine-aspartate-serine
RP-HPLC	reversed phase high performance liquid chromatography
SANS	small angle neutron scattering
SAS	small angle scattering
SAXS	small angle X-ray scattering
SPPS	solid phase peptide synthesis
TEM	transmission electron microscopy
TFA	trifluoroacetic acid

Abstract

The self-assembly peptide hydrogels used as tissue culture scaffolds have drawn great attention in recent years. They have the advantages of natural polymer hydrogels including biocompatibility, biodegradability and the advantages of synthetic materials such as controlled structural properties and mechanical properties. Furthermore, the bioactive ligands which can promote bioactivities and control cell behaviours can be easily introduced to the peptide backbone through peptide synthesis. One particular self-assembly FEFEFKFK peptide was chosen in this project.

FEFEFKFK peptide used in this project has been reported to self-assemble in solution, forming hydrogels with a 3D fibrous network structure above a critical gelation concentration. In this project, the self-assembly and gelation properties of FEFEFKFK peptide were further investigated, assessing the effect of pH and ionic strength on the self-assembly and gelation behaviour. The biomimetic nanofibrous hydrogels of FEFEFKFK were also assessed for their ability to support human dermal fibroblast cells. The protocols of gel preparation were developed for both 2 dimensional (2D) and 3 dimensional (3D) cell culture. A short peptide sequence homoarginine-glycine-aspartate (hRGD) has been introduced onto the amide end of the self-assembly peptide instead of bioactive ligand arginine-glycine-aspartate (RGD), creating hydrogels with a fibrous network with functionalised groups at the fibre surface. The functionalised peptide hydrogels enhanced cell adhesion on gel surface, with cell interaction assessed using various imaging and spectroscopic techniques. A preliminary 3D cell culture study also showed potential of these peptide gels to be used for encapsulated human dermal fibroblast cell studies.

Declaration

No portion of the work referred to in the thesis has been submitted in support of an application for another degree or qualification of this or any other university or other institute of learning.

Copyright

i. The author of this thesis (including any appendices and/or schedules to this thesis) owns certain copyright or related rights in it (the “Copyright”) and s/he has given The University of Manchester certain rights to use such Copyright, including for administrative purposes.

ii. Copies of this thesis, either in full or in extracts and whether in hard or electronic copy, may be made only in accordance with the Copyright, Designs and Patents Act 1988 (as amended) and regulations issued under it or, where appropriate, in accordance with licensing agreements which the University has from time to time. This page must form part of any such copies made.

iii. The ownership of certain Copyright, patents, designs, trade marks and other intellectual property (the “Intellectual Property”) and any reproductions of copyright works in the thesis, for example graphs and tables (“Reproductions”), which may be described in this thesis, may not be owned by the author and may be owned by third parties. Such Intellectual Property and Reproductions cannot and must not be made available for use without the prior written permission of the owner(s) of the relevant Intellectual Property and/or Reproductions.

iv. Further information on the conditions under which disclosure, publication and commercialisation of this thesis, the Copyright and any Intellectual Property and/or Reproductions described in it may take place is available in the University IP Policy (see <http://www.campus.manchester.ac.uk/medialibrary/policies/intellectual-property.pdf>), in any relevant Thesis restriction declarations deposited in the University Library, The University Library’s regulations (see <http://www.manchester.ac.uk/library/aboutus/regulations>) and in The University’s policy on presentation of Theses.

Acknowledgements

I would like to thank my supervisors Dr Alberto Saiani, Dr Aline F. Miller and Dr Julie Gough for giving me the opportunity to undertake a PhD project in their research group. Their guidance and encouragement helped me fulfil all the tasks and overcome all the problems during my PhD.

I would also like to thank School of Materials, the Alumni Funding of the University of Manchester and Peptisyntha for their financial support to the PhD project, the opportunity to attend workshops and conferences.

I would like to thank all the postdocs and PhD students in the Polymersandpeptides Research Group for the very friendly working environment. All the activities, discussions and advices helped me enjoying my life as a PhD student.

I would like to thank all my dearest friends for their friendship, encouragement and support. Particular mention must go to Bo Yuan who has offered me great support, advices and the most memorable experience being abroad.

Finally, I would like to thank my parents for their love and constant support.

Chapter 1 Introduction

1.1 Overview

There is a great increasing interest in self-assembling peptide systems in recent years. As a material, peptides are naturally biocompatible and biodegradable. They can be easily synthesised and manipulated. Hydrogels formed by self-assembling peptides have shown great potential to be used in the field of tissue engineering. Peptide hydrogels are good candidates as tissue culture scaffolds as well as drug delivery vehicles. Some peptide hydrogels can also be directly injected into the tissues to create nanofibre microenvironments that promote cell recruitment.¹ With the understanding of the self-assembly process and the gelation properties of peptide hydrogels, it helps tailoring the peptides for diverse biomedical applications.

To further study the relationship between the conformations and functions of self-assembling peptides, various self-assembling peptide systems have been developed.

To have a better control of the gel properties for further biomedical studies, it is essential to understand the self-assembly process of the peptide. The aim of the project was to deepen the understanding of the self-assembly process of FEFEFKFK peptide and to adapt the peptide hydrogel for being used as a tissue culture scaffold. Another objective was to link a functional peptide sequence onto this peptide and to assess the bioactivity of the functionalised peptide.

This dissertation report has five chapters. Chapter 1 gives the literature review and the objectives of this project. A brief introduction to the extra cellular matrix (ECM) is given followed by the requirements of scaffold design to mimic the ECM. Due to the high water content and similar structural and mechanical properties to the ECM, various types of hydrogels have been used as tissue culture scaffolds. Here in this review, the self-assembling peptide hydrogels are emphasised. Different self-assembling peptide systems are introduced.

Chapter 2 introduces the materials and methodologies used in the project. The basic mechanisms of the technology and the details of all the experiments are presented. It contains all the techniques for the characterisation of peptide synthesis and gelation

properties, as well as the techniques and assays for the assessment of bioactivity of the peptide hydrogels.

Chapter 3 and Chapter 4 present all the results and discussions of this project. Chapter 3 focuses on the study of the self-assembly and gelation properties of FEFEFKFK peptide and the influences of external stimuli such as pH and ionic strength. At the end, the preparation of hydrogels for cell culture studies is presented. Chapter 4 focuses on the synthesis and characterisation of the functionalised peptide hydrogel as well as the performance of the hydrogels in biological studies.

Chapter 5 gives the general conclusion of this project and possible future work.

1.2 ECM and cells

Tissue engineering is commonly defined as "an interdisciplinary field that applies the principles of engineering and life sciences toward the development of biological substitutes that restore, maintain, or improve tissue function or a whole organ".² Tissue engineering can be approached by: (1) replacing cells that offer the required function with isolated cells or cell substitutes; (2) delivering tissue inducing matter to the required position; (3) culturing cells in scaffolds.³ As it has such an important role in tissue engineering, tissue culture scaffold should be well designed to mimic the ECM in order to meet some basic requirements for tissue reconstruction.

1.2.1 ECM

Tissues are not solely made up of cells. Most tissues are composed of cells and large amounts of ECMs which fill in the extracellular space. Cells are packaged and protected by the ECM from external forces. The mechanical integrity, rigidity and elasticity of tissues are also contributed by the ECM. The mechanical functions are crucial especially to tissues like skin, tendons and bones. Besides the mechanical functions, the size and properties of ECMs can affect the transport of nutrients and cell migrations within the tissues. ECMs can also influence the cell viability, migration, orientation, proliferation, differentiation and even gene expression.^{4,5}

Although different tissues have different ECMs, most ECMs are made up of similar types of macromolecules. Different proportions and variants of those macromolecules contribute to the different physical properties of different tissues. The main components of ECMs are

polymerized protein fibres. The dominant fibrous proteins are collagens. Those fibres form a 3-dimensional (3D) network which acts as a scaffold. ECMs are also made up of proteoglycans and non-collagenous glycoproteins. At the beginning of the formation of ECMs, the hydrophobic effect plays an important role in protein-protein interactions, whilst electrostatic interactions help the associations between protein and carbohydrate.⁴ In general terms, ECMs are polysaccharide rich gels with 3D fibrous network structure formed by protein fibres.

The structural protein fibres are always decorated with some accessory proteins that serve specialised functions. Those proteins usually consist of hundreds of functional domains. Through years of study, some of the specific functions like cell binding can be localised to specific domains. One of them is a three amino-acid oligopeptide, arginine-glycine-aspartate (RGD), which was recognised as a cell adhesion site in many ECM glycoproteins such as fibronectins.⁵ Fibronectins act as the linkages between cells and collagen fibres, so cells can migrate through the ECM. The ability of fibronectin to bind to cells is a great help during wound healing. For example, it can bind to platelets to assist blood clotting and it can help cells move to the injured tissue area.⁶ Fibronectin can also influence the cell morphology, differentiation and cytoskeletal organization which are all based on the ability to promote cell adhesion.

Fibronectin was found to contain three structural units called type I, type II and type III as shown in Figure 1.1.⁷

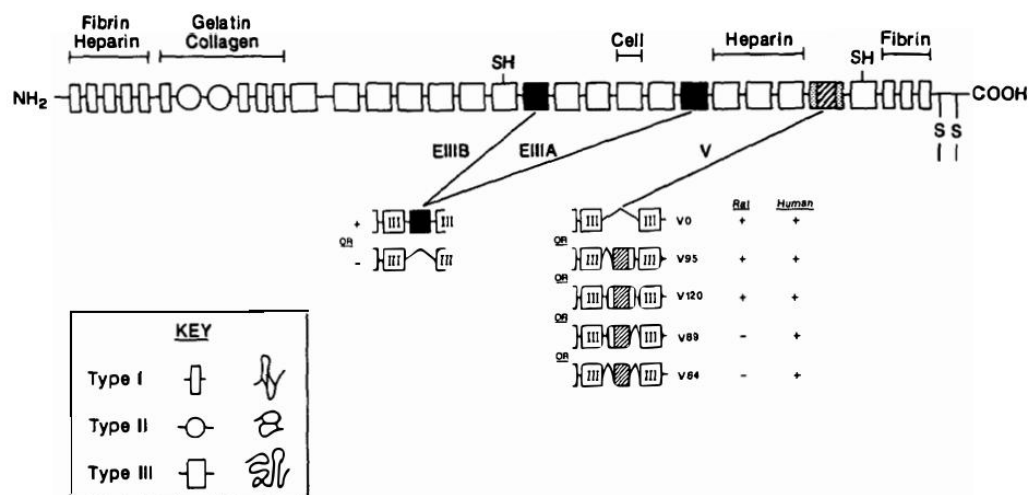


Figure 1.1 The general structure of the fibronectin polypeptide, location of its binding sites, and the alternatively spliced fibronectin variants.⁷

Three different structure units were assembled in a specific order. Different combinations

of structure units represent different binding domains or ensure the correct spatial arrangements of those domains. The 10th type III unit (10th FnIII) marked as 'Cell' is the binding domain where fibronectin binds to integrin receptors on cells.⁸ From the structure of this unit, it can be seen that a short peptide sequence RGD was located at the apex of the loop (Figure 1.2).

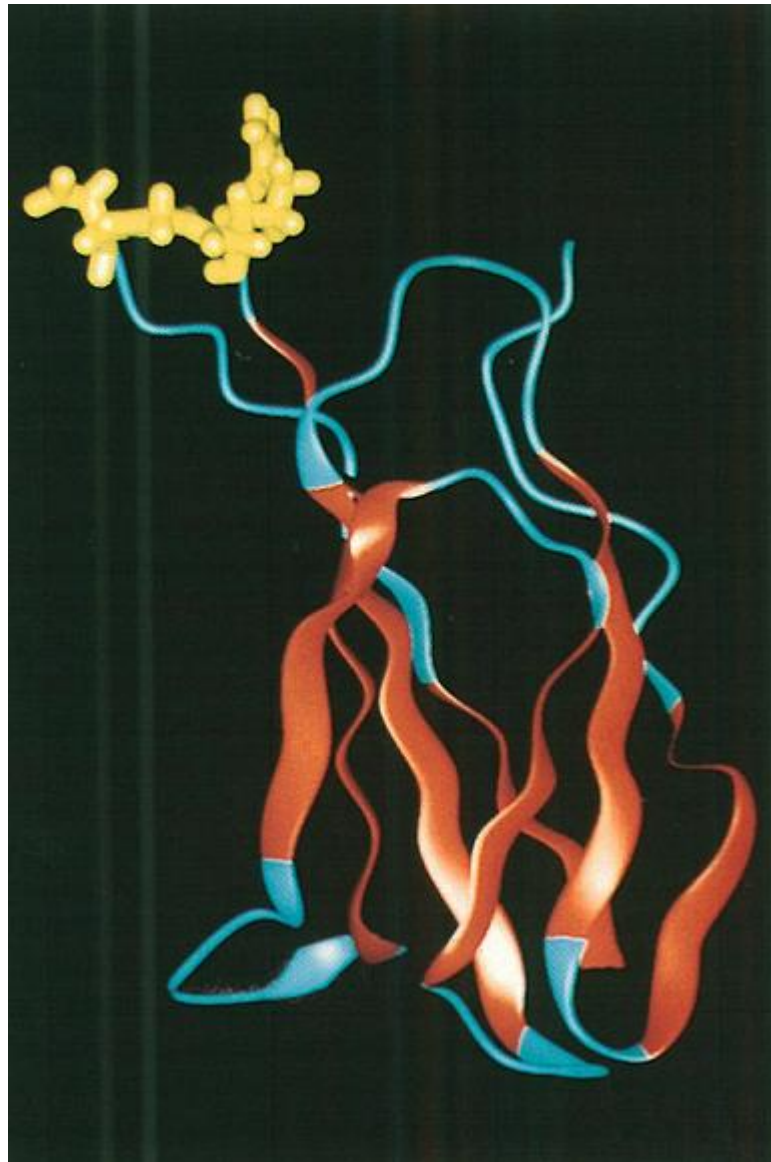


Figure 1.2 Ribbon representation of the 10th FnIII unit, highlighting secondary structure elements and the RGD motif.⁹

The position of this RGD sequence proved to be crucial for optimal cell adhesion. Being at the apex of the loop, the RGD sequence is extended from the centre of the molecule which ensures the exposure of RGD to the integrin receptors on cells. When the accessibility of RGD decreased, the cell adhesion was significantly weakened.¹⁰

To locate the cell adhesive domains in fibronectin, proteolytic and chemical cleavages were introduced. Initially the fibronectin was cleaved into 3 parts.¹¹ The one that can promote cell adhesion was further degraded. A segment which is 40 times smaller than fibronectin was found to maintain the ability of cell attachment.¹² With the help of smaller protein fragments and the synthesis of shorter peptides, the cell adhesion activity was finally localised. A tetrapeptide arginine-glycine-aspartate-serine (RGDS) was reported in 1984.¹³ When arginine (R), glycine (G) or aspartate (D) was replaced by lysine (K), alanine (A) or glutamine (E) respectively, the substitutions had no cell adhesion activity. However, the changes in S did not affect the bioactivity.¹⁴ The RGD sequence was proven to be the cell binding site on fibronectin.

1.2.2 Cell adhesion to ECM

Cells bind to RGD through the integrin receptors on the cell membrane. An integrin is a transmembrane protein. It consists of two subunits, α and β . So far 18 α subunits and 8 β subunits have been discovered. From the combinations of these two subunits, a family of more than 24 integrins have been identified.¹⁵ The first integrin-binding site found was RGD in fibronectin¹⁵ and the fibronectin receptor was integrin $\alpha_5\beta_1$.¹⁶ Later on, at least 7 more integrins which can recognise the RGD sequence were identified and RGD was also found in many other cell-adhesion proteins.¹⁷ During the previous studies, fibronectin was cleaved into fragments. It was found that the RGD sequence on the large fibronectin fragment preferred to bind to $\alpha_5\beta_1$ integrin, whilst the fragment with mainly the 10th FnIII preferred to bind to $\alpha_v\beta_{13}$ integrin.¹⁸ It was inferred that RGD has a more rigid conformation in the large fibronectin fragment and RGD with more rigid conformation prefers to bind to $\alpha_5\beta_1$ integrin.

Figure 1.3 illustrates the integrin mediated cell attachment. On one side, integrins bind to adhesion proteins which also bind to structural proteins through other binding sites. On the other side, integrins bind to adaptor proteins which are attached to the cytoskeleton. Thus, the linkage between the cytoskeleton and ECM is established.¹⁵

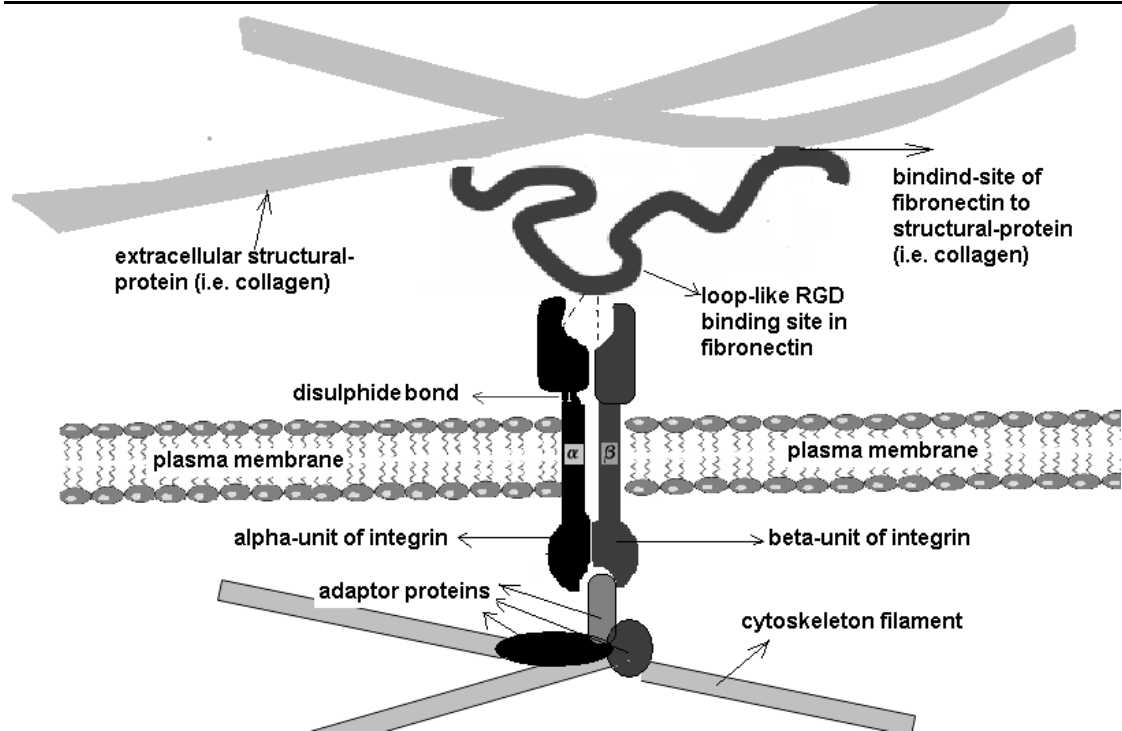


Figure 1.3 An illustration of cell adhesion to ECM through ligand-integrin interaction.¹⁹

This linkage between cell and ECM is crucial for many cell types. It was found that the cell growth, proliferation and even survival are dependent on the attachment to a scaffold.²⁰ Actively migrating cells need cell adhesion to the ECM for traction and guidance, whilst stationary cells need cell adhesion to the ECM for support and orientation.⁴ For most cell types, no cell adhesion to a substrate leads directly to cell apoptosis.

1.2.3 Human dermal fibroblast cells

ECMs are produced by cells. The largest volumes of ECMs are secreted by cells in connective tissues. Cells called fibroblasts are responsible for the secretion of most connective tissues. Fibroblast cells are usually not connected with neighbouring cells in the ECM and they respond to the external force to the tissue. Fibroblasts are favoured for cell culture studies because they are known to be the easiest of cells to grow in culture.^{4, 20}

The cells used in this project are human dermal fibroblast (HDF) cells. Morphologically, when grown in a monolayer, HDFs are flat, spindle-shaped; whilst in 3D environment HDFs are elongated and have many dendrites.²¹ HDFs that successfully attach to a scaffold will proliferate and secrete their own ECMs such as fibronectin and collagen I. A very important thing that needs to be taken into consideration before culturing HDFs is that HDFs have limited lifespan. The cultures stop proliferation after numerous passages and

morphologically cells become large and spread.²² This phenomenon is called cellular senescence. Cell cultures need to be taken before this occurs. The examples of the morphology of HDFs in two-dimensional (2D) cell culture are presented in Figure 1.4.

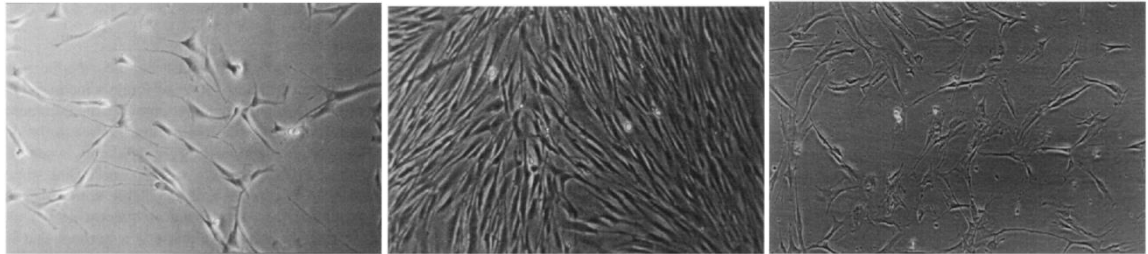


Figure 1.4 Fibroblasts in culture. Left: sub-confluent culture at 5th passage in which the cells are amoeboid and migratory. Middle: confluent culture at 5th passage showing characteristic swirling pattern. Right: culture at 12th passage showing senescent phenotype. Original magnification, 120X.²²

1.3 Scaffold design to mimic ECM

In natural ECM, complex biomolecules and resident cells coexist within a 3D-network of interlaced protein-nanofibres. To mimic the characteristics of natural ECM, a scaffold needs to (1) imitate the structural architecture; (2) be biocompatible; (3) direct and control cell behaviour; (4) be simple.²³

To mimic the characteristics of natural ECM, a scaffold needs to be highly porous with suitable pore size and high surface area. The large pores can provide enough space for cell growth and vessel generation. The fibres should be small enough so one cell can reach a lot of fibres to find its 3D orientation. A scaffold material has to be not only biodegradable, but also degrade at a similar rate as the formation of new tissue. There are also mechanical integrity and biocompatibility requirements for scaffolds. Finally, a scaffold should have a good interaction with cells, such as cell attachment, growth, migration, differentiation, but not encourage any unfavourable tissue reaction.^{23, 24}

To promote cell adhesion to the scaffold material, bioactive ligands are commonly introduced. Among all the cell-adhesive ligands, RGD peptide is the most widely investigated. It was applied to various fields studying the cell behaviour *in vitro* or *in vivo* and designing scaffolds. The RGD sequence proved to be the cell binding site on fibronectin. However, it does not belong to fibronectin alone. RGD peptide was found in many other proteins as well. Compared with the whole proteins, short peptides have similar effects on cell behaviour, but are more resistant to denaturation and proteolysis, less

expensive, easier to be synthesised and modified.^{23, 25, 26}

In order to play the role of a cell adhesive ligand, the RGD sequence has to be strongly linked to the scaffold material, because cells can only attach to the scaffold when the binding point can bear the contractile forces.²⁷ Not only this, the soluble RGD sequences would act like competitors to the immobilised RGD sequences. The soluble RGD sequences would bind to the integrin receptors on cells which reduces cell attachment to the immobilised RGD sequences on the scaffold.²⁸ The best way is to covalently link RGD peptides to the polymeric scaffold. This can be achieved by grafting on the scaffold surface, grafting to the polymer chains and tailing to the polymer backbones.²³ Before RGD peptides can be mobilised on the scaffold, functionalized polymer scaffolds need to be prepared. Various methods can be utilized to introduce the functional groups, including blending, co-polymerization, alkaline hydrolysis and oxidation. Then RGD peptides can be strongly anchored on the polymer via those functional groups. Disulphide bonds were found to be less stable compared to chemical bonds formed through other functional groups. Disulphide exchange may result in a reduction of immobilised RGD peptide which will lead to a decrease in cell adhesion.²⁷

Other variables that need to be taken into account before introducing RGD peptide into polymers are whether cell-adhesive interactions need to be 2D or 3D. The RGD sequence should be linked on the surface only or inside the scaffold accordingly. RGD modified peptides have been shown to optimize the performance of those surfaces for supporting cell adhesion.²⁹ The surface modification technology makes it easier to control all the factors during academic research and may be helpful to gain the basic knowledge of cell behaviours. However, it is too far from the real environment in tissue and could not be used straightway as scaffolds. This can be overcome by bulk modification where RGD peptides are introduced into the whole material. Cells can be encapsulated into the biomaterials which can support cell responses just as in natural ECM and may even be injected into native tissues for tissue engineering applications.²⁶ RGD peptides have been bulk immobilized into commonly used synthetic gels to study the interactions between the RGD sequence and cell functions.³⁰ Those bulk modified gels can also be used for drug delivery,³¹ targeting tumour cells,³² bone regeneration³³ and other biomedical applications.

Before being linked to the scaffold material, RGD is commonly incorporated with other amino acids to form longer peptides. There are some factors that are known to affect the

performance of immobilized RGD peptides. The design of the RGD peptide sequence affects the bioactivity of the material. Different conformations of RGD peptides lead to different selectivity to the cell receptors.^{34, 35} The activity of RGD peptide depends on whether the C-terminal carboxyl group is blocked or not. For example, the activity may stay in such an order: RGD (inactive) <RGD-NH₂<RGDS<GRGDSP.³⁶ The density of RGD peptide needs to reach a minimum in order to affect the cellular response. If the average density is too low, a cluster of RGD peptide can also support cell adhesion.³⁷ The amount of amino acids used as a spacer between RGD and the scaffold material will also affect the performance of RGD peptide. As discussed previously, the accessibility of the RGD sequence affects the ability of this short peptide to bind to the integrin receptors on cells. A long spacer helps RGD peptide form a cluster which increases the regional density of RGD peptide. A long spacer also ensures the RGD peptide can reach the receptors on cell surfaces. Both result in the promotion of cell attachment.²⁷ However, too long a spacer will lead to a weak binding and make the cell behave oppositely, owing to the preference of tight binding to stiffer surfaces of cells.³⁸ Using two amino acids as a spacer has been reported in most of the literatures. To sum up, all the factors that will affect the interaction between RGD peptide and the integrin receptor on cells should be taken into consideration during the scaffold design.

The biochemical, structural and mechanical properties of the scaffold are all very important to determine the tissue functions. Although scientists realized the importance of the mechanical properties decades ago, it is only recently that a lot of studies have been performed on the effect of the scaffold mechanical properties. Sometimes they even have more impact than the chemical stimuli.³⁹ A lot of dysfunctions and diseases can be related to the changes of the tissue's mechanical properties; the mechanical properties of the scaffold materials can also affect the normal tissue development. Cells within developing tissues not only sense the external mechanical stimuli, but also sense the mechanical microenvironment around them. The response of cells to those mechanical signals depends on cell types.⁴⁰

To study the influence of scaffold mechanics on fibroblast behaviours, a variety of hydrogels have been used. In 1997, Pelham and Wang developed a collagen-coated polyacrylamide hydrogel to perform a direct demonstration on the influence of the scaffold mechanical properties. A series of chemically identical gels with the Young's modulus ranging from 10 to 70 N m⁻² were prepared. It was observed that 3T3 fibroblasts migrated

faster on the gels with low modulus. However, less cell spreading and more round cell shape were found on those gels.⁴¹ Using the same gel preparation method, a series of gels with the Young's modulus ranging from 4.4 to 12.4 kPa were prepared by Guo and his colleagues. They found that 3T3 fibroblasts moved away from each other and spread on the stiffer gel surfaces, while on the softer gels, cells moved toward each other and formed tissue-like structures. This suggested that substrate mechanics can determine the direction of cell migration and association.⁴²

Later on, Ghosh and his colleagues developed a physiologically relevant ECM mimic composed of hyaluronan and fibronectin. The gels were prepared with elastic modulus of 4270 Pa, 550 Pa and 95 Pa, as measured by oscillatory rheometry respectively,⁴³ which are within the physiological range.^{44, 45} It was found that HDFs adapted a more stretched and organized phenotype on the stiffer gels. Faster cell migration was also observed on the softer gels. However, normal HDFs proliferation was only noticed on the stiffest gels.⁴⁶

More recently, in Brown's group, plastic compressed collagen hydrogels were developed. A series of hydrogels were prepared with the Young's modulus of 42 kPa, 143 kPa and 2240 kPa which are also within the physiological range.⁴⁷ HDFs were seeded on top of the gel surface and 3 times higher cell proliferation rate was observed on the stiffer gels compared to a compliant substrate.⁴⁸

All previous studies taken on gel surfaces for 2D cell culture showed that fibroblasts prefer stiffer gels with modulus within the physiological range.

The successful encapsulation and cultivation of HDFs were also found in short peptide-based bioactive hydrogels (elastic modulus ranging from 4 to 10 kPa),⁴⁹ chemically cross-linked Chitosan/Pluronic hydrogels containing fibroblast growth factor/heparin (elastic modulus ranging from 20 to 40 kPa),⁵⁰ alginate particle-embedded fibrin gel (compress modulus 1.3 kPa)⁵¹ and concentrated collagen hydrogels (elastic modulus ranging from 50 to 290 Pa).⁵² However, the effect of hydrogel mechanics on cell behaviours was not investigated in those 3D cell culture conditions. In recent studies, a series of collagen gels cross-linked by poly(ethylene glycol) dissucinimidyl ester with compressed modulus ranging from 0.7 to 2.2 kPa were developed. *In vivo* study showed that HDFs encapsulated in the stiffer gels had less cell spreading and low growth rate but formed dermis-like tissue, while HDFs encapsulated in the softest gel generated scar-like tissue.⁵³ This suggested HDFs prefer the stiffer gels within the physiological range in both

2D and 3D environment.

A simple spring model was used to explain the reaction of cells to the stiffness of the matrix. The matrix material is assumed to be isotropic and is the spring in the model which follows Hooke's Law: $F = -kx$. F is the cellular force to stretch the material, x is the displacement of the material, and constant k represents the intrinsic property of the material which is related to its shear modulus. A softer matrix has a smaller k , so small force is enough for cells to pull the gel surface to a certain distance; while the stiffer matrix has a relatively larger k , so much larger force is needed for the stiffer gels.³⁸

It can be clearly seen that the control of the gel network strength is crucial to determine the tissue function. To control the gel network strength, it is important to understand what can affect the gel network strength. A gel is a system which forms when a polymer is cross-linked through chemical or physical bonds that can entrap a large volume of fluid. The gel network strength is directly related to the strength of the cross-linking junctions, the number of the junctions and the strength of the segments between the junctions. It has been noticed in many gel systems that increasing the strength of the cross-linking junctions^{54, 55} and the number of the cross-linking junctions⁵⁶⁻⁵⁸ resulted in the increase of gel strength. Thicker fibres between the junctions were noticed to increase the gel strength,⁵⁵ while in another system, the gel strength decreased with increasing fibre diameter. This could be due to the increase of the fibre rigidity which leads to the decrease of the strength of the cross-linking junctions and the number of the junctions.⁵⁹

The gel network strength can also be affected by the gel concentration. Theoretical models for the chemical gels have been developed and the power law relation between the modulus and the concentration ($G \sim C^n$) was found in nearly all systems studied. The modulus and the concentration in the physical gels also fit in the power relation. The exponent n relies on the conformation of the segments between the network junctions.⁶⁰

A model based on F-actin gels was developed by Mackintosh et al. The exponent n is 11/5 for the semi-flexible fibrils when the fibril persistence length is much smaller than the mesh size of the gel network, while the exponent n is 5/2 for the densely cross-linked gels when the fibrillar segment length is equivalent to the mesh size.⁶¹

Another theoretical model for the chemical gels was developed by Jones and Marques.⁶² In that theory, the exponent n was determined by the fractal dimension (D_F) of the segments

linking at the network junctions. D_F is defined as:

$$S \propto L^{1/D_F}$$

Equation 1.1

where S is the end to end distance of the segment and L is the contour length. For a system with frozen junctions, the power law is expressed as:

$$G_r \approx C^{(3+D_F)/(3-D_F)}$$

Equation 1.2

while for a system with a freely hinged network, the relation is expressed as:

$$G_e \approx kTC^{3/(3-D_F)}$$

Equation 1.3

The fractal dimension can indicate the compactness of the segments linking at the network junctions: the higher the value of D_F the more compact the structure.⁶³

This theory was successfully applied by Guenet to several thermo-reversible gels which belong to the family of physical gels.⁶⁴ a physical gel is able to go through phase transitions between liquid and solid states due to external stimuli such as temperature,^{54, 65} pH,⁶⁶ ionic strength,⁶⁷ electric field,⁶⁸ solvent composition⁶⁹ and light.⁷⁰

External stimuli used in this project are temperature, pH and ionic strength, hence the gels respond to these three stimuli were discussed.

The most common thermoreversible hydrogels are modified cellulose hydrogels.⁵⁴ Copolymers composed of poly(ethylene oxide) (PEO)-poly(propylene oxide) (PPO) and their modified forms form another common type of thermoreversible hydrogel.⁷¹ Poly(N-isopropyl acrylamide) (PNIPAAm) is also a commonly used polymer to prepare temperature responsive hydrogels. PNIPAAm was grafted onto a hydrophilic backbone and acted like cross-linking junctions responding to the temperature stimulus. Poly(acrylic acid) (PAA),⁷² poly(vinyl alcohol) (PVA),⁷³ polyacrylamide⁷⁴ and cationic poly(N,N-dimethylaminoethyl methacrylate) (PDMA+)⁶⁵ have been used to graft PNIPAAm side chains.

pH responsive gels are composed of ionisable polymers with a pKa value between 3 and 10. Weak acids and bases such as carboxylic acids, phosphoric acids and amines can be good candidates as the ionisable groups. Classical monomers include acrylic acid (AAc),⁷⁵

methacrylic acid (MAAc),⁷⁶ maleic anhydride (MA)⁷⁷ and N,N-dimethylaminoethyl methacrylate (DMAEMA).^{78, 79} Another well studied model microgel is poly(EA/MAAc/BDDA) (ethylacrylate, methacrylic acid and 1,4-butanediol diacrylate).⁸⁰ Here BDDA is the cross-linking monomer and can be replaced by ethyleneglycol dimethacrylate (EGD)⁸¹ and poly(ethylene glycol) dimethacrylate (PEGD)⁸². Later on, this model microgel was used to form gel composites which also exhibited pH-dependent swelling.⁸³ A dual pH responsive gel was also developed based on this model microgel.⁸⁴

FEFEFKFKFEFEFKFK peptide was reported to form hydrogels in the presence of salt while remaining highly soluble in pure H₂O.⁶⁷ Other gels that respond to a change in ionic strength also often include ionisable monomers such as itaconic acid⁸⁵ or methacrylamido propyl trimethyl ammonium chloride (MAPTAC)⁸⁶. Some cellulose derivatives can also be used to form ionic strength sensitive hydrogels.⁸⁷

The reversibility of physical gels gives them a great advantage with many applications such as in drug delivery or in tissue engineering.

1.4 Hydrogel as scaffold in tissue engineering

Both synthetic materials and natural macromolecules have been used as scaffolds. Even some inorganic materials are involved in bone and mineralized tissue engineering studies. Materials used as tissue culture scaffold can be divided into two categories: materials used in a solid state and materials used in a gel form.³ The most common materials used in a solid state include linear aliphatic polyesters,⁸⁸⁻⁹¹ some other synthetic polymers including polyphosphoester,⁹² polyphosphazene,⁹³ poly(propylene fumarate),⁹⁴ polyanhydride⁹⁵ and poly(ortho esters),⁹⁶ natural macromolecules including collagen,⁹⁷ silk,⁹⁸ polysaccharide⁹⁹ and processed ECM materials,³ inorganic materials¹⁰⁰ and composite materials.¹⁰¹ Materials used in a solid state usually do not dissolve or melt in the tissue culture media or body fluid. However, the surgery is needed when those materials are implanted *in vivo* and it is difficult for those materials to fill tissue defects with an irregular shape.¹⁰² Materials in a gel form can overcome those issues and compared to the solid state materials, hydrogels have high water content which provides a hydrated 3D microenvironment for cell culture in which it is easier to incorporate cells with bioactive molecules.³⁰ Water plays an important role in the ECM which is the major component of connective tissues. It is the reason that connective tissues are flexible, resilient and can withstand external pressure.

Connective tissues have high water content, such as 80 % water in cartilage and 60 % water in tendon. The water content in hydrogels can be over 99 %, which is a better mimic of ECM compared to the solid-state materials.⁴

Hydrogels used as scaffolds can come from natural materials, synthetic polymers or even a hybrid which may have the advantages of both the natural materials and synthetic materials.¹⁰³

1.4.1 Natural materials

Hydrogels of natural origin are attractive because of their similarity to the ECM, good biological performance and chemical versatility.¹⁰⁴ The most commonly used natural materials are derived from mammalian ECM including collagen, hyaluronic acid (HA), fibrin, alginate and chitin.

Collagen is the most abundant component in native ECM and is one of the earliest natural materials used as a mimic of the ECM. Unmodified collagen has been used in porous solid-state as mentioned before as well as in a gel form. Collagen gels have been used for the regeneration of vocal cord,¹⁰⁵ the repair of spinal cord¹⁰⁶ and the restoration of cartilage defects.¹⁰⁷ Cells can be suspended in collagen solutions at room temperature and then gelation occurs at 37 °C. By this way, collagen gels with encapsulated cells can be used *in situ*.¹⁰⁸

HA is another natural material being widely used as a tissue culture scaffold. It presents in all mammals, especially in soft connective tissues. It can be degraded by enzymes in the body and by reactive oxygen intermediates. Unmodified HA has a high rate of degradation which is its important advantage. Cells encapsulated in HA can be easily recovered by the degradation of HA.¹⁰⁸

Fibrin also shows promise as an injectable scaffold. Commercially fibrin hydrogels are produced by the combination of purified allogeneic fibrinogen and purified thrombin. The big advantage of fibrin hydrogel is that fibrinogen can be gained from the patient's own plasma, thus there is less risk of a foreign body reaction. There are some other advantages including high efficiency of cell seeding and even cell distribution. There are also some disadvantages such as the high degradation rate, the low mechanical strength and the shrinkage of hydrogels when cells form flat sheets.¹⁰⁹

Alginate extracted from brown seaweed algae has been widely used for cell encapsulation. It is a linear block copolymer composed of D-mannuronic acid (M) and L-guluronic acid (G) residues. The ratio of M:G is determined by the origin of alginate and the ratio of M:G can affect the pore size of the hydrogel, the stiffness of the hydrogel and the cell adhesion to the hydrogel. Multivalent cations can be used to trigger the gelation process which gives alginate the potential to gel *in situ*. The big disadvantages of alginate gels are the poorly regulated degradation and poor cell adhesivity.^{108, 110}

Chitin and its derivatives are another category of materials that have attracted great attention in recent years. They have been used as tissue culture scaffolds for the regeneration of bone and cartilage and for wound care. Chitin has good biological activities including biodegradability, biocompatibility, non-toxicity and especially promotion in wound healing. The only disadvantage is its poor mechanical properties.¹¹¹

1.4.2 Synthetic polymers

Synthetic polymers are also used to form hydrogels used as tissue culture scaffolds. The structure of the polymer networks can be easily controlled on the molecular scale. The properties of hydrogels such as the rate of biodegradation, the mechanical strength and the bioactivity can be easily manipulated.¹¹²

Hydrogels which are made of poly(ethylene glycol) (PEG) and its derivatives are one of the most widely used synthetic scaffolds. PEG gels were used as scaffolds for tissues like bone, cardiovascular, cartilage and vascular. PEG is a hydrophilic polymer which results in the inhibition of protein binding and cell adhesion. The advantages of PEG are the biocompatibility, limited immunogenicity and low antigenicity. Because of the inert properties, PEG gels can be used to prevent unwanted cell/scaffold interactions. On the other hand, to promote cell behaviour, bioactive ligands have to be introduced to the polymer network.^{108, 113}

PVA is another well known synthetic polymer used for tissue engineering. As with PEG, PVA gels can also be obtained by photopolymerization, which provides hydrogels with the potential to be used *in situ*. PVA has no cell adhesivity but it has pendant alcohol groups which can be binding sites for biological molecules.¹⁰⁸ PVA hydrogels have a higher degradation rate than PEG hydrogels, thus PEG/PVA copolymer hydrogels are commonly used to control the degradation rate. PVA hydrogels also have other good properties such as

higher mechanical strength, low coefficient of friction and similar structural properties to cartilage.¹¹⁴ Those show PVA hydrogels have a great potential to be used for articular cartilage replacement and indeed a PVA hydrogel named SalubriaTM is already in the market as such a replacement.

Another common synthetic polymer is PNIPAAm. The most important characteristic of PNIPAAm hydrogel is the thermal responsive behaviour. PNIPAAm hydrogel has a lower critical solution temperature (LCST) which is around 32 °C and may vary by copolymerising with other comonomers. Below the LCST, PNIPAAm is hydrophilic while above the LCST, it becomes hydrophobic. This special property of PNIPAAm hydrogels can be used to control the cell adhesion to the polymer hydrogel.¹¹⁵ Like all other synthetic materials, the biggest problem for PNIPAAm is the non-biodegradability which can only be solved by copolymerization with other comonomers or the usage of biodegradable cross-linkers.

1.4.3 Designed peptides

Both synthetic materials and natural macromolecules have been used as scaffolds. Natural materials have advantages of being bioactive, being biocompatible and promoting cell functions. However, the disadvantages are also very obvious. Their physical properties, in particular the mechanical properties, are difficult to control and they have a high possibility of contamination and a short life time. There are also issues such as unpredictable degradation behaviour, reproducibility from batch-to-batch and possible denaturation during manufacturing and processing.¹¹⁶ On the other hand, synthetic gels are easier to design and manipulate, but biocompatibility and biodegradation is the primary concern. The toxicity of the small molecules introduced during the synthesis and after the degradation should also be taken into consideration. Further modifications are also needed to mimic native ECM. One of the most important modifications is introducing binding ligands into the system, with the active peptide sequence linked to the synthetic gel materials.³⁰ This lead to the development of peptide based hydrogels which exploit the natural self-assembly capability of these molecules. Among all the synthetic gels, self-assembled oligopeptide hydrogels have attracted a lot of attention because they combine the advantages of both natural and synthetic materials. Furthermore, the active peptide sequence can be easily introduced through peptide synthesis.

1.5 Self-assembling peptides

1.5.1 Amino acids

Amino acids are the building blocks of peptides. There are 20 α -amino acids in nature. They have a common structure as shown in Figure 1.5 A with only one exception: proline shown in Figure 1.5 B. R is the side group which differs in every amino acid.¹¹⁷

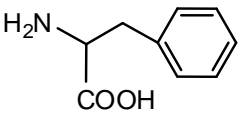
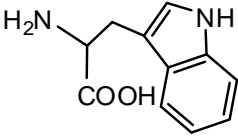
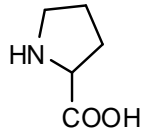
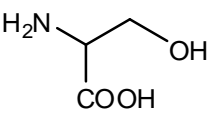
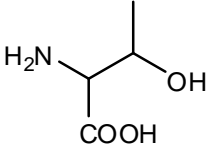
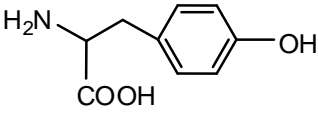
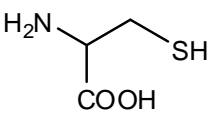
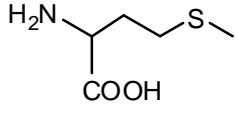
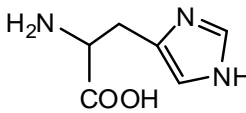
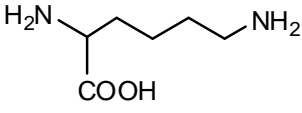


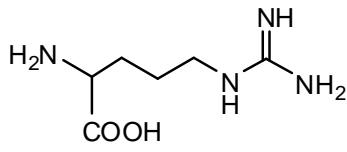
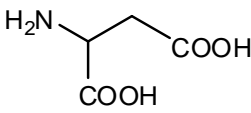
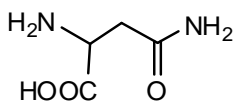
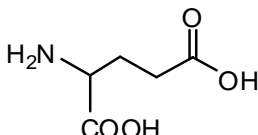
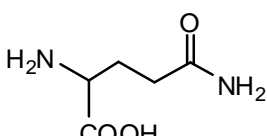
Figure 1.5 A) The common structure of amino acid; B) the structure of proline.

Thus 20 amino acids can be classified by different types of R as listed in Table 1.1.¹¹⁸

Table 1.1 20 Natural amino acids and their structures.

R	Amino acid	Three letter code	One letter code	structure
alkyl	glycine	Gly	G	
	alanine	Ala	A	
	valine	Val	V	
	leucine	Leu	L	
	isoleucine	Ile	I	

hydrophobic non-polar	phenylalanine	Phe	F	
	tryptophan	Trp	W	
	proline	Pro	P	
hydroxyl	serine	Ser	S	
	threonine	Thr	T	
	tyrosine	Tyr	Y	
sulphur-containing	cysteine	Cys	C	
	methionine	Met	M	
second amino	histidine	His	H	
	lysine	Lys	K	

	arginine	Arg	R	
carboxylic acid	aspartic acid	Asp	D	
	asparagines	Asn	N	
	glutamic acid	Glu	E	
	glutamine	Gln	Q	

The aromatic rings in F and W can introduce π - π stacking interactions which is one of the driving forces of peptide self-assembly.^{119, 120} Enzyme introduced peptide degradation also often occurs at the site next to these amino acids. The special structure of P makes it a bending or twisting site in the peptide structure. Sulphur containing amino acid C can form disulphide bonds between each other which is key to the 3D structure of the peptide molecule. Amino acids with hydrophilic side groups can introduce charges to the whole peptide molecule. The electronic interactions between peptide molecules is another important driving force of peptide self-assembly.¹¹⁸

1.5.2 Peptide formation

One peptide bond can be formed by a simple condensation reaction between two amino acids as illustrated in Figure 1.6.¹²¹

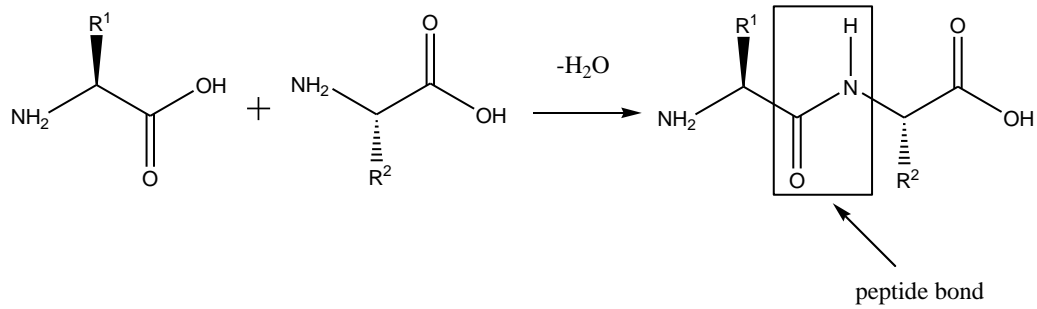


Figure 1.6 The illustration of the formation of one peptide bond.

The structure of a peptide has four levels.

The primary structure of a peptide molecule is the peptide sequence often named by listing the amino acid from the N-terminus to the C-terminus.

The secondary structure is the stereo organization of the primary structure including α -helix, β -sheet and turn. The first two structures are illustrated below.

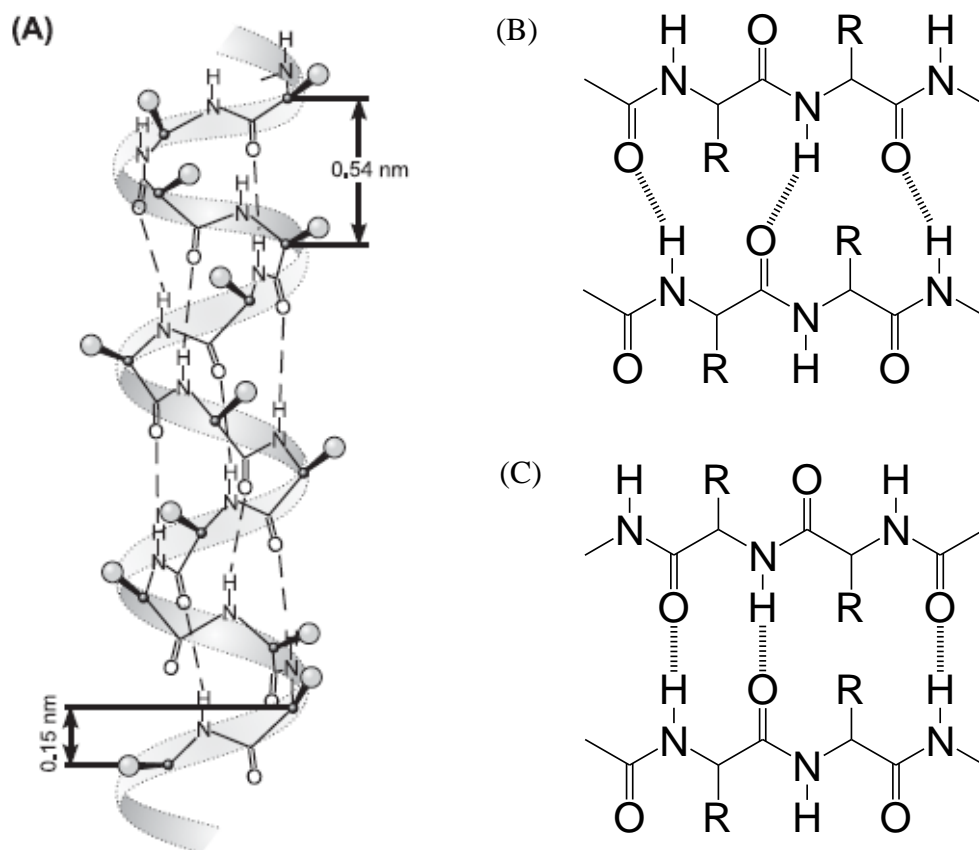


Figure 1.7 The illustration of the structure of A) α -helix;¹²¹ B) parallel β -sheet and C) anti-parallel β -sheet.

Hydrogen bonding plays an important role in the stabilization of the secondary structure. α -helix is the most common conformation of peptide molecules. Hydrogen bonds form

between amino acids in the same molecule. On the other hand, β -sheet structure forms through hydrogen bonding between amino acids in different molecules. The hydrophobic effect also plays an important role in the formation of β -sheet. β -sheet can be further divided into two classes: the parallel β -sheet and the anti-parallel β -sheet. Turns are the positions where a peptide molecule folds and turns are the reason that peptide molecules can form a compact conformation.¹²¹

The tertiary structure is a 3D organization of the secondary structures. This structure is more easily affected by the external forces such as hydrophobic forces, electrostatic forces and van der Waals forces rather than being governed by the intrinsic properties alone. The quaternary structure is the 3D arrangement of more than one peptide molecule. This structure is stabilized by similar forces as the tertiary structure and is important for proper protein functions.¹²¹

1.5.3 Self-assembling peptides systems

A lot of self-assembling peptide systems have been developed. With the understanding of the relationship between the peptide conformation and the function, the peptide systems can then be tailored for specific applications. Here several self-assembling peptide systems are classified by the structure of the peptide.

Peptides with aromatic structure

The shortest self-assembling peptide is aromatic FF, first identified by Gazit and colleagues.¹²² This dipeptide was found during the study of Alzheimer's β -amyloid polypeptide. It can self-assemble into nanotubes with a micro-scale persistence length and a remarkable mechanical strength. Combined with their biocompatibility and good thermal and chemical stability, these peptide nanotubes show a great potential to be used as biosensors.¹²³ Later the discovery of their high stiffness made them more attractive to be used for biocompatible nanodevices.¹²⁴ By the modification of the amine group, Fmoc-FF was discovered and recognised as the smallest structural unit to form amyloid-like fibres. This peptide was found to form a rigid gel in aqueous solution. The rigid gel was then assessed for its biocompatibility as a tissue culture scaffold.¹²⁵

Parallel work on Fmoc-FF peptide has been done by Ulijn et al.¹¹⁹ It was found that with the help of hydrogen bonding and π - π stacking, dipeptides linked with Fmoc groups can

self-assemble into hydrogels with a fibrous network under physiological conditions. These gels have been proven to support 3D chondrocyte cell culture.¹²⁶

The self-assembly process and the mechanical properties of the peptide hydrogel were found to be controlled by the change of pH.^{127, 128} The mechanical properties can also be affected by the alternation of peptide sequences.^{129, 130} The control over the mechanical properties could be very useful when tailoring the gel properties for further applications.

Bioactive ligands can also be introduced to the dipeptide system. A recent study showed a RGD modified system was created by simply mixing Fmoc-FF and Fmoc-RGD solutions together which were then adjusted to pH 7 and left at 37 °C for the gelation to occur. Fmoc-RGD contributed to the formation of fibrous network from π - π stacking. By using pure Fmoc-FF gels and Fmoc-FF/Fmoc-RGE gels as control, the RGD modified gels showed a support for cell adhesion and proliferation for dermal fibroblast cell culture.⁴⁹

Peptides with surfactant-like structure

Stupp and Hartgerink worked on peptide-amphiphile (PA) molecules which are made up of a peptide head and an alkyl tail. The hydrophobic tails gather together forming a hydrophobic core, and peptides help to form fibrous strands through hydrogen bonds forming the outer surface of a rod-like structure.¹³¹ The gelation is triggered when polyvalent ions are added into the system, which is the case in the physiological environment.¹³² Cells can be mixed in the PA solutions and then cultured in the 3D environment after the gelation has been triggered.¹³³ Cell migration, proliferation and differentiation were observed within the hydrogel.¹³⁴

Bioactive ligand RGD can be introduced to the peptide end which stays on the outer surface of the rod. SHED and DPSC cell lines were used and the results of cell culture show that both dental stem cell lines are compatible with the modified system; and cell adhesion, proliferation and differentiation are also promoted.¹³⁴

Peptides with α -helix structure

This system was developed by Woolfson and colleagues. The structure of α -helices bring side chains of amino acid residues three or four apart together. When those side chains are hydrophobic, α -helices gain amphipathic structures which can then self-assemble in aqueous solution via the hydrophobic effect and bury the hydrophobic side chains in the

middle of helical bundles which are also called helical coiled coils. This mechanism is illustrated in Figure 1.8.¹³⁵

Most of the coiled coils are presented by a heptad repeat shown in Figure 1.8 C. The hydrophobic amino acids are often assigned to position *a* and *d* while the polar amino acids are located at other positions. It can be easily seen from the heptad repeat that residues from position *a* and *d* will form the hydrophobic side of the helix. More α -helices with such structure can assemble into a left-handed supercoil through the hydrophobic association. There may be two, three, four or even more α -helices that come together, and the assemblies can be either parallel or anti-parallel.¹³⁶

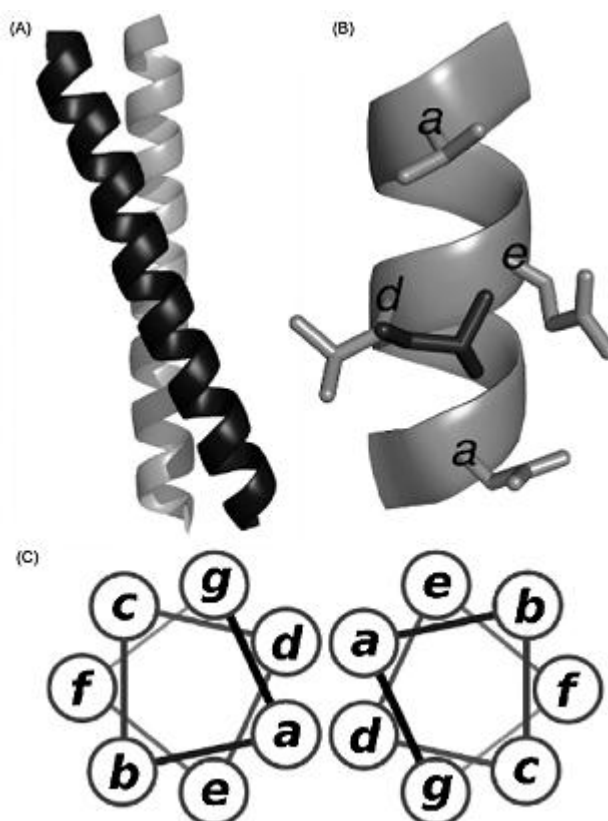


Figure 1.8 Images of (A) a dimeric coiled coil illustrating the left-handed supercoil, (B) the knobs-into-holes interactions, 'hole' residues are shown in grey and labelled with their positions in the heptad repeat, the 'knob' residue is shown in black. (C) heptad repeat.¹³⁵

Hydrogelating self-assembling fibres (hSAFs) was designed in the Woolfson lab. These hSAFs form physically cross-linked self-supporting hydrogels in water. The alternation of peptide sequence can affect the thickness of fibres, the gelation process and thus the gel properties.¹³⁷ This is a big advantage as the gel properties can be tailored for different applications. Another advantage of this gel system is that the gelation only occurs on mixing. Therefore the assembly process is well controlled as well, and the gels can be used

for *in situ* applications. *In vitro* studies were taken to assess the bioactivity of these hydrogels and promising results were gained giving hSAFs a great potential to be used as a mimic of the ECM.¹³⁸

Peptides with β -hairpin structure

Pochan and Schneider made MAX1 ($\text{H}_2\text{N-VKVKVKVKV}^{\text{D}}\text{PPTKVVKVKVKV-CONH}_2$), a 20 amino acid peptide. This peptide shows a random coil structure when dissolved in water, and then it can be triggered to fold to a β -hairpin structure and form a rigid hydrogel by adding Dulbecco's modified Eagle's medium (DMEM), a cell culture medium. The self-assembly process is demonstrated in Figure 1.9.¹³⁹

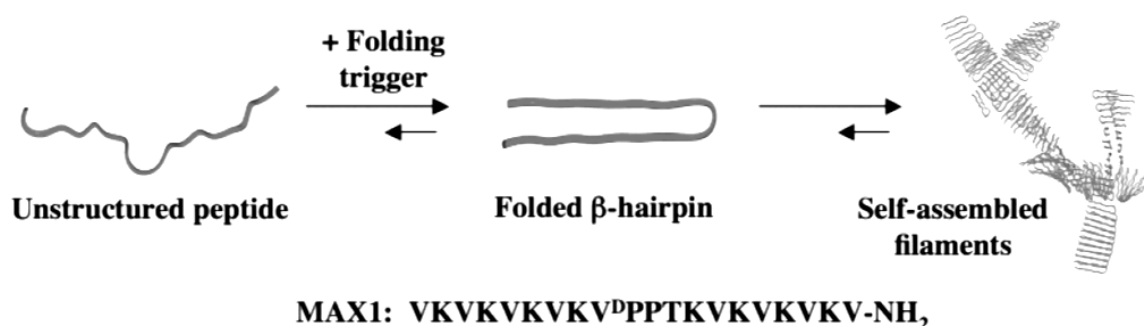


Figure 1.9 MAX1 folding and self-assembly¹³⁹

MAX1 is composed of many valine and lysine residues. The side groups of lysine will be positively charged if $\text{pH} < 7$. The repulsion forces make MAX1 molecules stay in an extended conformation. The external stimuli such as increasing the pH or adding salts will result in a decrease of the repulsion force, therefore triggering the molecular folding. Further molecular self-assembly is driven by the hydrophobic effect of valine residues and the intermolecular hydrogen bonding.⁵⁶ A series of MAX1 type of peptides were designed and the various external stimuli including pH, salt, temperature and enzyme were used as gelation triggers.⁵⁹ The gelation process and the mechanical properties of MAX1 type peptides can be affected by the variation of the peptide concentration, the change of pH, temperature and ionic strength.¹⁴⁰⁻¹⁴² The potential of this type of hydrogel to be used in cell culture has also been assessed.¹³⁹

Peptides with β -sheet structure

The most well studied self-assembling peptides are the ones with β -sheet structure. Several groups are working on the development of this type of peptide system.

Zhang and his co-workers have developed one type of peptide named “ionic complementary peptides”. This kind of peptide has an alternating hydrophobic and hydrophilic structure, which forms β -sheet rich fibres in aqueous solution. The first ionic complementary peptide AEAEAKAKAEAEAKAK (AEAK16-II) was discovered from a yeast protein named Zuotin.¹⁴³ In aqueous solution, the hydrophobic residues of A come together burying the two hydrophobic surfaces in between two peptide sheets as shown in Figure 1.10. The positively and negatively charged hydrophilic surfaces also pack together through ionic interactions. The peptide fibres with β -sheet stack were obtained accordingly. By increasing the repeat units of AEAK16-II from 2 to 4, AEAKAEAKAEAKAEAK (AEAK16-I) can be obtained. By substituting E with D and K with R, two more ionic complementary peptides RADARADARADARADA (RADA16-I) and RARADADARARADADA (RADA16-II) were gained. The self-assembly processes for all four peptides are the same and are illustrated in Figure 1.10.¹⁴⁴

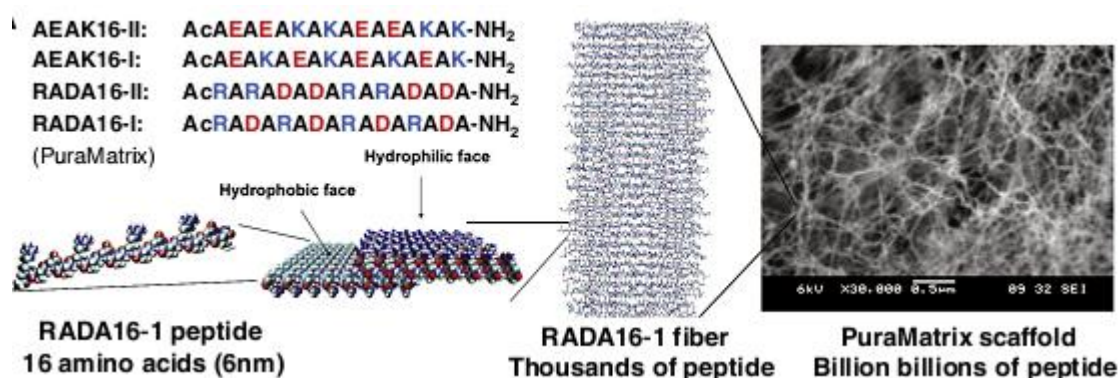


Figure 1.10 β -Sheet forming short peptides with alternating ionic complementary properties: peptide sequences of 4 β -sheet 16-mer peptides, including the commercially available RADA16-I (PuraMatrixTM). Structure and assembly of RADA16-1 peptide into fibres and nanofibrous scaffolds (electron microscopy image of RADA16-I is shown).¹⁴⁴

These peptide gels were found to support cell attachment of various mammalian cells. Some of the gels have also been shown to support cell proliferation, differentiation,¹⁴⁵ active migration and the extensive production of their own ECM.¹⁴⁶ Among them, the most studied peptide is RAD16-I, which is commercially available now and the trade name is PuraMatrix.¹⁴⁷

Zhang and his group designed a series of self-assembling peptides modified by biologically active motifs for specific cell culture studies. One example is coupling pure peptide RADA16-I to a lot of motifs including RGD containing peptide DGR (DGRGDSVAYG) and PRG (PRGDSGYRGDS). Compared with the pure peptide, this designer peptide

proved to considerably encourage mouse pre-osteoblast cell proliferation, differentiation and migration. Compared with natural materials with lots of unidentified components like collagens, the experiments with the designer peptide gels are more controllable and reproducible.¹⁴⁸

A shorter peptide with eight amino acids was developed later. A different self-assembly model was proposed. Instead of stacking, FKFEFKFE peptide formed fibres with a left-handed helix conformation with one hydrophobic surface and one hydrophilic surface. Two fibres come together driven by the hydrophobic effect and form a double helix. The construction of the double helix was shown in Figure 1.11.¹⁴⁹ This model was confirmed by the observation of the helical ribbon intermediate during self-assembly as well as by an analysis of the intermediate using molecular dynamics.¹⁵⁰

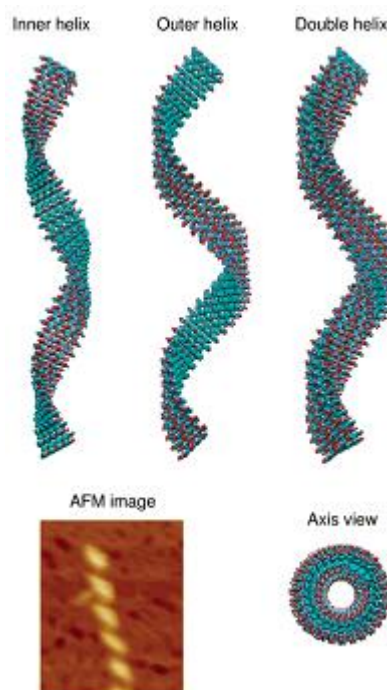


*Figure 1.11 Molecular modelling and simulation of a left-handed double helical β -sheet.*¹⁴⁹

To understand the self-assembly process and to control the gelation, the amino acid sequence was systematically varied. This series of oligopeptides self-assembled in salt solution and formed hydrogels above a critical salt concentration. It was noticed that increasing side-chain hydrophobicity decreased the critical salt concentration.¹⁵¹ This is in good agreement with the molecular model as the hydrophobic effect is one of the driving forces during the gelation. It was also found that increasing the number of repeat units first decreased than increased the critical salt concentration.¹⁵¹ Increasing the number of repeat

units not only increases the hydrophobic effect but also increases the entropic effect as the peptide is longer. It was believed that the result was due to the competition between the two effects.¹⁵¹ The shear modulus of those gels was also measured. A reverse trend of first increasing then decreasing of the shear modulus by increasing peptide length was observed. This could be due to the competition of increasing the area of interaction between molecules and decreasing the molecules effective length because of possible folding back of the longer molecules. However, there was no significant difference among peptides with varied hydrophobic side chains or peptides with varied charged side chains.¹⁵² Another attempt to vary the peptide sequence was to truncate one terminal amino acid. This small modification dramatically changed the self-assembly process. FKFEFKF formed thin fibrils (~3.7 nm) and broad nanotapes (~19.2 nm); while KFEFKFE only assembled at neutral pH.¹⁵³

Another aspect which can affect the self-assembly and gelation process of FKFEFKFE is the pH of the system. It was found that by increasing the pH of the system from 3.5 to 4.0, the time of gelation was decreased from hours to minutes. However, the mechanism of gelation remained the same.¹⁵⁴ The sensitivity of self-assembly to pH and ionic strength of the solution are due to the ionisable side chains.

FKFEFKFE can be functionalised prior to self-assembly with polyethylene glycol groups to inhibit bacterial motility¹⁵⁵ or with an epitope to modulate adaptive immune responses.¹⁵⁶ Bioactive ligand RGD can also be introduced to FKFEFKFE. A nanoribbon structure was obtained when coated by RGD segments. The functionalised nanoribbons showed great potential to be used as a selective intracellular drug delivery carrier.¹⁵⁷ RGD modified FKFEFKFE peptide was also used to study the influences of the matrix stiffness and the binding site density on microvascular network formation of endothelial cells and the morphology of human mesenchymal stem cells. By mixing the normal FKFEFKFE with RGD modified FKFEFKFE in different ratios, the gel stiffness was altered in the range between ~60 to 6000 Pa. It was found that no network formation and little cell elongation was noticed in the gels without RGD modified FKFEFKFE. When RGD was present, increased cell number and cell length were noticed within the stiffer gels. Robust microvascular network formation also occurred but the extent of this formation decreased with the increasing gel stiffness.¹⁵⁸ Those studies show a great potential of FKFEFKFE to be used for biomedical applications.

The peptide used in this project is FEFEFKFK which is another variation of FKFEFKFE sequence. Instead of the alternation of positively charged side chains and negatively charged side chains in FKFEFKFE, FEFEFKFK has two negatively charged side chains together and two positively charged side chains together. As a member of the ionic complementary peptide family, FEFEFKFK was postulated to have a similar self-assembly and gelation mechanism as FKFEFKFE. TEM and AFM were used to visually confirm the presence of fibres in FEFEFKFK solutions. Further analysis of the TEM images revealed a regular helical fibre or twisted structure. The existence of the anti-parallel β -sheet structure was confirmed by FTIR.⁵⁸ FEFEFKFK can form gels above 7 mg ml^{-1} . Using small angle neutron scattering (SANS), FEFEFKFK was found to form fibrillar structures with radii of 1.7 nm below the critical gelation concentration. The mesh size of the gel network was derived above the critical gelation concentration ranging from 15 to 30 nm depending on the gel concentration.¹⁵⁹ The stiffness of FEFEFKFK hydrogels was examined with an oscillatory rheometer and it can be easily altered by varying the peptide concentration. The hydrophobic effect of peptide side chains on the self-assembly and gelation properties was also investigated by replacing F with L and V. Similar network topologies were found for each peptide. However, the stiffness of hydrogels was dramatically changed: the lower the hydrophobicity, the higher the elastic modulus. The biggest difference between the high elastic modulus and the low elastic modulus reached up to 100 times at the same gel concentration.⁵⁷

Similar to FKFEFKFE, FEFEFKFK can also be functionalized by introducing a polymer or peptide sequence to FEFEFKFK molecule prior to self-assembly. Previous studies showed that FEFEFKFK was successfully conjugated with PNIPAAm to form a reversible double thermoresponsive hydrogel which has a LCST at $30 \text{ }^\circ\text{C}$ and a melting temperature at $75 \text{ }^\circ\text{C}$.^{160, 161} The mechanical properties of this conjugated FEFEFKFK gel can be manipulated by mixing with normal FEFEFKFK in different molar ratios.^{162, 163} Combining the responsive behaviour and the tuneable mechanical properties, hydrogels of the mixture can be good candidates for tissue engineering or drug delivery system. FEFEFKFK can also be functionalized with short peptide sequence such as 6 histadine (H). The mixtures of H functionalised FEFEFKFK and normal FEFEFKFK in the presence of nanogold particles were examined with TEM. As the nanogold particles can covalently bind to H, the positions of the nanogold particles indicated the presence of H functionalised FEFEFKFK which confirmed the well distributed incorporation of H

functionalised FEFEFKFK throughout the fibrillar structure.¹⁶⁴ HHHHHH was believed to stick out of the edge of peptide fibrils.⁵⁷

Bovine chondrocytes were used to test the biocompatibility of FEFEFKFK hydrogels. Cells stayed round and alive in 2D and 3D cell culture environments. The deposition of ECM was also observed under both cell culture conditions. This study showed FEFEFKFK hydrogels can be good candidates as scaffolds for cartilage tissue engineering.¹⁶⁵

The Aggeli group also designed peptide with the β -sheet structure. This peptide system showed a concentration dependent self-assembly behaviour. As shown in Figure 1.12, peptides with one hydrophobic and one hydrophilic surface adopt a β -strand conformation and form anti-parallel β -sheet tapes at low concentrations. When the concentration increases, the hydrophobic surfaces attract each other and form ribbons. Further increasing concentration results in stacks of ribbons forming fibrils. Fibrils eventually twist together forming fibres. Fibres can entangle to form hydrogels.¹⁶⁶ Among all developed peptides, the most studied one is QQRFEWEFEQQ (P11-4). It can self-assemble to form fibres with an anti-parallel β -sheet tape structure at pH 4.2 when the concentration is below 10 mg ml⁻¹. When the concentration is higher than 10 mg ml⁻¹, it can form a hydrogel in cell culture medium which can then be used as an injected scaffold in tissue engineering.¹⁴⁷

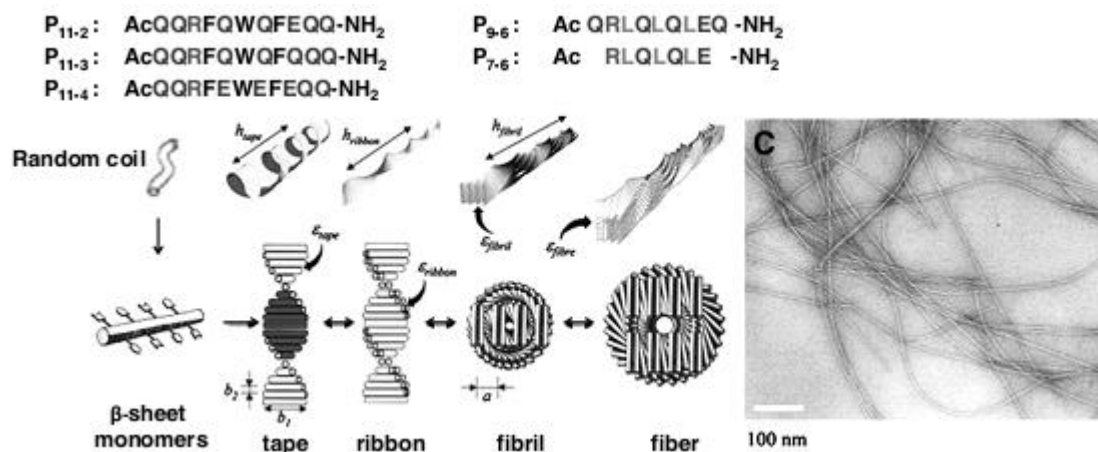


Figure 1.12 Short amphiphilic β -sheet peptides that self-assemble into anti-parallel nanotapes and further aggregate into ribbons and higher order structures. In a recent paper, shorter sequences (P9-6 and P7-6) with aliphatic hydrophobic residues (in green) were demonstrated to form fibrillar structures. (C) Transmission electron micrograph of a P11-4 gel in water (6.3 mM, pH 3) showing semi-rigid fibrils and fibers.¹⁴⁴

1.6 References

1. Davis, M. E.; Motion, J. P. M.; Narmoneva, D. A.; Takahashi, T.; Hakuno, D.; Kamm, R. D.; Zhang, S.; Lee, R. T., Injectable self-assembling peptide nanofibers create intramyocardial

microenvironments for endothelial cells. *Circulation* **2005**, 111, 442-450.

2. Langer, R.; Vacanti, J. P., Tissue engineering. *Science* **1993**, 14, (260), 920-926.
3. Ma, P. X., Scaffolds for tissue fabrication. *Materials Today* **2004**, 7, (5), 30-40.
4. Hukins, D. W. L.; Weston, S. A.; Humphries, M. J.; Freemont, A. J., Extracellular matrix. In *Principles of Medical Biology*, Elsevier: 1996; Vol. 3, pp 181-232.
5. Kreis, T.; Vale, R., *Guidebook to the Extracellular Matrix, Anchor, and Adhesion Proteins*. 2nd ed.; A Sambrook & Tooze Publication at Oxford University Press: New York, 1999.
6. Plopper, G., The extracellular matrix and cell adhesion. In *Cells*, Lewin, B.; Cassimeris, L.; Lingappa, V. R.; Plopper, G., Eds. Jones and Bartlett Publishers: London, 2007; pp 645-702.
7. Ruoslahti, E., Fibronectin and its receptors. *Annual Review of Biochemistry* **1988**, 57, 375-413.
8. Potts, J. R.; Campbell, I. D., Fibronectin structure and assembly. *Current Opinion in Cell Biology* **1994**, 6, (5), 648-655.
9. Main, A. L.; Harvey, T. S.; Baron, M.; Boyd, J.; Campbell, I. D., The three-dimensional structure of the tenth type III module of fibronectin: An insight into RGD-mediated interactions. *Cell* **1992**, 71, (4), 671-678.
10. Leahy, D. J.; Aukhil, I.; Erickson, H. P., 2.0 A crystal structure of a four-domain segment of human fibronectin encompassing the RGD loop and synergy region. *Cell* **1996**, 84, (1), 155-164.
11. Pierschbacher, M. D.; Hayman, E. G.; Ruoslahti, E., Location of the cell-attachment site in fibronectin with monoclonal antibodies and proteolytic fragments of the molecule. *Cell* **1981**, 26, (2, Part 2), 259-267.
12. Ruoslahti, E.; Pierschbacher, M.; Hayman, E. G.; Engvall, E., Fibronectin: a molecule with remarkable structural and functional diversity. *Trends in Biochemical Sciences* **1982**, 7, (5), 188-190.
13. Pierschbacher, M. D.; Ruoslahti, E., Cell attachment activity of fibronectin can be duplicated by small synthetic fragments of the molecule. *Nature* **1984**, 309, (3), 30-33.
14. Pierschbacher, M. D.; Ruoslahti, E., Variants of the cell recognition site off fibronectin that retain attachment-promoting activity. *Proceedings of the National Academy of Sciences of the United States of America* **1984**, 81, (19), 5985-5988.
15. Cooper, G. M.; Hausman, R. E., *The Cell: A Molecular Approach*. 4th ed.; ASM Press: Washington, 2007.
16. Pytela, R.; Pierschbacher, M. D.; Ruoslahti, E., Identification and isolation of a 140 kd cell surface glycoprotein with properties expected of a fibronectin receptor. *Cell* **1985**, 40, (1), 191-198.
17. Ruoslahti, E., RGD and other recognition sequences for integrins. *Annual Review of Cell and Developmental Biology* **1996**, 12, 697-715.
18. Pytela, R.; Pierschbacher, M. D.; Ruoslahti, E., A 125/115 kd cell surface receptor specific for vitronectin interacts with the Arg-Gly-Asp adhesion sequence derived from fibronectin.

Proceedings of the National Academy of Sciences **1985**, 82, 5766-5770.

19. Zhou, M. Self-assembled Bioactive Fmoc-peptide Hydrogels for Skin Tissue Engineering. PhD dissertation, The University of Manchester, Manchester, 2009.
20. Alberts, B.; Johnson, A.; Lewis, J.; Raff, M.; Roberts, K.; Walter, P., *Molecular Biology of The Cell*. 5th ed.; Garland Science, Taylor & Francis Group: New York, 2008.
21. Rittié L.; Fisher, G. J.; Varga, J.; Brenner, D. A.; Phan, S. H., Isolation and culture of skin fibroblasts. In *Fibrosis Research: Methods and Protocols*, Walker, J. M., Ed. Humana Press: 2005; Vol. 117, pp 83-98.
22. Mansbridge, J., Dermal Fibroblasts. In *Human Cell Culture*, M.R.Koller; B.O.Palsson; J.R.W.Masters, Eds. Kluwer Academic Publishers: Great Britain, 2001; Vol. V, pp 125-172.
23. Wnek, G. E.; Bowlin, G. L., *Encyclopedia of biomaterials and biomedical engineering*. Marcel Dekker, Inc.: New York, 2004; Vol. 1, p 89-90.
24. Ma, P. X., Tissue Engineering. In *Encyclopedia of Polymer Science and Technology*, 3rd ed.; Kroschwitz, J. I., Ed. John Wiley & Sons: NJ, 2004.
25. Ratner, B. D.; Bryant, S. J., Biomaterials: Where we have been and where we are going. *Annual Review of Biomedical Engineering* **2004**, 6, 41-75.
26. Shin, H.; Jo, S.; Mikos, A. G., Biomimetic materials for tissue engineering. *Biomaterials* **2003**, 24, (24), 4353-4364.
27. Hersel, U.; Dahmen, C.; Kessler, H., RGD modified polymers: biomaterials for stimulated cell adhesion and beyond. *Biomaterials* **2004**, 24, 4385-4415.
28. Yamada, K. M.; Kennedy, D. W., Dualistic nature of adhesive protein function: fibronectin and its biologically active peptide fragments can autoinhibit fibronectin function. *The Journal of Cell Biology* **1984**, 99, (1), 29-36.
29. Perlin, L.; MacNeil, S.; Rimmer, S., Production and performance of biomaterials containing RGD peptides. *Soft Matter* **2008**, 4, 2331-2349.
30. Tibbitt, M. W.; Anseth, K. S., Hydrogels as extracellular matrix mimics for 3D cell culture. *Biotechnology and Bioengineering* **2009**, 103, (4), 655-663.
31. Oh, J. K.; Bencherif, S. A.; Matyjaszewski, K., Atom transfer radical polymerization in inverse miniemulsion: A versatile route toward preparation and functionalization of microgels/nanogels for targeted drug delivery applications. *Polymer* **2009**, 50, 4407-4423.
32. Aluri, S.; Janib, S. M.; Mackay, J. A., Environmentally responsive peptides next term as anticancer drug carriers. *Advanced Drug Delivery Reviews* **2009**, 61, (11), 940-952.
33. Sundelacruz, S.; Kaplan, D. L., Stem cell- and scaffold-based tissue engineering approaches to osteochondral regenerative medicine *Seminars in Cell & Developmental Biology* **2009**, 20, (6), 646-655.
34. Storrie, H.; Guler, M. O.; Abu-Amara, S. N.; Volberg, T.; Rao, M.; Geiger, B. e. a., Supramolecular crafting of cell adhesion. *Biomaterials* **2007**, 28, 4608-4618.

35. Maheshwaric, G.; Brown, G.; Lauffenburger, D. A.; Wells, A.; Griffith, L. G., Cell adhesion and motility depend on nanoscale RGD clustering. *Journal of Cell Science* **2000**, 113, 1677-1686.
36. Pierschbacher, M.; Ruoslahti, E., Influence of stereochemistry of the sequence Arg-Gly-Asp-Xaa on binding specificity in cell adhesion. *Journal of Biological Chemistry* **1987**, 262, 17294-17298.
37. Kantlehner, M.; Schaffner, P.; Finsinger, D.; Meyer, J.; Jonczyk, A.; Diefenbach, B.; Nies, B.; Hözemann, G.; Goodman, S. L.; Kessler, H., Surface coating with cyclic RGD peptides stimulates osteoblast adhesion and proliferation as well as bone formation. *ChemBioChem* **2000**, 1, (2), 107-114.
38. Georges, P. C.; Janmey, P. A., Cell-type-specific response to growth on soft materials. *Journal of Applied Physiology* **2005**, 98, 1547-1553.
39. Uibo, R.; Laidmae, I.; Sawyer, E. S.; Flanagan, L. A.; Georges, P. C.; Winer, J. P.; P.A.Janmey, Soft materials to treat central nervous system injuries: Evaluation of the suitability of non-mammalian fibrin gels. *Biochimica et Biophysica Acta - Molecular Cell Research* **2009**, 1793, (5), 924-930.
40. Levental, I.; Georges, P. C.; Janmey, P. A., Soft biological materials and their impact on cell function. *Soft Matter* **2006**, (3).
41. Pelham, R. J.; Jr., Y.-L. W., Cell locomotion and focal adhesions are regulated by substrate flexibility. *Proceedings of the National Academy of Sciences* **1997**, 94, 13661-13665.
42. Guo, W. h.; Frey, M. T.; Burnham, N. A.; Wang, Y. I., Substrate rigidity regulates the formation and maintenance of tissues. *Biophysical Journal* **2006**, 90, 2213-2220.
43. Ghosh, K.; Shu, X.; Mou, R.; Lombardi, J.; Prestwich, G.; Rafailovich, M., Rheological characterization of in situ cross-linkable hyaluronan hydrogels. *Biomacromolecules* **2005**, 6, 2857-2865.
44. Holt, B.; Tripathi, A.; Morgan, J., Viscoelastic response of human skin to low magnitude physiologically relevant shear. *Journal of Biomechanics* **2008**, 41, (12), 2689-2695.
45. Geerligs, M.; Oomens, C.; Ackermans, P.; Baaijens, F.; Peters, G., Linear shear response of the upper skin layers. *Biorheology* **2011**, 48, 229-245.
46. Ghosh, K.; Pan, Z.; Guan, E.; Ge, S.; Liu, Y.; Nakamura, T.; Ren, X.-D.; Rafailovich, M.; Clark, R. A. F., Cell adaptation to a physiologically relevant ECM mimic with different viscoelastic properties. *Biomaterials* **2007**, 28, (4), 671-679.
47. Boyer, G.; Zahouani, H.; Bot, A. L.; Laquieze, L., In vivo characterization of viscoelastic properties of human skin using dynamic micro-indentation. *Proceedings of the 29th Annual International Conference of the IEEE* **2007**, 4585-4587.
48. Hadjipanayi, E.; Mudera, V.; Brown, R. A., Close dependence of fibroblast proliferation on collagen scaffold matrix stiffness. *Journal of Tissue Engineering and Regenerative Medicine* **2009**,

3, 77-83.

49. Zhou, M.; Smith, A. M.; Das, A. K.; Hodson, N. W.; Collins, R. F.; Ulijn, R. V.; Gough, J. E., Self-assembled peptide-based hydrogels as scaffolds for anchorage-dependent cells. *Biomaterials* **2009**, 30, 2523-2530.
50. Choi, J. S.; Yoo, H. S., Chitosan/pluronic hydrogel containing bFGF/heparin for encapsulation of human dermal fibroblasts. *Journal of Biomaterials Science* **2013**, 24, (2), 210-223.
51. Hwang, C. M.; Ay, B.; Kaplan, D. L.; Rubin, J. P.; Marra, K. G.; Atala, A.; Yoo, J. J.; Lee, S. J., Assessments of injectable alginate particle-embedded fibrin hydrogels for soft tissue reconstruction. *Biomedical Materials* **2013**, 8, (1), 014105.
52. Helary, C.; Bataille, I.; Abed, A.; Illoul, C.; Anglo, A.; Louedec, L.; Letourneur, D.; Meddahi-Pelle, A.; Giraud-Guille, M. M., Concentrated collagen hydrogels as dermal substitutes. *Biomaterials* **2010**, 31, (3), 481-490.
53. Jeong, J. H.; Liang, Y.; Jang, M.; Cha, C.; Chu, C.; Lee, H.; Jung, W.; Kim, J. W.; Boppart, S. A.; kong, H., Stiffness-modulated water retention and neovascularization of dermal fibroblast-encapsulating collagen gel. *Tissue Engineering Part A* **2013**, 19, (11-12), 1275-1284.
54. Li, L.; Thangamathesvaran, P. M.; Yue, C. Y.; Tam, K. C.; Hu, X.; Lam, Y. C., Gel network structure of methylcellulose in water. *Langmuir* **2001**, 17, 8062-8068.
55. Boothroyd, S. Peptide Self-assembly: Controlling Conformation and Mechanical Properties. PhD dissertation, the University of Manchester, Manchester, 2011.
56. Ozbas, B.; Kretsinger, J. K.; Rajagopal, K.; Schneider, J. P.; Pochan, D. J., Salt-triggered peptide folding and consequent self-assembly into hydrogels with tunable modulus. *Macromolecules* **2004**, 37, 7331-7337.
57. Miller, A. F.; Saiani, A., Engineering peptide based biomaterials: structure, properties and application. *Focus on Oligos & Peptides/Chemistry Today* **2010**, 28, (1), 34-38.
58. Saiani, A.; Mohammed, A.; Frielinghaus, H.; Collins, R.; Hodson, N.; Kielty, C. M.; Sherratt, M. J.; Miller, A. F., Self-assembly and gelation properties of alpha-helix versus beta-sheet forming peptides. *Soft Matter* **2009**, 5, (1), 193-202.
59. Rajagopal, K.; Ozbas, B.; Pochan, D. J.; Schneider, J. P., Probing the importance of lateral hydrophobic association in self-assembling peptide hydrogelators. *European Biophysics Journal With Biophysics Letters* **2006**, 35, 162-169.
60. Guenet, J.-M., *Thermoreversible Gelation of Polymers and Biopolymers*. Academic Press Limited: London, 1992.
61. Mackintosh, F. C.; Kas, J.; Janmey, P. A., Elasticity of semiflexible biopolymer networks. *Physical Review Letters* **1995**, 75, (24), 4425-4428.
62. Jones, J. L.; Marques, C. M., Rigid polymer network models. *Journal De Physique* **1990**, 51, (11), 1113-1127.
63. Guilbaud, J.-B.; Saiani, A., Using small angle scattering (SAS) to structurally characterise

peptide and protein self-assembled materials. *Chemical Society Reviews* **2011**, 40, 1200-1210.

64. Guenet, J. M., Structure versus rheological properties in fibrillar thermoreversible gels from polymers and biopolymers. *Journal of Rheology* **2000**, 44, (4), 947-960.
65. Liu, R.; Leonardis, P. D.; Cellesi, F.; Tirelli, N.; Saunders, B. R., Cationic temperature-responsive poly(N-isopropyl acrylamide) graft copolymers: from triggered association to gelation. *Langmuir* **2008**, 24, 7099-7106.
66. McParlane, J.; Dupin, D.; Saunders, J. M.; Lally, S.; Armes, S. P.; Saunders, B. R., Dual pH-triggered physical gels prepared from mixed dispersions of oppositely charged pH-responsive microgels. *Soft Matter* **2012**, 8, 6239-6247.
67. Collier, J. H.; Hu, B.-H.; Ruberti, J. W.; Zhang, J.; Shum, P.; Thompson, D. H.; Messersmith, P. B., Thermally and photochemically triggered self-assembly of peptide hydrogels. *Journal of American Chemistry Society* **2001**, 123, 9443-9464.
68. Filipcsei, G.; Feher, J.; Zrinyi, M., Electric field sensitive neutral polymer gels. *Journal of Molecular Structure* **2000**, 554, (1), 109-117.
69. Boral, S.; Gupta, A. N.; Bohidar, H. B., Swelling and de-swelling kinetics of gelatin hydrogels in ethanol-water marginal solvent. *International Journal of Biological Macromolecules* **2006**, 39, (4-5), 240-249.
70. Sugiura, S.; Sumaru, K.; Ohi, K.; Hiroki, K.; Takagi, T.; Kanamori, T., Photoresponsive polymer gel microvalves controlled by local light irradiation. *Sensors and Actuators A: Physical* **2007**, 140, (2), 176-184.
71. Bromberg, L.; Temchenko, M.; Moeser, G. D.; Hatton, T. A., Thermodynamics of temperature-sensitive polyether-modified poly(acrylic acid) microgels. *Langmuir* **2004**, 20, 5683-5692.
72. Yin, X.; Hoffman, A. S.; Stayton, P. S., Poly(N-isopropylacrylamide-co-propylacrylic acid) Copolymers That Respond Sharply to Temperature and pH. *Biomacromolecules* **2006**, 7, (5), 1381-1385.
73. Nonaka, T.; Ogata, T.; Kurihara, S., Preparation of poly(vinyl alcohol)-graft-N-isopropylacrylamide copolymer membranes and permeation of solutes through the membranes. *Journal of Applied Polymer Science* **1994**, 52, (7), 951-957.
74. Muniz, E. C.; Geuskens, G., Compressive elastic modulus of polyacrylamide hydrogels and semi-IPNs with poly(N-isopropylacrylamide). *Macromolecules* **2001**, 34, (13), 4480-4484.
75. Philippova, O. E.; Hourdet, D.; Audebert, R.; Khokhlov, A. R., pH-Responsive Gels of Hydrophobically Modified Poly(acrylic acid). *Macromolecules* **1997**, 30, (26), 8278-8285.
76. Crook, C. J.; Smith, A.; Jones, R. A. L.; Ryan, A. J., Chemically induced oscillations in a pH-responsive hydrogel. *Physical Chemistry Chemical Physics* **2002**, 4, 1367-1369.
77. Xiao, C. M.; Tan, J.; Xue, G. N., Synthesis and properties of starch-g-poly(maleic anhydride-co-vinyl acetate). *Polymer Letters* **2010**, 4, (1), 9-16.

78. Brahim, S.; Narinesingh, D.; Guiseppi-Elie, A., Release Characteristics of Novel pH-Sensitive p(HEMA-DMAEMA) Hydrogels Containing 3-(Trimethoxy-silyl) Propyl Methacrylate. *Biomacromolecules* **2003**, 4, (5), 1224-1231.
79. Schmaljohann, D., Thermo- and pH-responsive polymers in drug delivery. *Advanced Drug Delivery Reviews* **2006**, 58, (15), 1655-1670.
80. Saunders, J. M.; Tong, T.; Le Maitre, C. L.; Freemont, T. J.; Saunders, B. R., A study of pH-responsive microgel dispersions: from fluid-to-gel transitions to mechanical property restoration for load-bearing tissue. *Soft Matter* **2007**, 3, (4), 486-494.
81. Lally, S.; Bird, R.; Freemont, T.; Saunders, B., Microgels containing methacrylic acid: effects of composition on pH-triggered swelling and gelation behaviours. *Colloid and Polymer Science* **2009**, 287, (3), 335-343.
82. Lally, S.; Liu, R.; Supasuteekul, C.; Saunders, B. R.; Freemont, T., Using osmotic deswelling of microgel particles to control the mechanical properties of pH-responsive hydrogel composites. *Journal of Materials Chemistry* **2011**, 21, (44), 17719-17728.
83. Supasuteekul, C.; Milani, A. H.; Saunders, J. M.; Lally, S.; Freemont, T.; Saunders, B. R., A study of hydrogel composites containing pH-responsive doubly crosslinked microgels. *Soft Matter* **2012**, 8, (27), 7234-7242.
84. McParlane, J.; Dupin, D.; Saunders, J. M.; Lally, S.; Armes, S. P.; Saunders, B. R., Dual pH-triggered physical gels prepared from mixed dispersions of oppositely charged pH-responsive microgels. *Soft Matter* **2012**, 8, (23), 6239-6247.
85. Caykara, T.; Dogmus, M., Swelling-shrinking behavior of poly(acrylamide-co-itaconic acid) hydrogels in water and aqueous NaCl solutions. *Journal of Macromolecular Science - Pure and Applied Chemistry* **2005**, 42 A, (1), 105-111.
86. Baker, J. P.; Stephens, D. R.; Blanch, H. W.; Prausnitz, J. M., Swelling equilibria for acrylamide-based polyampholyte hydrogels. *Macromolecules* **1992**, 25, (7), 1955-1958.
87. Akar, E.; Altinisik, A.; Seki, Y., Preparation of pH- and ionic-strength responsive biodegradable fumaric acid crosslinked carboxymethyl cellulose. *Carbohydrate Polymers* **2012**, 90, (4), 1634-1641.
88. Seyednejad, H.; Ghassemi, A. H.; van Nostrum, C. F.; Vermonden, T.; Hennink, W. E., Functional aliphatic polyesters for biomedical and pharmaceutical applications. *Journal of Controlled Release* **2011**, 152, (1), 168-176.
89. Bouten, C. V. C.; Dankers, P. Y. W.; Driessen-Mol, A.; Pedron, S.; Brizard, A. M. A.; Baaijens, F. P. T., Substrates for cardiovascular tissue engineering. *Advanced Drug Delivery Reviews* **2011**, 63, (4), 221-241.
90. Armentano, I.; Dottori, M.; Fortunati, E.; Mattioli, S.; Kenny, J. M., Biodegradable polymer matrix nanocomposites for tissue engineering: A review. *Polymer Degradation and Stability* **2010**, 95, (11), 2126-2146.

-
91. Chen, Q.-Z.; Harding, S. E.; Ali, N. N.; Lyon, A. R.; Boccaccini, A. R., Biomaterials in cardiac tissue engineering: Ten years of research survey. *Materials Science and Engineering: R: Reports* **2008**, 59, (1), 1-37.
92. Wang, S.; Wan, A. C. A.; Xu, X.; Gao, S.; Mao, H.-Q.; Leong, K. W.; Yu, H., A new nerve guide conduit material composed of a biodegradable poly(phosphoester). *Biomaterials* **2001**, 22, (10), 1157-1169.
93. Morozowich, N. L.; Nichol, J. L.; Mondschein, R. J.; Allcock, H. R., Design and examination of an antioxidant-containing polyphosphazene scaffold for tissue engineering. *Polymer Chemistry* **2012**, 3, (3), 778-786.
94. Henslee, A. M.; Gwak, D. H.; Mikos, A. G.; Kasper, F. K., Development of a biodegradable bone cement for craniofacial applications. *Journal of Biomedical Materials Research Part A* **2012**, 100A, (9), 2252-2259.
95. Griffin, J.; Delgado-Rivera, R.; Meiners, S.; Uhrich, K. E., Salicylic acid-derived poly(anhydride-ester) electrospun fibers designed for regenerating the peripheral nervous system. *Journal of Biomedical Materials Research Part A* **2011**, 97A, (3), 230-242.
96. Nair, L. S.; Laurencin, C. T., Biodegradable polymers as biomaterials. *Progress in Polymer Science* **2007**, 32, (8-9), 762-798.
97. Rosso, F.; Marino, G.; Giordano, A.; Barbarisi, M.; Parmeggiani, D.; Barbarisi, A., Smart materials as scaffolds for tissue engineering. *Journal of Cellular Physiology* **2005**, 203, (3), 465-470.
98. Altman, G. H.; Horan, R. L.; Lu, H. H.; Moreau, J.; Martin, I.; Richmond, J. C.; Kaplan, D. L., Silk matrix for tissue engineered anterior cruciate ligaments. *Biomaterials* **2002**, 23, (20), 4131-4141.
99. Lavergne, M.; Derkaoui, M.; Delmau, C.; Letourneur, D.; Uzan, G.; Le Visage, C., Porous polysaccharide-based scaffolds for human endothelial progenitor cells. *Macromolecular Bioscience* **2012**, 12, (7), 901-910.
100. Li, Z. X.; Kawashita, M., Current progress in inorganic artificial biomaterials. *Journal of Artificial Organs* **2011**, 14, (3), 163-170.
101. Stevens, M. M.; Mecklenburg, G., Bio-inspired materials for biosensing and tissue engineering. *Polymer International* **2012**, 61, (5), 680-685.
102. Lee, K. Y.; Mooney, D. J., Hydrogels for tissue engineering. *Chemical Reviews* **2001**, 101, (7), 1870-1882.
103. Dutta, R. C.; Dutta, A. K., Cell-interactive 3D-scaffold; advances and applications. *Biotechnology Advances* **2009**, 27, (4), 334-339.
104. Mano, J. F.; Silva, G. A.; Azevedo, H. S.; Malafaya, P. B.; Sousa, R. A.; Silva, S. S.; Boesel, L. F.; Oliveira, J. M.; Santos, T. C.; Marques, A. P.; Neves, N. M.; Reis, R. L., Natural origin biodegradable systems in tissue engineering and regenerative medicine: present status and some

moving trends. *Journal of the Royal Society Interface* **2007**, 4, (17), 999-1030.

105. Hahn, M. S.; Tepy, B. A.; Stevens, M. M.; Zeitels, S. M.; Langer, R., Collagen composite hydrogels for vocal fold lamina propria restoration. *Biomaterials* **2006**, 27, (7), 1104-1109.
106. Joosten, E. A. J., Biodegradable biomatrices and bridging the injured spinal cord: the corticospinal tract as a proof of principle. *Cell and Tissue Research* **2012**, 349, (1), 375-395.
107. Mimura, T.; Imai, S.; Kubo, M.; Isoya, E.; Ando, K.; Okumura, N.; Matsusue, Y., A novel exogenous concentration-gradient collagen scaffold augments full-thickness articular cartilage repair. *Osteoarthritis and Cartilage* **2008**, 16, (9), 1083-1091.
108. Slaughter, B. V.; Khurshid, S. S.; Fisher, O. Z.; Khademhosseini, A.; Peppas, N. A., Hydrogels in regenerative medicine. *Advanced Materials* **2009**, 21, (32-33), 3307-3329.
109. Ahmed, T. A. E.; Dare, E. V.; Hincke, M., Fibrin: A versatile scaffold for tissue engineering applications. *Tissue Engineering Part B-Reviews* **2008**, 14, (2), 199-215.
110. Hunt, N. C.; Grover, L. M., Cell encapsulation using biopolymer gels for regenerative medicine. *Biotechnology Letters* **2010**, 32, (6), 733-742.
111. Jayakumar, R.; Chennazhi, K. P.; Srinivasan, S.; Nair, S. V.; Furuike, T.; Tamura, H., Chitin scaffolds in tissue engineering. *International Journal of Molecular Sciences* **2011**, 12, (3), 1876-1887.
112. Peppas, N. A.; Hilt, J. Z.; Khademhosseini, A.; Langer, R., Hydrogels in biology and medicine: From molecular principles to bionanotechnology. *Advanced Materials* **2006**, 18, (11), 1345-1360.
113. Zhu, J., Bioactive modification of poly(ethylene glycol) hydrogels for tissue engineering. *Biomaterials* **2010**, 31, (17), 4639-4656.
114. Pan, Y.-S.; Xiong, D.-S.; Ma, R.-Y., A study on the friction properties of poly(vinyl alcohol) hydrogel as articular cartilage against titanium alloy. *Wear* **2007**, 262, (7-8), 1021-1025.
115. Guan, Y.; Zhang, Y., PNIPAM microgels for biomedical applications: from dispersed particles to 3D assemblies. *Soft Matter* **2011**, 7, (14), 6375-6384.
116. Kohane, D. S.; Langer, R., Polymeric biomaterials in tissue engineering. *Pediatric Research* **2008**, 63, (5), 487-491.
117. Solomons, T. W. G.; Fryhle, C. B., *Organic Chemistry*. 8th ed.; John Wiley & Sons, Inc.: USA, 2003.
118. Clayden, J.; Greeves, N.; Warren, S.; Wothers, P., *Organic Chemistry*. Oxford University Press: New York, 2001.
119. Smith, A. M.; Williams, R. J.; Tang, C.; Coppo, P.; Collins, R. F.; Turner, M. L.; Saiani, A.; Ulijn, R. V., Fmoc-diphenylalanine self assembles to a hydrogel via a novel architecture based on pi-pi interlocked beta-sheets. *Advanced Materials* **2008**, 20, 37-41.
120. Kayser, V.; Turton, D. A.; Aggeli, A.; Beevers, A.; Reid, G. D.; Beddard, G. S., Energy migration in novel pH-triggered self-assembled beta-sheet ribbons. *Journal of American Chemistry*

Society **2003**, 126, 336-343.

121. Sewald, N.; Jakubke, H. D., *Peptides: Chemistry and Biology*. Wiley-Vch Verlag GmbH: Weinheim, 2002.
122. Reches, M.; Gazit, E., Casting metal nanowires within discrete self-assembled peptide nanotubes. *Science* **2003**, 300, (5619), 625-627.
123. Yemini, M.; Reches, M.; Rishpon, J.; Gazit, E., Novel electrochemical biosensing platform using self-assembled peptide nanotubes. *Nano Letters* **2004**, 5, (1), 183-186.
124. Kol, N.; Adler-Abramovich, L.; Barlam, D.; Shneck, R. Z.; Gazit, E.; Rouso, I., Self-assembled peptide nanotubes are uniquely rigid bioinspired supramolecular structures. *Nano Letters* **2005**, 5, (7), 1343-1346.
125. Mahler, A.; Reches, M.; Rechter, M.; Cohen, S.; Gazit, E., Rigid, self-assembled hydrogel composed of a modified aromatic dipeptide. *Advanced Materials* **2006**, 18, (11), 1365-1370.
126. Jayawarna, V.; Ali, M.; Jowitt, T. A.; Miller, A. F.; Saiani, A.; Gough, J. E.; Ulijn, R. V., Nanostructured hydrogels for three-dimensional cell culture through self-assembly of fluorenylmethoxycarbonyl-dipeptides. *Advanced Materials* **2005**, 18, (5), 611-614.
127. Tang, C.; Smith, A. M.; Collins, R. F.; Ulijn, R. V.; Saiani, A., Fmoc-diphenylalanine self-assembly mechanism induces apparent pKa shifts. *Langmuir* **2009**, 25, 9447-9453.
128. Raeburn, J.; Pont, G.; Chen, L.; Cesbron, Y.; Levy, R.; Adams, D. J., Fmoc-diphenylalanine hydrogels: understanding the variability in reported mechanical properties. *Soft Matter* **2012**, 8, 1168-1174.
129. Hughes, M.; Frederix, P. W. J. M.; Raeburn, J.; Birchall, L. S.; Sadownik, J.; Coomer, F. C.; Lin, I.-H.; Cussen, E. J.; Hunt, N. T.; Tuttle, T.; Webb, S. J.; Adams, D. J.; Ulijn, R. V., Sequence/structure relationships in aromatic dipeptide hydrogels formed under thermodynamic control by enzyme-assisted self-assembly. *Soft Matter* **2012**, 8, 5595-5602.
130. Jayawarna, V.; Richardson, S. M.; Hirst, A. R.; Hodson, N. W.; Saiani, A.; Gough, J. E.; Ulijn, R. V., Introducing chemical functionality in Fmoc-peptide gels for cell culture. *Acta Biomaterialia* **2009**, 5, (3), 934-943.
131. Hartgerink, J. D.; Beniash, E.; Stupp, S. I., Peptide-amphiphile nanofibers: A versatile scaffold for the preparation of self-assembling materials. *Proceedings of the National Academy of Sciences* **2002**, 99, (8), 5133-5138.
132. Stendahl, J. C.; Rao, M. S.; Guler, M. O.; Stupp, S. I., Intermolecular forces in the self-assembly of peptide amphiphile nanofibers. *Advanced Functional Materials* **2006**, 16, (4), 499-508.
133. Beniash, E.; Hartgerink, J. D.; Storrie, H.; Stendahl, J. C.; Stupp, S. I., Self-assembling peptide amphiphile nanofiber matrices for cell entrapment. *Acta Biomaterialia* **2005**, 1, 387-397.
134. Galler, K. M.; Cavender, A.; Yuwono, V.; Dong, H.; Shi, S.; Schmalz, G.; Hartgerink, J. D.; D'Souza, R. N., Self-assembling peptide amphiphile nanofibers as a scaffold for dental stem cells. *Tissue Engineering: Part A* **2008**, 14, (12), 2051-2058.

-
135. Boyle, A. L.; Woolfson, D. N., De novo designed peptides for biological applications. *Chemical Society Reviews* **2010**, 40, (8), 4295-4306.
136. Boyle, A. L.; Bromley, E. H. C.; Bartlett, G. J.; Sessions, R. B.; Sharp, T. H.; Williams, C. L.; Curmi, P. M. G.; Forde, N. R.; Linke, H.; Woolfson, D. N., Squaring the circle in peptide assembly: from fibers to discrete nanostructures by de novo design. *Journal of the American Chemical Society* **2012**, 134, (37), 15457-15467.
137. Papapostolou, D.; Bromley, E. H. C.; Bano, C.; Woolfson, D. N., Electrostatic control of thickness and stiffness in a designed protein fiber. *Journal of American Chemistry Society* **2008**, 130, 5124-5130.
138. Banwell, E. F.; Abelardo, E. S.; Adams, D. J.; Birchall, M. A.; Corrigan, A.; Donald, A. M.; Kirkland, M.; Serpell, L. C.; Butler, M. F.; Woolfson, D. N., Rational design and application of responsive [alpha]-helical peptide hydrogels. *Nature Materials* **2009**, 8, (7), 596-600.
139. Kretsinger, J. K.; Haines, L. A.; Ozbas, B.; Pochan, D. J.; Schneider, J. P., Cytocompatibility of self-assembled β -hairpin peptide hydrogel surfaces *Biomaterials* **2005**, 26, (25), 5177-5186.
140. Lamn, M. S.; Rajagopal, K.; Schneider, J. P.; Pochan, D. J., Laminated morphology of nontwisting beta-sheet fibrils constructed via peptide self-assembly. *Journal of American Chemistry Society* **2005**, 127, 16692-16700.
141. Schneider, J. P.; Pochan, D. J.; Ozbas, B.; Rajagopal, K.; Pakstis, L.; Kretsinger, J. K., Responsive hydrogels from the intramolecular folding and self-assembly of a designed peptide. *Journal of American Chemistry Society* **2002**, 124, (50), 15030-15037.
142. Pochan, D. J.; Schneider, J. P.; Kretsinger, J.; Ozbas, B.; Rajagopal, K.; Haines, L., Thermally reversible hydrogels via intramolecular folding and consequent self-assembly of a de novo designed peptide. *Journal of American Chemistry Society* **2003**, 125, (39), 11802-11803.
143. Zhang, S.; Holmes, T.; Lockshin, C.; Rich, A., Spontaneous assembly of a self-complementary oligopeptide to form a stable macroscopic membrane. *Proceedings of the National Academy of Sciences* **1993**, 90, 3334-3338.
144. Loo, Y.; Zhang, S.; Hauser, C. A. E., From short peptide to nanofibers to macromolecular assemblies in biomedicine. *Biotechnology Advances* **2012**, 30, 593-603.
145. Zhang, S., Emerging biological materials through molecular self-assembly. *Biotechnology Advances* **2002**, 20, (5-6), 321-339.
146. Zhang, S., Fabrication of novel biomaterials through molecular self-assembly. *Nature Biotechnology* **2003**, 21, 1171-1178.
147. Kyle, S.; Aggeli, A.; Ingham, E.; McPherson, M. J., Production of self-assembling biomaterials for tissue engineering. *Trends in Biotechnology* **2009**, 27, (7), 423-433.
148. Yang, Y.; Khoe, U.; Wang, X.; Horii, A.; Yokoi, H.; Zhang, S., Designer self-assembling peptide nanomaterials. *Nano Today* **2009**, 4, 193-210.

149. Marini, D. M.; Hwang, W.; Lauffenburger, D. A.; Zhang, S.; Kamm, R. D., Left-handed helical ribbon intermediates in the self-assembly of a beta-sheet peptide. *Nano Letters* **2001**, 2, (4), 295-299.
150. Hwang, W.; M., M. D.; Kamm, R. D.; Zhang, S., Supramolecular structure of helical ribbons self-assembled from a beta-sheet peptide. *Journal of Chemical Physics* **2003**, 118, (1), 389-398.
151. Caplan, M. R.; Schwartzfarb, E. M.; Zhang, S.; Kamm, R. D.; Lauffenburger, D. A., Control of self-assembling oligopeptide matrix formation through systematic variation of amino acid sequence. *Biomaterials* **2002**, 23, (1), 219-227.
152. Caplan, M. R.; Schwartzfarb, E. M.; Zhang, S.; Kamm, R. D.; Lauffenburger, D. A., Effects of systematic variation of amino acid sequence on the mechanical properties of a self-assembling, oligo peptide biomaterial. *Journal of Biomaterials Science, Polymer Edition* **2002**, 13, (3), 225-236.
153. Lee, N. R.; Bowerman, C. J.; Nilsson, B. L., Sequence length determinants for self-assembly of amphipathic beta-sheet peptides. *Biopolymers* **2013**, 10.1002/bip.22248.
154. Savin, T.; Doyle, P. S., Electrostatically tuned rate of peptide self-assembly resolved by multiple particle tracking. *Soft Matter* **2007**, 3, 1194-1202.
155. Petkau-Milroy, K.; Brunsveld, L., Supramolecular chemical biology; bioactive synthetic self-assemblies. *Organic & Biomolecular Chemistry* **2013**, 11, 219-232.
156. Rudra, J. S.; Sun, T.; Bird, K. C.; Daniels, M. D.; Gasiorowski, J. Z.; Chong, A. S.; Collier, J. H., Modulating adaptive immune responses to peptide self-assemblies. *ACS Nano* **2012**, 6, (2), 1557-1564.
157. Lim, Y.-b.; Kwon, O.-J.; Lee, E.; Kim, P.-H.; Yun, C.-O.; Lee, M., A cyclic RGD-coated peptide nanoribbon as a selective intracellular nanocarrier. *Organic & Biomolecular Chemistry* **2008**, 6, 1944-1948.
158. Stevenson, M. D.; Pirstine, H.; Hogrebe, N. J.; Nocera, T. M.; Boehm, M. W.; Reen, R. K.; Koelling, K. W.; AGARWAL, G.; Sarang-Sieminski, A. L.; Gooch, K. J., A self-assembling peptide matrix used to control stiffness and binding site density supports the formation of microvascular networks in three dimensions. *Acta Biomaterialia* **2013**, 10.1016/j.actbio.2013.04.002.
159. Saiani, A.; Mohammed, A.; Miller, A. F., 3D networks from self-assembling ionic-complementary octa-peptides. *Macromolecular Symposia* **2007**, 251, 88-95.
160. Stoica, F. Synthesis and Characterisation of the Thermoresponsive Copolymers and Peptide-Polymer Conjugates Based on Poly (N-isopropylacrylamide). PhD dissertation, University of Manchester, Manchester, 2008.
161. Stoica, F.; Alexander, C.; Tirelli, N.; Miller, A. F.; Saiani, A., Selective synthesis of double temperature-sensitive polymer-peptide conjugates. *Chemical Communications* **2008**, 4433-4435.
162. Maslovskis, A.; Saiani, A.; Miller, A. F., Thermoresponsive hydrogels from physical

mixtures of self-assembling peptide and its conjugate with PNIPAAm. *Macromolecular Symposia* **2010**, 296, 248-253.

163. Maslovskis, A.; Tirelli, N.; Saiani, A.; Miller, A. F., Peptide-PNIPAAm conjugate based hydrogels: synthesis and characterisation. *Soft Matter* **2011**, 7, 6025-6033.

164. Boothroyd, S.; Saiani, A.; Miller, A. F., Formation of mixed Ionic complementary peptide fibrils. *Macromolecular Symposia* **2008**, 273, 139-145.

165. Mujeeb, A.; Miller, A. F.; Saiani, A.; Gough, J. E., Self-assembled octapeptide scaffolds for in vitro chondrocyte culture. *Acta Biomaterialia* **2013**, 9, (1), 4609-4617.

166. Aggeli, A.; Nyrkova, I. A.; Bell, M.; Harding, R.; Carrick, L.; McLeish, T. C. B.; Semenov, A. N.; Boden, N., Hierarchical self-assembly of chiral rod-like molecules as a model for peptide beta-sheet tapes, ribbons, fibrils and fibers. *Journal of American Chemistry Society* **2001**, 98, (21), 11857-11862.

Chapter 2 Materials and methodology

2.1 Introduction

In this chapter the materials and methodology applied to the study of self-assembly and gelation properties of peptides for biomedical applications will be described. Both the basic theories of the techniques and the general procedures will be covered. All of the techniques used in this study can be classified into three groups: peptide synthesis and characterisation, peptide hydrogel preparation and characterisation and cell culture studies. They will be introduced in this chapter accordingly.

2.2 Peptide synthesis and characterisation:

2.2.1 Materials

All chemicals were used as received unless otherwise specified.

Fmoc-Lys(Boc)-Wang resin (100~200 mesh, loading: 0.66 mmol g⁻¹), Fmoc-Phe-OH, Fmoc-Lys(Boc)-OH, Fmoc-Glu(OtBu)-OH and 2-(6-Chloro-1H-benzotriazole-1-yl)-1,1,3,3-tetramethylaminium hexafluorophosphate (HCTU) were purchased from Novabiochem Co. and stored at -4 °C.

N, N-dimethylformamide (DMF 99.8%), N-methylpyrrolidone (NMP 99%), piperidine (99%), anisole (99%), N, N'-Diisopropylethylamine (DIPEA ≥99%), trifluoroacetic acid (TFA 99%), dichloro methane (DCM 99.9% biotech grade), diethyl ether, acetonitrile (HPLC grade with 0.1% formic acid and 0.01% TFA) were obtained from Sigma-Aldrich Co..

Ethanol absolute was supplied by Fisher Scientific.

Kaiser Test solutions A and B were prepared by A. Miller's group.

2.2.2 Solid phase peptide synthesis (SPPS)

To synthesise an acquired peptide, the primary structure was designed first then amino acids were coupled one by one from one end of the peptide backbone to the other. The strategy taken in this study was to start from the C-terminus of the peptide design and to

end at the N-terminus, which is illustrated in Figure 2.1:

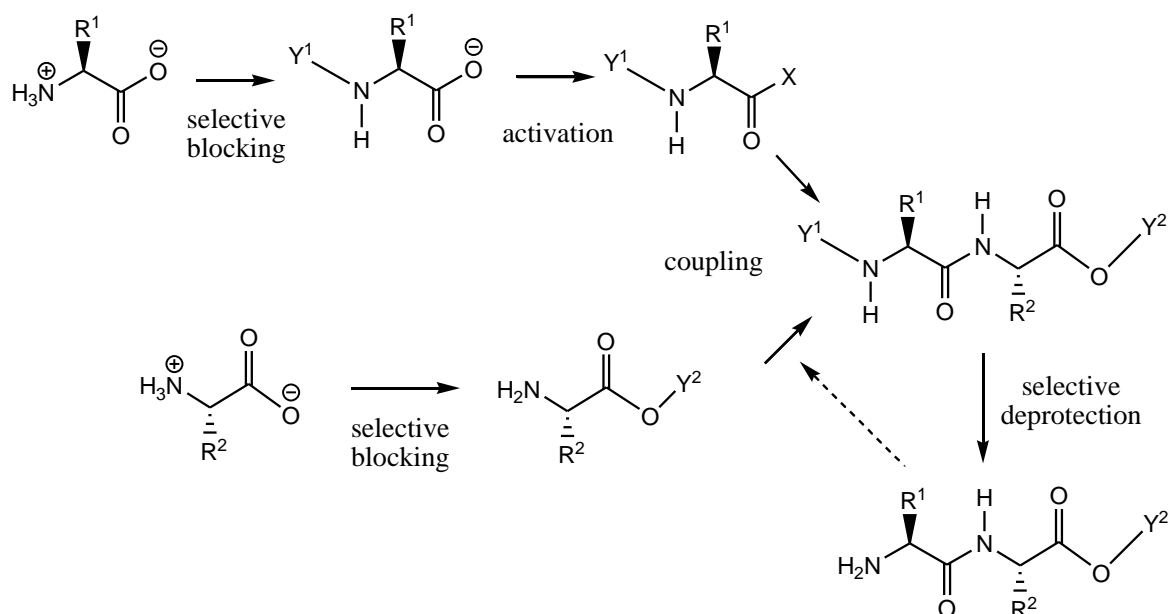


Figure 2.1 The multi-step process of peptide synthesis. Y^1 = amino-protecting group; Y^2 = carboxyl protecting group; R^1 , R^2 = amino acid side chains.¹

Firstly, to ensure the acquired peptide bond formations and to avoid the unwanted side reactions, amino acids were selectively protected. This included the side chain protection and the protection of the end functional groups. In the case presented here, the C-terminal amino acid should be C-protected, while the second amino acid should be N-protected. In this study, to protect the C-terminus of the first amino acid of the designed peptide sequence, said amino acid was connected to an insoluble polymer (Wang resin) through its carboxyl group.

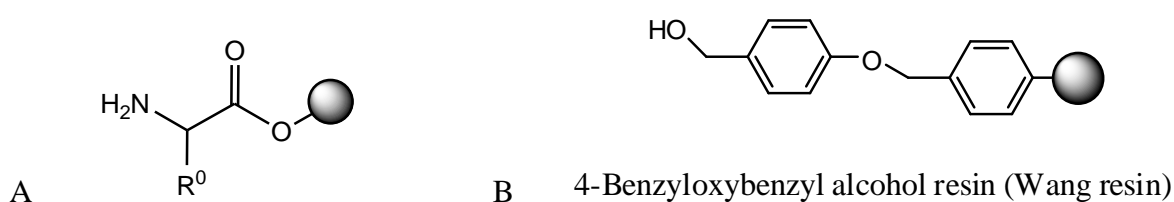


Figure 2.2 Structure of A) C-terminal amino acid linked to the resin; B) Wang resin

This peptide synthesis technology is known as solid phase peptide synthesis (SPPS).¹ Secondly, the protecting group of the amide group of the first amino acid was removed.

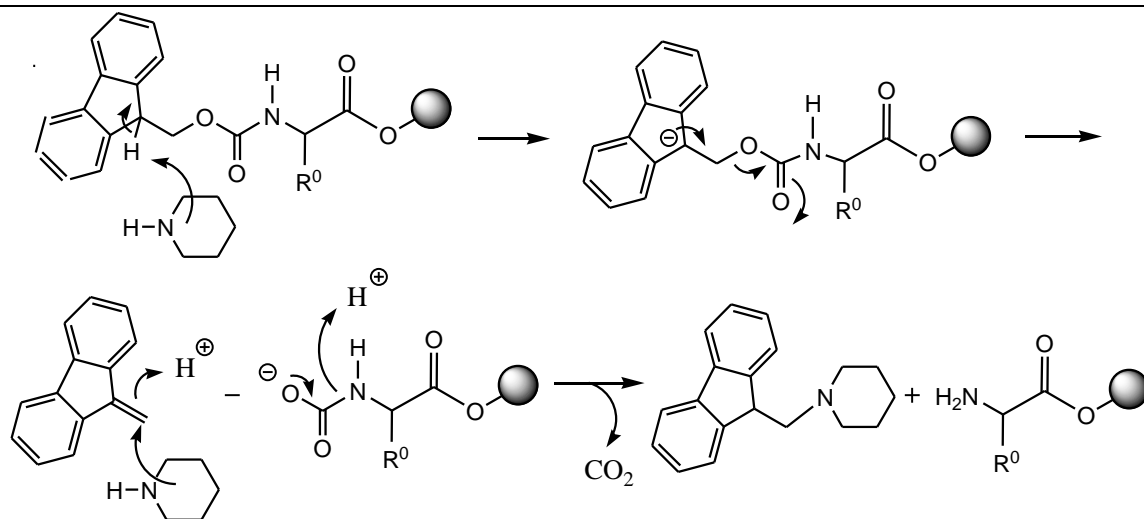


Figure 2.3 The mechanism of the Fmoc deprotection.¹

In the mean time the carboxyl group of the second amino acid was activated to provide a reactive intermediate.

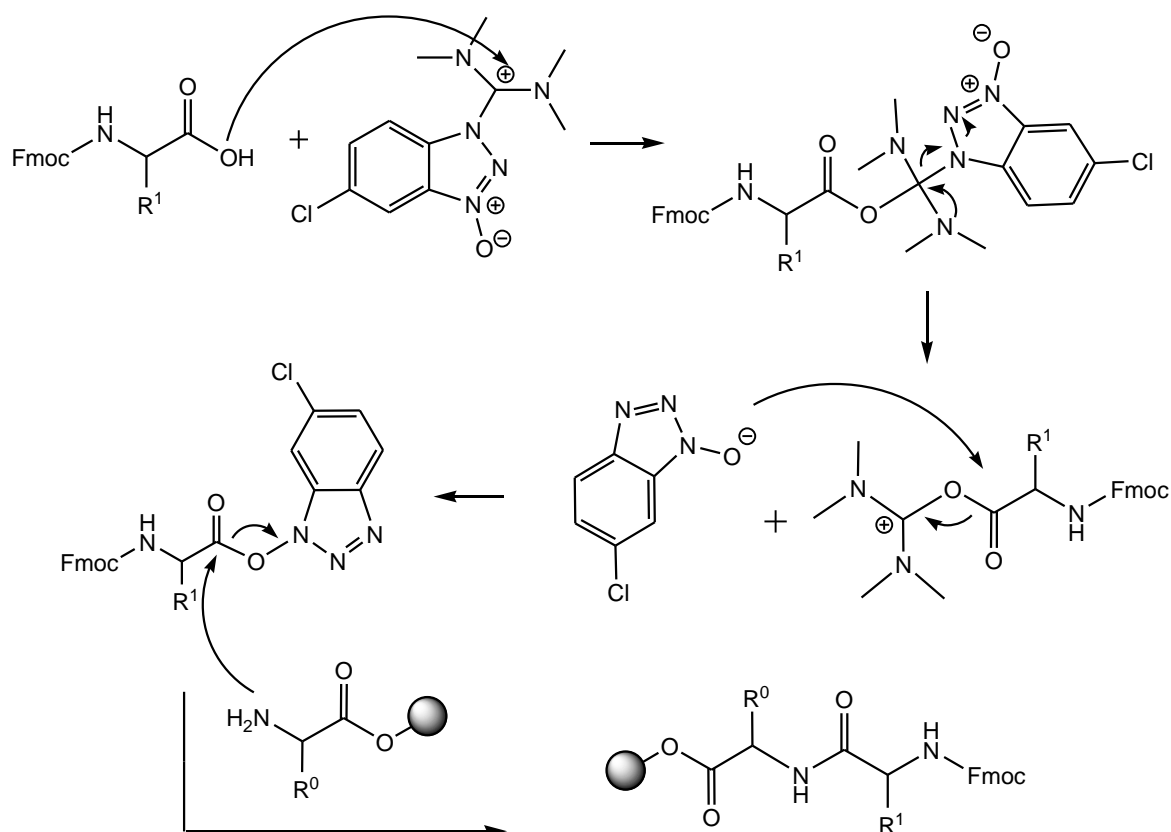


Figure 2.4 The mechanism of the activation and coupling reaction.²

This allows the coupling reaction, followed by the formation of peptide bond. One round after the other, the deprotection, activation and coupling were repeated until the designed sequence of the peptide formed. At the end of the synthesis, the product was dissolved in

the final cleavage cocktail while the insoluble polymeric support could be easily removed by filtration. In the meantime, all the protecting groups of both end groups and side groups were cleaved and the target peptide with the native primary structure was obtained.

In this study, SPPS was performed on a ChemTech ACT 90 peptide synthesiser. In a standard synthesis of the FEFEFKFK peptide, ~ 2.5 g Fmoc-Lys(Boc)-Wang resin (100~200 mesh, loading: 0.66 mmol g⁻¹) was pre-soaked in 30 ml DCM to allow the resin to swell. After 2 hours, 20 ml NMP was used to replace DCM to allow further swelling of the resin for 1 more hour. The reaction vessel was then emptied and a 30 ml mixture of piperidine and NMP with a ratio of 2:1 was added for 20 minutes to expose the amide group for the coupling step. A cleaning step was taken after the deprotection step. The resin beads were rinsed with 20 ml NMP for 5 times to wash out all the deprotection chemicals. A Kaiser test was performed to confirm the success of the deprotection.^{3, 4} Once the success of the deprotection step was confirmed, the second amino acid Fmoc-Phe-OH and HCTU were weighed at an 8 fold excess of the mole number of the K residue, and then dissolved in 40 ml DMF. The mixture solution was added into the reaction vessel along with 20 ml DIPEA and the coupling reaction was performed in the dark for 1 hour. The same cleaning step was taken followed by another Kaiser test. Once the coupling step was confirmed to be successful, the new cycle of the deprotection and coupling was repeated until the full length of the designed peptide was obtained. After the deprotection of the last amino acid, a final cleaning process was carried to ensure all the resin beads were clean, dry and ready for the cleavage. The resin beads were rinsed 3 times with 20 ml DMF for 15 minutes each time; followed by 2 times with 20 ml ethanol for 10 minutes each time and finally 2 times with 20 ml DCM for 10 minutes each time. The reaction vessel was gently agitated during the whole process. After the final cleaning, the resin beads were left to dry overnight. A 20 ml cleavage cocktail of TFA and anisole with a volume ratio of 19:1 were mixed with the beads and agitated for 3 hours to cause a complete reaction. The product solution was then added into a large excess of cold ether drop by drop. The peptide product precipitated in the cold ether and was separated by centrifugation. The purification of peptide product was undertaken by repeated precipitation in the cold ether and repeated centrifugation. Finally, the peptide product was dissolved in the distilled water, freeze dried and stored at -4 °C in a powder form.

Matrix-assisted laser desorption ionization-time of flight (MALDI-TOF) mass spectroscopy combined with reversed phase high performance liquid chromatography

(RP-HPLC) were used to prove the peptide was correctly synthesised as well as prove the purity of the peptides.

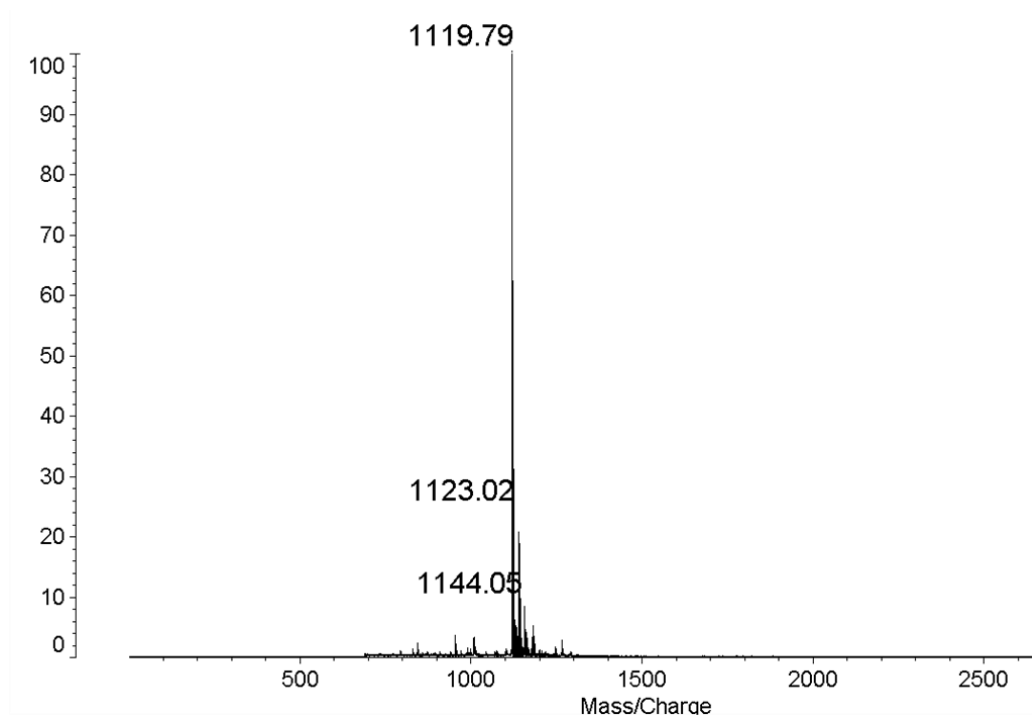


Figure 2.5 MALDI-TOF mass spectrum of FEFEFKFK in positive reflectron mode. The number beside each peak represents the molecular weight of $[M-H]^+$.

Figure 2.5 is the mass spectrum of FEFEFKFK. In this experiment, the electron charge was positive, so the value for the peak is the value of the molar mass of a cation associated molecule. The highest peak indicates the molar mass/charge of the major component within the analyte which is close to the molar mass $1121.3 \text{ g mol}^{-1}$ of FEFEFKFK in theory.⁵ This proved the major component within the product was FEFEFKFK. The small difference could be caused by the peak assignment during the calibration process. During the experiment, a standard sample was tested with the other samples. The molecular weight of this standard sample was known. After the experiment, the spectrum of this standard sample was analysed first. The values of the peaks on the spectrum were assigned to the known molecular weight of the standard sample. This is the calibration process. The values of the peaks on other spectra were calculated automatically.

Figure 2.6 exhibits the HPLC graph of FEFEFKFK, the peak area of which shows the proportion of each compound in the sample solution. Associated with the results of the mass spectroscopy, the highest peak can be assigned to FEFEFKFK and the percentage area of the largest peak among all peaks was used to estimate the purity of the peptide. Thus the designed peptide products with purity over 85 % were confirmed by HPLC and

mass spectroscopy (MS).

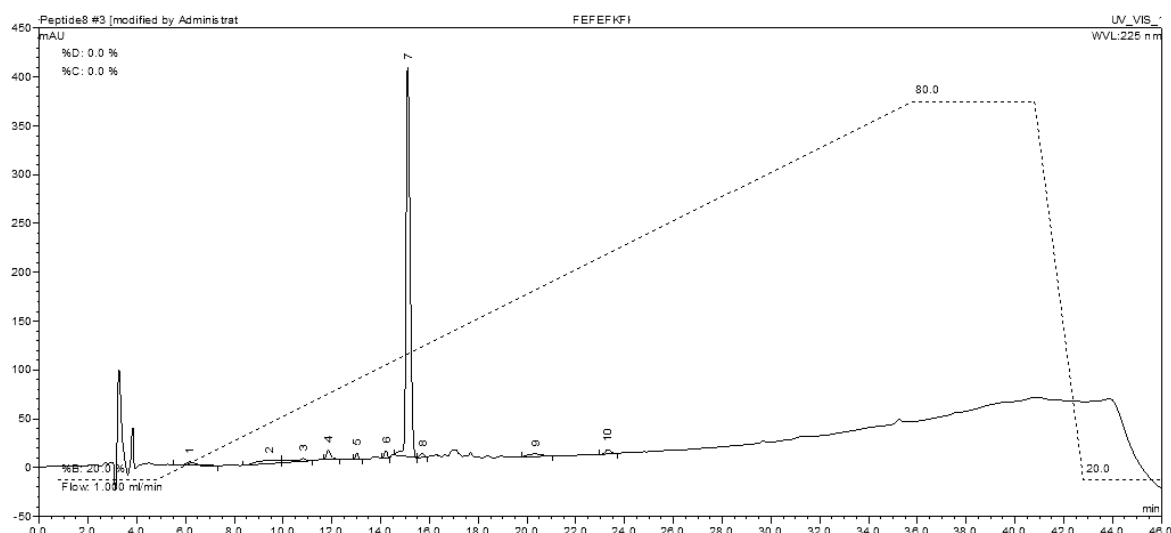


Figure 2.6 HPLC graph of FEFEFKFK.

The SPPS was not 100 % efficient. The impurities after peptide synthesis might have resulted from the miscoupling during the synthesis. Impurities with smaller molar mass could be peptides missing one amino acid or two; while impurities with larger molar mass could be peptides coupled with one more amino acid or two compared with the desired sequence. Because K was directly linked to the resin and the other K was coupled in the first two steps, K was unlikely missing in the process. As the peptide backbone grew longer, some molecules might have been hidden under other molecules or self-assembly would have occurred which also reduced the exposure of amino acid at the end of the peptide molecule. Thus one or two amino acids would appear missing on the final peptide molecule. On the other hand, the early deprotection of the end amino acid and a great amount of excess amino acids could result in one or two more amino acids appear on the final peptide molecule. When all the peptide molecules were dissolved in aqueous solutions, the short molecules incorporated into the fibrils and became the defects or branching points; while the long molecules stuck out of the edge of the fibrils or folded back which could inhibit the assembling of other molecules. The long molecules were not long enough to act like branches so a decrease of gel network strength was expected compared to the product with the higher purities. Although purities of peptide powder were slightly different between batches, the properties of peptide hydrogels, in particular mechanical showed no significant differences. This means the effects of the impurities on self-assembly and gelation properties of FEFEFKFK between batches were negligible.

2.2.3 Matrix-assisted laser desorption ionization-time of flight (MALDI-TOF) mass spectroscopy

MALDI-TOF was used to detect the molar mass of the peptide synthesised. In this project, reflectron detector and positive mode was used. In the experiment, after the sample plate was loaded, the whole system was vacuumed. The sample was directly exposed to a laser beam. After desorption and ionization, the analyte ions were accelerated in a field-free flight tube where high voltage was applied. The smaller ions travelled faster and reached the detector earlier, which was recorded as an electrical signal and transferred to intensity versus molar mass spectrum and showed on the computer screen. The molar mass of the analyte was indicated by the peaks.

The concentration of the sample for MALDI-TOF MS is around 1 pmol peptide in 1 μ l distilled water. To prepare the sample solution, 1 mg peptide was dissolved in 1 ml distilled water and then 1 μ l of this solution was diluted into 1 ml distilled water. This final solution had the right concentration. From the name of MALDI-TOF MS, matrix plays an important role in the experiment. It prevents the decomposition and association of the analyte and promotes the ionization of the sample.⁶ α -cyano-4-hydroxy-cinnamic acid was used as matrix which was dissolved in a mixture of acetonitrile, distilled water and formic acid solution (2 % v/v) at a ratio of 10:9:1. 1 μ l peptide solution and 1 μ l matrix solution were mixed, dropped onto a metal plate and dried in fume cupboard. Finally, the sample plate was placed inside the MALDI-TOF instrument and ready for tests.

2.2.4 Reversed phase high performance liquid chromatography (RP-HPLC)

An HPLC system consists of a stationary phase (column) and a mobile phase (solvent). When the sample is injected into the system, it is carried by the mobile phase flowing through the stationary phase. The different affinities between the sample components to the mobile phase and to the stationary phase result in the separation. The sample component attracts to the stationary phase and has a longer retention time, thus coming out of the column at the last. The sample component attracting to the mobile phase comes out of the column very quickly. When a non-polar material is chosen to be the stationary phase, the HPLC system is called RP-HPLC. When using this technique, the component with the highest hydrophobicity has the longest retention time.

A Dionex Ultimate 3000 HPLC was used to characterise the purity of the synthesised

peptide. The sample was prepared by dissolving 0.5 mg peptide in 1 ml distilled water and 0.5 ml acetonitrile solvent mixture. 100 μ l of sample solution was injected into the system. The flow rate was kept constant at 1 ml min⁻¹.

2.3 Gel preparation and characterisation:

2.3.1 Gel preparation and phase diagram

Three different sample preparation methods were performed for different studies.

1) Solutions and gels for transmission electron microscopy (TEM), small angle X-ray scattering (SAXS), Fourier transform infrared spectroscopy (FTIR) and the mechanical properties tests of the samples with no pH or adjusted ionic strength.

Peptide powder was weighed, mixed with a certain amount of distilled water to gain the acquired concentrations and vortexed. The mixture was then left in the oven at 90 °C. The sample vials were taken out 1 hour later to be vortexed again to ensure a homogenous gel and then put back into the oven. Followed by another 2 hours in the oven, the sample vials were then taken out and left on the bench. Transparent peptide solutions or hydrogels were observed during the cooling period until they reached room temperature. Without adding any NaOH or NaCl to the system, these samples had an original pH of 2.8. The experiments taken on these samples were performed at pH 2.8 at room temperature unless specified otherwise.

2) Solutions and gels for studying the pH effect.

1 M NaOH solution was prepared first. Distilled water was then mixed with 1 M NaOH solution at different volume ratios which resulted in a series of NaOH solutions at different concentrations. Peptide powder was weighed, mixed with a certain amount of NaOH solution to gain the acquired concentration and to get close to but slightly lower than the targeted pH. The sample vials were then vortexed and the mixture was left in the oven at 90 °C. Sample vials were taken out 1 hour later to be vortexed again to ensure a homogenous gel and then left on the bench to cool down. Once the samples were at room temperature, a pH meter was used to measure the actual pH value of the samples. Additional μ l of 1 M NaOH solution would be added if necessary to reach the targeted pH. The samples were usually prepared with more than 1 ml. Compared to the sample volume, the effect of the additional drops of NaOH solution on the peptide concentration was

negligible. Samples were then put back into the oven. Following by another 2 hours in the oven, the sample vials were then taken out and left on the bench. Peptide solutions or hydrogels were observed during the cooling period until they reached room temperature. The experiments done on these samples were performed at different pH levels at room temperature without any salt in the system unless specified otherwise.

3) Solutions and gels for studying the ionic strength effect.

2 M NaCl solution was prepared first. Distilled water was then mixed with 2 M NaCl solution at different volume ratios which resulted in a series of NaCl solutions at different concentrations. Peptide powder was weighed and mixed with a certain amount of NaCl solution to gain the acquired peptide concentration at the desired salt concentration. The sample vials were then vortexed and the mixture was left in the oven at 90 °C. The sample vials were taken out 1 hour later to be vortexed again to ensure a homogenous gel and then put back to the oven. After another 2 hours in the oven, the sample vials were then taken out and left on the bench. Peptide solutions or hydrogels were observed during the cooling period until they reached room temperature. The experiments done on these samples were performed at pH 2.8 at room temperature with different salt concentrations unless specified otherwise.

The samples for SANS tests were prepared in D₂O instead of H₂O. All other procedures were the same as mentioned above.

The experiments were usually performed on the next day after the samples were prepared.

The preparation of gels used in cell culture will be discussed later.

Three different types of phase diagrams were mapped out corresponding to three sample preparation methods. The sample vials were held in a hot water bath at a certain temperature for 15 minutes. The phase forms were recorded and then mapped out. For the samples prepared by method 1, the phase forms were recorded at different temperatures. For the samples prepared by methods 2 and 3, temperature was fixed to 25 °C. The pH value of the sample or the salt concentration of the sample was mapped against the sample concentration.

2.3.2 Transmission electron microscopy (TEM)

In the TEM instrument, an electron beam is generated by a field emission gun. Then electrons are accelerated inside a vacuum chamber and then run towards the sample. Electrons passing through the sample layer can be detected. The characteristics of the sample can be derived from the analysis of the density, phase and periodicity of the transmitted electrons. On the TEM images, the dark areas represent the thick sample areas or heavy atoms; whilst the bright areas have no sample. A thin sample layer at micron-scale is needed for a good observation under TEM. The samples like the peptide fibres are at nano-scale which appear transparent for electrons. Thus, a stain solution which contains heavy metal compounds is needed. The heavy metal atoms are attached to the fibre surfaces which appear dark under TEM while the fibre itself appears bright. This provides a good contrast for the observation of fibres morphology.⁷

A JEM'1220 electron microscope was used to characterise the structure of peptide hydrogels. 1 mg peptide was dissolved in 1 ml distilled water to prepare peptide solution at 1 mg ml⁻¹ concentration. The carbon coated face of copper grids was placed on top of 10 µl sample drop for 10 seconds, which was then blotted on filter papers. The grid was moved to a 10 µl distilled water drop for another 10 seconds and blotted again. Finally it was moved to a 10 µl drop of staining solution (4 wt% uranyl acetate) for 1 minute and blotted. The completely dried samples were then tested.

The micrographs obtained using TEM were analysed by ImageJ software. The diameters of random individual fibres were measured and the average diameter was used to present the size of the peptide fibre.

2.3.3 Small angle scattering (SAS)

In a small angle scattering (SAS) experiment, a sample is hit by a collimated, monochromatic beam and the beam scattered by the sample is monitored (Figure 2.7).

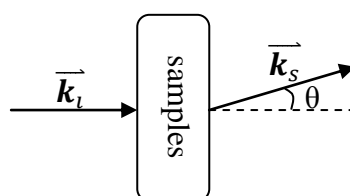


Figure 2.7 Illustration of a SAS experiment.

Given by the de Broglie relation, the neutron wavelength $\lambda = 2\pi/k$, where k is the size of the wave vector (\vec{k}). In an elastic scattering, the wavelength of the incident beam (λ_i) is the same as the wavelength of the scattered beam (λ_s), which also means $|\vec{k}_i| = |\vec{k}_s|$. The scattering vector \vec{q} (or the momentum transfer) is defined as $\vec{q} = \vec{k}_s - \vec{k}_i$. The size of it (q) is given as a function of the scattering angle (θ):⁸

$$q = |\vec{q}| = \frac{4\pi \sin(\theta/2)}{\lambda}$$

Equation 2.1

The scattered intensity for any isotropic sample is given as a function of q :

$$I(q) = BT_s\delta_s S(q)$$

Equation 2.2

where B is a constant and relates to the instrumental parameters and the contrast factor (K) of the scattered sample; T_s is the transmission of the scattered sample; δ_s is the thickness of the scattered sample; $S(q)$ is the scattering function. Both coherent scattering and incoherent scattering are included in $S(q)$, where the latter part does not contain any structural information of the sample and should be subtracted before data modelling. Thus⁹

$$I(q) = BT_s\delta_s S^{coh}(q)$$

Equation 2.3

$S^{coh}(q)$ can be described by

$$S^{coh}(q) = P(q) + Q(q)$$

Equation 2.4

where $P(q)$ is the form factor which comes from the intra scattering of the same objects and contains the structural information of the scattering objects; $Q(q)$ is the structure factor which comes from the inter scattering of the distinct scattering objects. In order to gain structure information of the scattering objects, experiments should be performed on diluted solutions where the scattering objects do not interact with each other, which means $Q(q)$ is negligible. Thus

$$I(q) = BT_s\delta_s P(q) = KCMP'(q)$$

Equation 2.5

where K is the contrast factor of the scattering object, C is the concentration of sample solution and $P'(q)$ is the form factor with no concentration and molar mass dependence.⁹

K used in this project is calculated by:

$$K = \frac{(a_p - Y_{ps} a_s)^2 N_A}{m_p^2}$$

Equation 2.6

where a_p is the scattering length of the peptide, which is the sum of the scattering length of each atom in one peptide molecule; a_s is the scattering length of the solvent, which is the sum of the scattering length of each atom in one solvent molecule; $Y_{ps} = \nu_p / \nu_s$ is the molar volume ratio, and the molar volume of one peptide molecule is the sum of the molar volume of each amino acid; m_p is the molar mass of one peptide molecule; $N_A = 6.022 \times 10^{23}$ is the Avogadro Number. The difference of K used in SANS and SAXS is due to the scattering length. In SAXS, the scattering length is proportional to the atom number, thus it has a better contrast between atoms with a bigger difference on the atom number. However, the scattering length in SANS has nothing to do with the atom number. It is well known that hydrogen has a negative scattering length while deuterium has a positive scattering length.¹⁰ This is a big advantage for examining biomaterials. The difference between the scattering lengths can also be used to study system with two objects. H₂O and D₂O co-solvents can be used. By varying the ratio between H₂O and D₂O, the scattering length of the co-solvent can be altered. Thus one object in the system could be studied by screening the other object. This has been successfully applied in the study of a mixture of FEFKFKFK and polymer conjugated FEFKFKFK.¹¹

The samples for SANS were prepared in the same way as explained in Section 2.3.1, except distilled water was replaced by D₂O. Experiments were carried out on both D22 in ILL Grenoble and in FRM Munich. By studying the scattering pattern, the structural properties of the samples can be revealed. It can be used as a complementary technique to TEM.

2.3.4 Fourier transform infrared spectroscopy (FTIR)

Every pair of neighbouring atoms in any molecule has a unique vibration frequency. When

the frequency of an infrared photon matches the unique vibration frequency, this pair of atoms will absorb the photon and get into an excited high energy level. The vibration frequency of pairing atoms can be affected by the conformation of the molecules and by the interactions between molecules. Thus by recording the absorbance frequency, characteristic IR spectrum can be obtained for any testing material. By comparing the spectra of the testing samples to IR spectra of the known samples, the intra and inter molecular structure of the testing samples can be discovered. The secondary structure of peptide can be presented by characteristic absorbance peaks within the amide I vibration zone, which is in the range of 1600-1700 cm^{-1} .¹²

The OMNIC software was used to fit the bands in the amide I region to determine the β -sheet content of the peptide samples. To find the position of each peak, band deconvolution and second derivative spectra were used. Comparing with the assignments of peaks from the literature,¹²⁻¹⁴ positions of peaks were assigned and fixed and a Gaussian function was applied to fit the original spectra. The full width half height of the bands was fixed to 6 and no baseline was chosen to get the best fit. The β -sheet content was estimated by the percentage area of β -sheet peak among all the secondary structure peaks.

A Thermo Nicolet 5700 spectrometer was used to study the peptide secondary structure in hydrogels. Solutions and hydrogels with different concentrations were prepared as described in 2.3.1. A background spectrum of distilled water was subtracted from all samples' spectra. Spectra were acquired in the 400 to 4000 cm^{-1} range with a resolution of 2 cm^{-1} over 128 scans.

2.3.5 Rheology

An oscillatory rheometry is often used for the rheology tests of the hydrogels. For a stress controlled rheometer, a stress varied sinusoidally is applied to the testing sample and the responding strain is recorded. For a Hookean solid, there is no phase difference between the applied stress and the responding strain; for a Newtonian fluid, the responding strain is completely out of phase. For a hydrogel, the phase difference in terms of phase angle (δ) is between 0 ° and 90 °. If δ is between 0 ° and 45 °, the gel has a solid-like behaviour whilst δ between 45 ° and 90 ° indicates the gel is liquid-like. The complex shear modulus (G^*) is defined as $G^* = \text{stress}/\text{strain}$. The elastic property of hydrogels is presented by the elastic modulus (G') which is defined as $G' = G^* \cos(\delta)$. The viscous property of hydrogels is presented by the viscous modulus (G'') which is defined as $G'' = G^* \sin(\delta)$. The phase

angle (δ) is defined as $\tan(\delta) = G''/G'$. Thus, for a gel with solid-like behaviour, $0 < \tan(\delta) < 1$, $G' > G''$; while for a gel with liquid-like behaviour, $\tan(\delta) > 1$, $G' < G''$. When $\tan(\delta) = 1$, $G' = G''$, this was considered the gel breaking point. The viscoelastic property of hydrogels can then be presented by these values and relationships between G' and G'' .

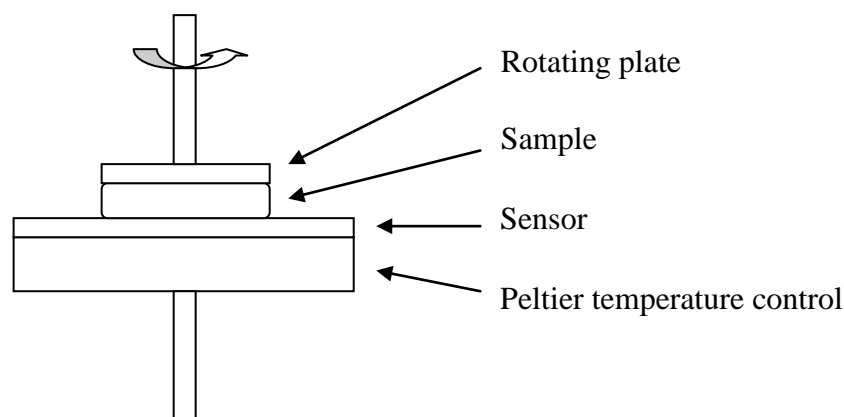


Figure 2.8 Rheometer with a parallel geometry

The mechanical property of peptide hydrogels was measured on an AR-G2 rheometer (TA instruments, UK) with a 20 mm diameter parallel plate geometry (Schematic representation was shown in Figure 2.8). During the process, the hydrogels were scooped out from the vial with a spatula and then loaded in the centre on the sensor plate. The upper plate was lowered down to a distance of 200 μm from the lower plate. A small amount of hydrogels were left in the gap between the two parallel plates while the excess hydrogels were removed with a spatula and recycled by the freeze drying technique. A solvent trap was utilized to decrease the evaporation of water and keep the concentration of the hydrogels constant. 3 minutes of relaxation time was allowed for the recovery of the hydrogels from being pressed by the plate.

Four different types of the rheological oscillation test were carried out.

1) Amplitude sweep

An amplitude sweep was taken for each new sample to determine the linear visco-elastic region (LVR) of the sample. The variation of the shear modulus with the increase of strain was recorded at an oscillation frequency fixed at 1 Hz at 20 $^{\circ}\text{C}$. Temperature was set to 37 $^{\circ}\text{C}$ for the gels used in the cell culture studies. In the LVR, the shear modulus is independent from the strain. For all samples tested, the LVR is below the strain of 5 %.

When the strain $> 10\%$, $G' < G''$ was observed for all samples which indicated the gel was broken.

2) Frequency sweep

A frequency sweep was taken in the LVR of all samples. A fixed strain of 1 % (in the LVR) was chosen in all frequency sweep tests. The variation of shear modulus and $\tan(\delta)$ with the increase of frequency were recorded at 20 °C and repeated at least 3 times for each sample. Temperature was set to 37 °C for the gels used in the cell culture studies. The independence of the shear modulus and $\tan(\delta)$ from the frequency was observed at the frequency lower than 5 Hz. The average value in this linear range was calculated to represent the mechanical properties of the peptide hydrogels. The error bars indicated the standard deviations of data obtained from the repeating experiments.

3) Temperature sweep

A temperature sweep was taken in the LVR of all samples. A fixed strain of 1 % and a fixed frequency at 1 Hz were chosen where the shear modulus was independent from the strain and frequency. 25 mg ml⁻¹ FEFEFKFK peptide hydrogel was heated up from 25 °C to 85 °C at a heating rate of 5 °C min⁻¹ then cooled back to 25 °C at the same rate for one cycle. The cycle was repeated twice.

4) Time sweep (recovery)

A time sweep was taken in the LVR of all samples. A fixed frequency at 1 Hz was chosen where the shear modulus was independent from the frequency. There were three stages during the recovery tests. In the first stage, the shear modulus was recorded with time for 5 minutes at a fixed strain of 1 % which is in the LVR of the peptide hydrogels. In the second stage, a strain of 150 % was applied for 5 seconds to break the gel which was confirmed by the sharp decrease of G' (where $G' < G''$). In the third stage, a fixed strain of 1 % was applied again to record the change of the shear modulus with time after the breakage. Temperature remained at 20 °C during all tests.

2.4 Cell culture and assays

2.4.1 Materials

Dermal fibroblast (C-013-5C human adult) was purchased from Cascade.

Dulbecco's modified eagle's medium (DMEM, 21885), fetal bovine serum (FBS, 21885), 0.25 % trypsin-EDTA (25200), Dulbecco's phosphate buffered saline (DPBS, 14190-250 no $\text{Ca}^{2+}/\text{Mg}^{2+}$) were purchased from Gibco.

Fibronectin (F2006 human plasma), bovine serum albumin (BSA, A7906), Triton® X-100 (T8787), dimethyl sulfoxide (DMSO), Antibody: anti-rabbit LgG (C2306) were purchased from Sigma.

Prolong antifade+Dapi (P36391), Live/dead assay (L3224), fluorescein phalloidin (F432) were purchased from Invitrogen.

Paraformaldehyde (30525-89-4) was purchased from Fisher.

Antibody: anti- $\alpha_5\beta_1$ (MAB1969 Mouse anti-human) was purchased from Chemicon.

Antibody: anti-fibronectin (ab32419 Rabbit anti-human) and anti-collagen I (ab21285 Rabbit anti-human) were purchased from Abcam.

2.4.2 Cell culture

HDFs were cultured in the cell culture medium consists of DMEM pre-mixed with 10 % FBS and 1% antibiotic-antimycotic solution. When confluent, cells were detached using trypsin (0.05%)-EDTA 4Na and transferred into a falcon tube. The cell culture medium with 10 times of the volume was added to neutralise the trypsin. Cells were centrifuged and the trypsin solution was removed. The cell pellet was re-suspended in the fresh cell culture medium and adjusted to the required cell concentration before seeding on or into the peptide hydrogels. A haemocytometer was used to count the cell numbers and calculate the cell concentrations accordingly.

After the initial seeding, cell morphology was observed under the Leica DM IL optical microscope while cells were still growing on or in the peptide hydrogels. The micrographs were taken with the attaching camera at different post culture days. The magnification of 20X was used unless specified otherwise.

2.4.3 Fluorescence microscopy:

In the fluorescence microscope, filtered light with a certain wavelength hit on the samples. Electrons absorbing the incident photon will jump into a high energy level and then when

electrons drop back to the ground energy level, a photon with lower energy will be emitted. The emitted photons can be recorded which can reveal the molecular arrangement of the tested samples.¹⁵

The fluorescence microscope Nikon ECLIPSE 50i with different excitation filters was used as an observation method in the F-actin staining assay, Live/Dead assay and immunostaining assays.

2.4.4 F-actin staining

fluorescein isothiocyanate (FITC)-conjugated phalloidin combined with the fluorescence microscopy was used to the observation of F-actin. During 2D cell culture, 4 % (w/v) paraformaldehyde was left on top of the gels for 30 minutes to fix the cells. The fixing solution was then removed and the gel surface was rinsed 3 times with PBS. Cells were permeabilized by 0.5 % (v/v) triton X-100 in PBS solution and left at 4 °C for 5 minutes. The solution was again removed and the gel surface was rinsed 3 times with PBS. 50 µg ml⁻¹ FITC-phalloidin solution was added and the samples were left in the dark. 3 hours later, the stain solution was removed and the samples were transferred onto microscope glasses and mounted with DAPI ProlongTM gold antifade reagent. A Nikon ECLIPSE 50i fluorescence microscope was used for the observation of F-actin. F-actin was stained green by FITC and observed with a filter of 495 nm and cell nucleolus was stained blue by DAPI and observed with a filter of 340 nm. For cells cultured in 3D environment, the hydrogels were soaked in the FITC-phalloidin solution overnight.

2.4.5 Cell counting

To dissolve the gel, 1 ml cell culture medium was added into one cell culture well. The partially broken gels and cell mixture was then transferred into a 2 ml vial and gently vortexed to further break down the gels, gaining a homogeneous cell suspension. 10 µl cell suspension was diluted with 10 µl trypan blue solution, staining the dead cells. The cell numbers in the diluted cell suspension were then counted using a haemocytometer and the cell concentrations and cell numbers in the original well were calculated accordingly.

2.4.6 Live/Dead assay

A live-dead assay uses the stain solutions to stain live cells and dead cells with different colours, so the cell viability can be easily observed under the fluorescence microscope. In

the assay kit, there are two solutions: calcein AM and ethidium homodimer-1 (EthD-1). Calcein AM can penetrate membranes of the living cells then be cut to calcein by the enzyme within the living cells. Thus the living cells appear green under the fluorescence microscope. EthD-1 can only get into the dead cells and stain the cell nuclei which results in the observation of the dead cells in red under the fluorescence microscope.

Cell viability was tested using a Live/dead assay. 300 μ l PBS containing 0.6 μ l of 4 μ M EthD-1 red assay solution and 0.15 μ l of 2 μ M calcein AM white assay solution was incubated on top of the gels for 20 minutes in the incubator at 37 °C. The staining solution was removed and the gels were transferred on to the microscope slides. The samples were mounted with Prolong gold anti-fade reagent, covered with the glass cover slips and observed using a Nikon Eclipse 50i fluorescence microscope with excitation filters of 494 nm (green, calcein) and 528 nm (red, EthD-1).

2.4.7 Immunostaining assay

The secretion of ECM molecules can be detected by the immunostaining assays. The deposition of ECM molecules was tested after 1, 3, 5, 7 and 14 days of cell culture. The same cell fixing and permeabilization process as F-actin staining were performed. Instead of laying the staining solution after the permeabilization, 1 % BSA in DPBS solution was used to block cells for 6 hours. The blocking solution was changed every 2 hours to ensure efficient blocking. The blocking solution was then replaced by the antibody solution. The primary rabbit anti-human fibronectin antibody was diluted 100 times in 1 % BSA solution (or the primary rabbit anti-human collagen I antibody was diluted 40 times in 1 % BSA solution) to gain the primary antibody solution. The gels were soaked in the antibody solution overnight at 4 °C. The antibody solution was then removed and the gels were rinsed 3 times with 1 % BSA solution and left in 1 % BSA solution for 1 hour. This was repeated 3 times to ensure no antibody solution was left in the system. The secondary antibody solution was then added. The secondary antibody solution was produced by diluting a Cy3-conjugated sheep anti-rabbit LgG antibody into 1 % BSA solution at a ratio of 1:100. After 6 hours, the secondary antibody solution was removed and the same washing step was repeated to ensure no secondary antibody solution was left in the system. The samples were then transferred onto microscope glasses and mounted with Prolong antifade reagent with DAPI. The samples were then observed under a Nikon Eclipse 50i fluorescence microscope with excitation filters of 547 nm (red, Cy3) and 340 nm (blue,

DAPI). The same protocol was used for both 2D and 3D cell culture.

2.5 References

1. Sewald, N.; Jakubke, H. D., *Peptides: Chemistry and Biology*. Wiley-Vch Verlag GmbH: Weinheim, 2002.
2. Balalaie, S.; Mahdidoust, M.; Najafabadi, R., 2-(1H-Benzotriazole-1-yl)-1,1,3,3-tetramethyluronium tetrafluoroborate as an efficient coupling reagent for the amidation and phenylhydrazination of carboxylic acids at room temperature. *Journal of Iranian Chemical Society* **2007**, 4, (3), 364-369.
3. Kaiser, E.; Colescott, R. L.; Bossinger, C. D.; Cook, P. I., Color test for detection of free terminal amino groups in the solid-phase synthesis of peptides. *Short Communications* **1969**, 595-598.
4. Sarin, V. K.; Kent, S. B. H.; Tam, J. P.; Merrifield, R. B., Quantitative monitoring of solid-phase peptide synthesis by the ninhydrin reaction. *Analytical Biochemistry* **1981**, 117, 147-157.
5. PepCalc.com Peptide property calculator. <http://www.innovagen.se/custom-peptide-synthesis/peptide-property-calculator/peptide-property-calculator.asp> (16/05/2012),
6. Gross, J. H., *Mass Spectrometry A Textbook*. Springer: Berlin Heidelberg, 2011.
7. Ayache, J.; Beaunier, L.; Ehret, G.; Boumendil, J.; Laub, D., *Sample Preparation Handbook for Transmission Electron Microscopy: Techniques*. Springer Science + Business Media, LLC: New York, 2010.
8. Imae, T.; Kanaya, T.; Furusaka, M.; Torikai, N., *Neutron in Soft Matter*. John Wiley & Sons, Inc.: Hoboken, 2011.
9. Guilbaud, J.-B.; Saiani, A., Using small angle scattering (SAS) to structurally characterise peptide and protein self-assembled materials. *Chemical Society Reviews* **2011**, 40, 1200-1210.
10. Pynn, R., Neutron scattering: a primer. *Los Alamos Science* **1990**, 19, 19-01.
11. Malslovski, A. Responsive Hydrogels using Self-Assembling Polymer-Peptide Conjugates. PhD dissertation, University of Manchester, Manchester, 2010.
12. Barth, A.; Zscherp, C., What vibrations tell us about proteins. *Quarterly Reviews of Biophysics* **2002**, 35, (4), 369-430.
13. Barth, A., Infrared spectroscopy of proteins. *Biochimica et Biophysica Acta* **2007**, 1767, 1073-1102.
14. Giacomelli, C. E.; Valenti, L. E.; Paci, M. B.; De Pauli, C. P., Infrared study of trifluoroacetic acid unpurified synthetic peptides in aqueous solution: Trifluoroacetic acid removal and band assignment. *Analytical Biochemistry* **2011**, 410, (1), 118-123.
15. Lakowicz, J. R., *Principles of Fluorescence Spectroscopy*. Springer Science + Business Media, LLC: Boston, 2006.

Chapter 3 Self-assembly and gelation properties of FEFKFK peptide

In this chapter, the studies of FEFKFK peptide self-assembly are presented. The gel properties of this peptide in particular the rheological properties were investigated. For a better control of the gel properties and further understanding the peptide self-assembly, the effects of pH and ionic strength on FEFKFK peptide were studied. A protocol for using this peptide hydrogel as 2D cell culture scaffold was developed with the understanding of the self-assembly and gelation process. The primary cell culture tests showed that the gel properties need further improvement for a better performance in the cell culture studies. Therefore the bioactive peptide sequence was introduced and the studies of self-assembly and gelation properties of the functionalized peptide are presented in the next chapter.

3.1 FEFKFK peptide

3.1.1 Self-assembly of FEFKFK peptide

In the polymers and peptides group, a library of eight amino acid peptides has been studied. The number of the amino acids was chosen based on a compromise between the cost, time and properties. Among all octapeptides, the ionic-complementary FEFKFK peptide (Figure 3.1) was selected for this project as it is known to form hydrogels with 3D fibrillar network structures in aqueous solutions. It is the mostly studied peptide among all the other peptides synthesised in the group, and has become the best candidate for biomedical researches.¹⁻⁷

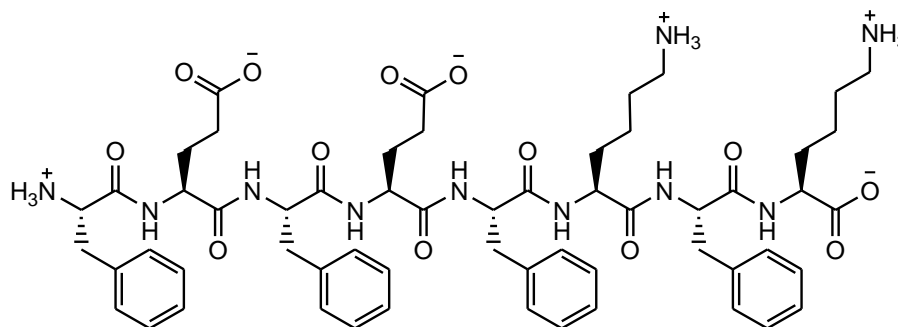


Figure 3.1 The molecular structure of FEFKFK peptide at neutral pH.

In the design of the FEFEFKFK peptide, glutamic acid and lysine were used to provide the negatively and positively charged side groups, respectively. Phenylalanine was used to provide the non-charged side group. The alternation of hydrophobic and hydrophilic amino acid was designed to tune the properties of the peptide. The charged side groups and non-charged side groups also provide peptides with one hydrophobic surface and one hydrophilic surface which aid the peptides to form β -sheet structures in water (Figure 3.2). A self-assembly model was previously proposed for similar peptide FKFEFKFE.⁸

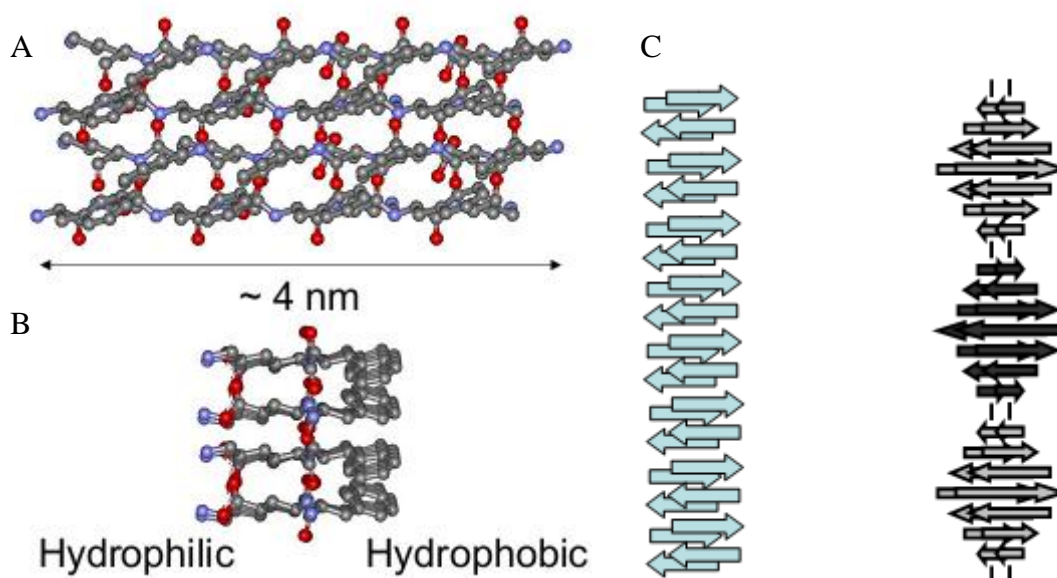


Figure 3.2 Schemes of an anti-parallel β -sheet structure formed by FEFEFKFK peptide (A—top view; B—side view);⁵ Schemes of the formation of the fibres by FEFEFKFK peptide (C).⁸

Figure 3.2 A and B show the self-assembly of an anti-parallel β -sheet structure taken by the FEFEFKFK peptide fibres. The anti-parallel β -sheet structure formed through hydrogen bonding of the peptide backbones. The hydrophobic side chains of phenylalanines stayed on one side of the fibres while the hydrophilic side chains of glutamic acids and lysines remained on the other side of the fibres. In the case of FKFEFKFE (Figure 3.2 C), the hydrophobic effect draws two fibres together which left the hydrophilic side groups outside the fibre surfaces.

To confirm the same self-assembly process occurred on the FEFEFKFK peptide, samples were prepared for the FTIR and TEM studies. The secondary structure of FEFEFKFK peptide was examined by FTIR. The samples at concentration of 10, 30 and 40 mg ml⁻¹ were tested. The strong sharp peaks around 1625 cm⁻¹ represent the presence of β -sheet structures. It was observed that the height of these peaks increased with increasing sample

concentrations. Although the sample at 10 mg ml^{-1} was a solution, the presence of β -sheet structure indicates that the self-assembly process had already occurred.

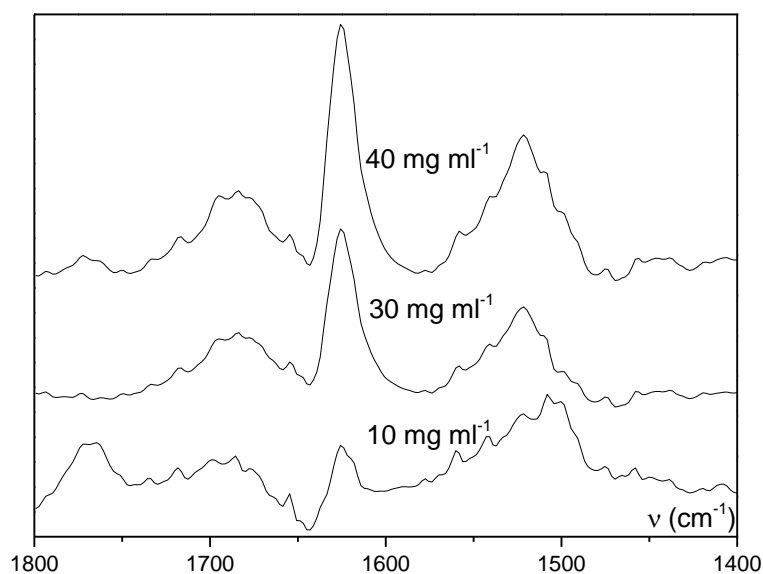


Figure 3.3 FTIR spectra of peptide hydrogels at concentrations of 10, 30 and 40 mg ml^{-1} all at pH 2.8.

The peak fitting analysis in the amide I region was processed for FEFEFKFK peptide at concentrations of 10, 30 and 40 mg ml^{-1} . The fitted FTIR spectrum of FEFEFKFK peptide at concentrations of 40 mg ml^{-1} is presented in Figure 3.4 (A).

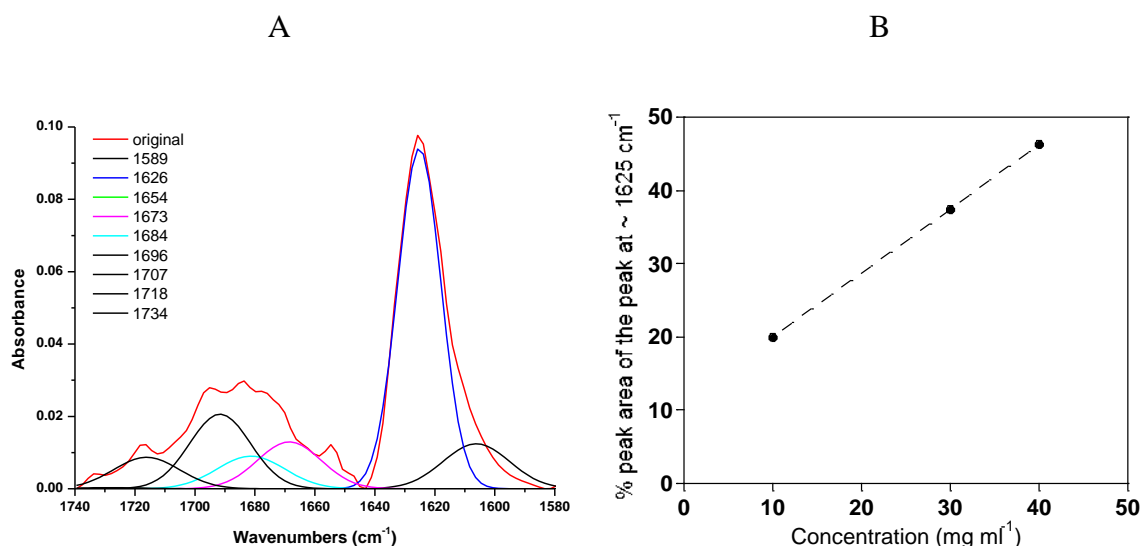


Figure 3.4 (A) Peak fitted FTIR spectra of FEFEFKFK peptide at concentration of 40 mg ml^{-1} at pH 2.8. (B) The percentage peak area of the peak at $\sim 1625 \text{ cm}^{-1}$ in the amide I region area as a function of peptide concentration.

In the amide I region, the positions of IR vibrations depend on the secondary structures of

peptides. Two characteristic peaks of the anti-parallel β -sheet peak were observed for each tested sample. These were the strong sharp peaks at $\sim 1625\text{ cm}^{-1}$ and the weak peaks at $\sim 1684\text{ cm}^{-1}$.^{9, 10} The peak at $\sim 1673\text{ cm}^{-1}$ was identified as residual TFA from the peptide synthesis.¹¹ The proportion of β -sheet structure in all the secondary structures adopted by the peptide was estimated at

$$\frac{A_{\beta}}{A_{all}} \times 100\%$$

Equation 3.1

where A_{β} is the area of the peak at $\sim 1625\text{ cm}^{-1}$ and A_{all} is the sum of the area of all the peaks in the amide I region. As presented in Figure 3.4 B, the % area of β -sheet peak increased with increasing peptide concentrations.

TEM was used to visualise the formation of peptide fibres.

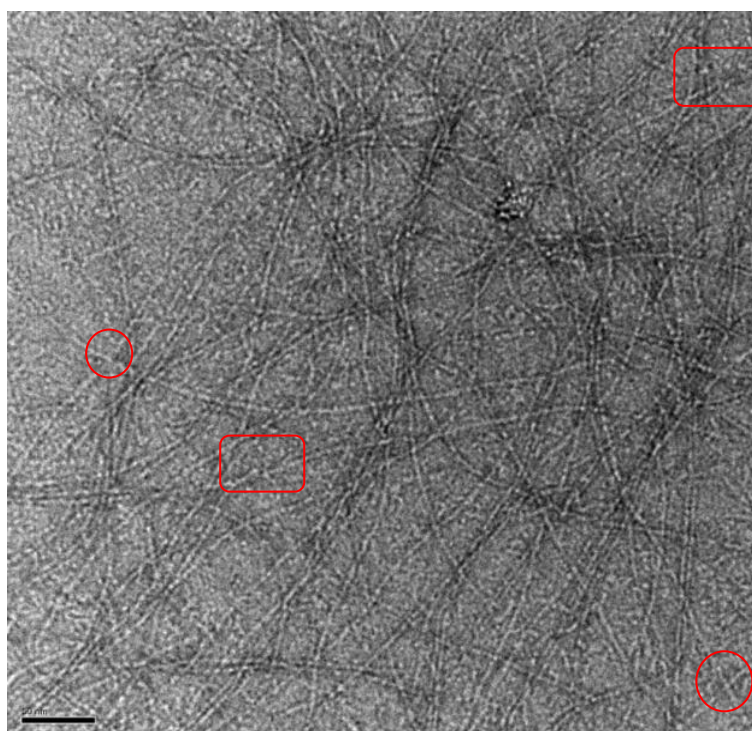


Figure 3.5 TEM micrographs of the diluted FEFKFK peptide hydrogel at pH 2.8. Boxes were used to indicate the presence of branched fibres; while circles were used to point out the entanglement of the fibres. The scale bar represents 50 nm.

The image analysis showed that the fibres had an average diameter of 3.5 nm. This confirms the previously proposed model, which concluded that the fully stretched length of the peptide backbone was approximately 4 nm.⁵ Both the branched fibres (boxes) and the entanglement of fibres (circles) were observed on the TEM images. Due to the drying

process during the sample preparation, all the peptide fibres were flattened and accumulated on the surface of the carbon grid. Although this observation is not conclusive evidence, it highlights the possible ways of the fibre association.

Both the TEM and FTIR results confirmed the previous studies on FEFKFK peptide.^{3, 12} This peptide can self-assemble in aqueous solution and form fibres with an anti-parallel β -sheet secondary structure. Currently, most of the previous research focused on the peptide solution, where the system is dilute enough to help gain the detailed structure information of peptide fibres and allow understanding of the self-assembling process. Although it is proved that FEFKFK peptide can form hydrogels in aqueous solutions, the gelation process and the hydrogel properties have not been previously fully investigated. Therefore this project will focus on the studies of the gelation process and the hydrogel properties of FEFKFK peptide.

3.1.2 Gel properties

To help understanding the formation of the fibrillar network and gelation process, the fibrillar model developed by Guenet was studied.¹³ In the Guenet fibrillar model, single fibril form at very low concentration, and connect to each other when the concentration increases. Some microgels of finite size form at concentrations just below the critical gelation concentration (C_{gel}), and an infinite network forms when the C_{gel} is reached. This will affect the mesh size and network elasticity as the concentration increases. When the concentration increases, the mesh size is expected to decrease, but the network structure is independent from a local point of view.

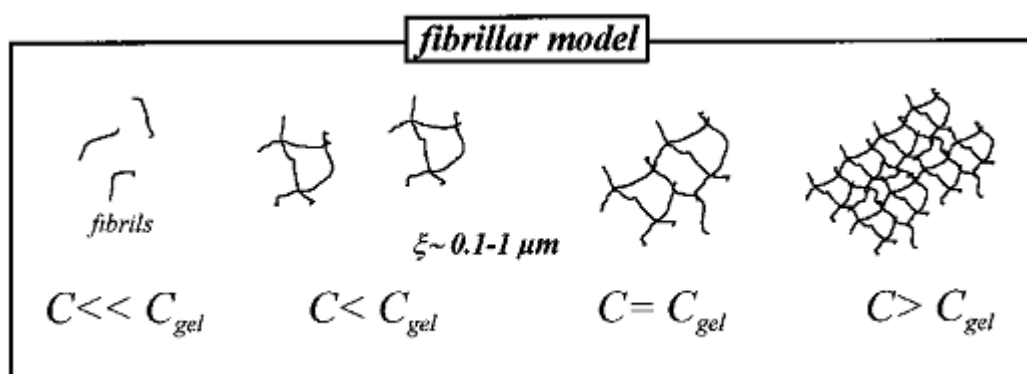


Figure 3.6 Schematic presentation of the fibrillar model suggested by Guenet. C_{gel} stands for the critical gelation concentration. ξ stands for the mesh size.¹³

In this project, the physical forms of the peptide and water mixtures were determined by

turning the sample vials upside down. The samples were called gels if they were self-supporting as shown in Figure 3.7 B. If the samples flowed to the bottom of the vials, they were called solutions. If the samples were self-supporting without any disturbance but flowed slowly to the bottom of the vials after a gentle pat on the vials, they were considered either a weak gel or a viscous liquid. The phase diagram of FEFEFKFK peptide was mapped out in this way. The physical forms of peptide and water mixtures at different temperatures were recorded. As shown in Figure 3.7 A, temperature is plotted against the peptide concentration. The dark grey circles represent the gel form; the light grey circles represent a weak gel or a viscous liquid, and the empty circles represent the liquid form.

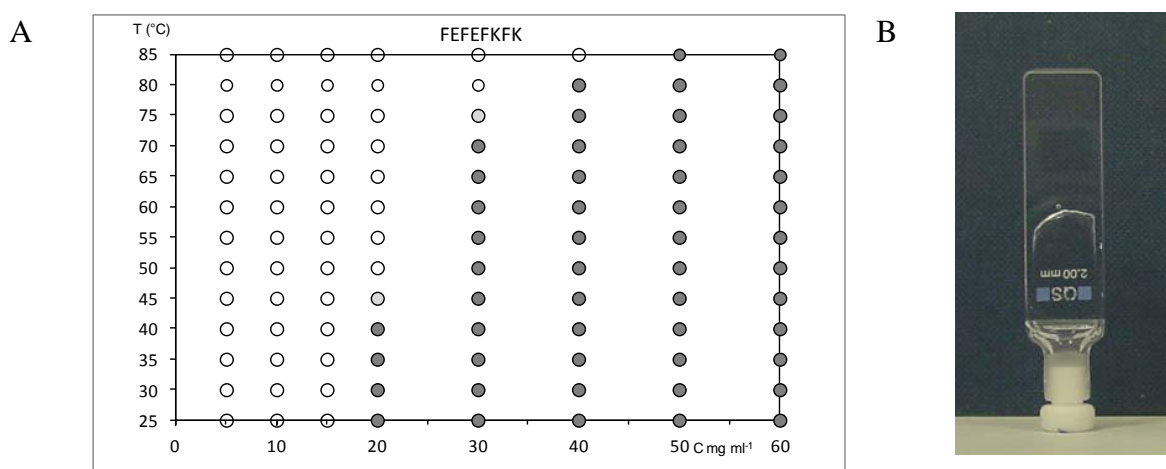


Figure 3.7 The phase diagram of FEFEFKFK peptide, where samples in the form of solution (empty circle), weak gel/viscous liquid (light filled circle) and gel (dark filled circle) were recorded. All samples were prepared at pH 2.8 (A), FEEFFKFK at 40 mg ml⁻¹ forms a self-supporting transparent hydrogel at pH 2.8 (B).

The C_{gel} of FEFEFKFK peptide at 25 °C is between 15 to 20 mg ml⁻¹. The area between the grey and white circles indicates the range where C_{gel} falls into. The C_{gel} increases when the temperature rises. For the peptide hydrogels at a fixed concentration, when temperature rises, the gels begin to melt. All the gels at concentrations above 20 mg ml⁻¹ were thermally stable at physiological temperature 37 °C. The gels with concentration higher than 50 mg ml⁻¹ were thermally stable up to 85 °C. At all concentrations, the melted gels could reform when cooled down again. This thermal reversible behaviour indicates that our peptide hydrogels are physically cross-linked. The hydrogel formation can be originated from a physically entangled network structure.

In the system studied in this project, the fibres correspond to the peptide rich phase and the solvent is the peptide poor phase. Under the influence of temperature, the system will undergo a transition between a liquid and a gel. For a constant concentration, the

temperature at the transition point can be called the critical gelation temperature (T_{gel}). As shown in Figure 3.7 A, the T_{gel} increased with increasing peptide concentrations. According to the Guenet fibrillar model, this was caused by the increase of the fraction of disordered materials at higher temperature, and the increase in C_{gel} when temperature rises could be attributed to this.

In the FTIR studies, fibres with the anti-parallel β -sheet structure were found in both the peptide solutions (10 mg ml^{-1}) and the peptide gels (30 mg ml^{-1} and 40 mg ml^{-1}). The existence of β -sheet fibres below the C_{gel} is in agreement with the Guenet model.

Such theory could be also applied to the TEM study of FEFEFKFK peptide. The cross-linked network structure was virtually proved using TEM as seen in Figure 3.5 . The TEM studies over a range of concentrations also confirmed the local network morphology remain unchanged.¹² However, due to the drying process during the sample preparation, microscopy cannot provide the fibre or mesh sizes of the network in the hydrated state. Small angle scattering (SAS) techniques were used to overcome this issue.

Both SANS and SAXS were used to study the structure of the peptide hydrogels. The absolute scattering intensity (I_A) was plotted against q value as well as the normalized scattering intensity (I_N) against q in the logarithmic scale for different concentrations. As seen in Figure 3.8, the scattering intensity increases with increasing gel concentration. A maximum or shoulder on the scattering curve appears in the 10 mg ml^{-1} to 50 mg ml^{-1} concentration range which is also known as the structure peak. The presence of the structure peaks indicates that the inter-particle effect was not negligible, which suggests the matters studied were too dense to draw information regarding single fibres. The scattering curve of sample at 5 mg ml^{-1} does not show any maximum, and the sample at 5 mg ml^{-1} is the only sample dilute enough to study the structure information of peptide fibres. The previous study on the fibre structure was also taken at this peptide concentration.³ However, the structure peaks can provide approximate geometrical information about the hydrogels.

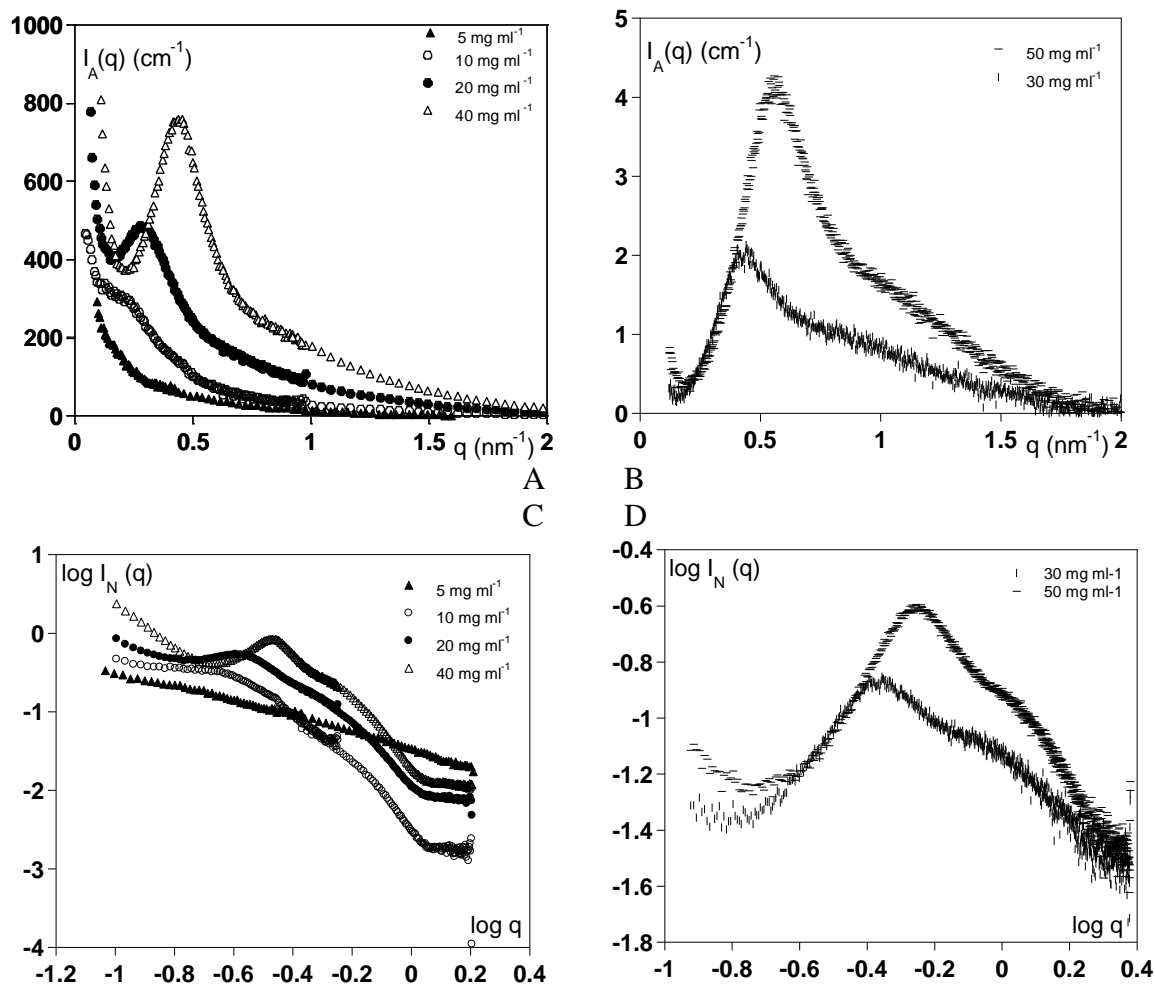


Figure 3.8 (A) SANS spectra of the FEFEFKFK peptide. The plot of I_A against q at 40 mg ml^{-1} (Δ), 20 mg ml^{-1} (\bullet) 10 mg ml^{-1} (\circ) and 5 mg ml^{-1} (\blacktriangle); (B) SAXS spectra of FEFEFKFK peptide. Plot of I_A against q at 30 mg ml^{-1} ($|$) and 50 mg ml^{-1} ($-$); (C) SANS spectra of the FEFEFKFK peptide. The plot of I_N against q in the logarithmic scale at 40 mg ml^{-1} (Δ), 20 mg ml^{-1} (\bullet) 10 mg ml^{-1} (\circ) and 5 mg ml^{-1} (\blacktriangle); (D) SAXS spectra of FEFEFKFK peptide. The plot of I_N against q in the logarithmic scale at 30 mg ml^{-1} ($|$) and 50 mg ml^{-1} ($-$). All the experiments were taken at pH 2.8.

Single structure peaks similar to those presented here were commonly detected when using SAS techniques to analyse the structure of fibrillar networks.¹⁴ The detection of the network structure at 10 mg ml^{-1} (below C_{gel}) indicates a fibrous network formed before gelation occurred, which is in agreement with the Guenet model. The Bragg's law can be applied to determine the approximate value of the characteristic distance of the network (d) from the q^* value (q value at the maximum or bump position on the scattering curve):¹⁴⁻¹⁶

$$d = \frac{2\pi}{q^*}$$

Equation 3.2

where the value of d was estimated as an approximate gel mesh size.^{3, 5, 15}

By combining the results gained by SANS and SAXS, the q^* value at the maximum or shoulder position on the scattering curve and the value of the corresponding gel mesh size d were measured and presented in Figure 3.9.

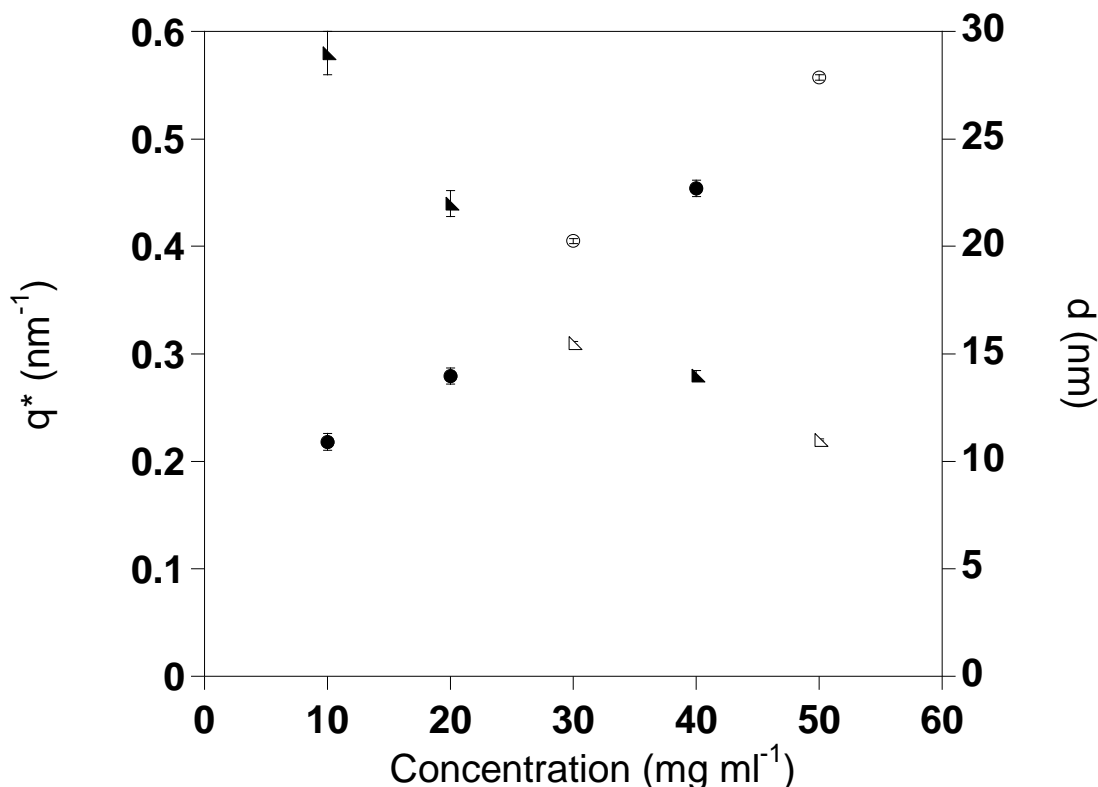


Figure 3.9 Plot of the q^* value (circle) and the mesh size d (triangle) against peptide concentration from SANS (solid) and SAXS (empty) scattering curves. Error bars are the standard deviation. All the experiments were taken at pH 2.8.

Although the q^* value and mesh size d were obtained by two techniques, the same trend against sample concentration was observed. The data obtained by two techniques were in agreement with each other. The q^* value increased from 0.22 to 0.56 nm⁻¹ when peptide concentrations increased from 10 to 50 mg ml⁻¹, while mesh size d decreased from 29 to 11 nm with increasing concentrations. This observation confirmed the interpretation of the meaning of d and is in agreement with the fibrillar model. The fibre density was expected to increase with increasing peptide concentrations; therefore a decrease in mesh size was anticipated. The value of d did not only match the magnitude of the mesh size observed under TEM in the previous studies, but also matched the value of size d previously reported.⁵ The values of mesh size obtained from either TEM or SAS were estimations.

So far in this section, both the morphology and the structure of the fibres and the network were studied. FEFEFKFK peptide could self-assemble in aqueous solutions and form fibres with the anti parallel β -sheet secondary structures. The fibre density increased with increasing peptide concentration. When the peptide concentration reached the critical gelation concentration, the transparent hydrogels would form with densely crosslinked fibrous network structure.

3.1.3 Rheological properties of peptide hydrogels

The rheological properties of this peptide need to be studied as it is an important character of hydrogels. The study of the peptide hydrogel network and structure may also help in understanding the deformation mechanism and mechanical properties of peptide hydrogel during the rheological studies. The rheological tests of FEFEFKFK peptide hydrogels under the different parameters are presented in this section.

3.1.3.1 Amplitude sweep

The linear viscoelastic region (LVR) is the region where G' and G'' are independent from the strain or stress applied; most rheological studies need to be conducted in this region. The first step in this rheological study is to determine the LVR of the FEFEFKFK peptide gels, and an amplitude sweep is usually performed for this purpose.

Figure 3.10 shows the strain sweep curves of the FEFEFKFK peptide hydrogels at different concentrations. At the low strain range (below 1 %), the elastic modulus G' , viscous modulus G'' and $\tan\delta$ are independent or slightly dependant from the strain. This low strain range is the LVR. The gel can be classified tougher, the greater the LVR can extend to the higher strain range. Otherwise, the gel would be deemed brittle.¹⁷ In the LVR, G' is higher than G'' , $\tan\delta < 1$. When G' dominates the LVR, the matter studied can be referred to as a gel with a solid-like behaviour.

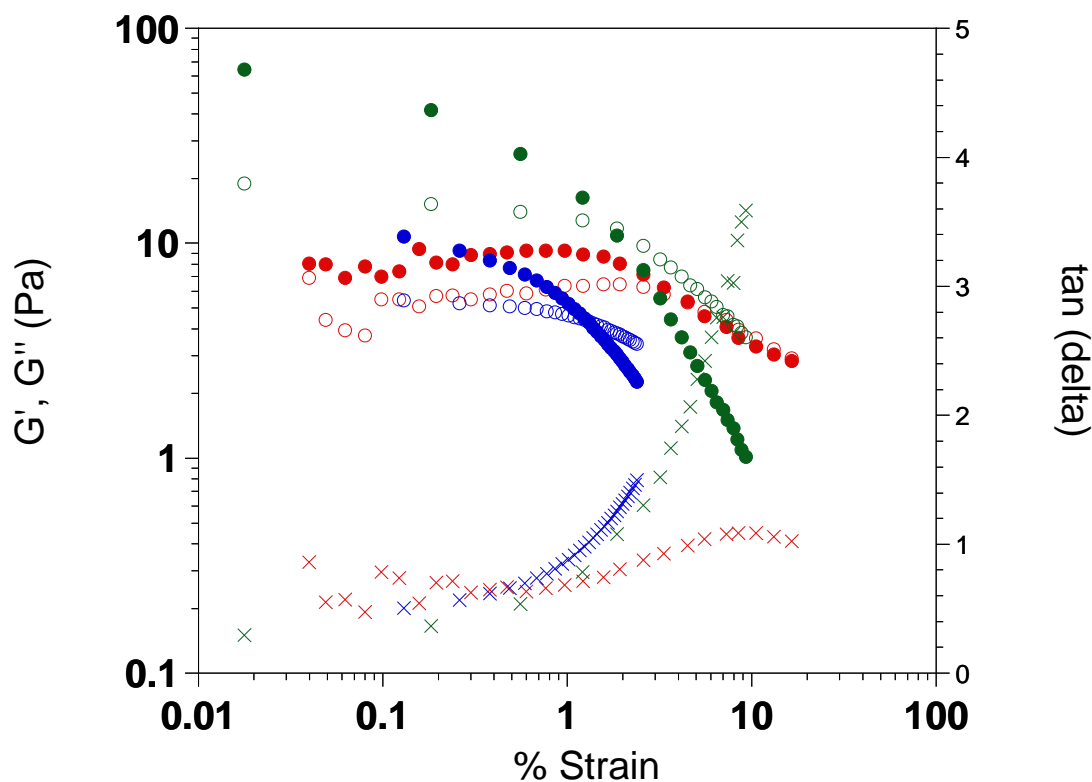


Figure 3.10 Plot of elastic modulus (G' , ●), viscous modulus (G'' , ○) and $\tan\delta$ (×) of FEFEFKFK peptide at 20 (red), 30 (blue) and 40 (green) mg ml^{-1} as a function of strain from 0.1 % to 100 % at 1 Hz at 20 °C in the logarithmic scale. All the experiments were taken at pH 2.8.

As peptide concentration increases, the value of $\tan\delta$ decreases, which means peptide gels at higher concentration show more solid-like behaviour. As shown in Figure 3.10, the values of G' in the LVR of all samples are below 100 Pa. With such small modulus, these FEFEFKFK gels are considered as weak gels. As the gel concentration increases, values of both G' and G'' increase, which indicates that stronger gels form at a higher gel concentration. When the strain is above 2 %, both G' and G'' begin to decrease; however, G' decreases faster than G'' resulting in a crossing point of the two data sets. This crossing point is called the breaking point of the gels. The value of $\tan\delta$ is 1 at this point, where $G'=G''$. The strain at this point is called the yield strain. No concentration dependence of the yield strain was observed for this peptide, and the gel breaks when the strain is higher than the yield strain. G'' dominates the higher strain range, which suggests the gel behaves more liquid-like after the breakage.

3.1.3.2 Frequency sweep

The strength of the peptide hydrogels were studied with frequency sweeps, which monitored the response of the hydrogels to an increasing frequency at 1 % strain at room

temperature.

Frequency sweeps of FEFEFKFK peptides at a range of concentrations above the C_{gel} are presented in Figure 3.11. G' is higher than G'' at all the concentrations in the frequency range studied confirming the solid-like behaviour observed previously with the amplitude sweeps. The value of $\tan\delta < 1$ in the frequency range also confirmed the testing samples are in the gel form. In the lower frequency range below 10 Hz, both G' and G'' of the hydrogels are independent from the frequency of concentrations above 30 $mg\ ml^{-1}$. For the gels at 25 and 30 $mg\ ml^{-1}$, both G' and G'' have weak dependence on frequency.

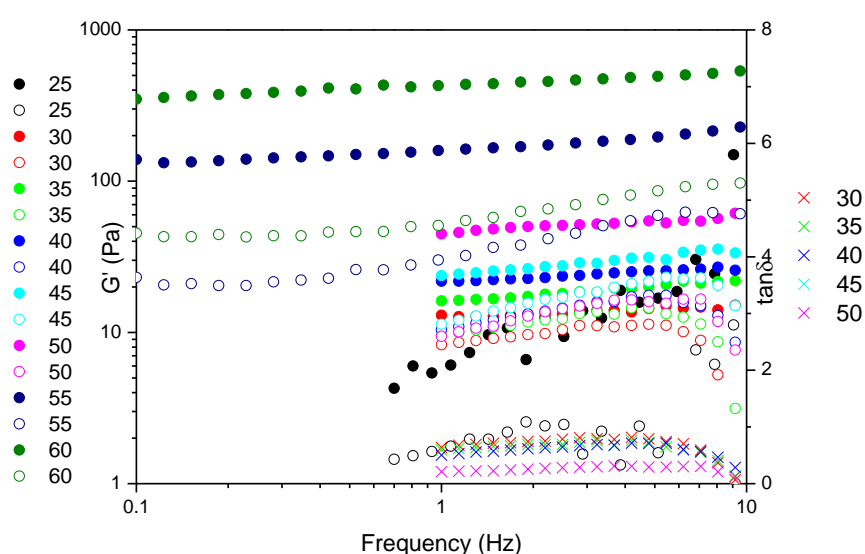


Figure 3.11 Plot of elastic modulus (G' , solid), viscous modulus (G'' , empty) and $\tan\delta$ (\times) of FEFEFKFK peptide at 25 (black), 30 (red), 35 (green), 40 (blue), 45 (cyan), 50 (purple), 55 (navy) and 60 $mg\ ml^{-1}$ (olive) as a function of frequency from 0.1 to 10 Hz at 1 % strain at 20 °C in the logarithmic scale. All the experiments were taken at pH 2.8.

The independence and very weak dependence on frequency in the lower range indicates a network possessing a long relaxation time and relatively permanent junctions.¹⁵ This rheological behaviour was studied by Ferry.¹⁸ In Ferry's theory, the plot of shear modulus as a function of time or frequency can show characteristic shapes for different polymeric systems. Eight polymeric systems were chosen for the illustration of different molecular responses: 1) a dilute polymer solution; 2) an amorphous polymer of low molecular weight; 3) an amorphous polymer of high molecular weight; 4) an amorphous polymer of high molecular weight with long side groups; 5) an amorphous polymer of high molecular weight below its glass transition temperature; 6) a lightly cross-linked amorphous polymer; 7) a very lightly cross-linked amorphous polymer and 8) a highly crystalline polymer. The

independence and very weak dependence on frequency in the lower range was often observed on system No.7. In the example given by Ferry, the number-average molecular weight of the polymer was only 4 times higher than the molecular weight between cross-linking points, but 30 times higher than the molecular weight between coupling entanglements. This demonstrates that on average, there were only a few cross-linked points on every initial molecule, while the branched structures were extensively entangled.¹⁸ For the FEFEFKFK peptide system, densely cross-linked fibres were observed by TEM. Most of the junctions were caused by fibre entanglements while some were caused by branching fibres.⁴ This network structure was similar to what is defined as a very lightly cross-linked amorphous polymer system.

To compare with the characteristic pattern in Ferry's theory, the stress relaxation modulus ($G(t)$) of FEFEFKFK peptide was calculated by the method of Ninomiya and Ferry:¹⁸

$$G(t) = G'(\omega) - 0.4G''(0.40\omega) + 0.014G''(10\omega)$$

Equation 3.3

where ω is the frequency and $\omega = t^{-1}$.¹⁹ $G(t)$ was plotted against t in Figure 3.12.

$G(t)$ at all studied concentrations show a similar trend with increasing t . In the short time range, $G(t)$ is decreasing and then flattens with increasing t . This range is called the transition zone and the value of $G(t)$ at the beginning of the plateau is called the plateau shear modulus (G_N). Since the relaxation time of the system was long, when in the transition zone, the entanglement points could be seen as fixed. Relative motions could only happen between network junctions instead of configuration rearrangements in the long distance range.

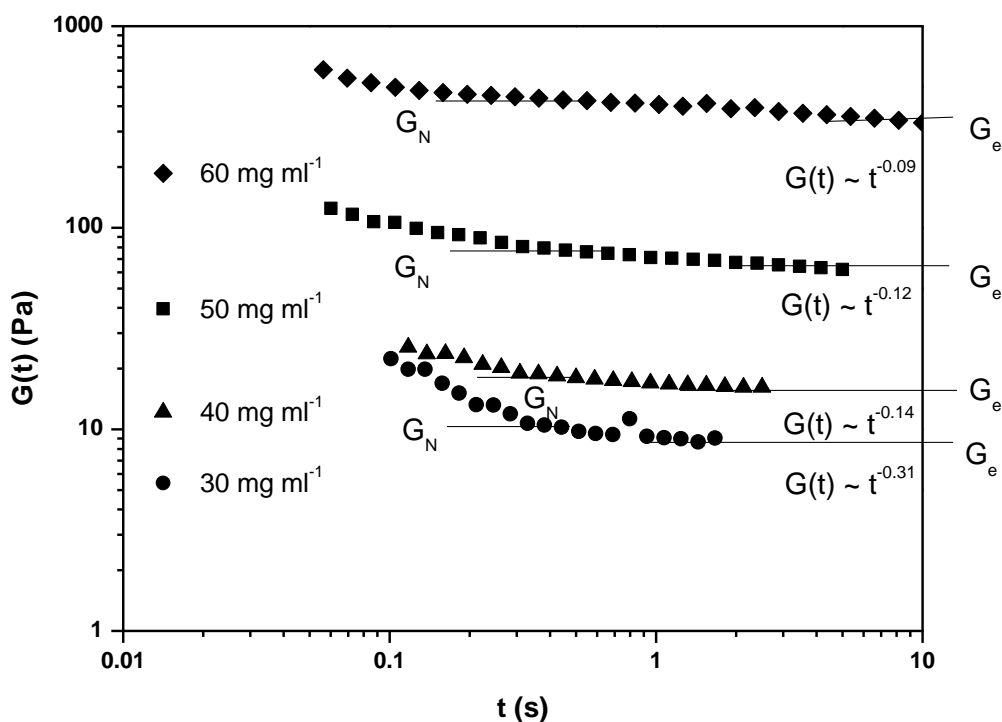


Figure 3.12 Plot of the stress relaxation modulus $G(t)$ as a function of t for peptide at concentrations of 30, 40, 50 and 60 mg ml^{-1} at 20 $^{\circ}\text{C}$ in the logarithmic scale. All the experiments were taken at pH 2.8. The value of $G(t)$ at the beginning of the plateau is called the plateau shear modulus (G_N). In the long time range, $G(t)$ was approaching the equilibrium state, which is called the equilibrium shear modulus (G_e).

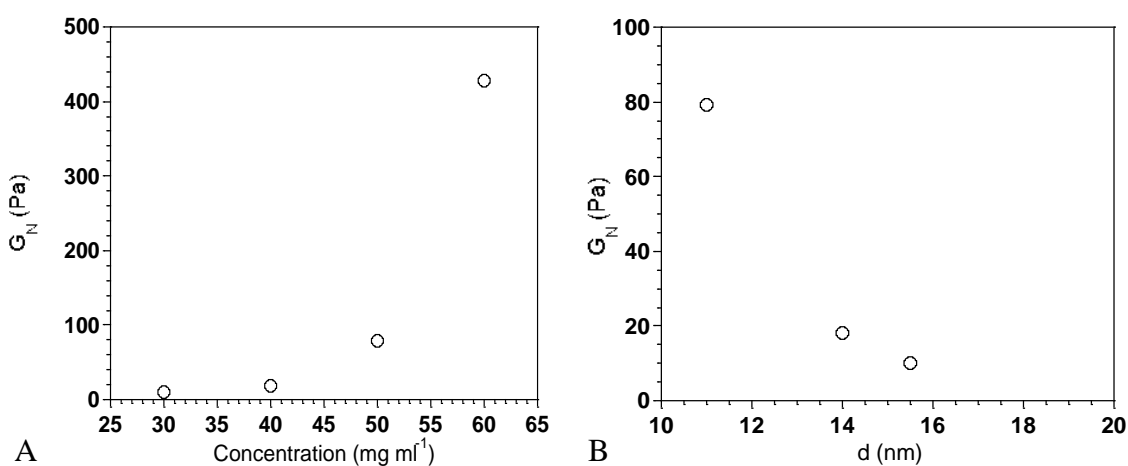


Figure 3.13 A) The plot of G_N against gel concentration; B) The plot of G_N against gel mesh size d . All the experiments were taken at pH 2.8.

Using the data extracted from Figure 3.12, G_N was plotted as a function of gel concentration in Figure 3.13 A. It can be seen that G_N increases with the increasing gel concentration. G_N is roughly inversely proportional to the distance between the entanglement points. As the distance between entanglement points can be considered as

the mesh size, using the value of the mesh size observed by SAS (Figure 3.9), G_N was plotted against the gel mesh size d (Figure 3.13 B). It can be seen from Figure 3.13 that the gel mesh size decreases with increasing gel concentrations. This is in agreement with the SAS results and the Guenet fibrillar model discussed in Section 3.1.2.¹³ The gel mechanical strength is related to the gel network structure and gel concentration.

The plateau region corresponds to the slow relaxation zone of gel. In this long time range, $G(t)$ was approaching the equilibrium state, which is known as the equilibrium shear modulus (G_e). The slight decrease of $G(t)$ from G_N to G_e in the slow relaxation zone could be attributed to the slippage of entanglements on the fibres with loose ends, enabling the long distance configuration to be rearranged.¹⁸

It was observed that the relationship between $G(t)$ and t followed a power law with an exponent of 0.09 to 0.31 for concentrations of 60 mg ml⁻¹ to 30 mg ml⁻¹. These exponents were found to be close to the exponents of the solvent-induced synthetic polymer gels rather than the crystallization-induced synthetic polymer gels or chemically cross-linked polymer gels.¹⁹ This indicated the network junctions of the peptide hydrogels were more likely to be physically entangled, and can be broken and possibly reformed under stress.

From Figure 3.11, it can also be seen that as the gel concentration increases, both G' and G'' increase while $\tan\delta$ decreases with increasing gel concentrations. The relationship between G' , G'' and the gel concentration (C) are presented and discussed below.

The average values of G' and G'' in the frequency independent region were calculated and used to represent the viscoelastic properties of the gel. As seen in Figure 3.14, G' increases with the increasing gel concentrations, which suggests that the gels were stronger at higher concentrations. G'' also increases with the increasing gel concentrations but at a slower rate. The difference between G' and G'' increased from less than 2 to 7 fold at the highest gel concentration. This indicates a stronger gel and a more solid-like behaviour at higher gel concentrations.

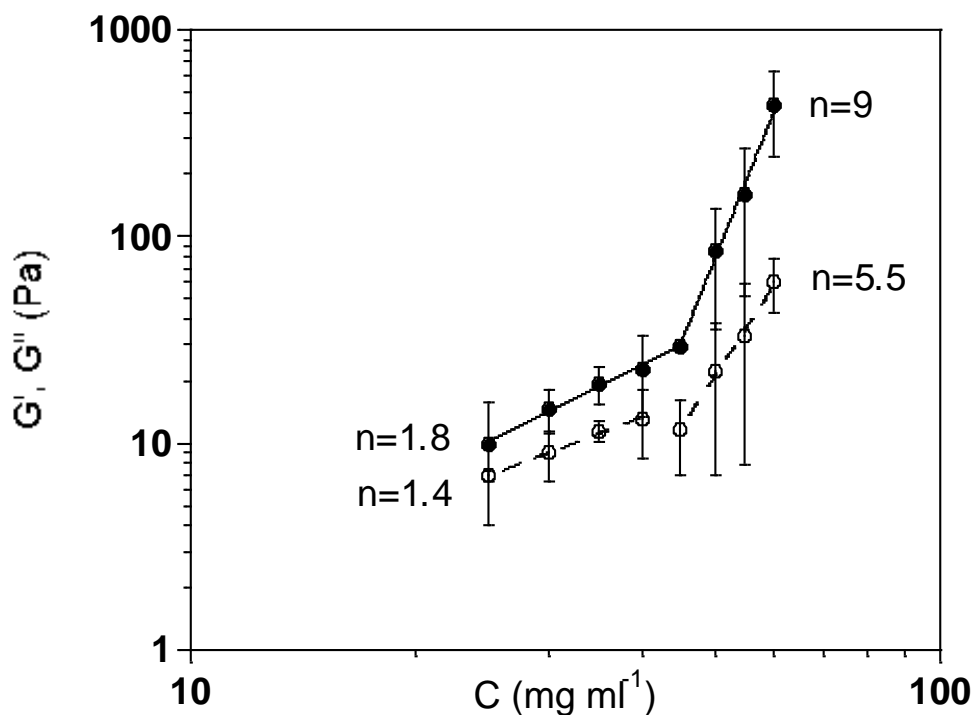


Figure 3.14 Plot of elastic modulus (G' , ●) and viscous modulus (G'' , ○) of FEFEFKFK peptide as a function of concentration (C) in the logarithm scale. n represents the slope of the fitted line. The solid line (—) represents a fitting of G' against concentration. The dash line (---) represents a fitting of G'' against concentration. All the experiments were taken at pH 2.8.

The values of G' ranging from 10 Pa to 450 Pa are on the same order of magnitude of other biopolymer hydrogels such as actin,²⁰ fibrin²¹ and collagen.²² The values of G' and the concentration of peptide hydrogels followed the power law ($G' \approx C^n$); however, two different slopes (exponent n) were observed. $n = 1.8$ was obtained for the concentrations below 45 mg ml^{-1} and $n = 9$ for the concentrations above. Two different slopes were also observed by data fitting of G'' . A sharp increase from 1.4 to 5.5 of the slope from fitted G'' data was also noticed for concentrations above 45 mg ml^{-1} .

As introduced in Chapter 1, Jones and Marques's theory²³ was successfully applied to several thermo-reversible gels by Guenet.¹³ When applied to the FEFEFKFK peptide system, for the rod-like structures such as the FEFEFKFK fibres, $D_F = 1$, which leads to $G_r \approx C^2$, while $G_e \approx C^{1.5}$.

In the case presented here, the slope in low concentration range is 1.8, which is between 1.5 and 2, and indicates an intermediate situation. The similar exponents were also observed in other thermoreversible gel systems including PMMA, agarose and carrageenans.¹⁹ The Jones and Marques theory was developed to explain the rheological

behaviours of thin and rigid fibres in chemically cross-linked gels. This could be the reason why the theory can also be applied to thermal reversible gels. The other condition of the theory is that the mesh size of the fibrillar network is larger than the cross sections of the fibres and network junctions. As discussed in the previous sections, a roughly estimated mesh size of the FEFKFK peptide at 50 mg ml^{-1} was 11 nm, while the average fibre diameter was around 4 nm. This could be the reason why an exponent of 9 observed in the high concentration range did not fit in the theory, and where the Jones and Marques theory might not be applicable. Such high exponent has not been reported for any gel system, and it does not fit into known models. However, if discussed under the frame of Jones and Marques theory, a higher fractal dimension will lead to a higher exponent. A higher fractal dimension means a more compacted structure between network junctions. As the concentration reached 50 mg ml^{-1} , the distance between network junctions was about 3 times longer compared with the average diameter of fibres. At a lower gel concentration, the distance between network junctions could be 7 times longer than the average diameter of fibres. The denser network structure at 50 mg ml^{-1} could be the reason for the dramatic increase of gel strength. However, such dense network can also lead to another possibility, and according to the fibrillar model,¹³ microgels form before the C_{gel} . When peptide samples were prepared in oven, the gels at the concentrations lower than 40 mg ml^{-1} including 40 mg ml^{-1} , could be melted (Figure 3.7). The fibres were evenly distributed in the whole system. However, when the gel concentration increased to 50 mg ml^{-1} , the gels could not be melted in the oven. Therefore, the gelation could occur locally once the peptide was mixed with distilled water, but the temperature was not high enough to allow the peptide fibres to be well distributed in the whole system. Although transparent gels were obtained, higher peptide concentration could exist locally within the gels. The sites with higher fibre density could act like reinforcements to other parts of the gel network, resulting in a dramatic increase of the gel network strength.

3.1.3.3 Temperature sweep

In Equation 1.3, the term kT indicated the elasticity of a network formed by freely hinged junctions which would be affected by the change in temperatures. Since FEFKFK peptide system could be in an intermediate state between freely hinged junctions and frozen junctions, it was interesting to investigate the rheological behaviour of FEFKFK hydrogels under the influence of temperature. The experiments were undertaken in the LVR at 1 % strain and the frequency was fixed at 1 Hz.

As shown in Figure 3.15 A, B and C, FEFEFKFK peptide at 25, 30 and 40 mg ml⁻¹ was heated up from 25 °C to 85 °C at 5 °C min⁻¹ and then cooled back to 25 °C at the same rate for one cycle. The cycle was repeated twice.

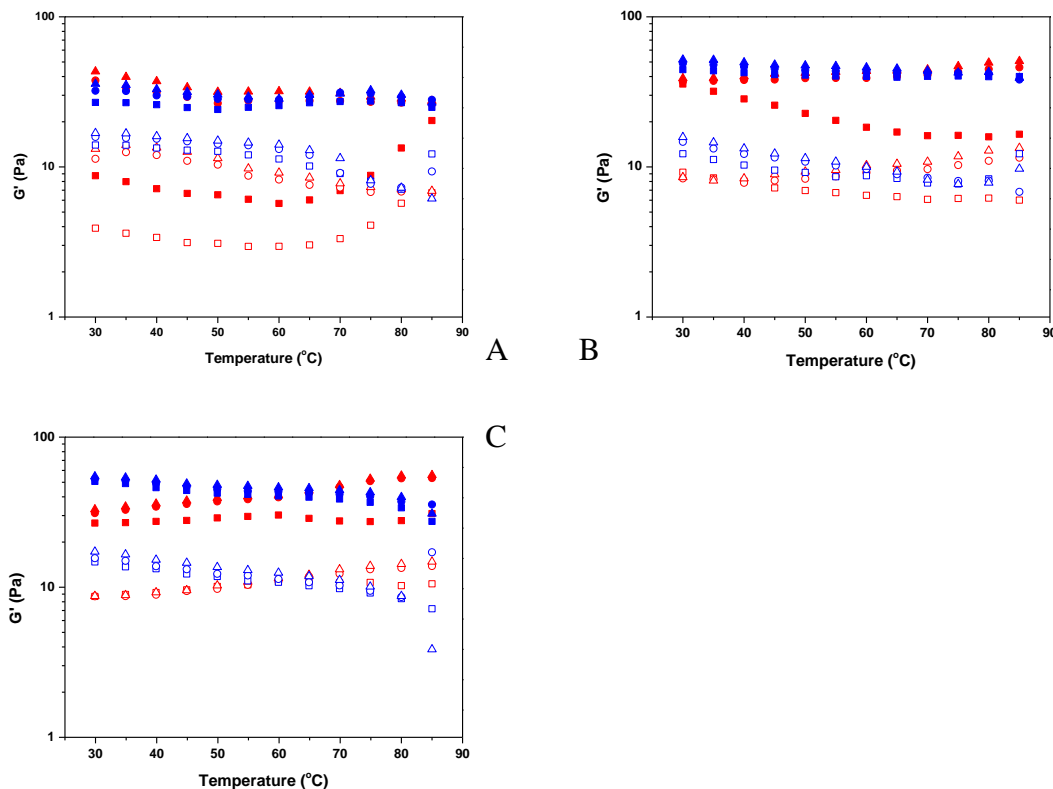


Figure 3.15 The plot of elastic modulus (G' , solid) and viscous modulus (G'' , empty) of the FEFEFKFK peptide at 25 (A), 30 (B) and 40 (C) mg ml⁻¹ as a function of temperature in the logarithmic scale. All the experiments were taken at pH 2.8. G' was marked red when the gels were heated up and blue when the gels were cooled down. The squares (■/□) represent the 1st heating and cooling cycle; the circles (●/○) represent the 2nd heating and cooling cycle; the triangles (▲/△) represent the 3rd heating and cooling cycle.

During the whole temperature sweep, all G' is higher than G'' which indicates a gel form of the sample. This is different from what was observed when mapping the phase diagram. This is because when determining a gel form by the tilting method, depending on the vials where samples are in, the weak gels could be considered as liquids. To look into each step of the temperature sweep, the gels at 25 mg ml⁻¹ is discussed in more details. During the first heating step, G' of 25 mg ml⁻¹ slowly decreased with increasing temperature until 65 °C, and G' then began to increase with increasing temperature. The G' value at 85 °C at the end of the 1st heating was greater than the G' value of the original gel. During the 1st cooling step, G' was independent from temperature. It should be noticed that the 1st heating step in this experiment was actually the second time the samples were heated, as

the real 1st heating was taken place during the sample preparation. G' remained nearly constant during the next two heating and cooling cycles, with only a small increase after each cycle.

The rheological behaviour reflects the conformation rearrangements of the fibres forming the network. From the previous discussion, we know that at 1 Hz, long distance conformation can be rearranged. The high temperature has the same effect on the conformation rearrangements as long relaxation time. During the 1st heating step, when the temperatures increased, not only the segments within the entanglement points could rearrange, but also the entanglement points linked to loose ends could slip. This caused the elasticity of the network to reduce slightly. From the phase diagram of the FEFEFKFK peptide (Figure 3.7), the critical gelation temperature at 25 mg ml^{-1} was approximately 65°C . This was also the temperature at which G' began to increase. Above 65°C , the gels could turn to viscous liquids, with the constant oscillation shear causing conformation rearrangements of all fibres. The fibres were oriented along the direction of the shear force, which led to a higher elasticity of the network. During the 1st cooling process, higher orientation of the fibres was maintained, corresponding to the constant higher G' value. As there was no further variation of G' , the increase in the network elasticity was permanent. During the following two heating and cooling cycles, more fibres could be oriented causing small increases in the G' value. The small G' value increase could be due to the slight evaporation of the solvent.

3.1.3.4 Time sweep (recovery)

It was postulated in the previous sections that the entanglement junctions of the network can be destroyed and reformed under shear stress. It is known that the gels can be broken under high shear stress, and in most biomedical applications, the gels will be deformed or broken during the transfer. It would be interesting to investigate whether the network structure of the gels could reform after a deformation or after being broken.

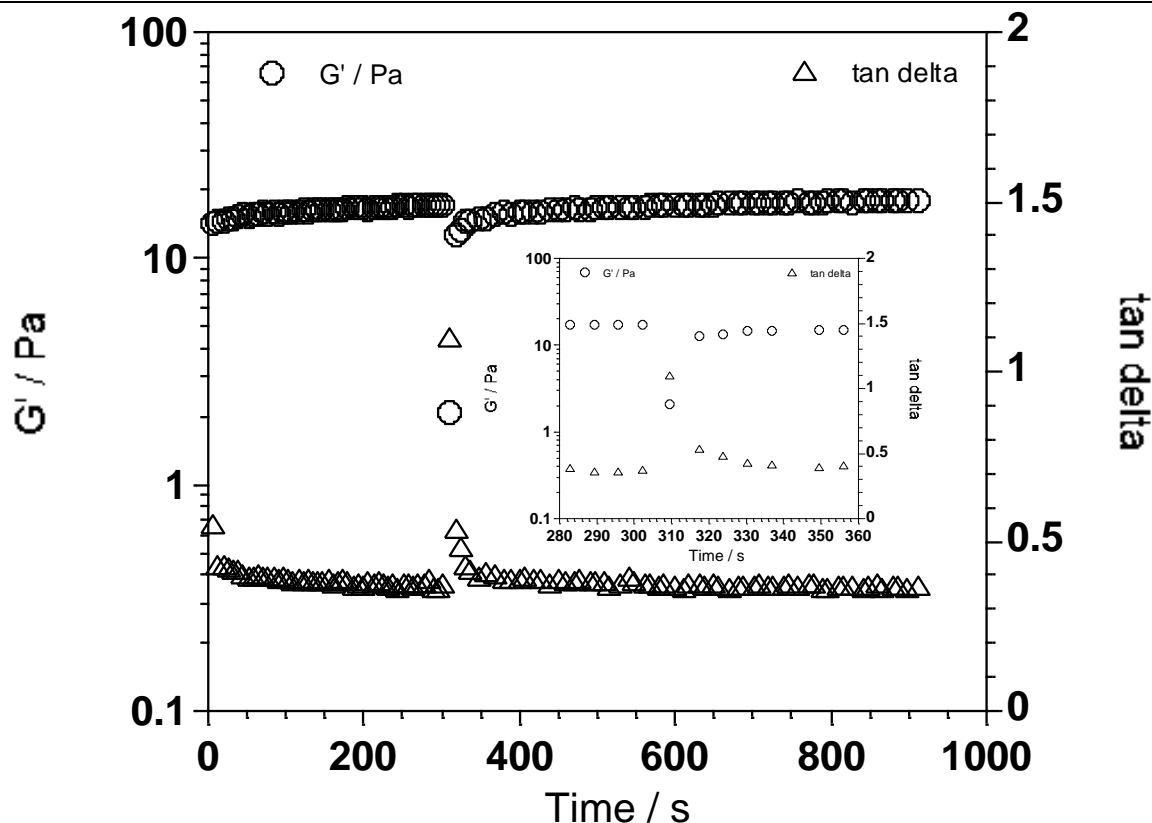


Figure 3.16 Plot of elastic modulus (G' , \circ) of FEFEFKFK peptide at 25 mg ml^{-1} as a function of time at 20°C at pH 2.8 in logarithmic scale. The inset is the magnified form of data from 280 to 360 seconds to give a closer look of the initial recovery process.

The recovery tests were taken at 1 % strain and 1 Hz as a function of time. The original mechanical property of the gel was recorded first. Then a 150 % strain was applied for 5 seconds to break the gel, which was confirmed by a sharp decrease of G' (where $G' < G''$) and $\tan\delta > 1$. A 150 % strain was chosen because it was larger than the yield strain ensuring gel breakage. The recovery process was monitored after the breakage.

FEFEFKFK peptides at different concentrations were tested. As can be seen in Figure 3.16, for the hydrogels at 25 mg ml^{-1} , the first plateau at early time points marked the original mechanical strength of the hydrogel. The sudden drop of G' was due to the breakage of the gel. The rebound of the mechanical strength was observed in less than 10 seconds after the applied strain was reverted back from 150 % to 1 %. A slow and steady recovery process was recorded after the initial 75% recovery. The gel recovered back to its original strength in less than 10 minutes. As discussed in the fibrillar model, the peptide gel network formed by microgel linkage before the critical gelation concentrations. The physically linked gel network could be broken by melting or applying the shear force, which was suggested to be similar to the reverse of the gelation process. Therefore the recovery process of the

peptide hydrogel after being melted or broken by shear force was postulated to be similar to that of the gelation process when the gel fractures into the smaller gel pieces and then reconnects through the physical entanglements. A thorough research was conducted on a similar peptide gel system by Pochan's group studying the mechanism of self-healing property in self-assembly peptide systems. Their study indicated that the gel network broke into large (>200 nm) hydrogel domains, which were percolated immediately resulting in the immediate reforming of the hydrogel during the recovery process.²⁴ A similar process could have been adopted by the FEFEFKFK hydrogel.

The recovery process of the peptide hydrogels proved that the gels were physically cross-linked, and the network junctions could reform after being destroyed. This recovery property provided the peptide hydrogel the possibility to be used as injectable materials.

3.2 pH and ionic strength effect on FEFEFKFK gel properties

3.2.1 Introduction

In Section 3.1, the gelation properties of the FEFEFKFK peptide were discussed. The gels showed a potential to be used as tissue culture scaffolds. In the previous section, all the samples were prepared in distilled water without any modification to the system. However, the tissue culture environment *in vitro* is more complicated. Tissue culture media are commonly used to mimic the body fluid environment and to provide nutrients for cells in the studies of tissue culture scaffolds. They usually contain various organic and inorganic salts, among which NaCl has much higher concentration than all the other salts;²⁵ resulting in NaCl being used to study the stability of the FEFEFKFK peptide hydrogels in the presence of salts. The role of some salts in tissue culture media is to provide pH 7 buffer solutions, which are vital physiological conditions for *in vitro* tissue culture studies and in the body. The stability of peptide hydrogels under the influence of pH was the other main factor considered in the project. In this chapter, the self-assembly and gelation properties of FEFEFKFK peptide under the effect of pH and ionic strength are discussed.

3.2.2 pH effect

3.2.2.1 Results

The peptide solutions and hydrogels at different concentrations were adjusted to various

pH values between pH 3 to pH 12. The phase diagram was mapped out. As observed in the last chapter, at pH 3, the C_{gel} is between 10 to 20 mg ml^{-1} . A clear liquid was obtained below the C_{gel} . At 10 mg ml^{-1} , a clear solution was observed at pH 3. A clear gel was obtained by increasing the pH of the 10 mg ml^{-1} clear solution from 3 to 5. As seen in Figure 3.17 A, the clear gels formed below pH 6. The gels gradually became cloudy when the pH of the gels was increased until pH 7. Further increases in pH resulted in the gels becoming clearer again at pH 9. However, at pH 11, the gels turned into liquids. The transition of the physical properties of the peptide gels as a function of pH suggested the possibility that the mechanical properties would change at various pH. Therefore rheological tests were carried out.

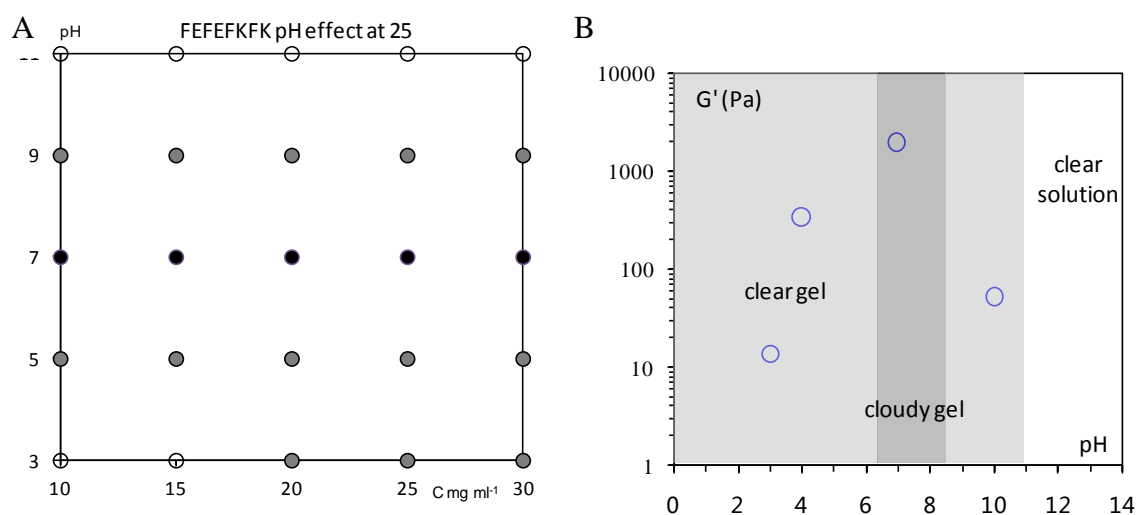


Figure 3.17 (A) The pH phase diagram of FEFEFKFK where samples in the form of solution (empty circle), transparent gel (dark filled circle) and cloudy gel (black dot) were recorded at 25 °C. (B) Plot of G' (○) of FEFEFKFK peptide at 30 mg ml^{-1} against pH.

The plot of G' as a function of pH was combined with the phase diagram of the FEFEFKFK peptide at the same concentrations. The G' value of the peptide at 30 mg ml^{-1} against the value of pH is presented in Figure 3.17 B. It can be seen that the value of G' increases with increasing pH below pH 7 which indicates the gel became stronger when approaching pH 7. It is also noticed that the gel became much weaker for pH > 7.

The gel properties at pH 2.8 were studied in the last section. The peptide fibres with anti-parallel β -sheet structures were detected with FTIR. When the gels turned into liquid above pH 11, FTIR was used again to study the secondary structure of peptide association in the liquid form. The highest pKa value among all the side and end groups of FEFEFKFK is 10.67 of the side chain of K. Therefore pH above this pKa value was chosen

to check the secondary structure of peptide association when the peptide was mostly charged. Three samples with high pH were prepared and the FTIR spectra of FEFEFKFK peptide at 30 mg ml⁻¹ and pH 10.79, pH 11.31 and pH 11.45 were compared with the FTIR spectra profile at pH 2.8 as shown in Figure 3.18.

The strong peak around 1625 cm⁻¹ together with the weak peak around 1684 cm⁻¹ indicates the existence of the anti-parallel β -sheet secondary structures. At pH 10.79, the peaks representing the existence of the anti-parallel β -sheet secondary structure were shifted, compared with the peaks at pH 2.8, which was clearly observed. However, these peaks were not seen in the spectra of FEFEFKFK peptide at pH 11.31 and pH 11.45. Instead the broad peaks of disordered structures dominated the amide I region.

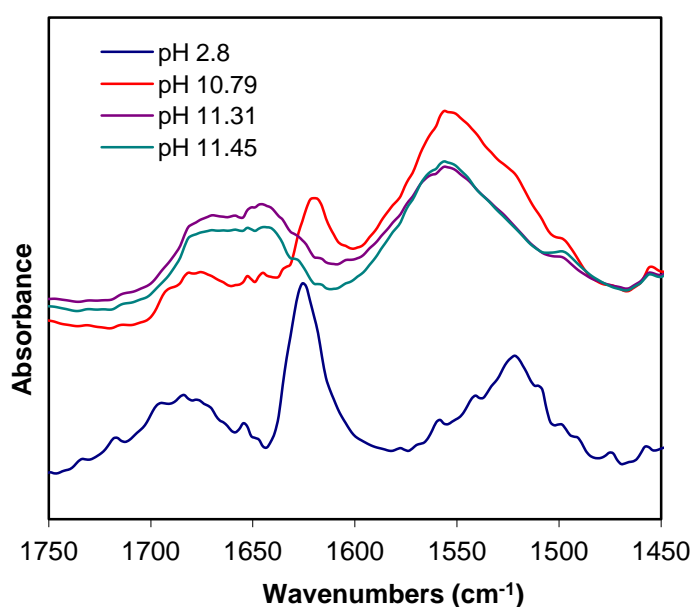


Figure 3.18 FTIR spectra of FEFEFKFK peptide at 30 mg ml⁻¹ at pH 2.8 (blue), pH 10.8 (red), pH 11.3 (purple) and pH 11.5 (green).

The SAS technique was used to study the fibre morphology of FEFEFKFK peptide. To obtain the structural information of a single fibre, the experiments had to be conducted in dilute conditions where the inter-particle scattering is negligible. Peptides at a low concentration of 10 mg ml⁻¹ were therefore studied. The samples at pH 2.8, 4, 5, 7 and 10 were prepared to investigate the effect of pH on fibre morphology.

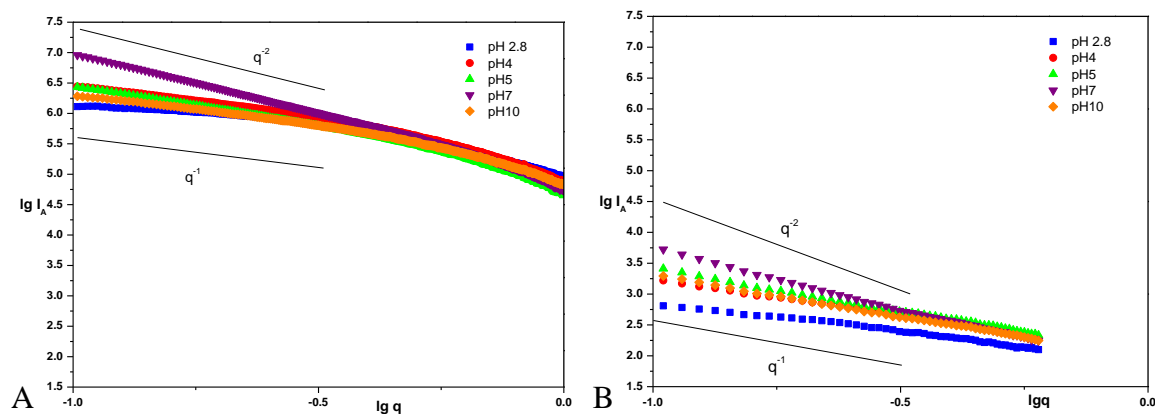


Figure 3.19 Plots of $\lg I_A$ against $\lg q$. (A) SAXS results of FEFEFKFK peptide at 10 mg ml^{-1} at pH 2.8 (blue), pH 4 (red), pH 5 (green), pH 7 (purple) and pH 10 (orange); (B) SANS results of FEFEFKFK peptide at 10 mg ml^{-1} at pH 2.8 (blue), pH 4 (red), pH 5 (green), pH 7 (purple) and pH 10 (orange).

Figure 3.19 presents the absolute scattering intensity I_A as a function of q at different pH in the logarithmic scale. No maximum of intensity is shown on the curves. This indicates the inter-particle scattering is negligible, and the experiments were taken in dilute conditions. The asymptotic form of the absolute intensity curves can be presented by a power law:²⁶

$$I_A \sim q^{-\alpha}$$

Equation 3.4

The value of the exponent α reveals the dimensionality of the scattered object. When I_A is plotted against q in the logarithmic scale, α equals to the slope of the line. All the curves in Figure 3.19 were fitted and the exponent values are listed in Table 3.1.

Table 3.1 The exponent values of the scattering intensity curves for FEFEFKFK peptide at 10 mg ml^{-1} at different pH.

pH	2.8	4	5	7	10
α by SAXS	0.9	1.1	1.4	1.9	1.1
α by SANS	0.9	1.2	1.5	2.1	1.4

For 10 mg ml^{-1} FEFEFKFK peptide samples at pH 2.8 and 4, the exponent α was around 1, which suggests the fibres might adopt rod-like structures in both solution and gels. For 10 mg ml^{-1} FEFEFKFK peptide sample at pH 7, the exponent α was approximately 2, suggesting the existence of a more compact structure in the gel. However, precipitations occurred at pH 7, which could affect the interpretation of the scattering pattern. For the

10 mg ml⁻¹ FEFKFK peptide sample at pH 5 and 10, the exponent α was not close to any integers. Non-integer exponents were also found in other systems and a fractal approach has been developed to analyse the structure information in these systems.¹⁴ In the fractal analysis for $1 < \alpha < 3$, the value of α equals to the mass fractal dimension (D_m), which reflections the compactness of the scattering matter. The structure becomes more compact as the value of D_m increases. For the 10 mg ml⁻¹ FEFKFK peptide, the value of α increased with increasing pH when the gels were acidic, and α reached a maximum at pH 7 before decreasing as the pH increased. According to the fractal concept, the peptide fibres became more compact when the pH was increased from 2.8 to 7. The fibres had the most compact structure at pH 7 before they became looser when the pH further increased.

As a rod-like structure was suggested by the previous result, Porod graphs which are used to estimate the dimension of scattered matters were drawn as shown in Figure 3.20 plotting $\ln qI_A$ against q^2 . For a rod-like structure in the low q range, the scattering density can be written as:

$$q^2 I_A(q) = \pi q \mu_L C_P \exp\left(-\frac{q^2 R_\sigma^2}{2}\right)$$

Equation 3.5

where R_σ is the cross-section radius of gyration of the scattered rod-like structure; μ_L is the linear mass and C_P is the sample concentration. Rewriting the equation will give another equation describing the relationship of $\ln[qI_A(q)]$ against q^2 .

$$\ln[qI_A(q)] = \ln(\pi \mu_L C_P) - \frac{q^2 R_\sigma^2}{2}$$

Equation 3.6

The linear curves could be obtained by fitting the original data, and the slopes of the lines would provide the dimensions of the fibres. The fitted curves are shown in Figure 3.20.

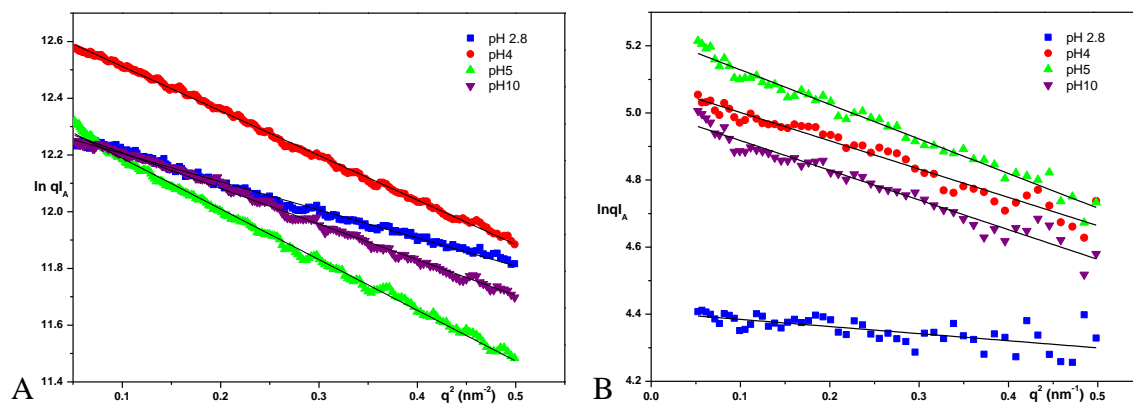


Figure 3.20 Porod plot ($\ln qI_A$ against q^2) of FEFEFKFK peptide at 10 mg ml^{-1} at pH 2.8 (blue), pH 4 (red), pH 5 (green) and pH 10 (purple) tested by SAXS (A) and SANS (B). The solid lines represent the best fit using Equation 3.6.

According to the analysis of Figure 3.19, the rod-like structure was not observed when 10 mg ml^{-1} FEFEFKFK peptide was at pH 7, and therefore the Porod curve at pH 7 was not fitted. The values of R_σ from the fitted curves are listed in Table 3.2.

Table 3.2 The value of R_σ of scattered fibres of 10 mg ml^{-1} FEFEFKFK peptide at different pH.

pH	2.8	4	5	7	10
R_σ (nm) by SAXS	1.4	1.8	1.9	N/A	1.6
R_σ (nm) by SANS	0.7	1.3	1.4	N/A	1.3

For $\text{pH} < 7$, the radius of the rod-like fibres increased with increasing pH. The fibres were thinner again when pH was over 7. The adequate fitting of the Porod curves using Equation 3.6 further indicated that a rod-like structure was taken for the FEFEFKFK peptide at 10 mg ml^{-1} at pH 2.8, 4, 5 and 10.

Figure 3.21 shows the Kratky curves of the FEFEFKFK peptide at 10 mg ml^{-1} and different pH. The bell-like shape of the curves at pH 2.8, 4, 5 and 10 also suggested a rod-like structure. By using Equation 3.7, a full cylinder model was fitted to the original data.⁵

$$q^2 I_A(q) = 4\pi q \mu_L C_P \left(\frac{J_1(qr)}{qr} \right)^2 + Cst$$

Equation 3.7

where r is the radius of the cylinder; μ_L is the linear mass of the cylinder; C_p is the peptide concentration; J_1 represents the first-order Bessel function and Cst is a constant. The fitted graphs are presented in Figure 3.21.

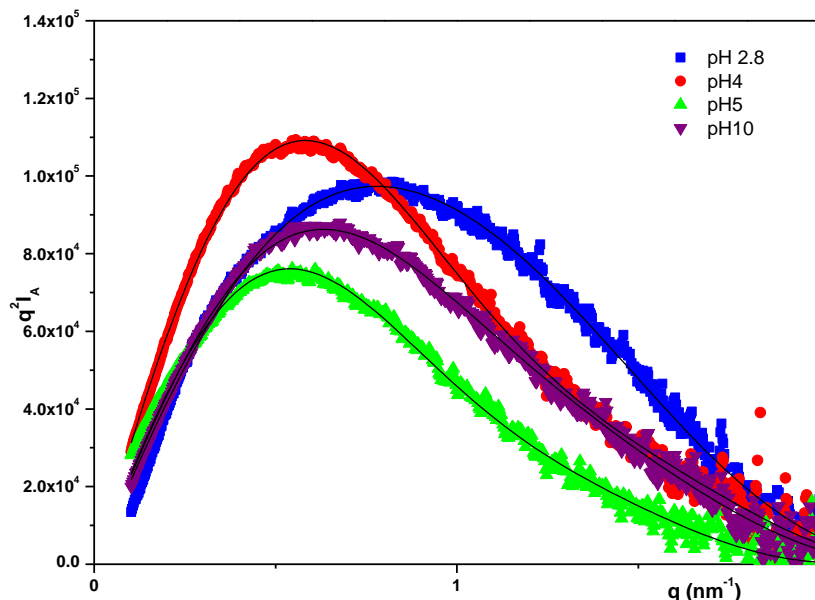


Figure 3.21 Kratky plot ($q^2 I_A$ against q) of FEFEFKFK peptide at 10 mg ml^{-1} at pH 2.8 (blue), pH 4 (red), pH 5 (green) and pH 10 (purple) tested by SAXS. The solid lines represent the best fit using Equation 3.7.

The values of r were obtained through data fitting and then presented in Table 3.3. The peptide fibres at pH 7 did not take the rod-like structure and could not be fitted by Equation 3.7.

Table 3.3 The value of the radius of the scattered fibres of 10 mg ml^{-1} FEFEFKFK peptide at different pH.

pH	2.8	4	5	7	10
r (nm) by SAXS	1.6	3.0	3.2	N/A	1.7

The rod-like fibres with radius of 1.6 nm have been found at pH 2.8 from the SAXS graphs. This also matches the results published before for the FEFEFKFK peptide.⁵ For $\text{pH} < 7$, the radius of the fibres increased with increasing pH. The fibres were thinner again when pH was over 7. As the radius of gyration and radius were related, this is in agreement with the analysis of the R_g obtained from the Porod graphs.

As opposed to the SAXS data, small shoulders were observed on all SANS curves in the

high q range. In order to fit the Kratky curves in the whole q range for the SANS graphs, another type of cylinder with a different radius was introduced to the model. In the new equation derived from Equation 3.7, the scattering intensity was given by:¹⁵

$$q^2 I_A(q) = 4\pi q C_P \left[w\mu_{L1} \left(\frac{J_1(qr_1)}{qr_1} \right)^2 + (1-w)\mu_{L2} \left(\frac{J_1(qr_2)}{qr_2} \right)^2 \right] + Cst$$

Equation 3.8

where 1 and 2 represent the two different types of rod-like structures and w is the weight fraction of the rod with radius r_1 . Fitted graphs are presented in Figure 3.22.

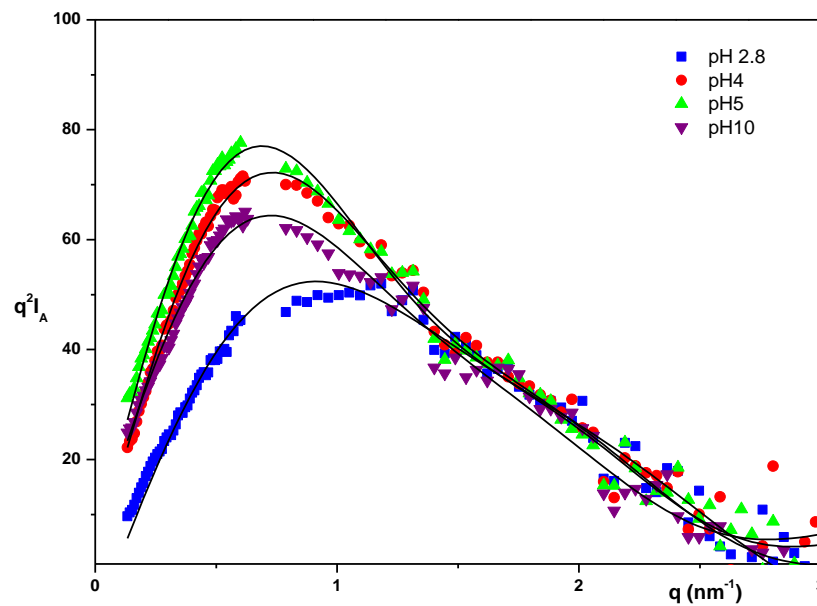


Figure 3.22 Kratky plot ($q^2 I_A$ against q) of FEFEFKFK peptide at 10 mg ml^{-1} at pH 2.8 (blue), pH 4 (red), pH 5 (green) and pH 10 (purple) tested by SANS. The solid lines represent the best fit by using Equation 3.8.

Table 3.4 The value of the radius of the scattered fibres of 10 mg ml^{-1} FEFEFKFK peptide at different pH.

pH	2.8	4	5	7	10
r_1 (nm)	1.1	1.2	1.3	N/A	1.4
r_2 (nm)	2.2	2.4	2.5	N/A	2.6
w	0.78	0.59	0.52	N/A	0.67

The values of r_1 , r_2 and w were obtained through data fitting and are presented in Table 3.4. The Kratky curve of the peptide gel at pH 7 was not in a bell shape and could not be fitted

using Equation 3.8.

The values of r_2 were twice the values of r_1 , suggesting that two or more fibres of radius r_1 could associate with each other to form a thicker fibre of radius r_2 . The association of fibres could be the formation of the network junctions¹⁵ and patterns taken shown in Figure 3.23.



Figure 3.23 Illustration of patterns that could be taken by the association of fibres.

The values of radius r_1 were smaller than those estimated previously. However, the trend of the change in radius for $\text{pH} < 7$ was the same. The value of r_1 increased with increasing pH for $\text{pH} < 7$. For $\text{pH} > 7$, the absence of the value the radius at $\text{pH} 7$ undetermined the observation of whether or not the value of r_1 decreased with increasing pH . The trend of the change in w was the opposite of r_1 . The weight fraction of the rods with radius r_1 decreased with increasing pH for $\text{pH} < 7$, while w increased for $\text{pH} > 7$. This trend indicates thicker fibres formed when the pH increased from 2.8 to 7, and less thick fibres were found when the pH increased up to 10. This could be due to more fibre association when pH increased from 2.8 to 7, and dissociation of fibres caused by further increasing pH up to 10. This suggested that not only the formation of fibres could be affected by the pH but also formation of network could be affected.

The discovery of the second radius was due to the long q range studied by SANS. By using SAXS, data at the high q range would be buried under the signal noises. This is the reason why two techniques were both used to gain more detailed information about the scattering objects.

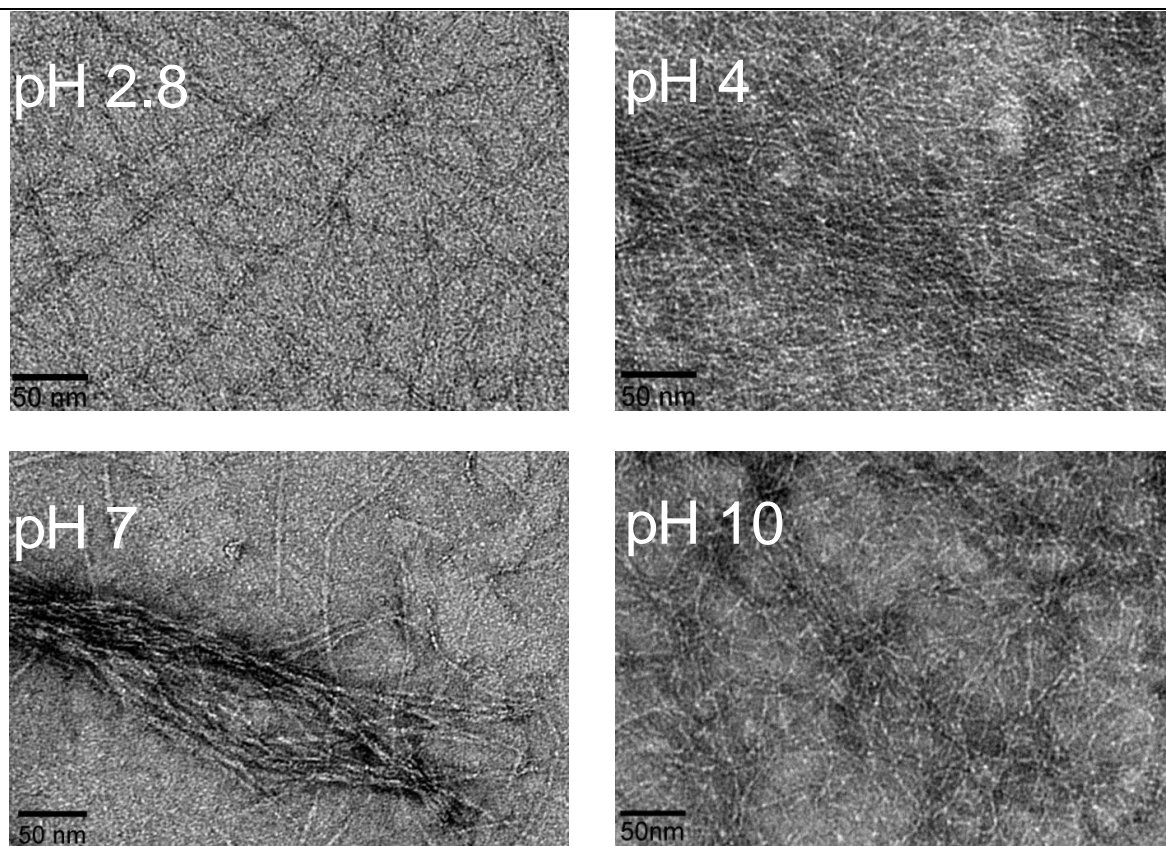


Figure 3.24 TEM images of FEFEFKFK peptide at different pH. Scale bars represent 50 nm.¹²

The network morphology was observed under TEM as shown in Figure 3.24. Diameters of the fibres increased with increasing pH for $\text{pH} < 7$. Diameters of the fibres decreased with increasing pH for $\text{pH} > 7$.¹² This is in agreement with the SAS results. It was also observed that a network structure composed of long thin rigid fibres formed at pH 2.8. When pH increased to 4, a much denser network structure with more long thin rigid fibres was noticed. Bundles of fibres were observed at pH 7. And at pH 10, bundles of fibres disappeared, and instead a dense network structure composed of long thin flexible fibres was found.

3.2.2.2 Discussion

In Chapter 3, the self-assembly model of the FEFEFKFK peptide suggested that by burying the peptide hydrophobic side chains, the hydrophilic side groups are left on the surface of the fibres. The electrostatic interaction between these charged side chains is one of the forces that contribute to the construction of the fibrillar network structure of the FEFEFKFK peptide.

From the chemical structure of the FEFEFKFK peptide (Figure 3.1 A), it can be seen that

the charges carried by the amino groups of the K side chains and N-terminal amino acid, and carboxyl groups of the E side chains and C-terminal amino acid can be affected by pH changes. The pK_a (K_a is the acidic dissociation constant) values of amino groups and carboxyl groups of the FEFEFKFK peptide are listed in Table 3.5.

Table 3.5 The pK_a values of amino groups and carboxyl groups of FEFEFKFK peptide from CRC Handbook of Chemistry and Physics.²⁷

Amino/carboxyl group	pK_a
N-terminal (F)	9.09
Side chain of K	10.67
Side chain of E	4.15
C-terminal (K)	2.15

The pK_a value is the pH value at which half of the amino/carboxyl groups are charged. The net charge of one peptide molecule can be calculated by summing the charges of all amino and carboxyl groups of that molecule. Since the charge state of each amino/carboxyl group varies at different pH, the net charge of peptide also varies where the pH is changed as shown in Figure 3.25.

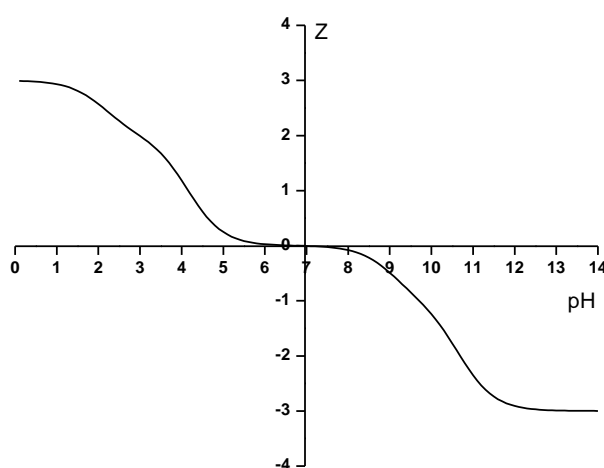


Figure 3.25 Plot of the net charge against pH of FEFEFKFK peptide.²⁸

Due to the presence of TFA residue from the peptide synthesis, the original peptide solution or peptide hydrogel has a pH of 2.8. At this pH, the net charge of the peptide is +2. The repulsion forces keep fibres away from each other. The fibrillar network is formed by

thin fibres.

The net charge of peptide reduces with increasing pH, which indicates the reduction of the repulsion force with increasing pH for $\text{pH} < 7$. This could result in the fibres getting closer to each other, forming thicker fibres and more entanglement junctions. At higher pH, thicker fibres were found in both SAXS and SANS studies for $\text{pH} < 7$. And a denser network structure was also observed in TEM images for pH 4 compared to pH 2.8.

When pH is approximately 7, the net charge is 0. Thin fibres could bundle together and form thicker fibres. However, if the fibres are too thick, the aggregation of fibres causes local precipitation, and the gel becomes cloudy in appearance.

When the pH is above 7 and below 11, peptides are negatively charged and the charge number increases. By increasing the charge number, the repulsion forces between fibres also increase. The thicker fibres dissociate into thinner fibres, and the gels appear clearer. The existence of thinner fibres was confirmed by SAXS and SANS results.

When the pH is above 11, both the amino and carboxyl groups are deprotonated; the charge number increases to its maximum. The disordered structures of FEFKFK peptide were found by FTIR. Both the association of fibres and formation of β -sheet structures could be affected by deprotonation and a higher charge. High fractions of disordered structures could have affected the gelation of the peptide above pH 11. Similar observations were found in other ionic complementary peptide system such as RADA16-I peptide.²⁹ This peptide is also neutral at pH 7 and the net charge of the peptide molecule is also affected by pH changes. It was reported that this system was affected by deprotonation and a higher charge at high pH.²⁹ Unordered structures of peptides in solutions were found to prevent the fibre formation. The formation of short fibres instead of long thin fibres caused the transition from gel to liquid.

The association and dissociation of fibres under the influence of pH was in agreement with the fractal analysis of SAXS and SANS data. The association of fibres increased the compactness of fibres while dissociation loosened the structure. Fibres were thickening with increasing pH for $\text{pH} < 7$, while fibres were thinner again for $\text{pH} > 7$. This was postulated by the self-assembly model and confirmed by the results of the SAS study. The same trend was also observed under TEM.¹² This could also explain the strengthening of the acidic peptide hydrogels with increasing pH. The thicker fibres increased the

mechanical strength of the fibrous network leading to stronger peptide hydrogels. The observations of all the data further confirmed the self-assembly model discussed in Chapter 3.

3.2.3 Ionic strength effect

The other important factor taken into consideration when studying the gel properties was the ionic strength. An ionic strength of around 200 mM^{30, 31} was reported for the media intended to be used in future experiments of this project. Therefore the study of the effect of ionic strength on the self-assembly and gelation properties were taken from a NaCl concentration range of 20 mM to 1 M. However, to have a better understanding of the effect of ionic strength on self-assembly and peptide gelation properties, other variables should not be changed at the same time. In order to compare with the previous work done on the original peptide hydrogels, no pH modification was applied on the gels used for ionic strength effect studies. Therefore all the results presented in this section were done at pH 2.8. However, this only helped to understand how ionic strength affects the self-assembly and gelation process. The conclusions can not be directly linked to the real gel state in the cell culture environment. From the discussion of the previous, it was shown that the peptide molecules have a +2 net charge at pH 2.8, which contributed to the charge of the side groups on K. The side groups of E are protonated at this pH. However, although the net charge of peptide molecules is zero at pH 7, the side groups of E and K are all charged. This results in a difference in the electrostatic environment for the salt ions to effect. It is still important to understand how ionic strength affects the peptide self-assembly and gelation properties but it should be noted that the conclusions drawn from this section should be used as a reference and not a direct guide for future cell culture studies.

3.2.3.1 Results

The peptide solutions and hydrogels at different concentrations with different amounts of NaCl in the system were prepared. The phase diagram under the effect of NaCl was mapped out.

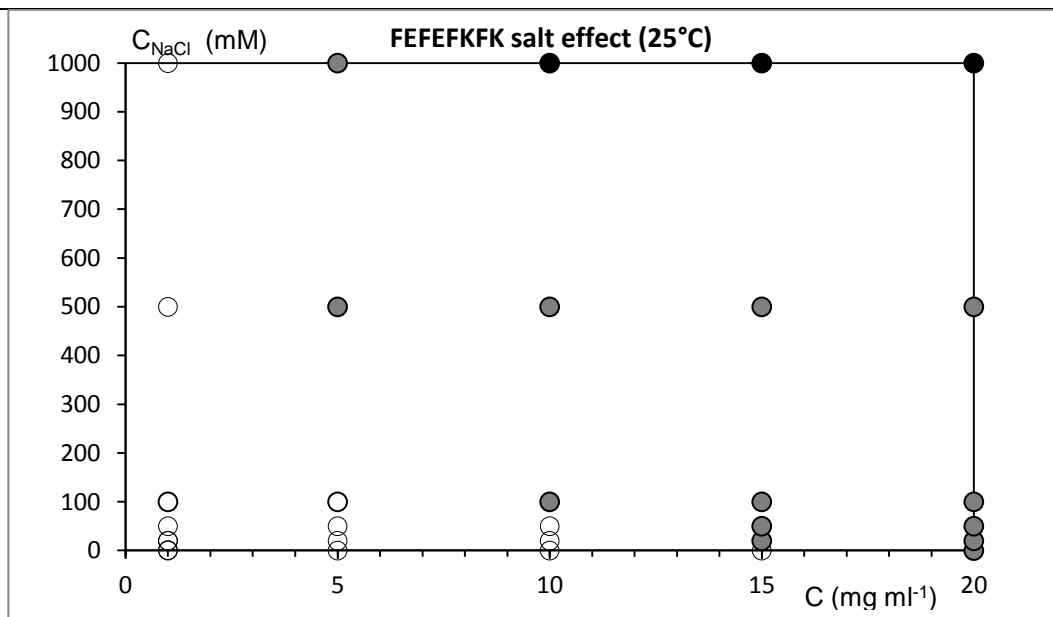


Figure 3.26 The phase diagram of FEFEFKFK peptide where samples in the form of solution (empty circle), transparent gel (dark filled circle) and cloudy gel (black dot) were recorded at 25 °C at different salt concentrations. All the samples were at pH 2.8.

Figure 3.26 is the phase diagram of the NaCl salt effect on FEFEFKFK peptide. The X-axis represents the peptide concentration and Y-axis represents the NaCl concentration. The peptide solutions remained liquid when the concentration was lower than 5 mg ml⁻¹. In the range of 5 mg ml⁻¹ to 15 mg ml⁻¹ without any salt in the system, the peptide system remained a solution; and when the salt concentration increased, transparent gels formed. Cloudy gels were observed with further increasing of the salt concentration. The C_{gel} of FEFEFKFK peptide without the addition of salt is between 15 to 20 mg ml⁻¹. When the concentration is higher than 15 to 20 mg ml⁻¹, the peptide always forms gels with or without salts. Semi-transparent gels were observed at NaCl concentration of 1 M for all the samples with concentrations greater than 5 mg ml⁻¹. Due to the change of physical forms, the mechanical properties were also expected to be affected by salt. To study the change in mechanical properties, the two concentrations of the sample, one below and one above the C_{gel} , were chosen to perform the rheological tests.

FEFEFKFK peptide at 10 and 20 mg ml⁻¹ were chosen for further mechanical tests.

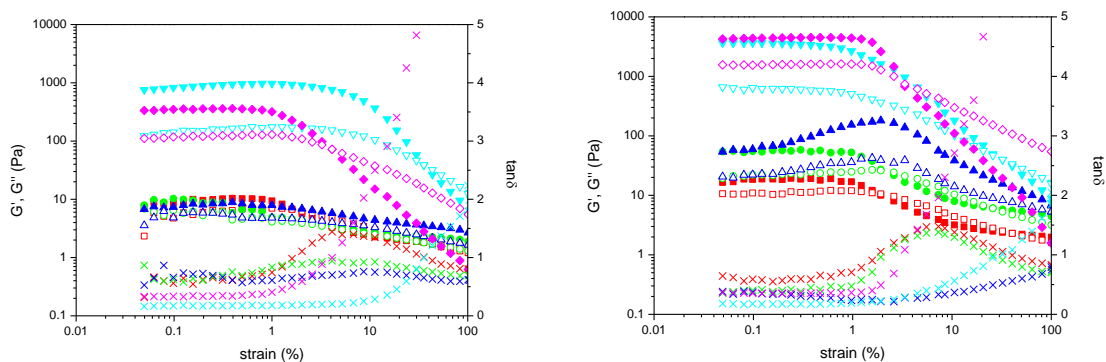


Figure 3.27 Plot of elastic modulus (G' , solid), viscous modulus (G'' , empty) and $\tan\delta$ (\times) of FEFEFKFK peptide at 10 (left) and 20(right) mg ml^{-1} at NaCl concentration of 20 (red), 50 (green), 100 (blue), 500 (cyan) and 1000 mM (purple) as a function of strain from 0.05% to 100% at 1 Hz at 20 °C in the logarithmic scale. All the experiments were taken at pH 2.8.

An amplitude sweep was performed first to locate the LVR of all samples. It can be seen that below 1% strain, all G' is higher than G'' and $\tan\delta < 1$, which indicates that all the samples were in the gel form. Values of G' , G'' and $\tan\delta$ were also independent from the variation of the applied strain below 1% strain, indicating that the LVR of the testing samples is below 1% strain. A frequency sweep was then performed at a fixed strain of 1%. It was also noticed on Figure 3.27 that the gels at a salt concentration of 1000 mM have lower yield strains than the gels at a salt concentration of 500 mM on both figures. This indicated a more brittle gel results at the highest salt concentration. The gels at the highest salt concentration were noticed by their semi-transparency on Figure 3.26, meaning small disruptions of the gel network, and could be the reason of the lower yield strain.

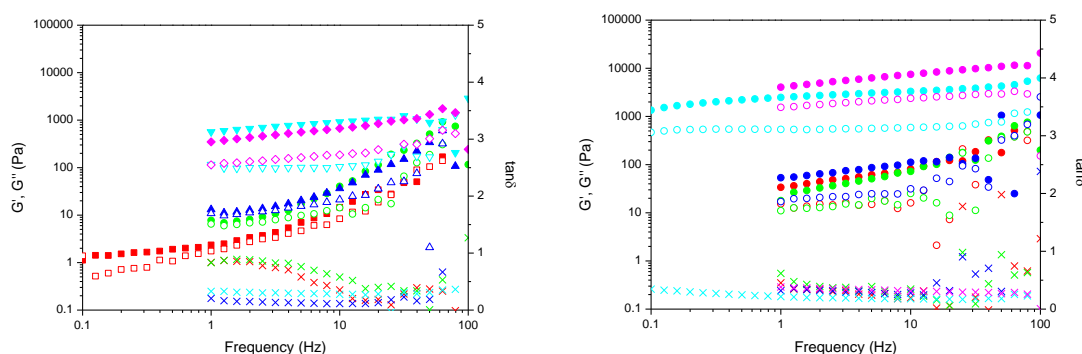


Figure 3.28 Plot of elastic modulus (G' , solid), viscous modulus (G'' , empty) and $\tan\delta$ (\times) of FEFEFKFK peptide at 10 (left) and 20(right) mg ml^{-1} at NaCl concentration of 20 (red), 50 (green), 100 (blue), 500 (cyan) and 1000 mM (purple) as a function of frequency from 0.1 to 100 Hz at 1% strain at 20 °C in logarithmic scale. All the experiments were taken at pH 2.8.

Frequency sweep of all samples were performed and at frequencies lower than 10 Hz, an

independence, or weak dependence of G' , G'' and $\tan \delta$ on frequency was observed. The average value of G' , G'' and $\tan \delta$ in the independent region and yield strain from Figure 3.27 of FEFEFKFK at 10 and 20 mg ml⁻¹ were plotted against the NaCl concentration as shown in Figure 3.29. It can be seen from the figure that for peptide at 20 mg ml⁻¹, the higher the salt concentration, the stronger the system, and the 10 mg ml⁻¹ peptide system experienced first an increase, then a decrease in G' before and after the salt concentration reached 500 mM. This could be due to more disruption of the gel network structure within the 10 mg ml⁻¹ gel at the highest salt concentration compared to the 20 mg ml⁻¹ gel. The gel at higher concentration has a denser network structure which could help maintain the strength of the gel network. The $\tan \delta$ value of 10 mg ml⁻¹ gel was close to 1 below the salt concentration of 100 mM, then decreased to 0.14 and 0.3 at salt concentrations of 500 mM and 1000 mM, respectively. This indicates that highly viscous solutions formed at lower salt concentrations, while real gels formed at higher salt concentrations for the gel at 10 mg ml⁻¹. The $\tan \delta$ value of 20 mg ml⁻¹ remained low in the whole salt concentration range. The value of yield strain experienced the opposite trend compared to $\tan \delta$. The maximum yield strain at salt concentration of 500 mM indicates the gels at other salt concentrations were all more brittle.

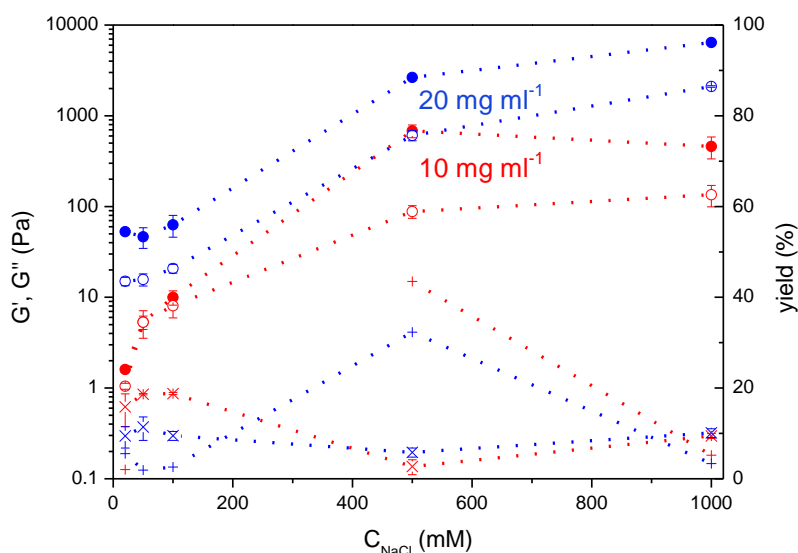


Figure 3.29 Plot of G' (solid), G'' (empty), $\tan \delta$ (\times) and yield strain ($+$) of FEFEFKFK peptide at 10 mg ml⁻¹ (red) and 20 mg ml⁻¹ (blue) against the salt concentration. All the experiments were taken at 1% strain at 20 °C at pH 2.8.

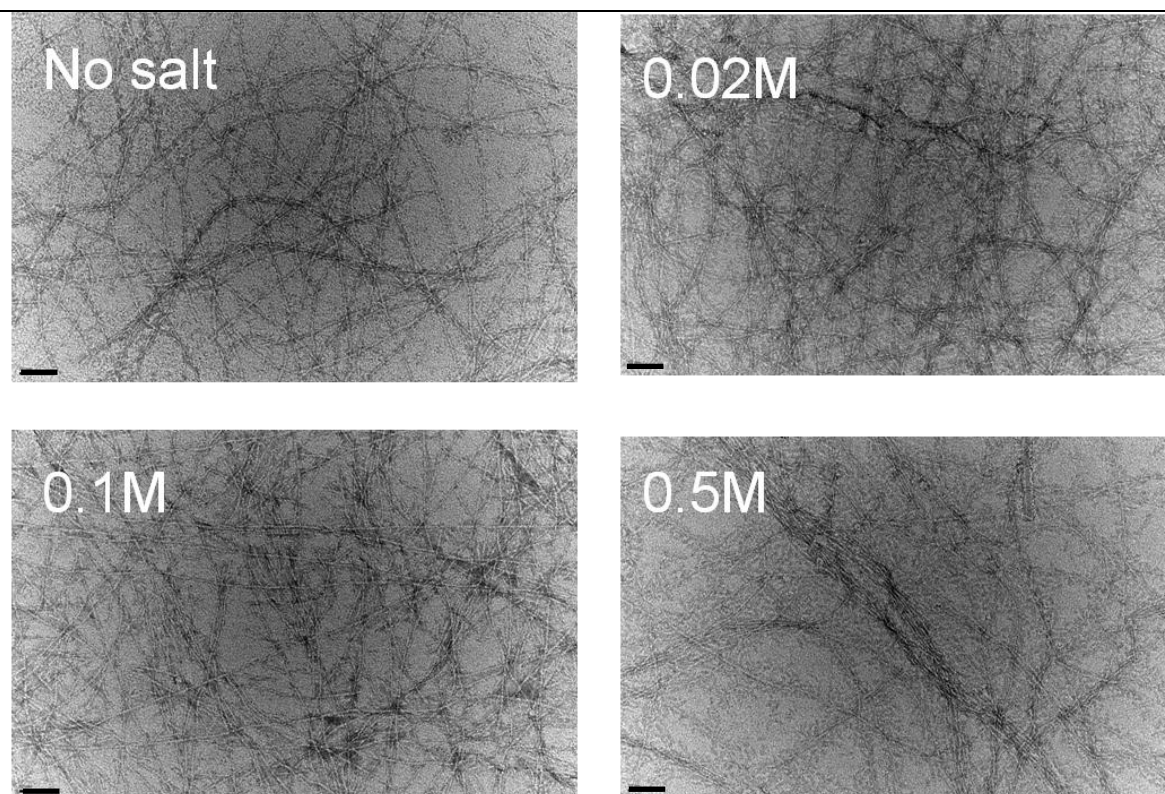


Figure 3.30 TEM images of FEFEFKFK peptide at different salt concentrations. Scale bars represent 50 nm. All the samples were at pH 2.8.

The salt effect on the gel properties suggested the self-assembly process could also be affected by the change in the ionic strength. TEM was used to observe the morphology of the fibrous network under the influence of different NaCl concentrations.

Densely cross-linked network structures were observed within the studied salt concentration range. Image analysis was used to measure the diameter of the fibres. The average diameters (d) of fibres at different NaCl salt concentrations (C_{NaCl}) were listed in Table 3.6:

Table 3.6 The average diameter d of peptide fibres at different salt concentrations at pH 2.8.

C_{NaCl} (M)	0	0.02	0.1	0.5
d (nm)	3.3	3.4	3.5	3.6

The image analysis showed a small increase in the diameters of single fibres with increasing salt concentration. However, the difference was too small to draw any conclusion. The average size of the single fibres in the no salt system had an average diameter of 3.3 nm. This matched the measurement in Section 3.1.1. When increasing the

salt concentration to 0.02 M, the diameter of the fibres did not seem to change, while some of the fibres were close or even parallel to each other. Further increasing of the salt concentration to 0.1 M, resulted in more fibres aligning closer and more parallel to each other. When the salt concentration reached 0.5 M, bundles of peptide fibres were observed. The fibre morphology also changed with increasing salt concentration. Very long thin and flexible fibres formed in the no salt system, and the fibres looked more rigid and stretched with increasing salt concentration. Due to the drying process during the sample preparation, the fibre morphology was observed under TEM in the dry state. With the help of the SAS technique, it is possible to study the system while it is hydrated. Combining the two techniques would provide more information on understanding the salt effect on the self-assembly process.

The SANS technique was used again to study the fibre morphology of FEFKFK peptide under the influence of different salt concentrations. To gain information about single fibre, the experiments were done in dilute conditions where the inter-particle scattering is negligible, and therefore peptide at a low concentration of 10 mg ml^{-1} was chosen. The samples with NaCl salt concentrations of 0 M, 0.1 M, 0.5 M and 1 M were prepared to deduce the fibre morphology.

Similar to the SAS data for the pH effect, SANS data for the salt effect was analysed using a similar approach. Figure 3.31 presents the absolute scattering intensity I_A as a function of q at different salt concentrations in the logarithmic scale. No maximum of intensity on the curves indicates that the inter-particle scattering is negligible, which also suggests the experiments were taken in dilute conditions. All the curves in Figure 3.31 were fitted using Equation 3.4 and the exponent values are listed in Table 3.7.

Table 3.7 The exponent values of scattering intensity curves for FEFKFK peptide at different NaCl salt concentrations at pH 2.8.

C_{NaCl} (M)	0	0.1	0.5	1
α	1.1	1.1	1.2	1.3

For 10 mg ml^{-1} FEFKFK peptide at all salt concentrations studied, the exponents α were all close to 1, which suggested the fibres might adopt rod-like structures in both solution and gels. For 10 mg ml^{-1} FEFKFK peptide at the salt concentration of 1 M, the exponent α was about 1.3, which could also be treated as non-integer. Using the fractal analysis, the

small increase of the exponent with increasing salt concentrations resulted in the peptide fibres becoming more compact with increasing salt concentrations.

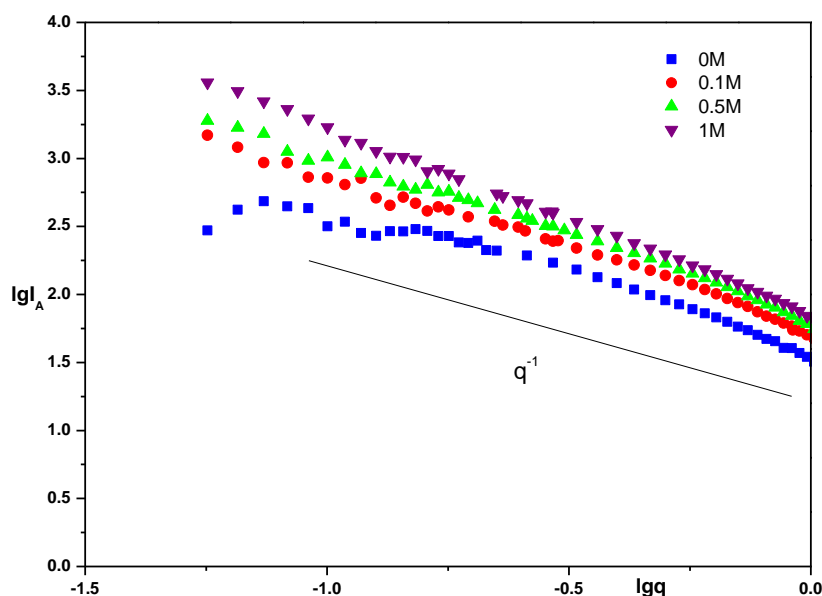


Figure 3.31 Plot of $\lg I_A$ against $\lg q$ of FEFEFKFK peptide at 10 mg ml^{-1} with the salt concentration at 0 M (blue), 0.1 M (red), 0.5 M (green) and 1 M (purple) tested by SANS. All the experiments were taken at pH 2.8.

As a rod-like structure was suggested by the previous result, the Porod graph is used to estimate the dimension of scattered matters was drawn as shown in Figure 3.32.

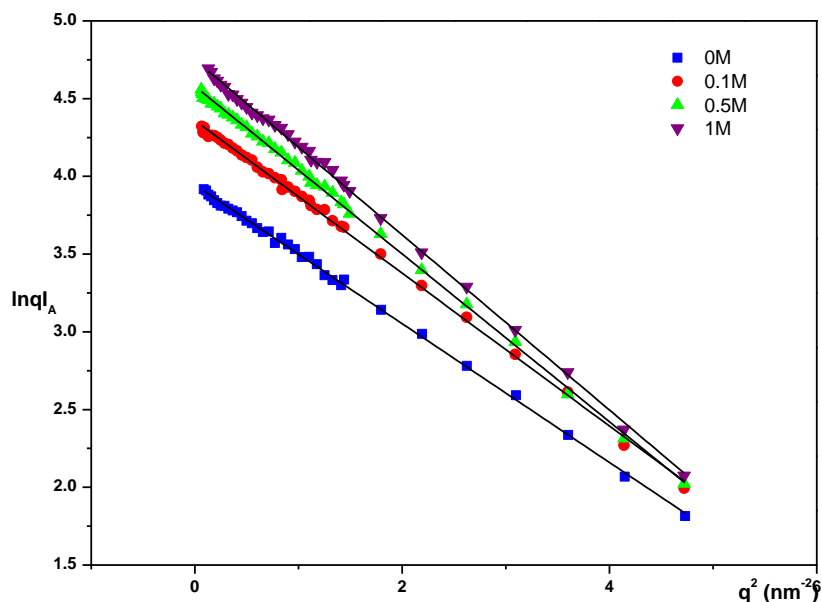


Figure 3.32 Porod plot ($\ln q I_A$ against q^2) of FEFEFKFK peptide at 10 mg ml^{-1} with the salt concentration at 0 M (blue), 0.1 M (red), 0.5 M (green) and 1 M (purple) tested by SANS. Solid lines represent the best fit by using Equation 3.6. All the experiments were taken at pH 2.8.

The fitting of the curves further proved the rod shape is an appropriate model for fitting the SAS data of the FEFEFKFK peptide. The values of R_σ from the fitted curves are listed in Table 3.8.

Table 3.8 The value of R_σ of scattered fibres of 10 mg ml^{-1} FEFEFKFK peptide at different salt concentrations.

C_{NaCl} (M)	0	0.1	0.5	1
R_σ (nm)	0.9	1.0	1.0	1.1

The radius of gyration slightly increased with increasing salt concentrations; however, the increase was very small. This is in agreement with the observation using TEM.

The Porod graph gives the dimension of the scattered matter irrespective of the shape of the scattered object. In order to further study the morphology of the fibres with a rod-like structure, Kratky curves of the FEFEFKFK peptide at 10 mg ml^{-1} and different salt concentrations were analysed (Figure 3.33). The bell-like shape of the curves at all salt concentrations also suggested rod-like structures in all systems. By using Equation 3.7, a full cylinder model was fitted to the original data. Fitted graphs are presented in Figure 3.33.

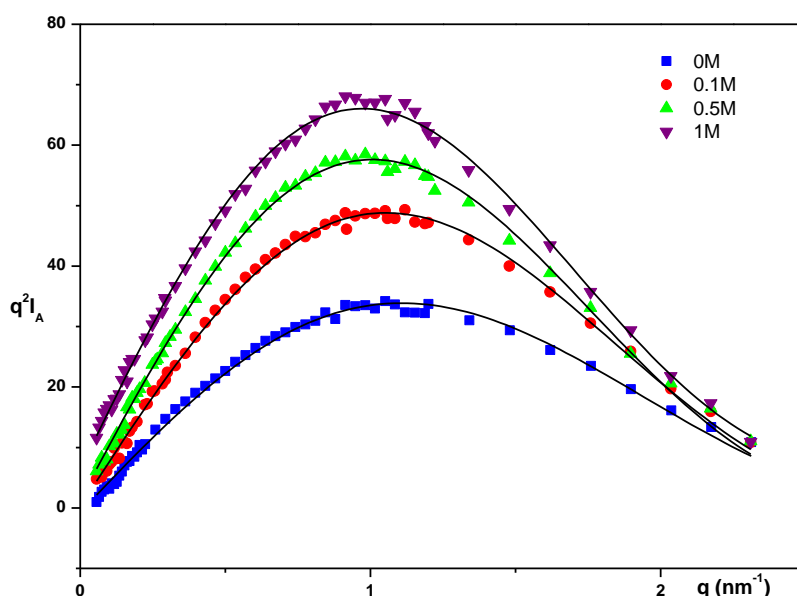


Figure 3.33 Kratky plot ($q^2 I_A$ against q) of FEFEFKFK peptide at 10 mg ml^{-1} with the salt concentration at 0 M (blue), 0.1 M (red), 0.5 M (green) and 1 M (purple) tested by SANS. Solid lines represent the best fit by using Equation 3.7. All the experiments were taken at pH 2.8.

The values of r were obtained through data fitting and are presented in Table 3.9.

Table 3.9 The value of radius of scattered fibres of 10 mg ml⁻¹ FEFEFKFK peptide at different salt concentrations at pH 2.8.

C_{NaCl} (M)	0	0.1	0.5	1
r (nm)	1.2	1.3	1.3	1.4

Rod-like fibres with a radius of 1.2 nm were found for the no salt peptide solutions. This matched the SANS results found when studying the pH effect of the FEFEFKFK peptide. The small increase in radius with the increasing salt concentrations also matched the trend observed by TEM. However, the radius obtained by SANS was smaller than the radius obtained by TEM at the same salt concentration. This could be due to the different sample preparation procedures. The fibres examined by SANS were in their hydrated states whilst the fibres studied by TEM were dried out during the preparation. The dried fibres were flattened on the grids, which could lead to larger diameters.

3.2.3.2 Discussion

The self-assembly model developed in previous chapters was also used to help understand the salt effect on the self-assembly and gelation properties of FEFEFKFK peptide. In the previous Section 3.2.2, it was reported that at pH 2.8, the amino groups of the FEFEFKFK molecules were positively charged, the carboxyl groups of the side chains of E were non-charged, and the carboxyl groups of C-terminus were negatively charged. The overall peptide fibres were positively charged with a charge of +2. The repulsion force kept fibres away from each other, and the fibrillar network was formed by thin fibres. Without changing the pH, all the samples studied in the Section 3.2.3 were at pH 2.8. Therefore all fibres were positively charged.

When NaCl salts were dissolved in the aqueous solution, the small Na⁺ and Cl⁻ ions would be attracted to the charged carboxyl and amino groups along the fibres. Without salts, the positively charged side chains would push the neighbouring fibres away from each other. And with salts, the small ions between the charged side chains would screen them from each other and reduce the repulsion forces between the neighbouring fibres. When the fibres came closer, more entanglement could occur, which resulted in the formation of a fibrous network structure. This could have caused the transition from liquid to gel form observed in the phase diagram. For peptides at higher concentrations, the gels with fibrous

network structure already formed. More entanglement could have resulted in a denser network structure leading to a stronger gel. This trend was observed during the rheology studies. When the salt concentration was further increased, the fibres got even more close to each other and forming bundles of fibres. More bundles of fibres may eventually precipitate from the system causing the formation of foggy gels as observed in the phase diagram. The higher the salt concentration, the more ions could be gathered around the fibres. This could explain the slight increase in the fibre diameter observed by both TEM and SANS. The gathered ions around the fibres could also decrease the flexibility of the fibres. More rigid fibres could be found at higher salt concentrations, which could also lead to stronger gels. This is also in agreement with the rheology studies.

3.3 2D cell culture protocol development on FEFEFKFK peptide gel

3.3.1 Introduction

With the understanding of the pH and salt effect on the FEFEFKFK gel, it was possible to predict the gel properties under the influence of cell culture media, and therefore enable the setting up of the gel preparation protocols. In this chapter, the development of the gel preparation protocol for the 2D cell culture and the preliminary tests in 2D cell culture will be discussed.

3.3.2 Gel preparation protocol development for 2D cell culture

In 2D cell culture, cells were seeded on the gel surface, and the gels needed to be relocated in the wells of a tissue culture well-plate from the original container. In order to get a good cell distribution on the gel surface, when in the wells, the gel surface needed to be uniform. This requirement could be met by transferring viscous solution or weak gel into the wells. The gelation could be triggered later on, and would promote a reproducible method for the gel preparation. If a gel form was transferred to the well directly, it would be very difficult to maintain the same uniform gel surface in each experiment. The phase diagram of FEFEFKFK was mapped out in the previous studies. It was noticed that when the concentration was lower than 30 mg ml^{-1} , the gels could be easily melted down at $90 \text{ }^\circ\text{C}$. The gelation occurred during the cooling process. When the gels were prepared, the

peptide powder and distilled water were sealed and heated at 90 °C until well mixed. Therefore the transferring requirement could be achieved by using the gels at low concentrations, and transferring the hot peptide solution quickly to the wells. Gels with a uniform surface were obtained after being cooled down.

Besides the uniform gel surface, there was another important factor that needed to be considered. It was known that physiological pH was a vital factor for culturing cells. However, the original peptide hydrogels were acidic, and the pH of peptide hydrogel had to be adjusted before cells were seeded. Usually NaOH or buffer solution was chosen to alter the pH of a system. Both of which were also tested in this project.

Firstly, NaOH solution was prepared. The required amount of NaOH solution was then mixed quickly with hot peptide solution in the 24-well plate for a pH neutral homogenous mixture. As discussed in the last chapter, pH can also be used as a gelation trigger. Because of the sharp pH increase in the system, the gelation would occur in minutes. It was essential to quickly transfer the mixture into wells to get a uniform gel surface. This also allows the peptide solution at low concentrations to be used. For example peptide solution at 10 mg ml⁻¹ does not form a gel during the cooling down process. But when the pH increases, gels can be obtained. To gain a stable pH and to also monitor the pH value of the gel in the wells, cell culture media were used to rinse the gel several times before seeding the cells. As a buffer solution, cell culture medium was able to maintain a stable pH value. The pH indicator in the cell culture medium also helped to monitor the pH value. This pH adjustment process was referred as Method 1. The FEFEFKFK gels prepared by Method 1 will be referred to as FEFEFKFK+NaOH.

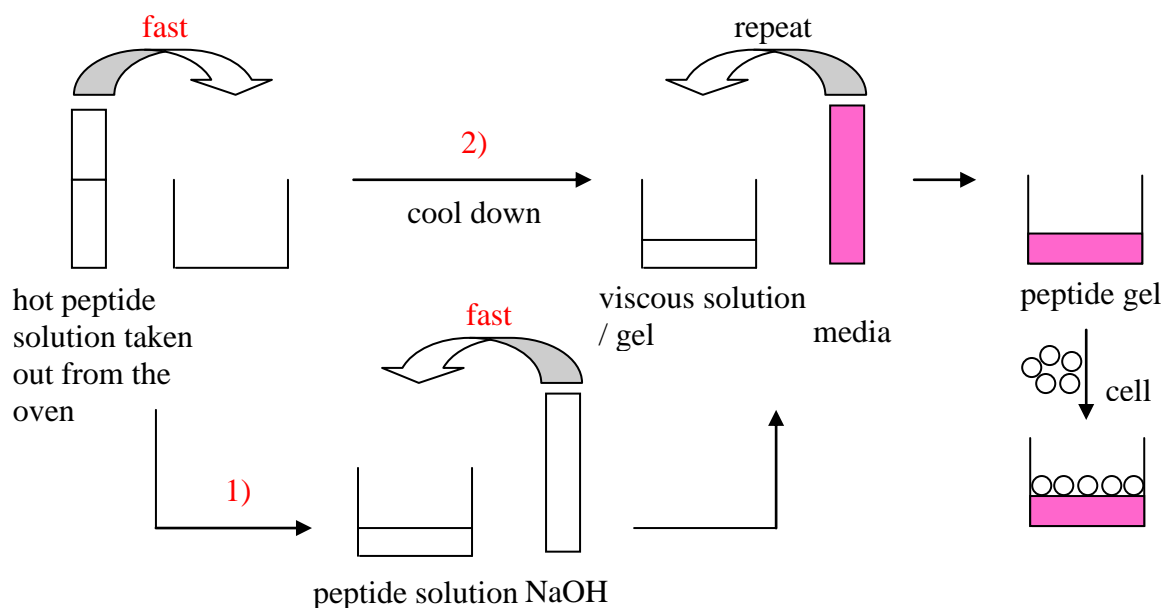


Figure 3.34 Scheme of the gel preparation for 2D cell culture

Secondly, cell culture media were used directly as a buffer solution to adjust the pH value. After the gels cooled down and formed a fairly rigid surface, a small amount of cell culture media was laid on top. At this stage, the gels were transparent while the cell culture media were pink due to the existence of the pH indicator. After several hours, the gels turned slightly yellow while the cell culture media were also yellow. This was caused by diffusion of ions between the media and gels. With a slight pH and salt concentration increases in the gel, the gels became stronger. The yellow solution was replaced by the fresh pink cell culture media. The replacement was repeated several times until the whole gel turned pink, which indicated a successful pH adjustment. It was noticed that, even when the peptide concentration was low, a highly viscous peptide solution could still support a thin layer of cell culture media on top. After the initial contact, the surface became slightly stronger, which then helped hold the cell culture media without the whole solution being diluted. This way of adjusting the pH was called Method 2. The FEFEFKFK gels prepared by Method 2 will be referred as FEFEFKFK in the future discussion.

By using these two methods, the pH of the peptide FEFEFKFK gels was adjusted to the physiological pH value. Salt diffusion occurred during the repeated media change, which also helped to alter the salt concentration of the peptide FEFEFKFK gels to the physiological salt concentration. The fact that FEFEFKFK gels can be optimised in this way also shows a good permeability of this octapeptide hydrogel. To be used as a tissue

culture scaffold, the hydrogels need to be permeable, so the nutrients can reach cells inside the gel and the metabolism waste can be washed out during media change. Finally, the gels were ready to be tested in 2D cell culture studies.

The gels used in the following 2D cell culture were all transparent. The only difference in the appearance compared with the gels in distilled water is the pink colour. The rheology tests were performed prior to cell seeding. And the results are presented in Figure 3.35.

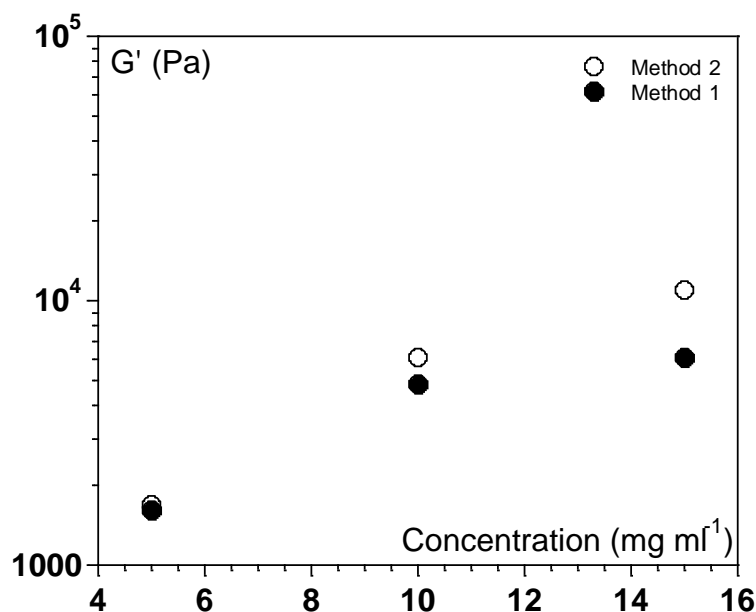


Figure 3.35 Plot of elastic modulus (G') against gel concentrations for the peptide gel prepared by Method 2 (empty) and Method 1 (solid) in the logarithmic scale. All the samples were at physiological conditions.

It can be seen that the gels prepared by Method 2 are slightly stronger at all gel concentrations. From the phase diagram (Figure 3.7), we know that the samples at concentrations of 5, 10 and 15 mg ml⁻¹ do not even form gels in distilled water at pH 2.8. The studies of the ionic strength effect alone in Section 3.2 (Figure 3.26) showed that when increasing ionic strength of the peptide samples at pH 2.8, a phase transition from a liquid to gel form occurred at concentrations of 5, 10 and 15 mg ml⁻¹. From the studies of the pH effect alone (Figure 3.17 A), we can see that a phase transition from a liquid to gel form occurred at concentrations of 10 and 15 mg ml⁻¹ when pH 5 was reached. These samples maintained the gel form up to pH 9. The sample at 5 mg ml⁻¹ was not studied when mapping the pH phase diagram. However, according to the studies of the pH effect on peptide self-assembly in Section 3.2, the association of peptide fibres in the sample of 5 mg ml⁻¹ was expected to increase with increasing pH. This is due to the decrease of the net charge of every single peptide fibre. In the preparation of the peptide hydrogels for the

cell culture studies, the gels were adjusted to physiological conditions, resulting in a neutral pH and ionic strength of around 200 mM. Both pH and ionic strength were proven to be gelation triggers on their own. At neutral pH, although the net charge of each peptide fibre is zero, all the amide and carboxyl groups of each peptide molecule are charged. Those charged groups can be affected by the salts present at physiological conditions. The combined action of both pH and ionic strength caused the gelation of peptide samples at concentrations of 5, 10 and 15 mg ml⁻¹ under physiological conditions.

3.3.3 2D cell culture protocol development

3.3.3.1 NaOH effect

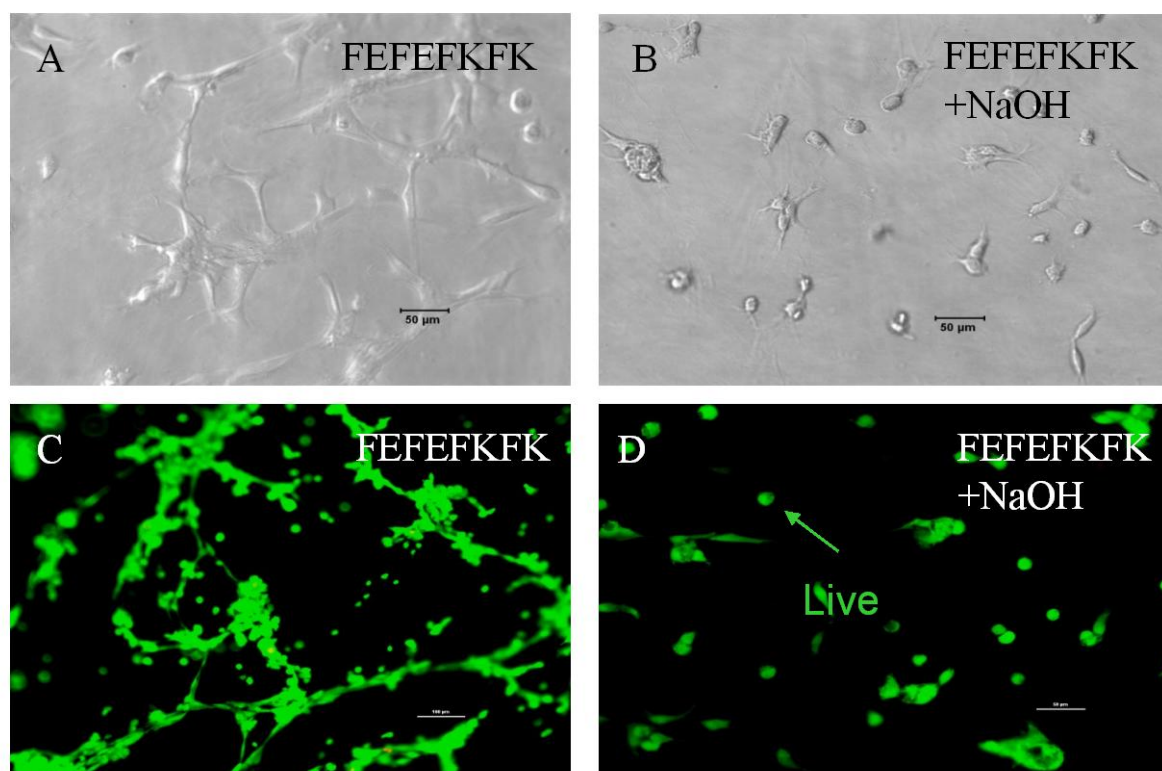


Figure 3.36 (A) Optical micrograph of chondrocyte cell morphology 7 days post cell culture on 10 mg ml⁻¹ gels prepared by Method 2; (B) Optical micrograph of chondrocyte cell morphology 7 days post cell culture on 10 mg ml⁻¹ gels prepared by Method 1; (C) Fluorescence micrograph of chondrocyte cell viability 7 days post cell culture on 10 mg ml⁻¹ gels prepared by Method 2 and (D) Fluorescence micrograph of chondrocyte cell viability 7 days post cell culture on 10 mg ml⁻¹ gels prepared by Method 1. Scale bars represent 50 μm. 5 × 10⁴ cells were seeded on top of the gel surface in each well.

The biggest difference between the gels prepared by Method 1 and Method 2 is the existence of NaOH in the system. Different cell morphology was observed between the two systems (shown in Figure 3.36). Several images were taken for every gel observed

using microscopy technique, and the percentage of cells with different morphology was calculated by image analysis. In future cell culture studies regarding cell morphology or cell number, the same protocol was applied.

It can be seen clearly that after day 7, cells had fully spread on the gel surface prepared by Method 2. The spreading shape indicated chondrocyte cells had differentiated into fibroblast cells. Cells on the gel surface prepared by Method 1 were less stretched. 168 cells were counted and 40% of the cells remained with a round shape 7 days post cell culture. Fluorescence micrographs were taken after the Live/dead staining. In the Live/dead staining assays, dead cells are stained red while live cells are stained green. All cells were alive on both of the FEFEFKFK gel surfaces up to 7 days. The strong effect of NaOH on the cell morphology suggested that by controlling the use of NaOH, different cell morphology can be manipulated in 2D cell culture.

3.3.3.2 Gel concentration effect

It was known from the last two chapters that the peptide gel concentrations would affect the mechanical properties, and the mechanical properties of the scaffold were known to affect the cell behaviours.³² Therefore the gel concentration effect on the cell behaviour was studied. As shown in Figure 3.37, it can be seen that cells on the FEFEFKFK peptide at a concentration of 5 mg ml⁻¹ were less elongated compared with cells on the FEFKFEFK peptide at concentrations of 10 mg ml⁻¹ and 15 mg ml⁻¹. From the optical micrographs, the cell morphology on FEFEFKFK peptide at the concentrations of 10 mg ml⁻¹ and 15 mg ml⁻¹ were the same. The overlapped rheological tests showed that the gels were stronger at higher concentrations. This could explain why chondrocyte cells were less elongated on the weakest gels. It is also known that when the scaffold is stiff enough, further increase of the mechanical strength does not make a big difference on cell behaviours. This could be the reason that similar cell morphology on the gels at concentrations of 10 mg ml⁻¹ and 15 mg ml⁻¹ were observed.

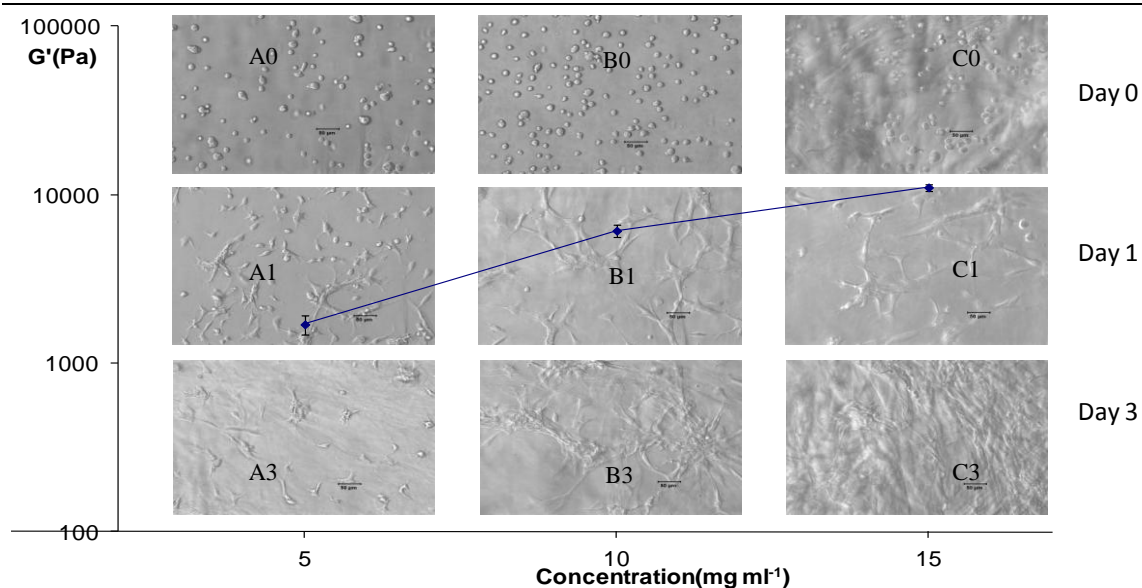


Figure 3.37 Optical micrographs of chondrocyte cell morphology at day0, day1 and day3 of cell culture on the gels prepared by Method 2 at the concentration of 5 mg ml^{-1} (A0, A1, A3), 10 mg ml^{-1} (B0, B1, B3) and 15 mg ml^{-1} (C0, C1, C3). Optical micrographs were overlapped with the rheological tests results of all three types of gels before cell seeding. All the samples were at physiological conditions. Scale bars represent $50 \mu\text{m}$. 5×10^4 cells were seeded on top of the gel surface in each well.

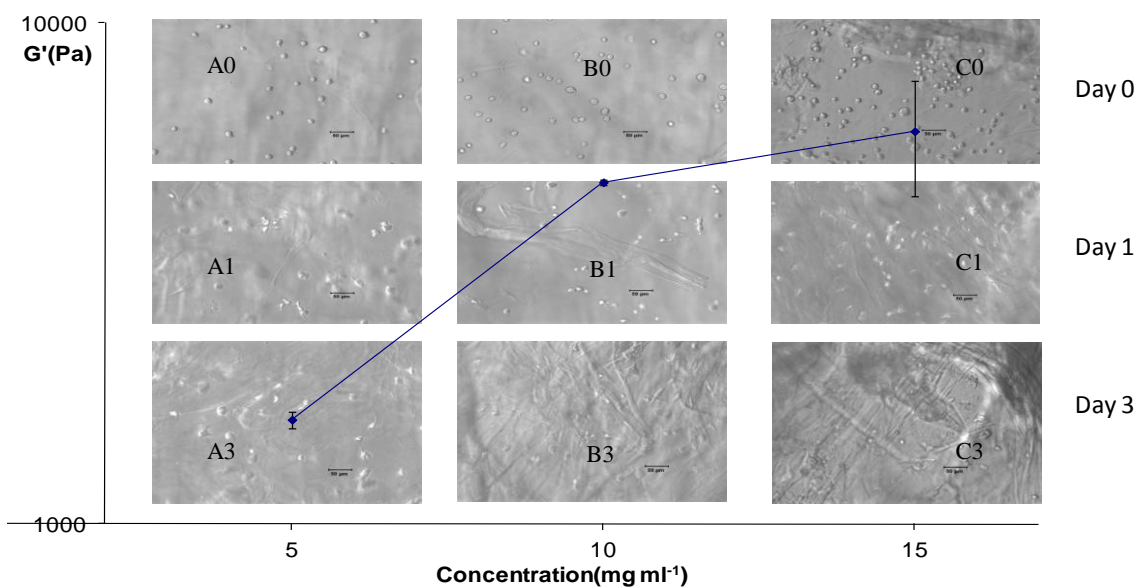


Figure 3.38 Optical micrographs of chondrocyte cell morphology at day0, day1 and day3 of cell culture on the gels prepared by Method 1 at the concentration of 5 mg ml^{-1} (A0, A1, A3), 10 mg ml^{-1} (B0, B1, B3) and 15 mg ml^{-1} (C0, C1, C3). Optical micrographs were overlapped with the rheological tests results of all three types of gels before cell seeding. All the samples were at physiological conditions. Scale bars represent $50 \mu\text{m}$. 5×10^4 cells were seeded on top of the gel surface in each well.

Figure 3.38 shows the optical micrographs on FEFEFKFK peptide gels prepared by Method 1. Cells retained their round shape morphology on all hydrogels. No difference of cell morphology was observed between the gels at different peptide concentrations.

Although the rheological tests showed the gels at higher concentrations had a significantly higher G' , which means the gels at higher concentrations were much stronger than those at lower concentrations, cells seeded on top of all three gels still had the same morphology.

Figure 3.39 showed the fluorescence micrographs of FEFKFK peptide stained by Live/dead after 7 days of cell culture. An average of 150 cells was counted on each gel. Over 99% of the cells were stained green on all the gel surfaces.

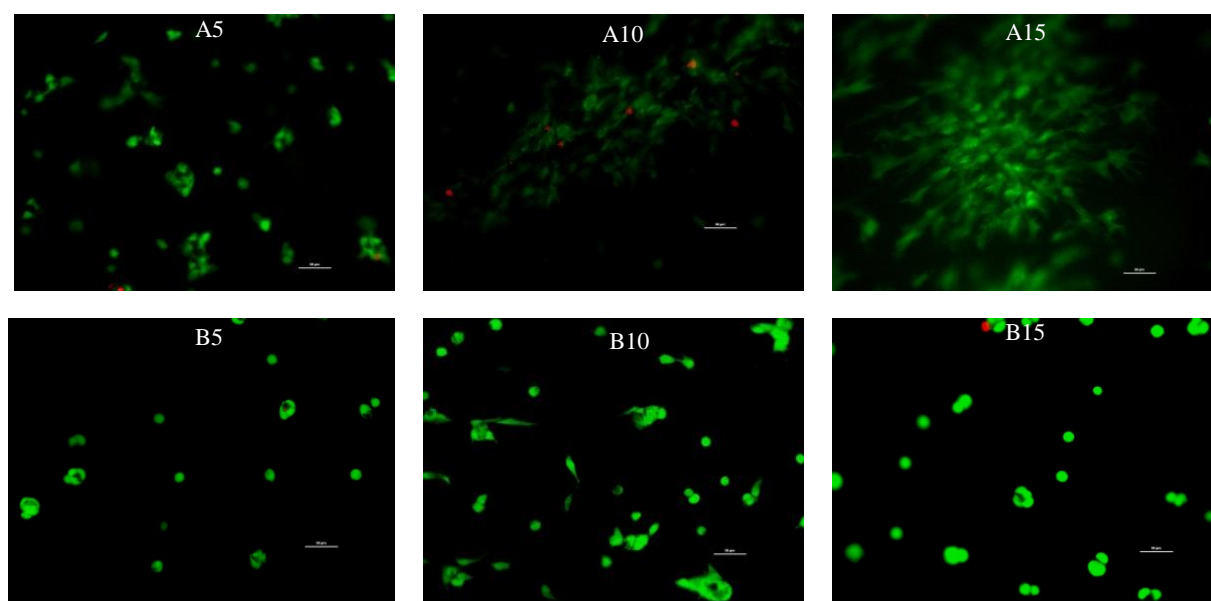


Figure 3.39 Fluorescence micrograph of chondrocyte cell viability 7 days post cell culture on the gels prepared by Method 1 (A5, A10, A15) and Method 2 (B5, B10, B15) at concentrations of 5 mg ml^{-1} (A5, B5), 10 mg ml^{-1} (A10, B10) and 15 mg ml^{-1} (A15, B15). Scale bars represent $50 \mu\text{m}$. 5×10^4 cells were seeded on top of the gel surface in each well.

In conclusion, cells were alive on the gels prepared by both methods at three different gel concentrations. This indicated that the FEFKFK peptide gels studied were biocompatible. There was no difference in cell morphology seeded on the gels prepared by Method 1. However, small differences were observed on the gels prepared by Method 2. Cells were less stretched at the lowest gel concentration, while above the concentration of 10 mg ml^{-1} , no big difference was seen between the different gels. This could be due to the gels being weaker at lower concentration, and cells preferred a stronger scaffold surface to attach to.

The cell behaviours of chondrocyte on FEFKFK peptide were more systematically studied by other researchers in Saiani's group.⁷ Other cell types such as stem cells were also used in the same group to examine the possibility of the FEFKFK peptide hydrogels to be used as tissue culture scaffolds. This project would mainly focus on the

cell behaviour of HDF cells.

3.3.3.3 2D cell culture protocol development for HDF cell

Using the work done on chondrocyte cells as a reference, a 2D cell culture protocol for HDF cells was developed. The effect of NaOH was examined again. Gels at a concentration of 20 mg ml^{-1} were prepared by Method 1 and Method 2 for the HDF cell studies.

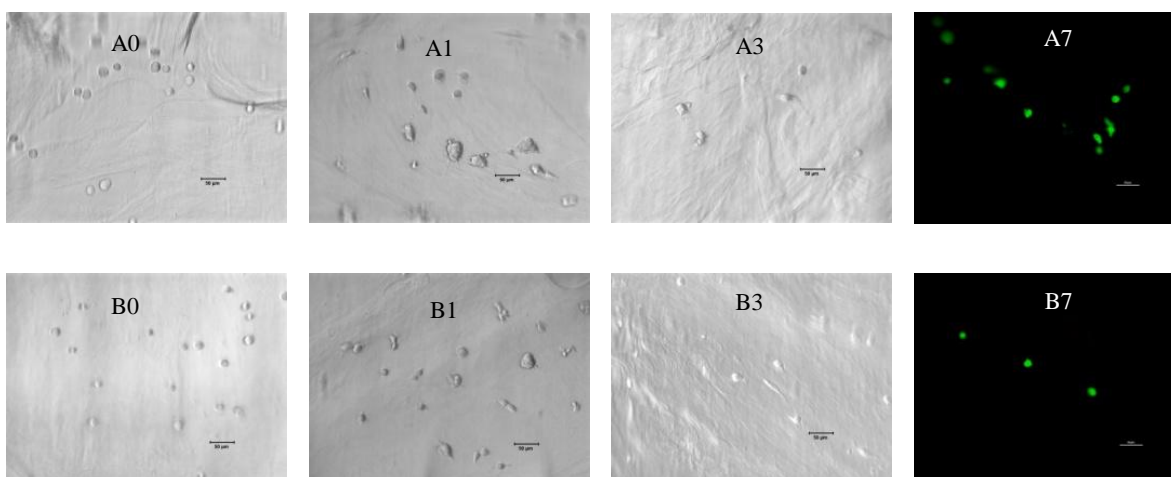


Figure 3.40 Optical micrographs of HDF cell morphology at day0, day1 and day3 of cell culture on the gels prepared by Method 2 (A0, A1, A3) and Method 1 (B0, B1, B3) at a concentration of 20 mg ml^{-1} . Fluorescence micrographs were also presented for HDF cell viability at day7 on the gels prepared by Method 2 (A7) and Method 1 (B7). Scale bars represent $50 \mu\text{m}$. 5×10^4 cells were seeded on top of the gel surface in each well.

As seen in Figure 3.40, cells were green on the fluorescence micrographs after staining by the Live/dead assay. This means cells attached to the gel surfaces after 7 days of cell culture were still alive. No big difference in the cell morphology was observed during cell culture time on the gels prepared by Method 1 and Method 2. The cells remained in a round shape as seeded on both gel surfaces. Clusters of cells were observed on gel surfaces but detached from the gel surfaces during the media change. As no cells spread on either gels with or without NaOH, the effect of NaOH on the cell morphology remained undiscovered. In order for cells to spread on scaffold surfaces, cells need to be firmly attached to the surface. Cells that took a round shape could be the result of a lack of cell attachment on the gel surface.

3.4 Summary

So far in this project, work has focused on the study of the gelation properties of FEFEFKFK peptide. In the beginning of this chapter, the self-assembly process and model proposed by Zhang *et al.* were briefly reviewed. It was confirmed that FEFEFKFK peptide formed nanofibres with anti-parallel β -sheet structure in aqueous solution. Those peptide fibres had a diameter around 3.5 nm which is similar with results published previously.³ The previous work done on FEFEFKFK mainly focused on understanding the self-assembly process and gaining information about the fibre structure. In the first section of this chapter, the main focus was on the investigation of the gel network structure and the gelation properties of FEFEFKFK hydrogels. When the concentration of peptide solution increased, a fibrillar network with a mesh size around 30 nm was observed before gelation occurred. The relationship between the gel network mesh size and gel concentrations was discussed. It was noticed that with increasing hydrogel concentration, the fibre density increased but the mesh size of the network decreased. The phase diagram of FEFEFKFK was mapped out and the thermoreversible behaviour was investigated using the oscillatory rheometry. A solid-like behaviour was observed for FEFEFKFK hydrogels at all concentrations during the rheology studies. Several models were discussed and used to analyse the rheological behaviour of FEFEFKFK hydrogels. The G' and peptide hydrogel concentration as well as the $G(t)$ and peptide hydrogel relaxation time both followed a power law relationship. The study of the power law relationships indicated a lightly cross-linked or entangled network structure in the hydrogels. It was interesting to note a second exponent above gel concentrations of 45 mg ml^{-1} when studying the power law. The possible causes of this large exponent were discussed; however, more work is needed to fully understand the phenomenon. Finally, the reversibility of this gel was investigated. The gel network could be damaged by increasing temperature or applying shear stress, but a quick recovery of the hydrogels was observed after the external stimuli were removed.

Factors including the high water content of the gels, fibrillar network structure, mechanical strength similar to the strength of the components of ECM and possibility of being injectable all promote the potential of this peptide gel system to be used as a mimic of ECM. The gel properties under the influence of the cell culture environment were discussed in the next section. The self-assembly and gelation properties of FEFEFKFK peptide under the influence of pH and ionic strength were then investigated. pH affected

the self-assembly and gelation properties of the FEFKFK peptide by altering the charges of the peptide molecules. Peptide molecules were positively charged in acidic solution. Increasing pH resulted in a decrease of repulsive forces between fibres, which then caused an increase in the mechanical strength of the hydrogels. Peptide molecules were negatively charged in basic solutions. Increasing pH resulted in an opposite observation. It was the first time SANS and SAXS were combined together when studying the pH effect on FEFKFK peptide fibres. A two radius model was used and discussed to obtain more information from the scattering curves. The ionic strength effect was demonstrated by the effect of NaCl. No work has been published regarding the effect of ionic strength on FEFKFK peptide hydrogels. It should be noted that the gels used in this study were not pH adjusted, and all work regarding the effect of ionic strength was taken at pH 2.8 of the original gels. Increasing salt concentration in hydrogels decreased the solubility of peptide molecule in aqueous solution, which promoted the formation of peptide fibres causing a more entangled network structure and strengthened the mechanical properties. Both pH and salt can be used to trigger the transition from a peptide solution to peptide hydrogel. The gel strength could be altered by changing the peptide concentration as well as the pH or salt concentrations. The information gained during the investigation could help engineer the gel properties to fit better with future applications.

Based on the studies of the first two sections, the development of the 2D cell culture protocol was presented in the final section of this chapter. By the time this project started, no cell culture work had been done on the FEFKFK hydrogels. It was very important to develop a cell culture protocol with good reproducibility in order for future cell work using this peptide hydrogel to be correlated. Two different hydrogel preparation methods were developed to meet the basic requirements for tissue culture scaffold. The preliminary tests were done on chondrocyte cells. Cells stayed alive on the gels prepared by either method; however, distinct morphologies of chondrocytes were observed. Chondrocytes remained round in shape on the gels with NaOH in the system, while chondrocytes changed to the fibroblast-like shape on the gels without NaOH in the system. It was interesting to see that the existence of NaOH would affect the differentiation of chondrocytes as NaOH is commonly used in biostudies. However the mechanism behind this phenomenon needs further research. HDF cells were also cultured on these gels for up to 7 days. It was promising to observe the good cell viability 7 days post cell culture. However, HDF cells all remained round on both gel surfaces. HDF takes a spindle-like

shape in a 3D environment and more elongated shapes in 2D. The round shape of HDF on both gel surfaces suggested the lack of cell attachment sites. Preliminary cell culture tests proved the biocompatibility of FEFEFKFK hydrogels and revealed the requirement of further surface modification to promote cell adhesion.

3.5 References

1. Miller, A. F.; Saiani, A., Engineering peptide based biomaterials: structure, properties and application. *Focus on Oligos & Peptides/Chemistry Today* 2010, 28, (1), 34-38.
2. Maslovskis, A.; Saiani, A.; Miller, A. F., Thermoresponsive hydrogels from physical mixtures of self-assembling peptide and its conjugate with PNIPAAm. *Macromolecular Symposia* 2010, 296, 248-253.
3. Saiani, A.; Mohammed, A.; Miller, A. F., 3D networks from self-assembling ionic-complementary octa-peptides. *Macromolecular Symposia* 2007, 251, 88-95.
4. Boothroyd, S.; Saiani, A.; Miller, A. F., Formation of mixed Ionic complementary peptide fibrils. *Macromolecular Symposia* 2008, 273, 139-145.
5. Saiani, A.; Mohammed, A.; Frielinghaus, H.; Collins, R.; Hodson, N.; Kielty, C. M.; Sherratt, M. J.; Miller, A. F., Self-assembly and gelation properties of alpha-helix versus beta-sheet forming peptides. *Soft Matter* 2009, 5, (1), 193-202.
6. Roberts, D.; Rocha, C.; Saiani, A.; Miller, A. F., Effect of peptide and guest charge on the structural, mechanical and release properties of beta-sheet forming peptides. *Langmuir* 2012, 28, 16196-16206.
7. Mujeeb, A.; Miller, A. F.; Saiani, A.; Gough, J. E., Self-assembled octapeptide scaffolds for in vitro chondrocyte culture. *Acta Biomaterialia* 2013, 9, (1), 4609-4617.
8. Marini, D. M.; Hwang, W.; Lauffenburger, D. A.; Zhang, S.; Kamm, R. D., Left-handed Helical Ribbon Intermediates in the Self-Assembly of a beta-sheet Peptide. *Nano Letters* 2002, 2, (4), 295-299.
9. Barth, A.; Zscherp, C., What vibrations tell us about proteins. *Quarterly Reviews of Biophysics* 2002, 35, (4), 369-430.
10. Barth, A., Infrared spectroscopy of proteins. *Biochimica et Biophysica Acta* 2007, 1767, 1073-1102.
11. Giacomelli, C. E.; Valenti, L. E.; Paci, M. B.; De Pauli, C. P., Infrared study of trifluoroacetic acid unpurified synthetic peptides in aqueous solution: Trifluoroacetic acid removal and band assignment. *Analytical Biochemistry* 2011, 410, (1), 118-123.
12. Boothroyd, S. Peptide Self-assembly: Controlling Conformation and Mechanical Properties. PhD dissertation, the University of Manchester, Manchester, 2011.
13. Guenet, J. M., Structure versus rheological properties in fibrillar thermoreversible gels

from polymers and biopolymers. *Journal of Rheology* 2000, 44, (4), 947-960.

14. Guilbaud, J.-B.; Saiani, A., Using small angle scattering (SAS) to structurally characterise peptide and protein self-assembled materials. *Chemical Society Reviews* 2011, 40, 1200-1210.
15. Miller, A. F.; Yan, H.; Frielinghaus, H.; Nykanen, A.; Ruokolainen, J.; Saiani, A., Thermoreversible lysozyme hydrogels: properties and an insight into the gelation pathway. *Soft Matter* 2008, 4, (6), 1313-1325.
16. Guinier, A.; Fournet, G., *Small-angle Scattering of X-rays*. John Wiley & Sons, Inc.: New York, 1955.
17. Kavanagh, G. M.; Ross-Murphy, S. B., Rheological characterisation of polymer gels. *Progress in Polymer Science* 1998, 23, (3), 533-562.
18. Ferry, J. D., *Viscoelastic properties of polymers*. 3rd ed.; John Wiley & Sons, INC.: New York, 1980.
19. Guenet, J.-M., *Thermoreversible Gelation of Polymers and Biopolymers*. Academic Press Limited: London, 1992.
20. Mackintosh, F. C.; Kas, J.; Janmey, P. A., Elasticity of semiflexible biopolymer networks. *Physical Review Letters* 1995, 75, (24), 4425-4428.
21. Janmey, P. A.; Euteneuer, U.; Traub, P.; Schliwa, M., Viscoelastic properties of vimentin compared with other filamentous biopolymer networks. *Journal of Cell Biology* 1991, 113, (1), 155-160.
22. Storm, C.; Pastore, J. J.; MacKintosh, F. C.; Lubensky, T. C.; Janmey, P. A., Nonlinear elasticity in biological gels. *Nature* 2005, 435, (7039), 191-194.
23. Jones, J. L.; Marques, C. M., Rigid polymer network models. *Journal De Physique* 1990, 51, (11), 1113-1127.
24. Yan, C.; Altunbas, A.; Yucel, T.; Nagarkar, R. P.; Schneider, J. P.; Pochan, D. J., Injectable solid hydrogel: mechanism of shear-thinning and immediate recovery of injectable beta-hairpin peptide hydrogels. *Soft Matter* 2010, 20, 5143-5156.
25. Invitrogen Technical Resources - Media Formulations 21885 - DMEM, low glucose, GlutaMAX(TM), pyruvate. http://www.invitrogen.com/site/us/en/home/support/Product-Technical-Resources/media_formulation.313.html (27 09 2011),
26. Roe, R.-J., *Methods of X-ray and Neutron Scattering in Polymer Science*. Oxford University Press: New York, 2000.
27. CRC handbook of chemistry and physics. In 92nd ed.; Haynes, W. M., Ed. CRC Press: Boca Raton, 2011.
28. PepCalc.com Peptide property calculator. <http://www.innovagen.se/custom-peptide-synthesis/peptide-property-calculator/peptide-property-calculator.asp> (16/05/2012),
29. Ye, Z.; Zhang, H.; Luo, H.; Wang, S.; Zhou, Q.; Du, X.; Tang, C.; Chen, L.; Liu, J.; Shi, Y.-k.; Zhang, E.-y.; Ellis-behnke, R.; Zhao, X., Temperature and pH effects on biophysical and

morphological properties of self-assembling peptide RADA16-1. *Journal of Peptide Science* 2008, 14, 152-162.

30. Yan, H.; Nykanen, A.; Ruokolainen, J.; Farrar, D.; Miller, A. F., Protein fibrillar hydrogels for three-dimensional tissue engineering. *Research Letters in Nanotechnology* 2009, 2009.

31. Ji, Z.; Jin, X.; George, S.; Xia, T.; Meng, H.; Wang, X.; Suarez, E.; Zhang, H.; Hoek, E. M. V.; Godwin, H.; Nel, A. E.; Zink, J. I., Dispersion and stability optimization of TiO₂ nanoparticles in cell culture media. *Environmental Science & Technology* 2010, 44, (19), 7309-7314.

32. Genes, N. G.; Rowley, J. A.; Mooney, D. J.; Bonassar, L. J., Effect of substrate mechanics on chondrocyte adhesion to modified alginate surfaces. *Archives of Biochemistry and Biophysics* 2004, 422, 161-167.

Chapter 4 Functionalized peptide and HDF cell culture

4.1 Introduction

To improve cell attachment to biomaterials, a variety of bioactive ligands can be introduced to enhance the bioactivity of a scaffold. Among all the bioactive ligands, RGD is the most well-known and commonly used, providing binding sites to a variety of cells including human dermal fibroblast (HDF) cells. At this stage, a peptide synthesis company Peptisyntha was involved in this project. A short peptide 3-mercaptopropionyl-homoarginine-glycine-aspartic acid-tryptophan-proline (Mpr-hRGDWP) was provided by the company. In this sequence, an amino acid derivative homoarginine (hR), with one more CH_2 group on the side chain (Figure 4.1) compared to R, was used to replace R in the RGD sequence. A great amount of work has been conducted investigating how RGD functions, including studying the alternative sequences of RGD. For example, glutamic acid (E) was used to replace aspartic acid (D). With only one less CH_2 group on the side chain of E, RGE showed no bioactivity at all.¹ Similarly, when arginine (R) was replaced by lysine (K) or when glycine (G) was replaced by alanine (A), the cell binding ability was reduced.² So far, no substitution of RGD has been found to have the same bioactivity. hRGD has not been reported as a substitution of RGD before, thus the bioactivity of this peptide remain unknown. The previous work done on finding the substitution of RGD was always replacing one of the amino acid with another amino acid having a similar structure. However, the replacements were all more hydrophobic than the original amino acids. Here in this project, although hR has one more CH_2 on the side chain than R, it does not reduce the charged side groups as K would do. The extended side chain might help the charged side groups to be exposed to the cell. Hence, it has a high possibility to be used as a replacement of R. The effect of hRGD on cell adhesion was examined in this project, which has not been studied by others.

In this chapter, the results presented demonstrated how hRGD was successfully linked to FEFKFK peptide. The functionalised peptide formed gels in aqueous solutions and the gels were characterised by various techniques. It was postulated that the octapeptide would self-assemble into fibres while hRGDs present on the fibre surfaces. The cells may then recognise hRGDs and bind to them. Therefore in the later part of this chapter, the results of cell behaviours both on the gel surface and within the gels were included to show the

influence of the peptide modification on cell behaviours.

4.2 Functionalised peptide hydrogel

4.2.1 Peptide synthesis

The Mpr-hRGDWP peptide was introduced to the backbone of FEFEFKFK peptide by the solid phase peptide synthesis and the functionalised Mpr-hRGDWPFEFEFKFK peptide (``hRGD``) was gained.

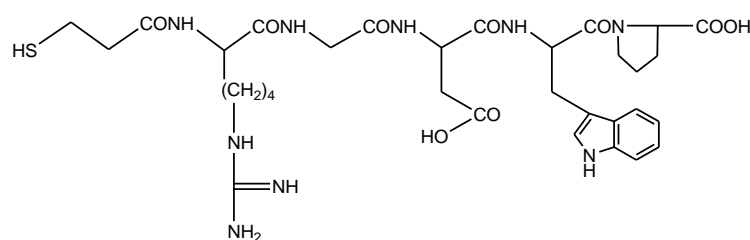


Figure 4.1 The structure of Mpr-hRGDWP.

The HPLC spectrum of the product after the first coupling to link Mpr-hRGDWP onto FEFEFKFK clearly showed two major peaks (Figure 4.2 C). HPLC elution solutions of those two peaks were then collected and examined by MALDI-TOF MS. Figure 4.2 A is the MS spectrum of peak 1 in Figure 4.2 C. Since a positive mode was used during the tests. The mass/charge ratio of the peak is the value of the molar mass of a cation associated molecule. The major peak showed a mass/charge ratio of 1121.52 which was very close to the molar mass of one H associated FEFEFKFK (1122). Figure 4.2 B is the MS spectrum of peak 2 in Figure 4.2 C. The major peak showed a mass/charge ratio of 1836.05 which was very close to the molar mass of one H associated ``hRGD`` (1835). Then a second coupling was performed and the final product after the coupling was run through HPLC again. After the second coupling, peak 1 significantly shrank while the area of peak 2 was enlarged to 60 % (Figure 4.2 D).

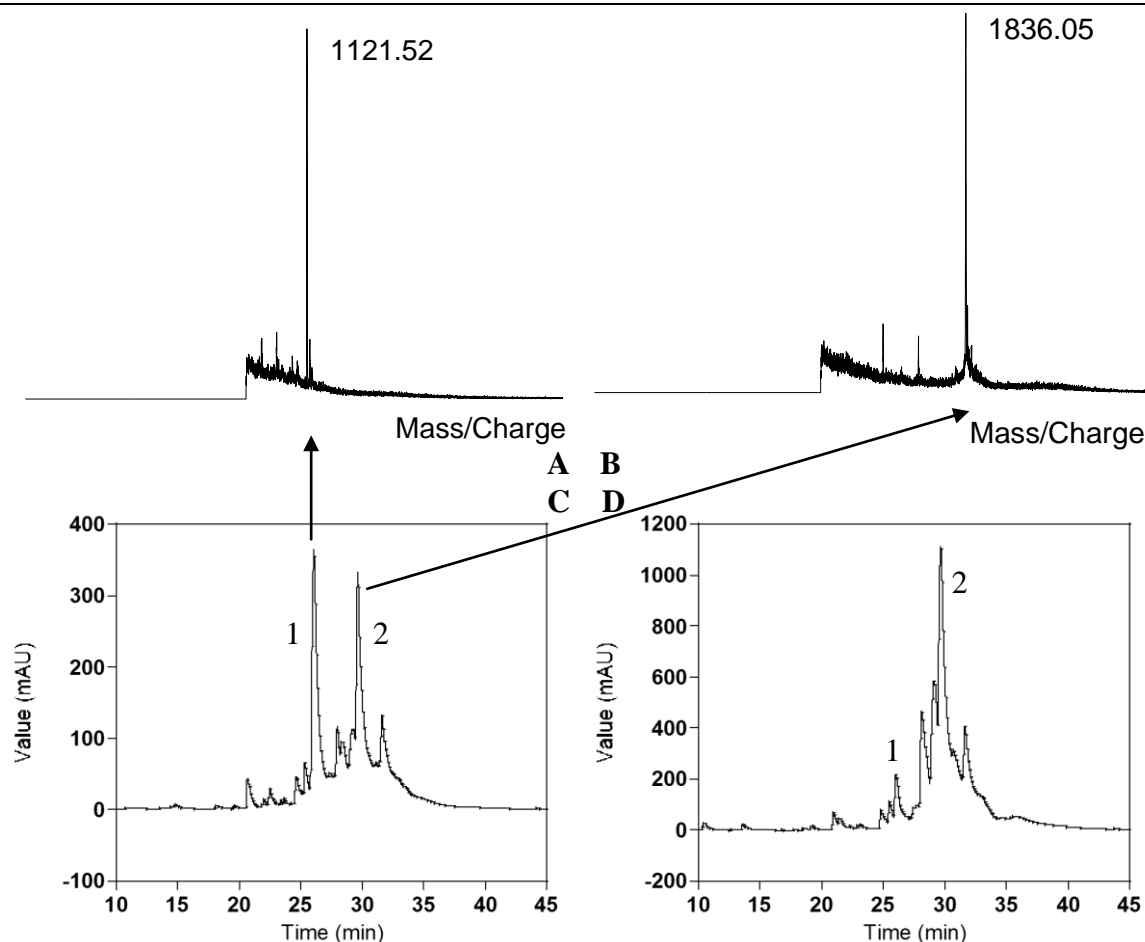


Figure 4.2 A, B) MALDI-TOF MS spectra of two HPLC elution solutions corresponding to the two major peak 1 and 2 in HPLC spectra respectively; The number beside each peak represents the molecular weight of $[M-H]^+$. C) HPLC spectrum of the product after the first coupling to link Mpr-hRGDWP on FEFEFKFK; D) HPLC spectrum of the product after repeating the coupling.

Further LC-MS tests (done by Peptisyntha) showed that the final product contained ``hRGD``, ``hRGD``+F, ``hRGD``+F+F, FEFEFKFK, FEFEFKFK+F. This suggested that most impurities in the final product came from miscoupling during the synthesis of FEFEFKFK. In total, around 80 % of the final products were functionalised with the short hRGD peptide. In summary, Mpr-hRGDWP was successfully linked to FEFEFKFK. The final product was named by its major component ``hRGD`` peptide.

The previous studies showed that FEFEFKFK in water can self-assemble into fibres with an anti-parallel β -sheet structure, and macroscopically form transparent hydrogels (Section 3.1). After being coupled twice with Mpr-hRGDWP, 80 % of peptides were loaded with Mpr-hRGDWP. Further experiments on the self-assembly and gelation properties of ``hRGD`` (the functionalized peptide) were described as follows.

4.2.2 Functionalised peptide hydrogel properties

By comparing ``hRGD`` with FEFEFKFK, it can help to gain a better understanding of the self-assembly and gelation properties of ``hRGD``, the role of ``hRGD`` in cell culture studies and how cell behaviour could be related to the properties of the gel matrix. The comparison between the two peptides should be taken in the same experimental conditions. Thus, the hydrogel properties of the functionalised peptide were also examined at pH 2.8.

The samples of the functionalised peptide were also prepared as described in Section 2.3.1 and the phase diagram of ``hRGD`` was mapped (Figure 4.3).

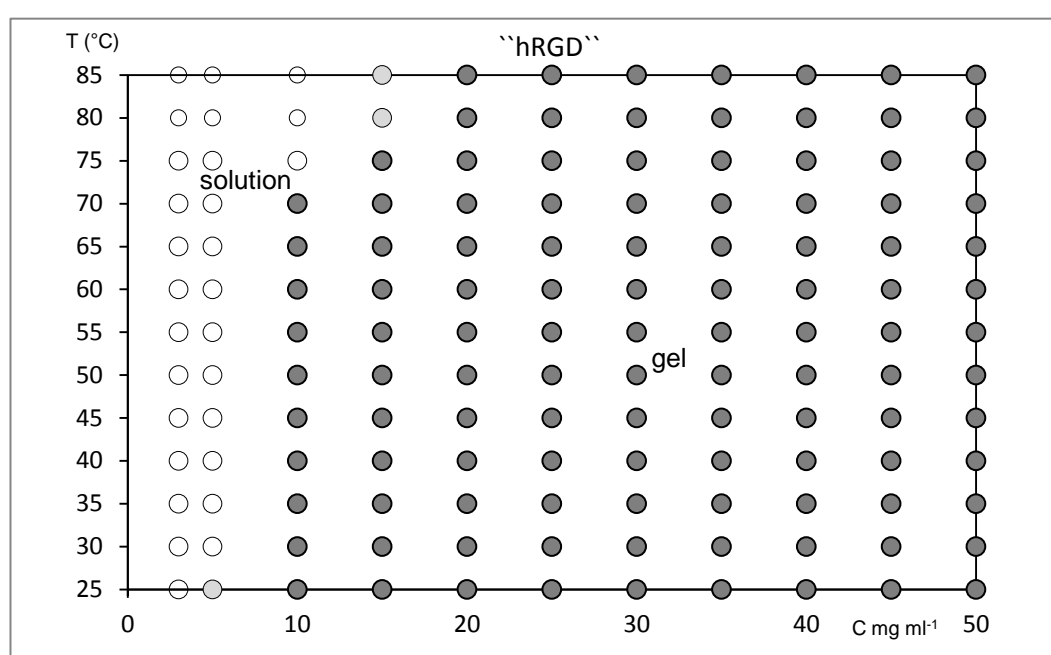


Figure 4.3 The phase diagram of ``hRGD`` peptide shows the variation of gel (dark solid circle), viscous liquid (light solid circle) and solution (empty circle) as a function of temperature. All the samples were at pH 2.8.

As shown in Figure 4.3, the critical gelation concentration of ``hRGD`` was between 5 to 10 mg ml⁻¹. All the gels were transparent and thermal-stable at 37 °C. Compared to FEFEFKFK (Section 3.1.2), ``hRGD`` started to gel at a lower concentration. The reason may be that when the octapeptide backbone in ``hRGD`` begins to self-assemble and form fibres, the Mpr-hRGDWP sequences extend out from the fibres act like positively charged branches providing more rigid fibres to form a 3D network. Thus, the gelation can occur at a lower peptide concentration.

With the postulation that Mpr-hRGDWP acts like branches and provides more positively charged side chains, the ``hRGD`` fibres would become more rigid, which should be more

resistant to shear force. Thus the ``hRGD`` gels should be stronger than the FEFEFKFK gels at the same peptide concentration. The mechanical strength of ``hRGD`` gels was tested using oscillatory rheometer. The results are shown below.

The amplitude sweep was carried out first to determine the LVR of all the samples. The LVR was noticed below 2% strain. It can be seen that all G' is higher than G'' in the LVR indicates all the samples are in the gel form. This can also be confirmed by the values of all $\tan\delta$ in the LVR which are smaller than 0.2. The gels with such small $\tan\delta$ have more solid-like behaviours. As concentration increases, both G' and G'' increases in the LVR. 1 % strain in the LVR was chosen for the frequency sweep.

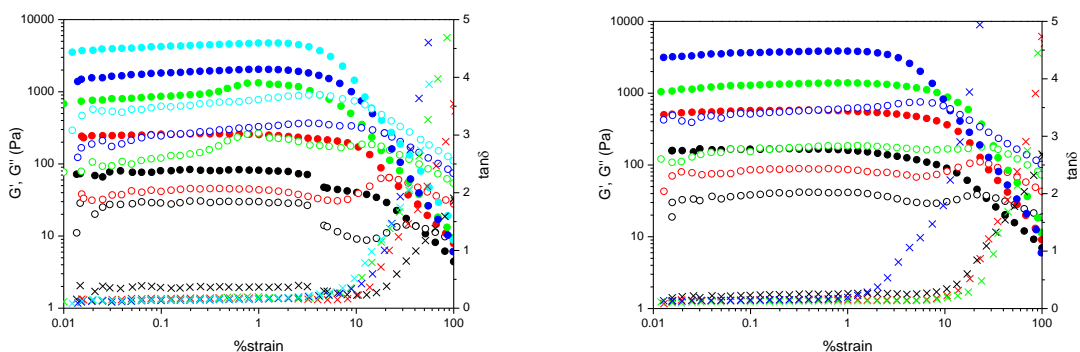


Figure 4.4 Plot of elastic modulus (G' , solid), viscous modulus (G'' , empty) and $\tan\delta$ (\times) of ``hRGD`` peptide at 10 (black), 20 (red), 30 (green), 40 (blue) and 50 (cyan) on the left while 15 (black), 25 (red), 35 (green), 45 (blue) on the right as a function of strain from 0.01% to 100% at 1 Hz at 20 °C in the logarithmic scale. All the samples were at pH 2.8.

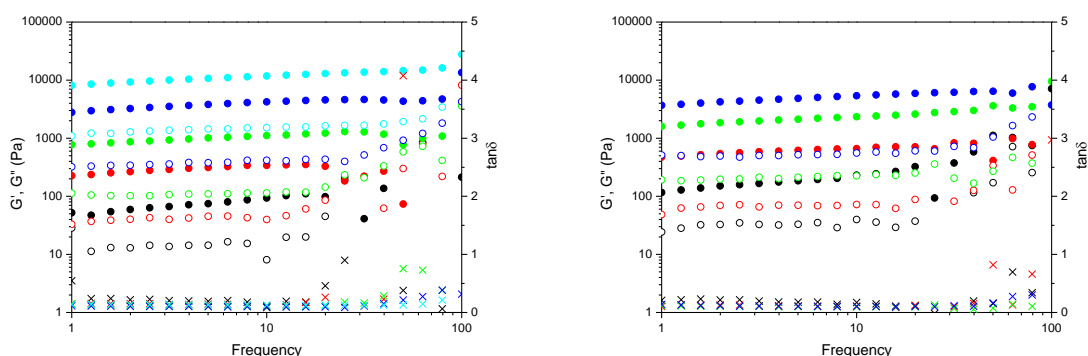


Figure 4.5 Plot of elastic modulus (G' , solid), viscous modulus (G'' , empty) and $\tan\delta$ (\times) of ``hRGD`` peptide at 10 (black), 20 (red), 30 (green), 40 (blue) and 50 (cyan) on the left while 15 (black), 25 (red), 35 (green), 45 (blue) on the right as a function of frequency from 1 to 100 Hz at 1% strain at 20 °C in the logarithmic scale. All the samples were at pH 2.8.

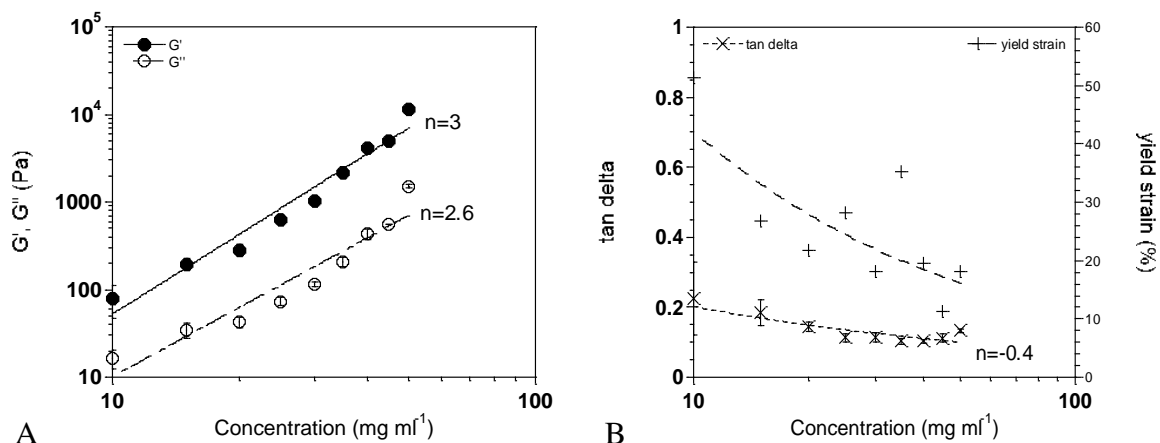


Figure 4.6 A) Plot of elastic modulus (G' , ●), viscous modulus (G'' , ○) of hRGD peptide as a function of concentration in the logarithmic scale. B) Plot of $\tan \delta$ (×) and yield strain (+) of hRGD peptide as a function of concentration. G' , G'' and $\tan \delta$ are the average values in the frequency independent region in Figure 4.5 and were tested at 1 % strain; the yield strain is from Figure 4.4 and was tested at 1 Hz; n represents the slope of the fitted line which is also the power law exponent. The solid line (—) represents a fitting of G' against concentration. The large/small dash line (- - -) represents a fitting of G'' against concentration. The small dash line (-----) represents a fitting of $\tan \delta$ against concentration. All the samples were at pH 2.8.

All the samples show independence from frequency when below 10 Hz. It can be seen again that all G' is higher than G'' in the frequency independent region as well as the small $\tan \delta$ of all the samples. The mechanical properties of those gels were presented by the average value of G' , G'' and $\tan \delta$ in the frequency independent region which were plotted against peptide concentration in Figure 4.6. The yield strain was also obtained from Figure 4.4 and plotted against peptide concentration. The relations between G' and C as well as G'' and C follow the power law, and the slopes of the fitted lines are 3 and 2.6 respectively. According to $\tan \delta = G''/G'$, the relation of $\tan \delta$ and C should also follow the power law with an exponent of -0.4. This perfectly matches the value gained from the experiments. In general, the yield strain of peptide hydrogels slightly decreases with increasing gel concentrations. This indicates the gels are more brittle at high concentrations.

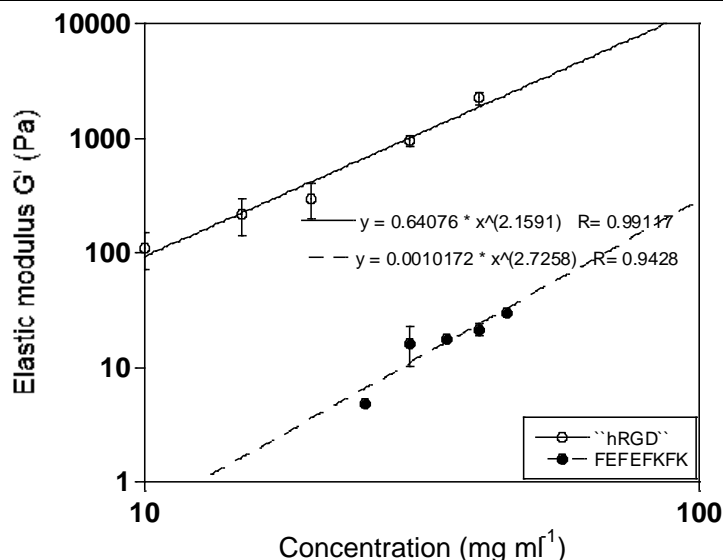


Figure 4.7 Plot of G' of the hRGD (empty circle) and FEFEFKFK gels (solid circle) as a function of peptide concentrations. The solid line (—) represents a fitting of G' of the hRGD gels against concentration. The dash line (---) represents a fitting of G' of the FEFEFKFK gels against concentration. All the samples were at pH 2.8.

The average values of G' at lower gel concentrations were plotted against the concentrations of the hRGD gels in Figure 4.7 to compare with the mechanical strength of FEFEFKFK gels tested in Chapter 3. The hRGD gels are stronger at the same concentration. The relation between G' and the hRGD gel concentrations below 40 mg ml⁻¹ also follows a power law with an index around 2.2. This exponent indicates an entangled network structure inside the peptide gels.³ When the data from the whole concentration range were used, an exponent of 3 was obtained, which means a faster increase of G' at higher hRGD gel concentrations. The mechanism behind this could be similar to the sharp increase of G' of FEFEFKFK peptide at high gel concentrations. Octapeptide FEFEFKFK itself forms both branching fibres and entangled fibres. The gel structure could be considered close to chemically cross-linked gels. In hRGD gels, the Mpr-hRGDWP at the end of the molecule might inhibit the formation of branching fibres. At the meantime Mpr-hRGDWP can serve as positively charged branches. It was noticed in the previous study that rigid short peptide sequence introduced to FEFEFKFK would stick out from the edge of the fibril.⁴ It can be seen in Figure 4.1 that the two linking amino acids are rigid and bulky, thus the end of hRGD was expected to stick out from the edge of the fibril, which can be treated as branches. The two linkers could make individual fibres more rigid which can increase the strength of the network.

4.2.3 Fibre morphology and network structure

The fibre structures of the ``hRGD`` gels were examined by FTIR. A series of the ``hRGD`` peptide gels were prepared. As shown in Figure 4.8, all the samples had a strong peak around 1625 cm^{-1} which represented the existence of the β -sheet structures, and a weak peak around 1690 cm^{-1} which means that the β -sheet structure was an anti-parallel β -sheet⁵. This suggested that ``hRGD`` also forms fibres with an anti-parallel β -sheet structure similar to those of FEFKFKFK.

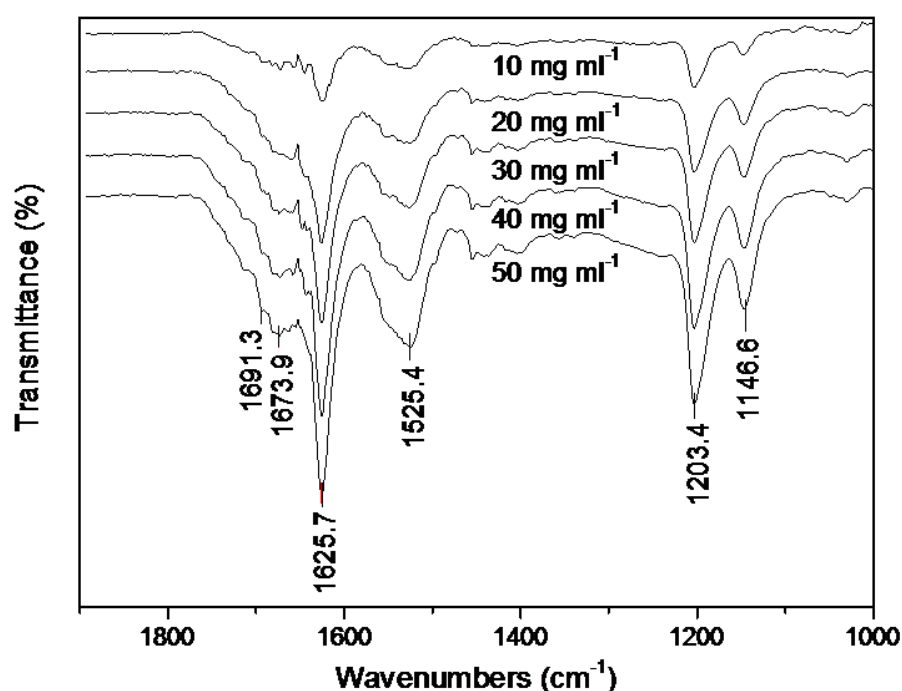


Figure 4.8 FTIR spectra of ``hRGD`` peptide at different concentrations. All the samples were at pH 2.8.

TEM was used to visually confirm the fibre morphology. A dense fibrillar network structure was observed for the self-assembled ``hRGD`` fibres. The average fibre diameter is 4.0 nm. This is close to the average fibre diameter of 3.5 nm described in Chapter 3, but slightly increased. This could be because the fibres were formed by FEFKFKFK sequence in the backbone of ``hRGD``, while the Mpr-hRGDWP attached to the surfaces of the fibres.

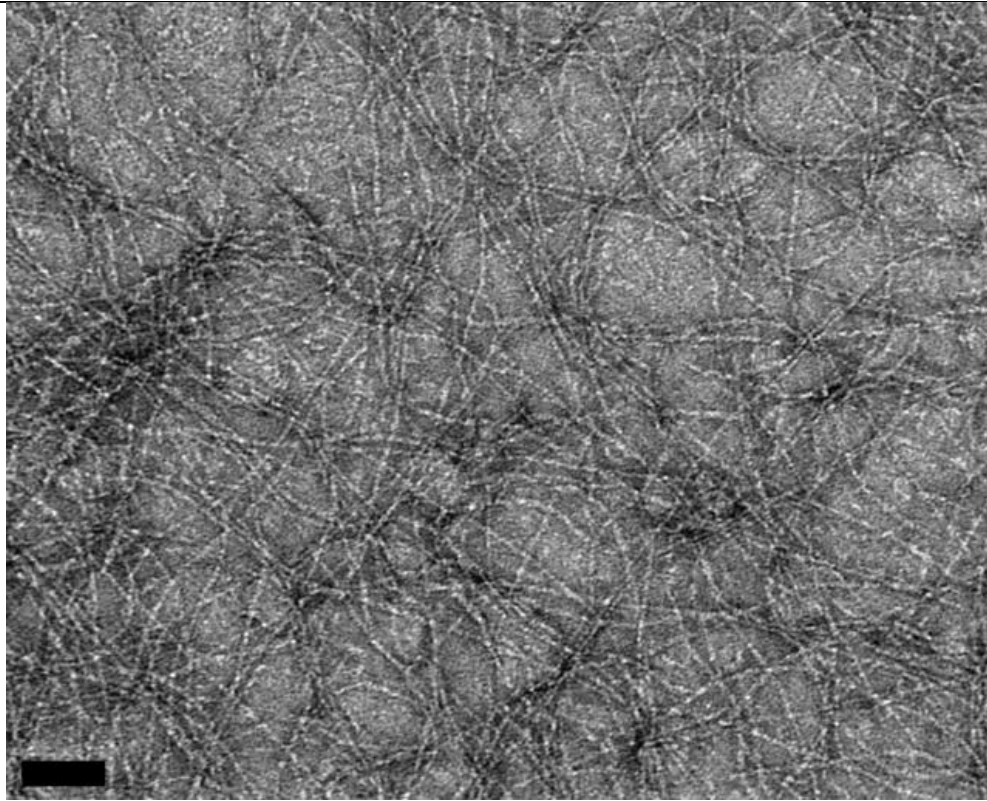


Figure 4.9 TEM image of 5 mg ml^{-1} hRGD peptide solution at pH 2.8 shows a dense fibrillar network. Scale bar presents 50 nm.

As a complementary technique of TEM, the SANS technique was used to study the fibre morphology of hRGD peptide. To gain the information of a single fibre, the experiment has to be done in the dilute regime where the inter-particle scattering is negligible. The samples at the concentrations of 3 mg ml^{-1} , 5 mg ml^{-1} , 10 mg ml^{-1} and 20 mg ml^{-1} were prepared to see what the fibre morphology was.

Figure 4.10 presents the absolute scattering intensity I_A as a function of q at different salt concentrations in the logarithmic scale. No maximum of intensity shows on the curves but a small shoulder can be seen on the curve of the 20 mg ml^{-1} hydrogel. This indicates the inter particle scattering is negligible except for the 20 mg ml^{-1} hydrogel, which also means the experiments were taken in the dilute regime for samples at 3 mg ml^{-1} , 5 mg ml^{-1} and 10 mg ml^{-1} . Different models were used to study the SANS pattern, but all the patterns were developed for dilute samples. Hence only the samples at 3 mg ml^{-1} , 5 mg ml^{-1} and 10 mg ml^{-1} were analysed from now on. All the curves in Figure 4.10 of the low q range were fitted by Equation 3.4 and the exponent values were all around 1.2, which was close to 1. The exponent α is equal to 1 for thin rods. This suggested the fibres both in solutions and gels might adopt rod-like structures.

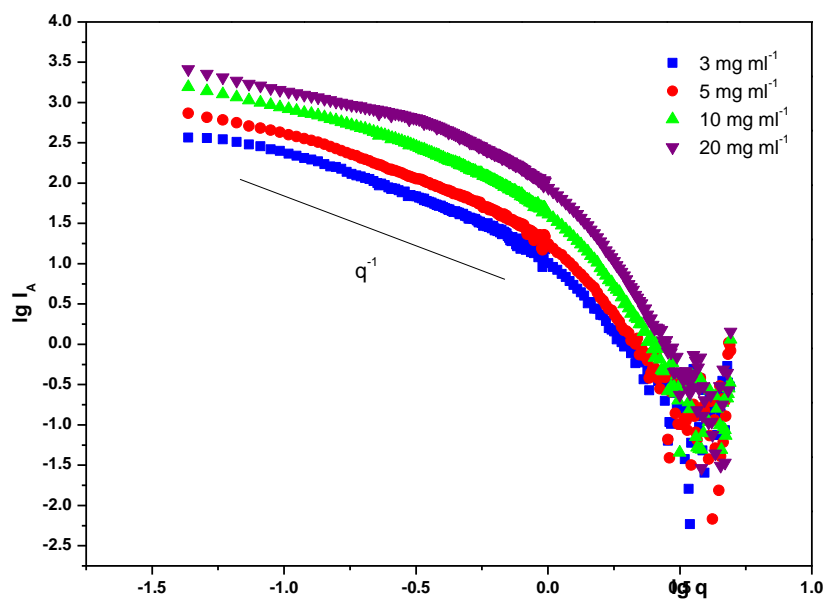


Figure 4.10 Plot of $\lg I_A$ against $\lg q$ of ``hRGD`` peptide at concentrations of 3 mg ml^{-1} (blue), 5 mg ml^{-1} (red) and 10 mg ml^{-1} (green) and 20 mg ml^{-1} (purple) tested by SANS. All the samples were at pH 2.8.

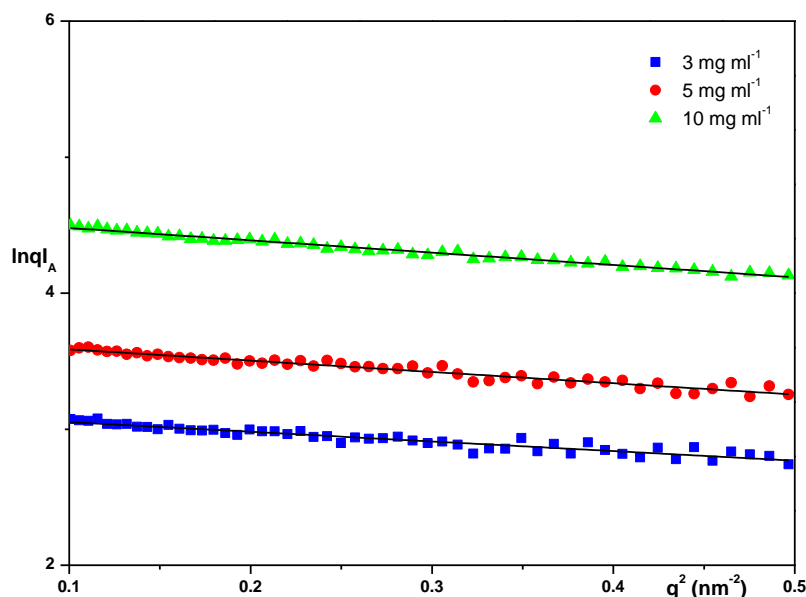


Figure 4.11 Porod plot ($\ln q I_A$ against q^2) of FEFEFKFK peptide at concentrations of 3 mg ml^{-1} (blue), 5 mg ml^{-1} (red) and 10 mg ml^{-1} (green) tested by SANS. Solid lines represent the best fit by using Equation 3.6. All the samples were at pH 2.8.

Since a rod-like structure was suggested by the previous result, the Porod graphs which are used to estimate the dimension of scattered matters were drawn as shown in Figure 4.11 which were the plots of $\ln q I_A$ against q^2 . The linear curves should be gained by fitting the original data with Equation 3.6 and the slopes of the lines would provide the dimensions of the fibres. The fitted curves were shown in Figure 4.11. The values of R_σ from the fitted curves were 1.2 for all the 3 samples. This further confirmed the fibres both in solutions

and gels had the same thickness.

The Porod graph gives the dimensions of the scattered matter without regard to the shape of the scattered object. In order to further study the morphology of the fibres with a rod-like structure, the Kratky curves of ``hRGD`` peptide at different concentrations were analysed (Figure 4.12). The bell-like shape of the curves at all concentrations suggested rod-like structures in all systems. By using Equation 3.7, a full cylinder model was fitted to the original data. The fitted graphs were presented in Figure 4.12.

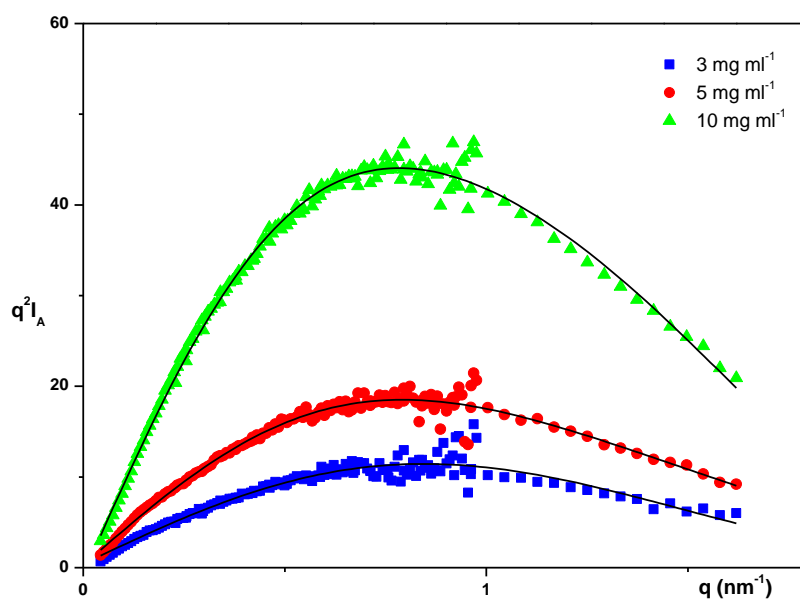


Figure 4.12 Kratky plot (q^2I_A against q) of peptide ``hRGD`` at concentrations of 3 mg ml^{-1} (blue), 5 mg ml^{-1} (red) and 10 mg ml^{-1} (green) tested by SANS. Solid lines represent the best fit by using Equation 3.7. All the samples were at pH 2.8.

The values of r were obtained through data fitting. The rod-like fibres with radii of 1.6 nm were found at all peptide concentrations. This is very close to the diameter of FEFKFK peptide fibres which suggested the fibres were formed by the FEFKFK sequence of the ``hRGD`` backbones. The same fibre radii also suggested the fibres both in solutions and gels had the same thickness. Similar observation was found in FEFKFK system.⁶ However, the radius obtained by SANS was smaller than the radius obtained by TEM. This could be caused by the different sample preparation procedures. The fibres examined by SANS were in their hydrated states while the fibres studied by TEM were dried out during the preparation. The dried fibres were flattened on the grids which could lead to larger diameters.

4.3 2D HDF cell culture

4.3.1 2D HDF cell culture protocol development

As discovered in the previous chapter, NaOH had a significant influence on the spreading of chondrocyte cells. To prevent the possible inhibition effect of NaOH on the HDF cell spreading, the ``hRGD`` gels were prepared in Method 2 as described in Section 3.3.2.

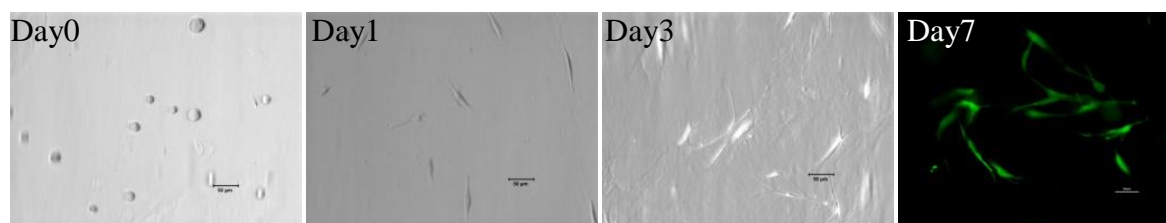


Figure 4.13 Optical micrographs of HDF on ``hRGD`` gel surfaces during 7 days of cell culture show the cells adopt a spindle shape. Fluorescence micrograph shows the living (green) and dead (red) cells on gel surfaces 7 days post cell culture. Scale bars represent 50 μm . 5×10^4 cells were seeded on top of the gel surface in each well.

The same HDF cell density used in Section 3.3.5 were also applied here. Within the first 24 hours of culture, over 95 % out of 105 counted HDF cells started to spread on the ``hRGD`` gel surfaces, which indicated a direct cell adhesion. The spindle like elongated cell morphologies were observed 1 day and 3 days post culture. This cell morphology was also confirmed by fluorescence microscopy, which showed the cells stained by Live/dead assay solutions at 7 days post culture. All cells stained green, it demonstrated that after 7 days of culturing, All cells were alive on the ``hRGD`` gel surface as well. As discovered in Section 3.3.5, the cells were alive after 7 days of culturing, however, the HDF cells remained round or just started spreading on both FEFKFKFK gels with or without NaOH. Compared to those, the ability of HDF cells to spread on the ``hRGD`` gels shows a greatly improved cell adhesion.

It has been reported before that HDF cells had better cell adhesion on the stiffer gel surfaces⁷. To estimate the influence of the mechanical properties on cell behaviours, the rheology tests were performed on the three gels mentioned above. The gels were tested before cell seeding after 1, 3 and 7 days of cell culture on the gel surface.

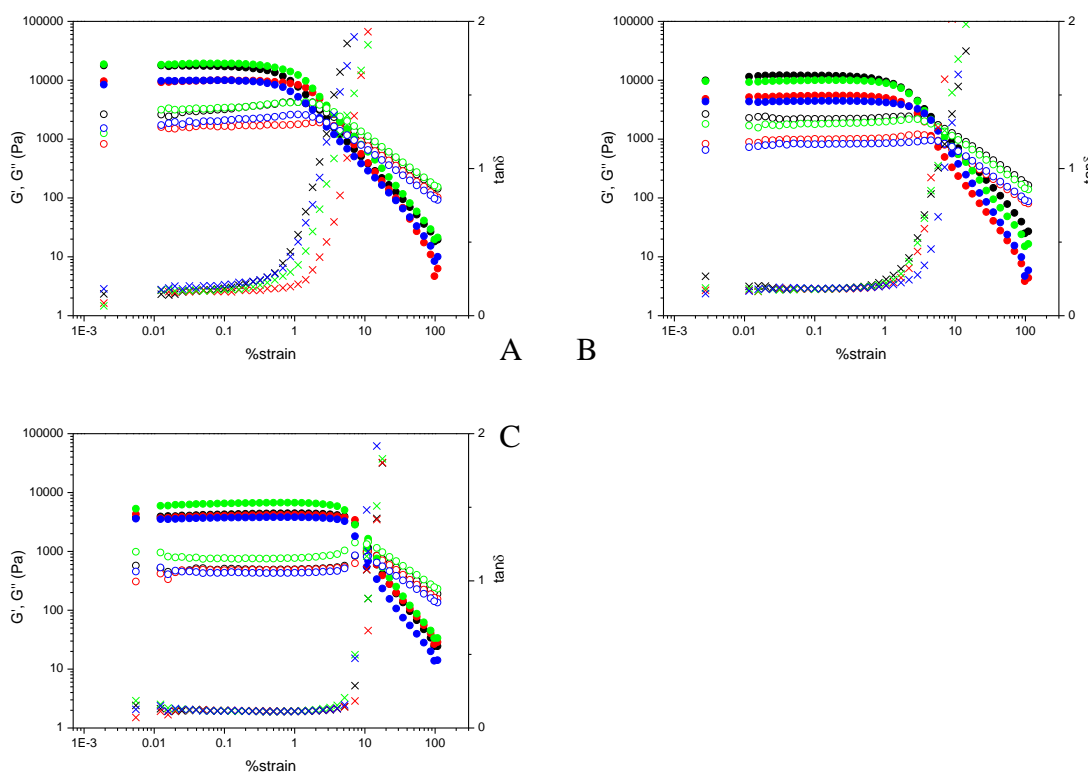


Figure 4.14 Plot of elastic modulus (G' , solid), viscous modulus (G'' , empty) and $\tan\delta$ (\times) of FEFKFK (A) at cell culture day0 (black), day1 (red), day3 (green) and day7 (blue); FEFKFK+NaOH (B) at cell culture day0 (black), day1 (red), day3 (green) and day7 (blue) and ``hRGD`` (C) at cell culture day0 (black), day1 (red), day3 (green) and day7 (blue) as a function of strain from 0.01% to 100% at 1 Hz at 37 °C in the logarithmic scale. All the samples were at physiological conditions.

The amplitude sweep was carried out first to determine the LVR of all the samples. The LVR was noticed below 1 % strain. It can be seen that all G' is higher than G'' in the LVR indicates all the samples are in the gel form. This can also be confirmed by the values of all $\tan\delta$ in the LVR is smaller than 0.2. The gels with such small $\tan\delta$ have more solid-like behaviours. As cell culture time increases, no big difference of G' and G'' was observed in the LVR. 1% strain in the LVR was chosen for the frequency sweep.

All the samples show independence from frequency when below 100 Hz in Figure 4.15. It can be seen again that all G' is higher than G'' in the frequency independent region as well as the small $\tan\delta$ of all the samples. The mechanical properties of those gels were presented by the average value of G' , G'' and $\tan\delta$ in the frequency independent region which were plotted against the cell culture time in Figure 4.16. The yield strain was also obtained from Figure 4.14 and plotted against peptide concentration.

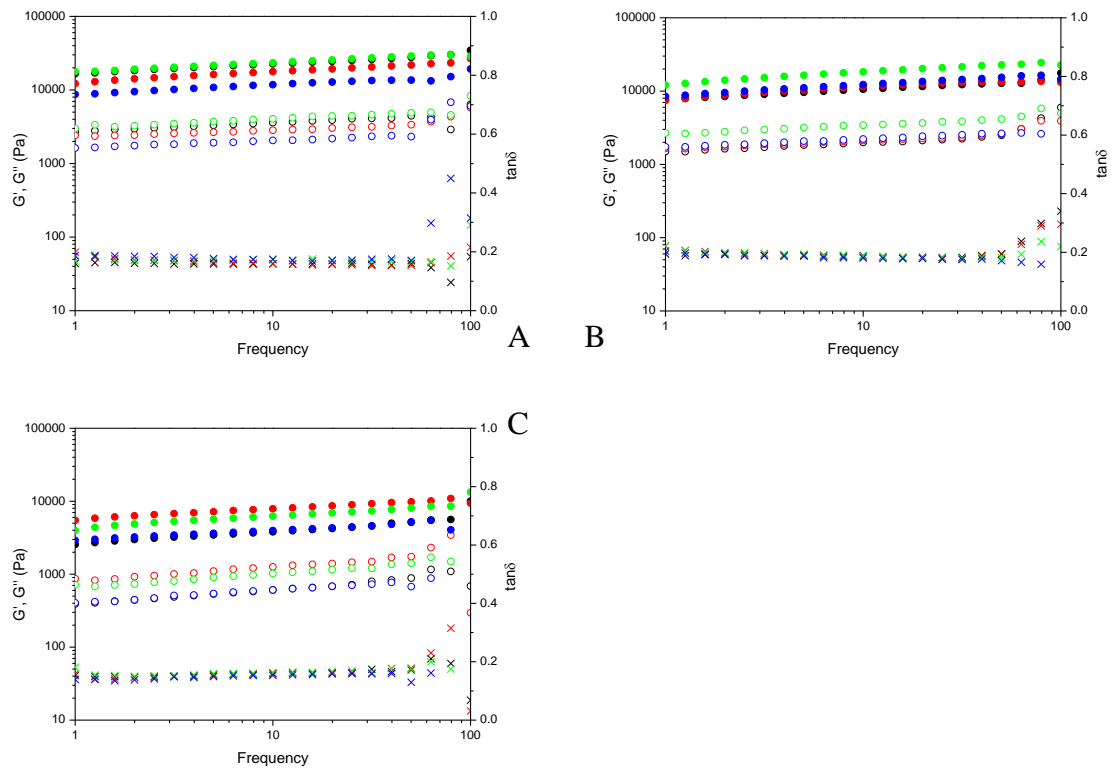


Figure 4.15 Plot of elastic modulus (G' , solid), viscous modulus (G'' , empty) and $\tan\delta$ (\times) of FEFKFKFK (A) at cell culture day0 (black), day1 (red), day3 (green) and day7 (blue); FEFKFKFK+NaOH (B) at cell culture day0 (black), day1 (red), day3 (green) and day7 (blue) and ``hRGD`` (C) at cell culture day0 (black), day1 (red), day3 (green) and day7 (blue) as a function of frequency from 1 to 100 Hz at 1% strain at 37 °C in the logarithmic scale. All the samples were at physiological conditions.

From Figure 4.16 we can see that the mechanical properties of all three gels did not vary much during the 7 days of cell culture. The values of G' are around 10000 Pa and $G' > G''$ for all tested samples indicate the gels were strong and had solid-like behaviours. The values of G' of the ``hRGD`` gels were the smallest during the cell culture time indicate the ``hRGD`` gels were the weakest among all three types of gels. However, the yield strain of the ``hRGD`` gels were the biggest during the cell culture time among all three types of gels. This means that ``hRGD`` gels, although weak, but were tougher than the FEFKFKFK gels during 7 days of cell culture. To directly compare the strength of all three gels, the values of G' of all three samples were plotted against the cell culture time and the results were presented in the same figure (Figure 4.17).

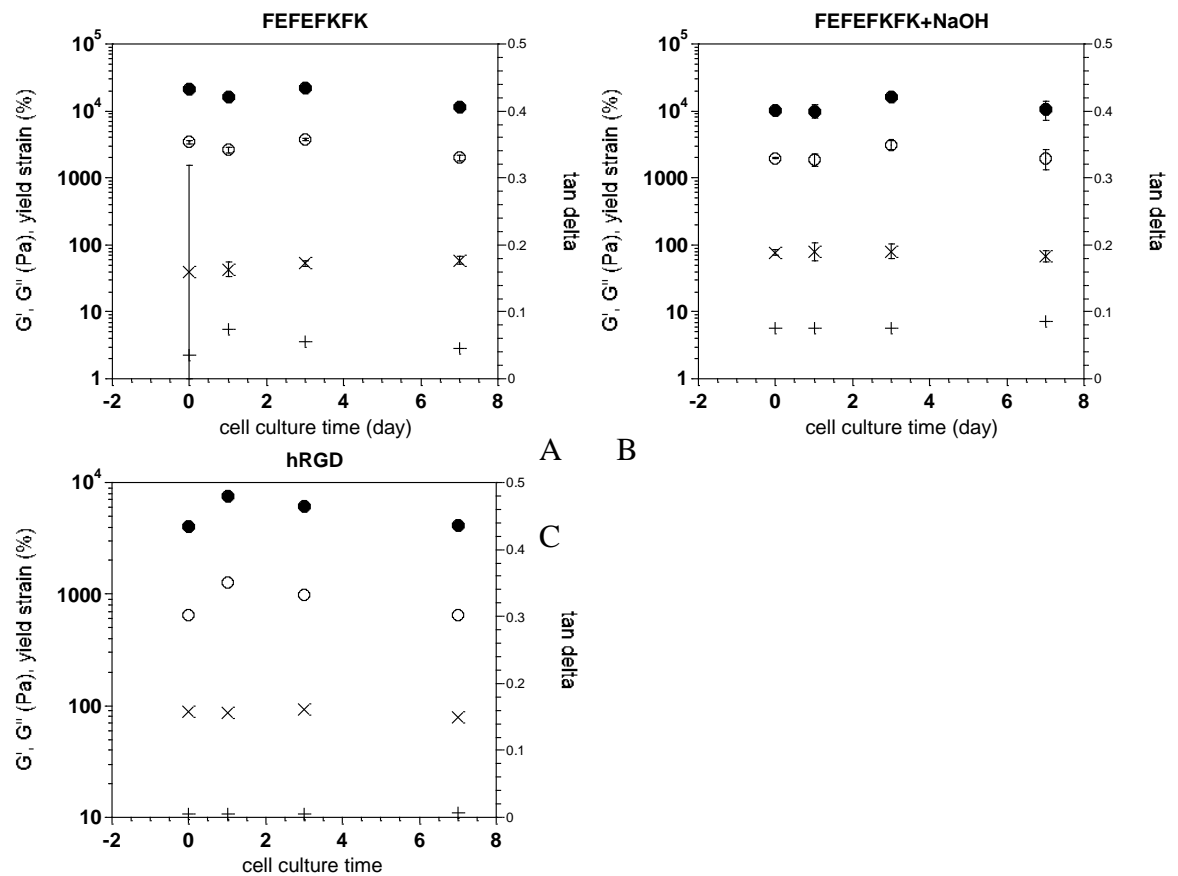


Figure 4.16 Plot of elastic modulus (G' , ●), viscous modulus (G'' , ○), $\tan \delta$ (×) and yield strain (+) of FEFEFKFK (A), FEFEFKFK+NaOH (B) and hRGD (C) gel as a function of cell culture time at 37 °C in the logarithmic scale. G' , G'' and $\tan \delta$ are the average values in the frequency independent region in Figure 4.15 and tested at 1 % strain; the yield strain is from Figure 4.14 and tested at 1 Hz. All the samples were at physiological conditions.

Although there were some variations in the mechanical strength of each type of the gels during 7 days, it can be clearly seen (Figure 4.17) that during the whole cell culture period, the hRGD gels were the weakest. The previous studies demonstrated that before pH adjusting, the hRGD gels were stronger than the FEFEFKFK gels. The fact that they were weaker here in the cell culture environment could be the result of the change in pH and the presence of salt. As discussed in Chapter 3, when the pH and the salt concentration increased, the electric repulsion force between the fibres became weaker; the small fibrils then bundled together and formed thicker fibres but the network structure became less dense, which made the gels stiffer but brittle. In the hRGD gels, the Mpr-hRGDWP sequence was considered to be the positively charged branches which made the hRGD gels stronger than the FEFEFKFK gels at pH 2.8. The possible reason was the branches make fibres more rigid which resulted in higher gel network strength. When pH increased

to 7, hR was positively charged and D was negatively charged. Hence the net charge of the branches is zero. Combined with the salt screening effect, the repulsion force caused by the branches reduced to the minimum. However, those side chains were still rigid and bulky. The stereo effect could also prevent small fibrils come too close to each other, thus less thick fibres under the influence of pH and salt. The ``hRGD`` gels are weaker than the other two gels as indicated by the low G' value; however, the bigger yield strain (Figure 4.14 and Figure 4.16) indicates a tougher gels than the other two gels.

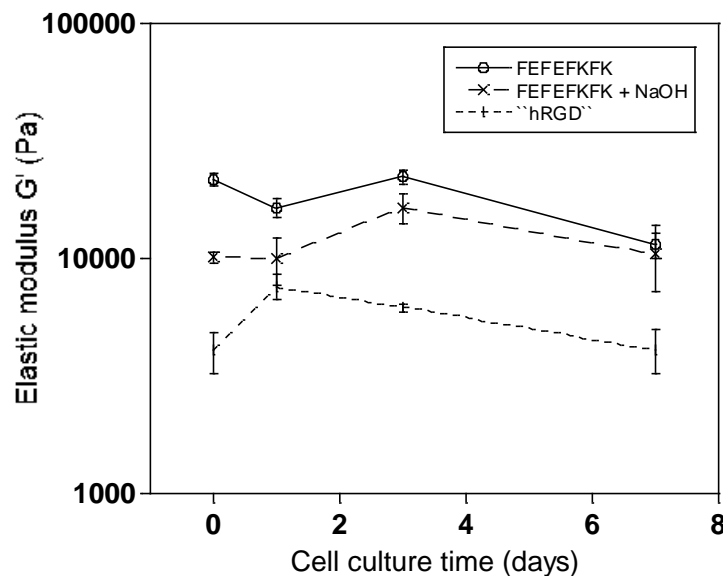


Figure 4.17 The change of mechanical strength of the gels during the 7 day cell culture; \circ represents the FEFKFK gels prepared by Method 2 (Section 3.3.2); \times represents the FEFKFK gels prepared by Method 1 (Section 3.3.2); $|$ represents the ``hRGD`` gels prepared by Method 2 (Section 3.3.2). All the samples were at physiological conditions.

Since the weakest gel provided better cell adhesion, it is possible that the incorporated hRGD sequence was the key for the improvement. If the cells recognised hRGD the same way as they recognise RGD, then the ``hRGD`` gels would provide more binding sites than the FEFKFK gels for cells to attach to, thus improving cell attachment. This should be confirmed by further investigations.

So far, ``hRGD`` peptide was used for all the characterisations without mixing with FEFKFK peptide. However, a lot of work has indicated that the density of normal RGD sequences played an important role in mediating cell adhesion. It was also noticed that, when the RGD density was high enough, more RGD did not further improve cell attachment.⁸ The density of the hRGDs was expected to play an important role in promoting cell adhesion as well. To use the functionalised peptide more efficiently, a preliminary test based on the observation of the HDF cell morphology was performed. The

peptide mixtures with different mole percentages of ``hRGD`` in the whole mixture were prepared by Method 2 (Section 3.3.2).

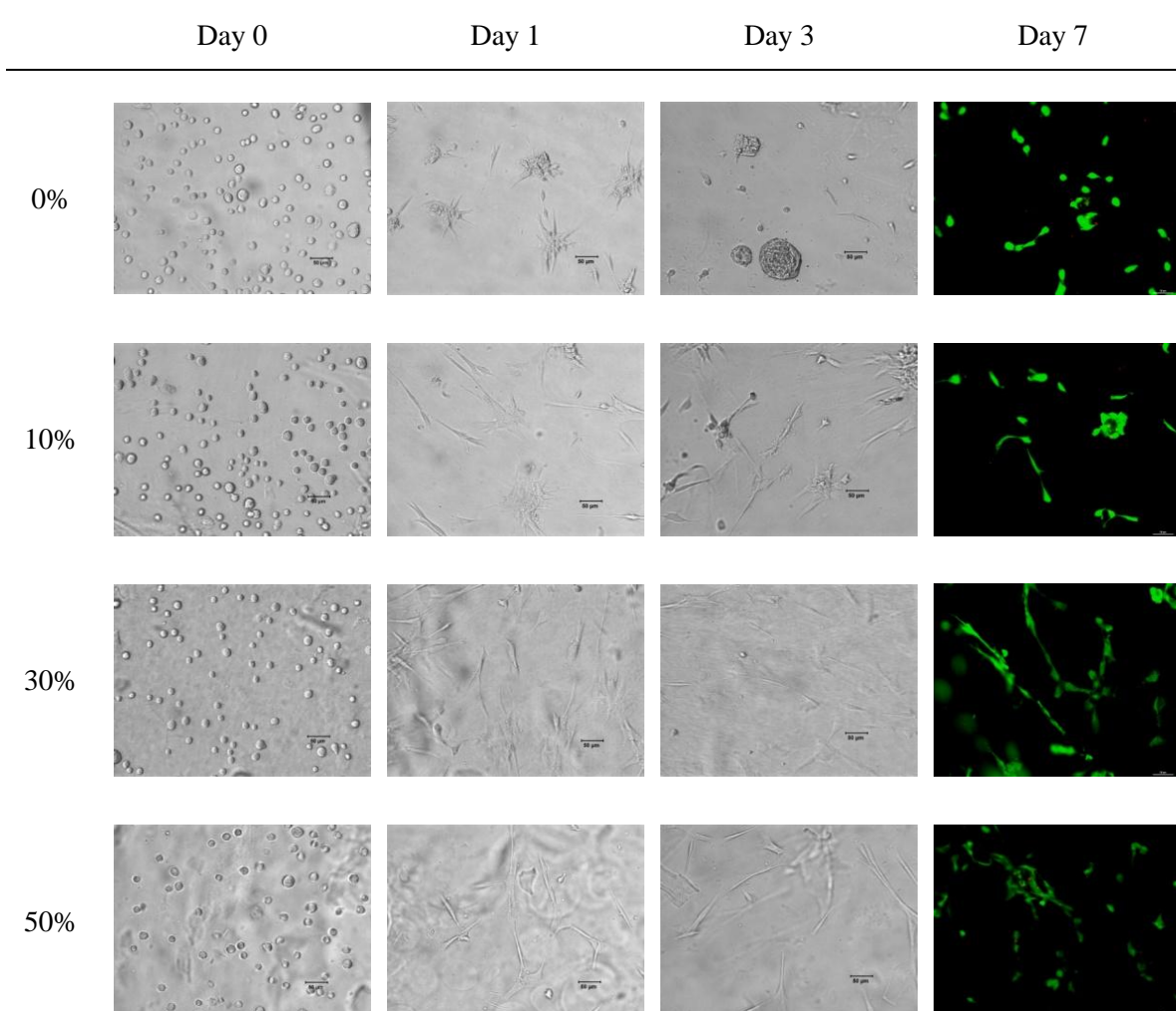


Figure 4.18 Optical micrographs of HDF on the ``hRGD`` gel surfaces with different loading ratios of ``hRGD`` peptide show cell morphologies during 3 days of cell culture. The fluorescence micrographs show the living (green) and dead (red) cells on the gel surfaces 7 days post cell culture. 5×10^4 cells were seeded on top of the gel surface in each well.

In this test, the mixtures with 0%, 10%, 30% and 50% ``hRGD`` were prepared. The required amount of FEFKFK peptide was dissolved in distilled water and melt at 90 °C to prepare a solution. According to the discussion in Chapter 3, there would be two possible situations. In the solution, FEFKFK peptide self-assembled into fibrils and the fibrils would be either too short or the fibril density would be too low to form any network structure; or the self-assembled fibrils formed microgels but the fibre density was not dense enough to form a network structure through the whole system. Then this solution was used to dissolve the required amount of ``hRGD`` at 90 °C. The previous co-assembly studies of systems composed of two self-assembling peptides showed that two peptides

would self-assemble independently and two types of fibrils would both exist in the gels formed.^{9, 10} Since the mixture was still in a liquid form, there were also two possibilities for ``hRGD`` fibres as well. The fibril length would be too short or the fibril density would be too low to form any network structure or the fibrils form microgels but not dense enough to form network structure through the whole system. Either way, ``hRGD`` peptide would self-assemble into hRGD rich fibres compared to pure FEFEFKFK fibres. When the gelation was triggered later on, two distinct fibres would both exist in the network structure forming hRGD rich and hRGD poor regions. The previous studies showed that the incorporation of rigid peptide sequence⁴ or binding sites¹¹⁻¹³ will not affect the structure of the template peptide. The octapeptide part of the ``hRGD`` peptide was expected to self-assemble into fibrils while Mpr-hRGDWP would stick out of the edge of the fibrils. This allows the functionalised part to be exposed for cell recognitions. In this way, the hRGD side chains would appear as clusters in the hRGD rich regions. The clusters of RGD peptides rather than equally distributed RGD peptides were preferred for enabling cell attachment as reported.¹⁴ Thus, the clusters of hRGDs were expected to be favourable for the HDF cell binding.

Less than 5 % out of 115 counted cells were seen to have spread on gel surfaces with 0 % ``hRGD`` loading. This confirmed the previous studies on the FEFEFKFK peptide prepared by Method 2. The cell spreading started within 24 hours after the cells were seeded on all the ``hRGD`` loaded gels. However, the cells were less spread on the gels with 10 % ``hRGD`` loading; while there was no significant difference in cell morphology between the gels with 30 % and 50 % ``hRGD`` loading (Figure 4.18). The cells stained green by the Live/dead assay confirmed the observed differences in cell morphology and also demonstrated that all cells were alive after 7 days of cell culture. If hRGDs acted as binding sites for the cell attachment, low loading would offer less binding sites thus led to less cell spreading. However, when the number of binding sites was sufficient for cell adhesion, more binding sites would not be able to further improve the cell adhesion. This could be the reason why no large difference was seen between the gels with 30 % and 50 % ``hRGD`` loading. To reduce the possible effect of batch differences due to the various purities of synthesised peptides, only the gels with 50 % ``hRGD`` loading were used for the further experiments.

To conclude, the gels were prepared using Method 2 (Section 3.3.2) for 2D HDF cell culture study. The FEFEFKFK gels were used as a negative control. The gels with 50 %

``hRGD`` loading were used to study the ``hRGD`` influence on cell attachment. If not specified, in the following sections, ``hRGD`` will be used to refer to the gels with 50 % ``hRGD`` loading.

4.3.2 Long term 2D cell culture

4.3.2.1 Cell morphology

The HDF cell attachment can be visually examined by observing the cell morphology under the microscopes. If the HDF cells are firmly attached to the scaffold, they will spread and maintain an elongated shape. The cells were cultured on all gel surfaces for 15 days, and optical micrographs were taken (Figure 4.19) to record the cell morphology changes. At day 1, over 95% out of 268 counted cells were spread on the ``hRGD`` gels; while on the FEFEFKFK gels, less than 40% out of 189 counted cells were spread. Some small aggregates of cells formed on the FEFEFKFK gels. This indicated cell possibly preferred to attach to each other than to the gel surface. Some cells adopted a spindle shape on the FEFEFKFK gels. This could be due to the existence of serum in the cell culture medium. In serum, there are various proteins including those containing bioactive ligands for cell attachment. As the gels were pre-soaked in the serum containing cell culture medium, some proteins could be absorbed by the gel and physically bound to the gel surfaces. When the cells were seeded, they could have assisted cell attachment and spreading on the gel surfaces. At day 3, all the cells adopted a spindle like shape on the ``hRGD`` gels. In contrast, larger aggregates of cells were present and minimal cell spreading was observed on the FEFEFKFK gels. The cell number on the FEFEFKFK gels decreased which may be due to the detachment of the cell aggregates. After 5 days of culture, all the cells were spread on the ``hRGD`` gels. Some of the cells moved together and were aligned into a line. In some regions, local orientation of the cells was observed. This may be caused by the fibre arrangement in the gels. When the gels were transferred into the well-plates, shear forces were applied as the gels flowed through the pipette tip, possibly causing slight orientation of the fibres. This could then influence cell behaviours, causing the cells to migrate or spread along the fibres and inducing local orientation. On the FEFEFKFK gels, the large aggregates of cells disappeared and single cells were distributed evenly on the gel surfaces. Over 85 % out of 243 counted cells started spreading, but not to the same extent as the cells cultured on the ``hRGD`` gels. After 7 days, the cell density increased on both gels. Although the cells spread on both gels, the cells had a more elongated morphology on

the ``hRGD`` gels. At day 15, the cell densities continued to increase on both gels with no significant changes in the cell morphology. The cells began to form a network-like structure on the ``hRGD`` gels while the cells remained isolated on the FEFEFKFK gels. This difference could be caused by the difference of cell numbers on the two gels. There might not be enough cells on the FEFEFKFK gels to form the network-like structure.

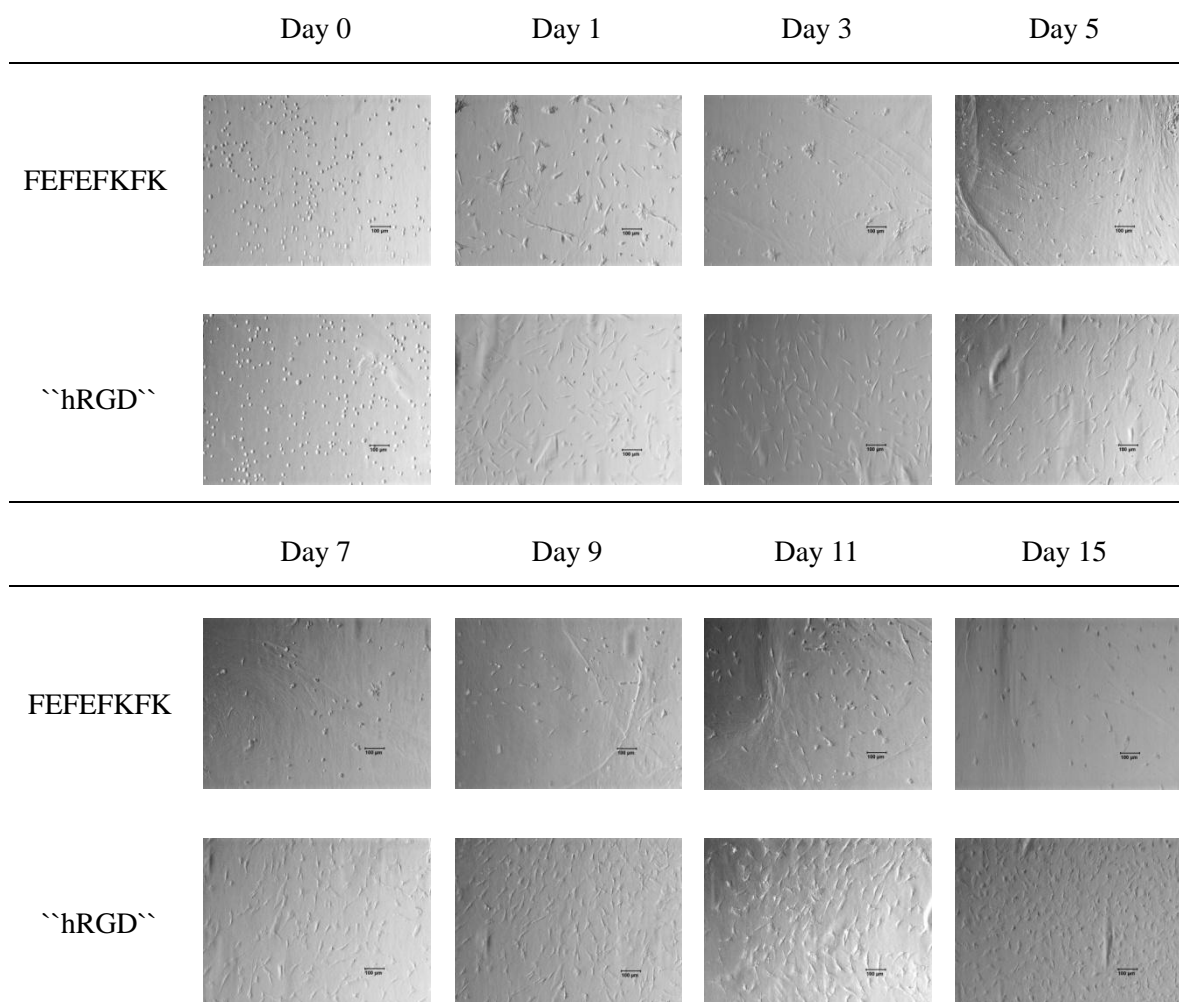


Figure 4.19 Optical micrographs of the HDF cells grow on the FEFEFKFK gels and the ``hRGD`` gels show cell morphologies during the 15 days of cell culture. Scale bars represent 100 μm . 5×10^4 cells were seeded on top of the gel surface in each well.

The optical micrographs provided a general idea of the cell morphology during the 2 weeks of cell culture. However, the lack of contrast in the images made it difficult for a more detailed observation on the cell morphology. Thus, F-actin staining assay was used to further analyse the cell morphology changes. Because some FITC-phalloidin was absorbed by the peptide hydrogel, a light green background was observed under the fluorescence microscope. However, this green background did not disturb the observation of the existence of F-actin. F-actin of the cells was still stained clear enough to provide high

contrast fluorescence micrographs (Figure 4.20).

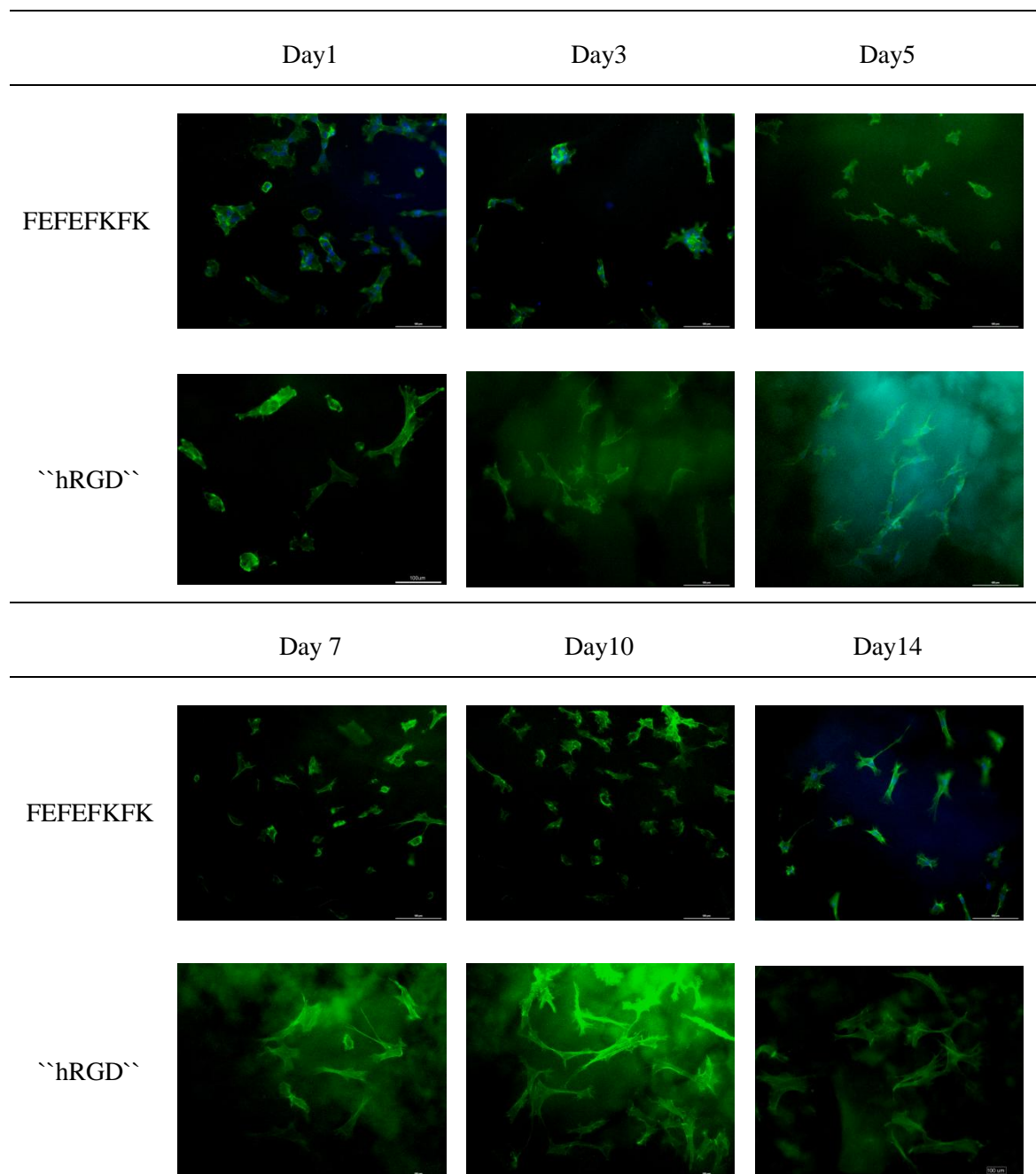


Figure 4.20 Fluorescence micrographs show phalloidin-stained F-actin (green) of cells on gel surfaces during 14 days of cell culture. Scale bars represent 100 μm . 5×10^4 cells were seeded on top of the gel surface in each well.

At day 1, the cells started to spread on the ``hRGD`` gels. There were still some round cells present. On the FEFEFKFK gels, the spread cells were also present. This confirmed the results detected by the optical microscope. At day 3, over 95 % out of 256 counted cells took an elongated shape on the ``hRGD`` gels. On the FEFEFKFK gels, protrusion structures from the cells were also observed. Those details were not able to be seen on the optical micrographs. At day 5, cell spreading occurred on both gel surfaces, while the cells

were more elongated on the ``hRGD`` gels. From day 7 to day 14, the cells were even more lengthened on the ``hRGD`` gels and began to form a network-like structure. The stress fibres can also be seen clearly. On the FEFEFKFK gels, the cells were well distributed and isolated from each other. The cells extended but not elongated much until day 14. At day 14, the elongated shapes were taken by over 90 % out of 438 counted cells. The stress fibres were also seen in cells. This may be because the cells began to secrete their own ECM which contained bioactive ligand for them to bind to. Compared to the ``hRGD`` gels, the FEFEFKFK gels also supported cell adhesion. However, this could be caused by the protein absorption.¹⁵ The link between proteins and the gels were weak and could not support strong local adhesion when the cells tried to spread. While on the ``hRGD`` gels, the hRGD sequences were permanently linked to the fibres via peptide bonds. If the cells bound to these sequences, the binding would be strong enough to support the cell extension and migration. This might lead to more spread cells on the ``hRGD`` gels compared to on the FEFEFKFK gels.

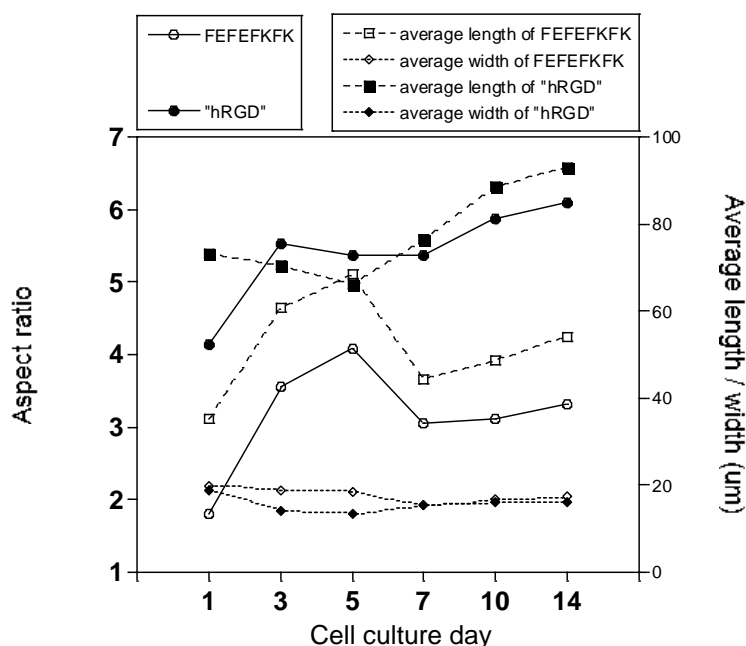


Figure 4.21 The aspect ratios (circle), average lengths (square) and average widths (diamond) of the cells in 14 days of cell culture; the ``hRGD`` gels are presented by solid symbols; the FEFEFKFK gels are presented by empty symbols. 5×10^4 cells were seeded on top of the gel surface in each well.

With the better contrast of fluorescence micrographs, cell spreading can also be quantified via photo analysis software. An average of 400 cells was counted for each sample. Here the aspect ratios of the cells on both gels were measured and presented with the average length and width of the cells on both gels (Figure 4.21). In general, the cells on the ``hRGD`` gels

had a larger aspect ratio and average length, while the average width were similar to the cells on the FEFKFKFK gels. This quantitative image analysis confirmed the impression given by the direct observation of fluorescence micrographs that the cells were more elongated on the ``hRGD`` gels than on FEFKFKFK gels.

On the ``hRGD`` gels, the average cell length and cell width were slightly decreased in the first 5 days post cell culture, then the average cell length began to increase slowly but steadily from day 5 to day 14, while the average cell width stopped decreasing. As a result, the aspect ratio of the cells increased between day 1 and day 3, and then kept steady between day 3 and day 7, and began to slowly increase again after day 7. This could be caused by the cells initially attaching to the proteins absorbed by the gels. The previous studies on FKFEFKFE and other β -sheet derived peptide hydrogels showed the ability of protein absorption with the presence of serum. Initial cell elongation was observed because of the binding to the cell-adhesive proteins in serum and through rapid ECM synthesis of the cells.¹⁶ These bindings were not stable, as the protein assisting cell attachment could be replaced or washed out during medium changes.¹⁵ This could then result in some cells losing their attachment sites, which in turn would affect cell morphology. However, after 5 days, the cells originally bound to the stable sites (possibly via hRGD) were continuing to elongate whilst the cells which had lost their initial attachment had recovered and attached to more stable sites. Thus, the average cell length would increase again.

On the FEFKFKFK gels, the average cell length increased 3 times in the first 5 days post cell culture, followed by a large decrease between day 5 and day 7. After 7 days, the average length slowly increased again. The average width remained more stable with a small decrease between day 5 and day 7. Consequently, the change of aspect ratio followed a same trend as that of the average length. This could be caused by the detachment of the cells. As described above, some cells could attach to the proteins physically bound to the gels which may be subsequently washed out during medium changes. The cells attached to these sites could then be washed out as well. The cells attached to the proteins left on the gel surfaces or the cells produced their own ECM could be the ones remained on the gel surface. Those cells might still try to reach out for neighbouring cells, preferred binding sites, or start to spread on their own ECM. Either way, their numbers could be the reason why the average cell length increased. However, after 5 days post cell culture, if those cells could not reach the neighbouring cells due to either lack of migration ability or low cell density, the cells might shrink back to less elongated morphology. If the ECMs were

secreted, then the cells would slowly spread again.

In conclusion, more cells were observed to have spread on the ``hRGD`` gels than on the FEFEFKFK gels, and the spread cells on the ``hRGD`` gels had more elongated morphology. Those all proved a positive effect of the ``hRGD`` gels on cell adhesion and spreading.

4.3.2.2 Cell proliferation

The effect of the gels on cell adhesion can also be examined by measuring the cell proliferation as the gel surface that provides better cell adhesion will also support higher initial cell population. The gels with cells on top were able to be dissolved easily with an excess of cell culture medium and disruptive pipetting. The cell number in this cell suspension (a mixture of cells, diluted gels and excess medium) was then counted. Compared to the traditional cell proliferation assays, this direct approach largely simplified the procedure and avoided background absorbance which may occur when the gels are assessed using quantitative colorimetric assays. This is also a notable advantage of this peptide gel system as the cells can be easily retrieved for analysing using alternative techniques including RNA extraction for PCR analysis and flow cytometry.

The cell numbers on both gels were plotted against cell culture days in Figure 4.22 A. More cells attached to the ``hRGD`` gel surface from the beginning, and the ``hRGD`` gels maintained a higher cell population during the entire cell culture period. The cell numbers had been increasing steadily on the ``hRGD`` gels during 14 days of culture time. While on the FEFEFKFK gels, the cell number decreased in the first 3 days and then increased afterwards. The initial decrease could be due to the detachment of cell aggregates or cells washed out by binding to unstable absorbed proteins on the gel surface. All the results matched what was observed under the optical microscope, as the positive effect of the ``hRGD`` gels on cell adhesion was reinforced again by cell proliferation tests.

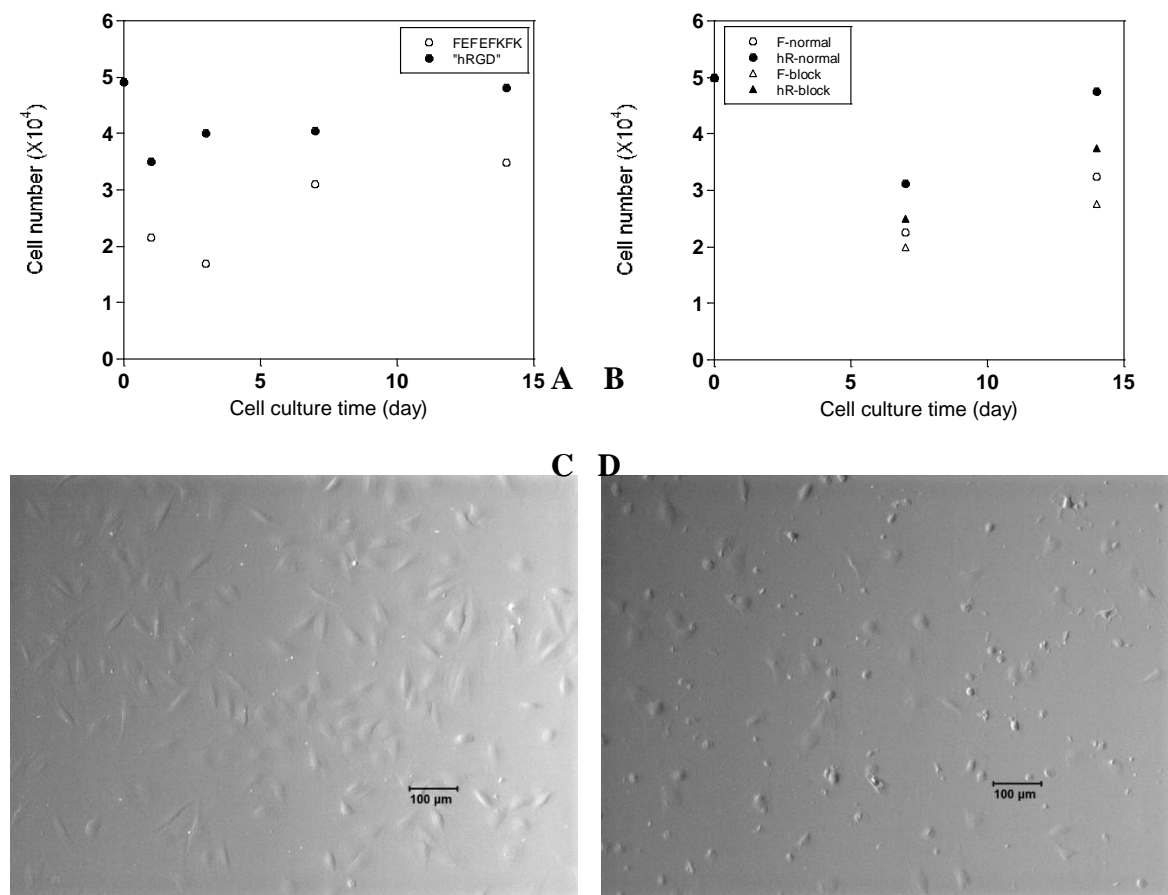


Figure 4.22 A) Plot of cell numbers against cell culture days in the 14 days of cell culture; \circ represents FEFEFKFK; \bullet represents hRGD; B) Plot of cell numbers against cell culture days in integrin blocking tests; circles represent the normal cells; triangles represent the blocked cells; empty symbols represent FEFEFKFK; solid symbol represent hRGD; C,D) optical micrograph of normal cells (C) and integrin blocked cells (D) on fibronectin coated glass surface 4 hours post cell culture; Scale bars represent 100 μm . 5×10^4 cells were seeded on top of the gel surface in each well.

4.3.2.3 Integrin blocking test

Integrin $\alpha 5 \beta 1$ within the HDF cell membranes was blocked with an antibody and then the cells were seeded on the fibronectin coated glass surface to test the blocking efficiency. Figure 4.22 C shows the normal cell morphology on the fibronectin coated glass 4 hours post cell culture. All cells were spread on the glass surface. However as seen in Figure 4.22 D, when the cells were incubated with the antibody solution and then seeded on the fibronectin coated glass, over 85 % out of 176 counted cells were rounded or not attached. This demonstrated that by blocking the integrin $\alpha 5 \beta 1$, cell adhesion to fibronectin was inhibited, which means the main binding sites on the scaffold surface were offered by RGD sequence which is known to be the sequence recognised by integrin $\alpha 5 \beta 1$. The cell

attachment of the blocked cells could be due to inefficient integrin blocking. However, even if the blocking is not sufficient for preventing all the cell attachment, it was sufficient to distinguish the difference in cell adhesion between the normal cells and the integrin-blocked cells on the same FN-coated surface. Thus, this integrin blocking test could be used for the diagnosis of the binding sites.

Figure 4.22 B shows the results of the integrin blocking tests on the ``hRGD`` gels and the FEFEFKFK gels. It can be clearly seen that the unblocked cells seeded on the ``hRGD`` gels had the highest cell numbers 14 days post cell culture; the blocked cells seeded on the ``hRGD`` gels had the second highest cell numbers, followed by the normal cells seeded on the FEFEFKFK gels; the blocked cells seeded on the FEFEFKFK gels had the lowest cell numbers. The previous section showed that higher initial cell attachment would result a high cell population after 14 days cell culture. This could mean the initial cell adhesion was increasing from blocked cells on FEFEFKFK to normal cells on FEFEFKFK, then blocked cells on ``hRGD``, ended with normal cells on ``hRGD``.

The difference between the normal cells and the blocked cells on the FEFEFKFK gels could be caused by the absorption of proteins on the gel surfaces. Integrin $\alpha 5\beta 1$ of normal cells would bind to the RGD sequences of the proteins on the gel surfaces, while the integrin blocked cells could not bind to those RGD sequences, therefore better cell adhesion for normal cells on the FEFEFKFK gels. This also proved that integrin blocking tests could be performed on the gel surfaces as well.

The difference of the cell numbers between the normal cells on the FEFEFKFK gels and the blocked cells on the ``hRGD`` gels could be caused by inefficient integrin blocking and more binding sites on ``hRGD`` gels. However, although the blocking was not 100 %, there was still a significant difference observed when tested on the fibronectin coated glass surfaces. This means that most of the integrin should have been blocked. In this case, only when there were several times more binding sites on ``hRGD`` than FEFEFKFK, it would cause the number of the cells attached to the ``hRGD`` gel surface among the small amount of unblocked cells during the blocking test is higher than the number of the cells attached to the FEFEFKFK gel surface among the normal cells. More binding sites on the ``hRGD`` gels could be offered by more proteins absorbed by ``hRGD`` gels, but it is unlikely for the ``hRGD`` gels to have several times more protein absorption than the FEFEFKFK gels. The other more likely explanation would be that the hRGD sequences

were able to provide binding sites for integrin $\alpha 5\beta 1$ with the 50 % loaded gels having sufficient hRGD sequences exposed on the gel surfaces for enhanced cell attachment. The amount of hRGDs would be more stable and in excess compared to the non-specific adsorption of proteins by the FEFKFKFK gels. Thus, the number of the unblocked cells bound to hRGD would have a chance to exceed the number of normal cells bound to the proteins absorbed by the FEFKFKFK gels.

The difference between the normal cells and the blocked cells on the ``hRGD`` gels could be caused by either the absorption of proteins on the gel surfaces, which is the same source for cell adhesion difference on the FEFKFKFK gels; or integrin $\alpha 5\beta 1$ could specifically recognise the hRGD as has been previously reported for the RGD sequence. If it was the latter reason, integrin within the normal cell membrane could bind to hRGD, while the cells with blocked integrin could not bind to hRGD, thus fewer cells attached to the gel surface. Or it could be both together caused the best cell adhesion of normal cells on ``hRGD``.

Although with the serum present in the cell culture medium, it added another factor which could have affected the experiment results; it would still be a very good explanation for all the results gained so far, that hRGD can help cell adhesion through the same way as RGD. To draw a more exclusive conclusion, further optimisation on integrin blocking and serum free tests could be implemented.

4.3.2.4 Synthesis of ECM

One important role of a scaffold is to support normal cell functions which include the synthesis of their own ECM. The steady cell spreading and cell proliferation after the 7 days post cell culture on the FEFKFKFK gels suggested that there might be ECM secreted to assist the cell adhesion and subsequent proliferation. The type of ECM investigated here was fibronectin, which contains RGD sequences and serves as a linker between the cells and other molecules within ECM.

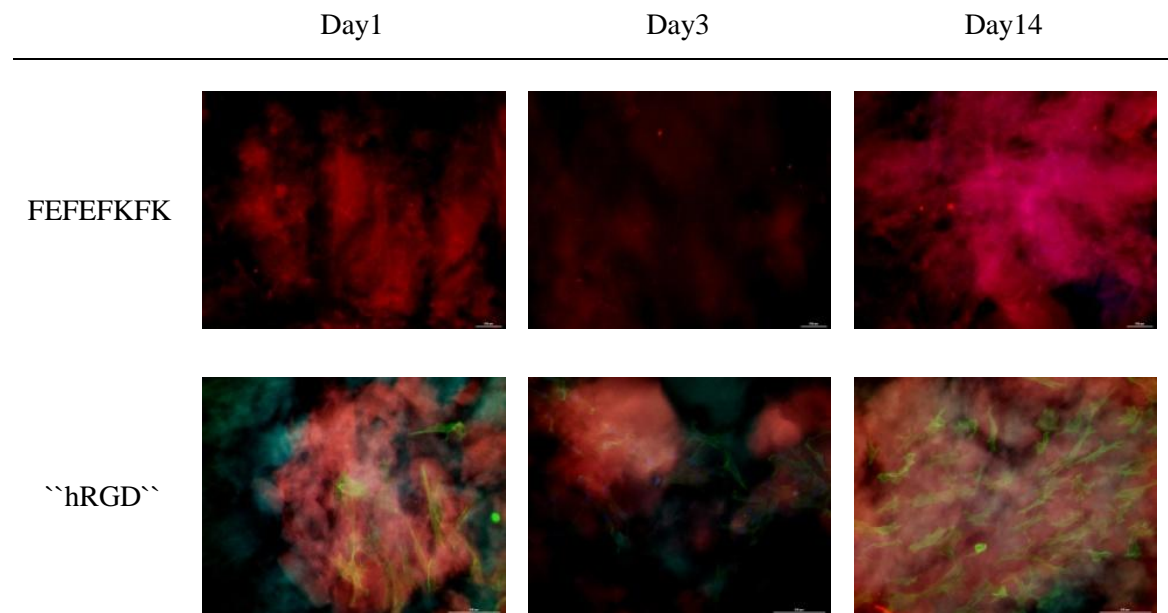


Figure 4.23 Fluorescence micrographs of fibronectin secreted on the FEFEFKFK and the ``hRGD`` gels in 14 days of cell culture. Scale bars represent 100 μm . 5×10^4 cells were seeded on top of the gel surface in each well.

Figure 4.23 shows fibronectin staining on both FEFEFKFK and hRGD functionalised gels. Unfortunately, due to the dye absorption by the gel, a large amount of background fluorescence was present and it was difficult to see clearly the secretion of fibronectin. On the FEFEFKFK gels, some red spots were highlighted at day 1 and day 3. The positions of those spots were overlapped with the positions of the HDF cells on the gel surfaces. It was conjectured that the red spots could be fibronectin produced inside the cells or secreted under the cells. At day 14, a fibrous network could be seen with a lighter red colour along with highlighted red spots. This could be the secretion of fibronectin large enough to form a fibrous network structure. The formation of the fibronectin network could also be the reason why the cell adhesion on the FEFEFKFK gels increased between day 7 and day 14. On the ``hRGD`` gels, the background was too strong to see any highlighted red stained fibronectin. In the fibronectin staining assay, the primary rabbit anti-human fibronectin antibody was used to locate the fibronectin secreted by HDFs. The secondary antibody was used to locate the primary antibody and show red colour under the fluorescence microscope. Since the immunogen of the primary antibody is the recombinant full length human protein,¹⁷ the primary antibody is only attracted to the fibronectin secreted by HDFs. Hence the strong background was not due to hRGD being stained by the assay solutions. The F-actin staining assay (green) was used with fibronectin staining assay (red) to help locate the position of cells. The gels demonstrated large absorption of both staining

solutions which resulted in green and red background fluorescence. The background fluorescence could be due to remaining antibodies trapped within the gels. However, whilst the green fluorescence was all over the field of view, the red fluorescence was localised in cell rich regions. As cell culture progressed, the cell number increased and the area of the red regions increased too. This could be attributed to the secretion of fibronectin. More quantitative assays could be used to further confirm the secretion of fibronectin by cells on both peptide gels.

4.4 3D HDF cell culture

The major advantage of hydrogels used as tissue culture scaffold is that the gels can provide a 3D environment as a mimic of the ECM. After being proved biocompatible in a 2D environment, it was important for the two gels of FEFEFKFK and ``hRGD`` to be assessed for 3D cell culture. 3D cell culture has different requirements for the gels than 2D cell culture, thus the 3D cell culture protocol was developed first.

4.4.1 Gel preparation protocol development for 3D HDF cell culture

In the section describing 2D gel preparation, it was mentioned that a uniform gel surface was crucial for an even cell distribution on the gel surface. In the gel preparation for 3D tests, it was more important to ensure a homogeneous cell distribution within the gels. Due to the residue from peptide synthesis, peptide gels were acidic after first prepared. This was the reason the gels were washed with cell culture medium several times until they were at neutral pH in 2D cell culture. During the washing steps, the salt concentration in the gels was also adjusted to the physiological salt concentration. In the 3D cell culture studies, both pH and salt concentration needs to be adjusted prior to the cell encapsulation and gel setting. From the study of the pH effect on the gel properties, it was found that the gels were very rigid between pH 6.5 to pH 7, but the mechanical strength sharply decreased above pH 7. According to these observations, the peptide powder was dissolved in distilled water, melted in an oven and cooled down to form clear gels. NaOH was then added to obtain pH 7-8, which created a cloudy gel. More NaOH solution was added in drop wise until the gels became clear again at pH 9.5-10. Subsequently, 10 times concentrated phosphate buffered saline (PBS) was added to adjust the pH to approximately pH 9. This step also brought the final salt concentration of the gel to be the physiological salt concentration.

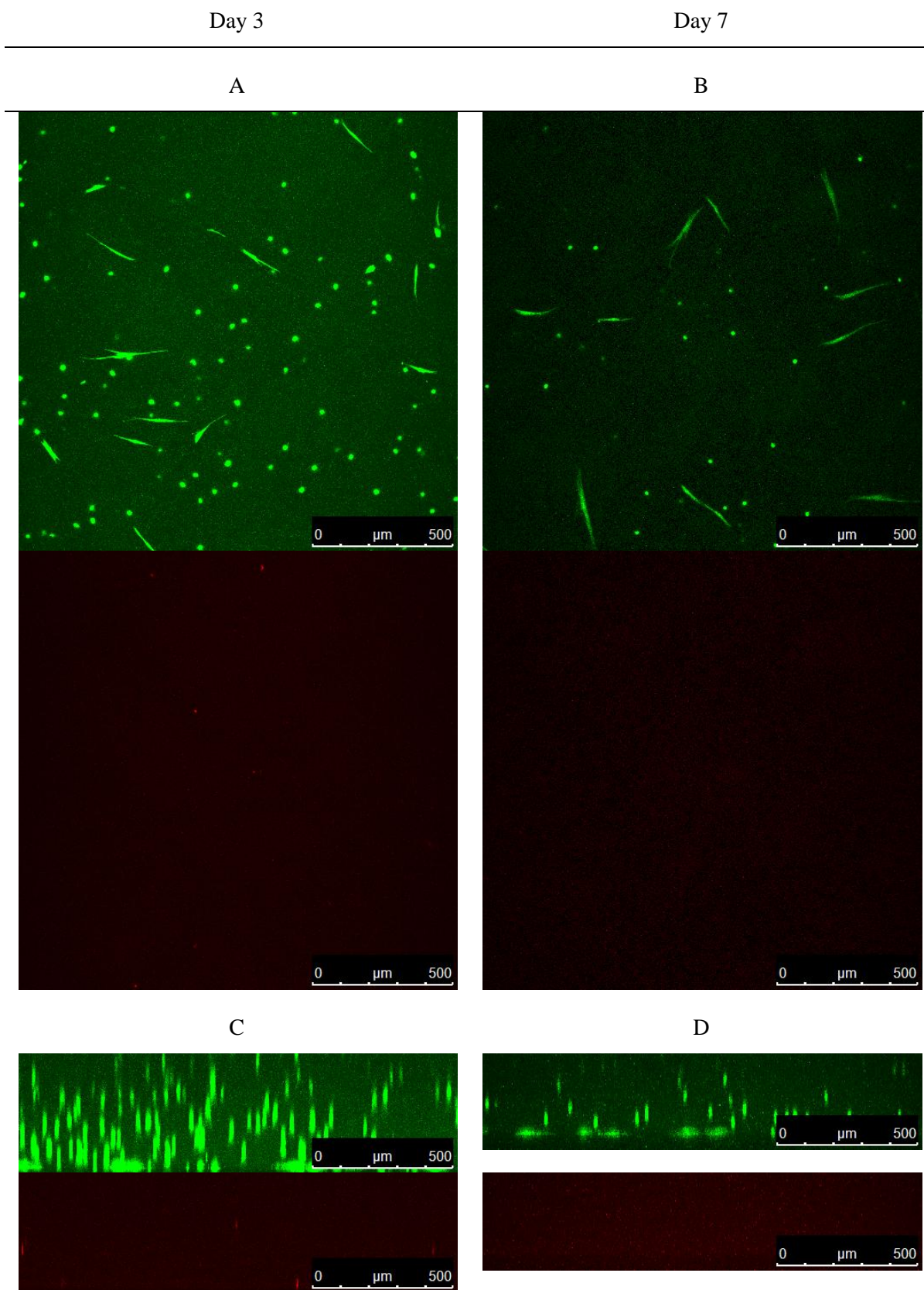


Figure 4.24 Fluorescence micrographs of HDF cells in the FEFEFKFK gels at 3D cell culture day 3 (left) and day 7(right). Scale bars represent 500 μm . Cell density was $10^6 \text{ cell ml}^{-1}$ gel.

At this stage, the gel was soft enough to be well mixed with the cells and the pH was

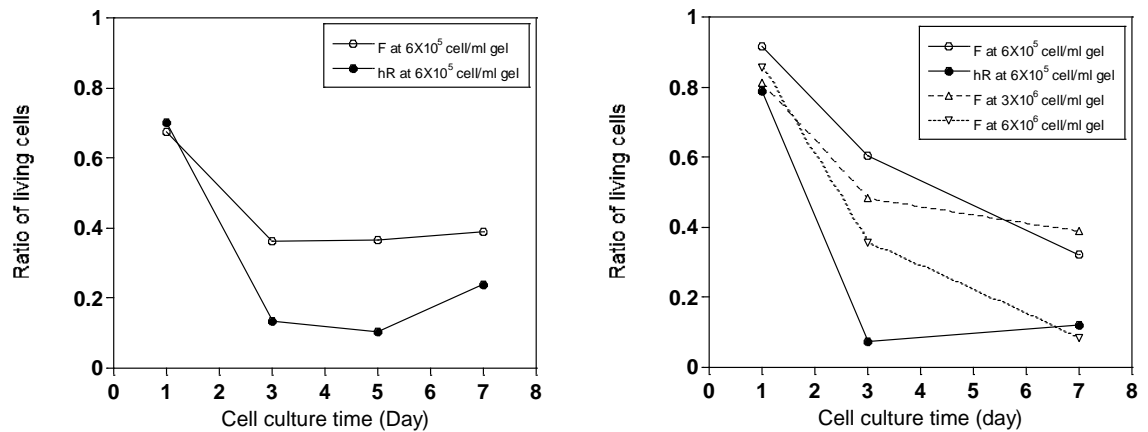
tolerable for initial cell seeding. The addition of the cell suspension also helped to reduce the pH further, aiding cell survival. Then the cell-gel constructs were transferred to the cell culture wells to set for 10 minutes at 37 °C. A Live/dead assay combined with confocal microscopy was used to detect cell viability and cell distribution within the gels.

The living cells (green) and dead cells (red) were observed through two channels thus the images from two channels were both presented. Figure 4.24 A and Figure 4.24 B are top-down views of the cell-gel construct. The encapsulated cells were alive and well distributed throughout the gel after 7 days of cell culture. Figure 4.24 C and Figure 4.24 D are side views of the cell-gel construct. The spread cells were observed at the interface between the gels and the cell culture wells, which were the wider cells on the side view images. The cells inside the FEFKFK gels maintained rounded. Very few dead cells were observed after 3 days of cell culture while no dead cells were seen at day 7. The side view image taken at day 7 was shorter than the one taken at day 3. This could be due to the medium changing in the cell culture period, top layer of gels were slowly washed away and the gels became thinner. The observation under the confocal microscope confirmed that the 3D gel preparation protocol used in this project met the requirements for the 3D cell culture. It provided a good cell distribution inside the gels and the cells survived from the initial seeding environment. For further investigations, a 3D cell culture protocol needs to be developed.

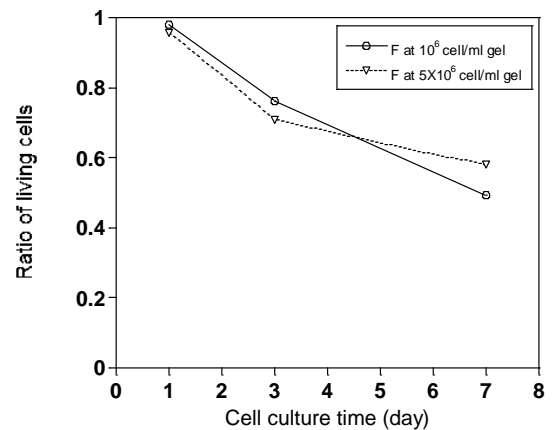
4.4.2 3D HDF cell culture protocol development

High cell viability was one of the aims for a proper cell culture protocol. The cell viability was represented by the ratio of living cell numbers in total cell numbers. The ratio was obtained by counting the cell number and analysing fluorescence micrographs of Live/dead assay results. An average of 1500 cells was counted for each sample during the image analysis.

A) 24 well-plate: medium changed every other day as 2D cell culture protocol



B) 24 well-plate: medium changed 3 times a day



C) Insert: medium changed every other day as 2D cell culture protocol

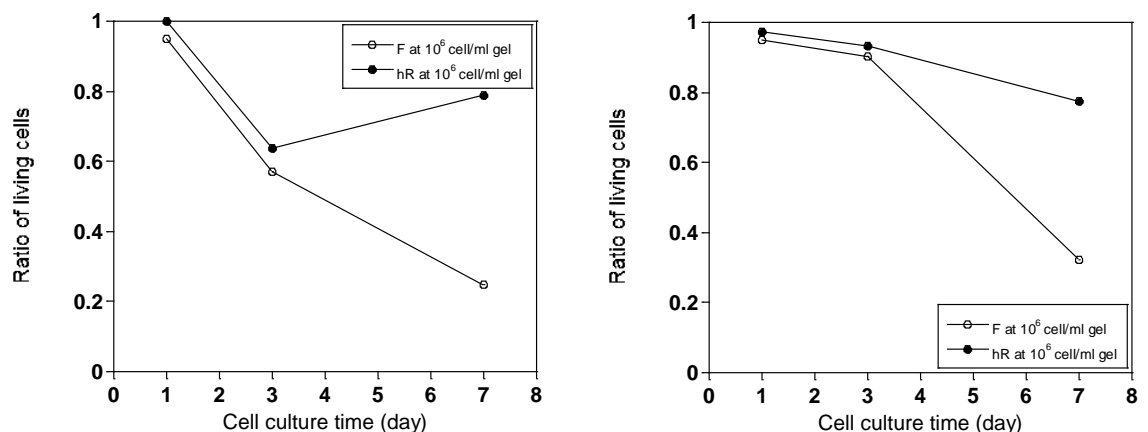


Figure 4.25 The ratio of living cells using different cell culture protocols. Left column is the results of cell counting. Right column is the results of image analysis of Live/dead assay results. Empty symbols represent the FEFEFKFK gels; solid symbols represent the ``hRGD`` gels.

Initially, after a cell-gel construct was set, culture medium was placed on top of it and changed at day 1 followed by every other day. This was the same protocol used in 2D cell culture studies. Figure 4.25 A shows the ratio of living cells cultured in this way in a 7 days' culture. The figure on the left is the results of cell counting at a cell density of 6×10^5 cell ml⁻¹gel. In both the FEFEFKFK and the ``hRGD`` gels, the ratio of the living cells sharply decreased between day 1 and day 3 and then slowly increased between day 3 to day 7. However, the ratio was still below 40 % at day 7. Similar results were gained by analysing the fluorescence micrographs of live/dead staining shown in the figure on the right. At the same cell density, the ratio of living cells kept decreasing in the FEFEFKFK gels and eventually dropped below 40 % at day 7. In the ``hRGD`` gels, although the ratio of the living cells increased slightly after the initial drop, the percentage of living cells was still below 20 %. The cells were seeded in the FEFEFKFK gels at the cell density of 3×10^6 cell ml⁻¹gel and 6×10^6 cell ml⁻¹gel, which resulted in a further decrease in the ratio of living cells. Previous fluorescence micrographs taken under the confocal microscope showed that, the living cells were distributed evenly in depth of gels during 7 days of cell culture. That suggested the cell-gel construct had a good permeability for nutrients and waste, thus ensuring all cells inside the gels were treated equally. The low ratio of living cells could be caused by insufficient medium changes. Initial environmental shock probably caused the cell death. Without enough medium changes, the toxins released by the dead cells could not be removed from the system in time. Those toxins would affect the neighbouring cells and cause even more cell death. The higher the cell density was, the more toxic accumulated in the gels, thus lower living cell ratio.

In order to address this, the medium was then changed 3 times a day. However, due to gel contamination, the cell-gel construct used for cell counting was disposed and the data could not be collected. Here, we only present the result from the remaining cell-gel construct used for Live/dead assays. It can be clearly seen on Figure 4.25 B that the living cell ratios increased to around 20 % at both cell densities. Although the ratio was increased, the final ratio of living cells at day 7 was still around 50 %. Therefore, a more efficient ways of getting rid of the toxic waste and transporting nutrients needs to be developed.

Instead of a 24 well-plate, an insert in a 12 well-plate was used. The surface area of a well in a 24 well-plate and an insert in a 12 well-plate was very similar. However, the gels in the inserts not only contact cell culture medium from the top surface, but also from the bottom. With a large amount of medium surrounding the insert, the released toxins could be diluted

to a very low concentration. The medium was placed on top and outside of the insert after the setting of the cell-gel construct, and then changed at day 1 followed by every other day. A cell density 10^6 cell ml^{-1} gel was chosen as previous results showed that higher cell density resulted in higher cell death if the medium changes were not sufficient. However, if the cell density is too low, in a 3D environment, there would not be enough neighbouring cells to communicate with each other. A cell density of 10^6 cell ml^{-1} gel was considered to be an appropriate seeding density for 3D cell culture studies and was used in the following experiments. In the ``hRGD`` gels, the ratio of living cells calculated by cell counting demonstrated the same trend as observed previously (Figure 4.25 C). The percentage of living cells decreased between day 1 and day 3 then increased between day 3 and day 7. The percentage of living cells calculated by image analysis however showed a continuous but slow decreasing trend. Both results showed a great improvement in living cell ratio by reaching 80 % at day 7. However, in the FEFEFKFK gels, the ratio of living cells decreased continuously until reaching 30 % at day 7. This could be due to the noticed gel thinning and softening during medium changes, which was not a preferred environment for HDF cells. As discussed previously, the influence of pH and salt on the FEFEFKFK gels causes thicker fibres with a less dense network. However, the side chain within the ``hRGD`` gels helped form more rigid fibres and less bundles of fibres which maintained the network density. As a result, the large amount of cell culture medium would have a bigger influence on the FEFEFKFK gels, because the fibres in the FEFEFKFK gels would be easier to be washed out than those within the ``hRGD`` gels. Gel thinning and softening was observed with the naked eye, this should be confirmed by rheological tests in the future. Further tests on the ``hRGD`` gels showed that if culture medium was changed every day, the final ratio of living cells at day 7 could reach up to 97 %. To conclude this section, the inserts in a 12 well-plate could be a good choice for 3D cell culture studies.

Although the 3D cell culture protocol could be further optimised, the high cell viability in the ``hRGD`` gels provided the possibility to apply some preliminary tests on culturing HDF cells in the 3D environment.

4.4.3 3D HDF cell culture

A Live/dead assay was applied to investigate the cell viability and the cell morphology (Figure 4.26).

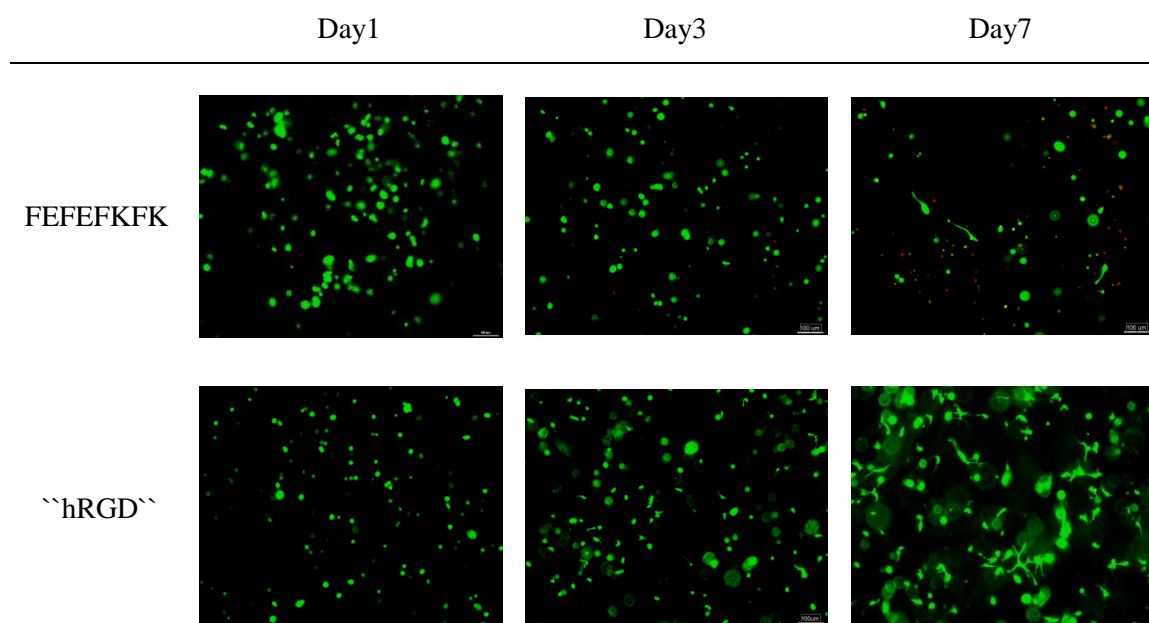


Figure 4.26 Fluorescence micrographs of 3D HDF cell culture in the FEFEFKFK and ``hRGD`` gels during 7 days of cell culture. Scale bars represent 100 μm . Cell density was $10^6 \text{ cell ml}^{-1}$ gel.

In FEFEFKFK gels, over 99 % out of 1530 counted cells were alive (green); less than 1% dead cells (red) were seen under the fluorescence microscope at day 1. All cells adopted the rounded morphology. At day 3, dead cells were observed with the majority of the cells alive. All cells still maintained the rounded morphology. However, at day 7, over 75 % out of 736 counted cells were dead with the remaining living cells largely rounded and some cell spreading. The spreading of the cells could be caused by several reasons. In the 2D cell culture, the gels were pre washed with cell culture medium several times, thus some proteins were trapped on the gel surface and helped initial cell spreading. In the 3D cell culture, no gels were washed prior to cell culture. Thus there was not enough protein trapped inside the gel to help cell spread. After the medium was changed during the 7 days of cell culture, trapped proteins could be enough to help the cells spread on the gel surfaces. The other reason could be that, although with continuous cell death, living cells struggled to survive but still produced their own ECM to help the cell spreading. Both conjectures need to be confirmed further by locating cell positions using confocal microscopy and by quantitative or qualitative ECM analysis assays. In the ``hRGD`` gels, over 99 % out of 1437 counted cells were alive at day 1, and had a rounded morphology. Some dead cells were seen at day 3, but the majority of the cells were alive with some spreading observed. By day 7, over 99% out of 1286 cells were still alive with a high degree of cell spreading into spindle and polyhedral morphologies. In some regions, the cells had formed

connections with each other and formed networks. This further reinforces the conclusion drawn from the 2D cell culture studies, that the ``hRGD`` gels help improving cell adhesion. Future studies should assess the cell proliferation. Or higher cell concentration could be used to study the difference at early cell culture stage.

Cell morphology was also confirmed by F-actin staining at day 7 (Figure 4.27). In the FEFEFKFK gels, the rounded morphology of the cells can be seen more clearly, with some cells forming small protrusions. In contrast, the cells in the ``hRGD`` gels demonstrated more extensive spreading with both the lamellipodia and the filopodia observed.

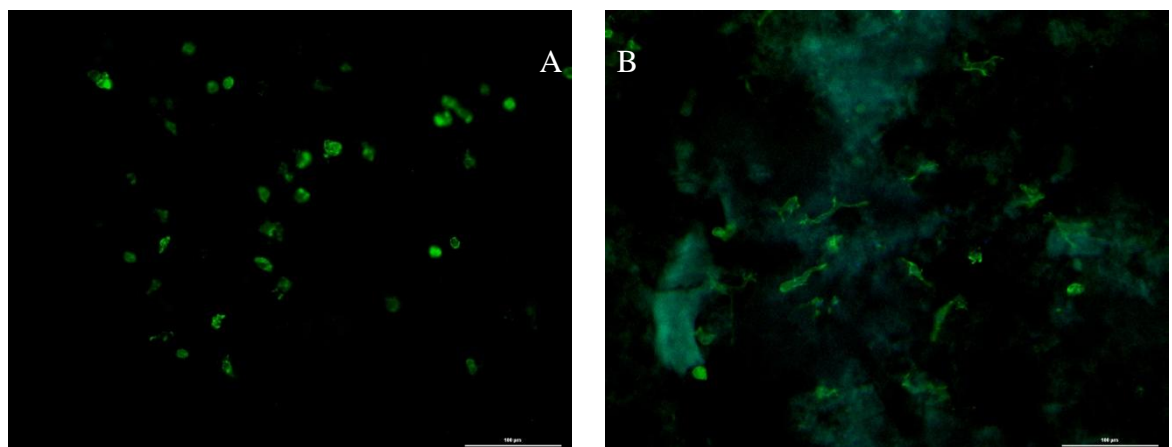


Figure 4.27 Fluorescence micrographs of stained F-actin of HDF cells in the FEFEFKFK (A) and ``hRGD`` (B) gels at day 7 post cell culture. Scale bars represent 100 μm . Cell density was 10^6 cell ml^{-1} gel.

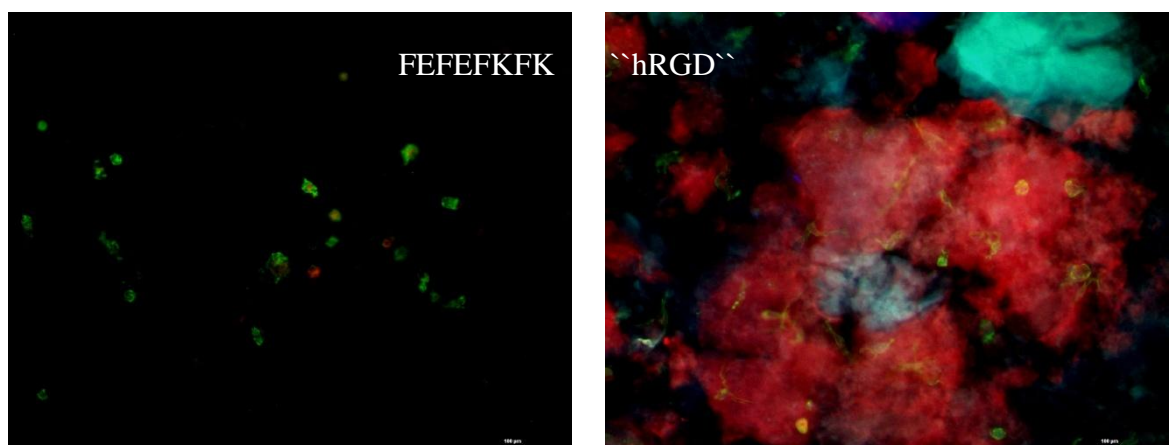


Figure 4.28 Fluorescence micrographs of F-actin assay result (green) and collagen I assay result (red) at day 7 post cell culture. Scale bars represent 100 μm . Cell density was 10^6 cell ml^{-1} gel.

To investigate the production of ECM molecules by cells at day 7, further analyses were carried out. For this purpose, collagen I antibody was used. In the FEFEFKFK gels, no red staining was observed indicating no or limited amounts of collagen I produced by cells. In

the ``hRGD`` gels, the cell rich regions stained red, similar to what was observed in the 2D cell culture studies. The red region could not be confirmed as collagen I, but it does suggest the deposition of collagen I in ``hRGD`` gels after 7 days in cell culture.

4.5 Summary

The oligopeptide Mpr-hRGDWP was successfully introduced into the FEFEFKFK peptide backbone. When dissolving the peptide in water, the ``hRGD`` peptide self-assembled into fibres with an anti-parallel β -sheet structure. The fibres had the same thickness as the octapeptide. The peptide gels formed when the gel concentrations were above the C_{gel} . Due to the side chains attached to the fibres, the ``hRGD`` gels had a stronger 3D fibrillar network structure. The self-assembly process and gel properties were characterised using various techniques. However, all studies of the gel properties were taken at pH 2.8 in order to have a good comparison with the octapeptide. The results of cell reactions to these hRGD modified gels were shown in the following part of this chapter.

Subsequently, both the FEFEFKFK and the ``hRGD`` gels were applied to the 2D and 3D HDF cell culture studies. Both gels were proved to be biocompatible, and can sustain cell growth up to 14 days in 2D and 7 days in 3D cell culture studies. The cell culture time for gels to be stable and for cells to stay alive is relatively long compared to the other peptide systems reported. Although the results on 3D cell culture were from preliminary tests, they are very promising results which shows that the gels used in this project can be good candidates as cell culture scaffolds in both 2D and 3D cell culture environment. The exact role of hRGD in supporting cell attachment needs further investigation. However, it was confirmed that the ``hRGD`` gel did enhance cell adhesion and proliferation in 2D cell culture compared to the FEFEFKFK gel. This proves the FEFEFKFK gels can be functionalised to improve the performance in cell culture studies. Further experiments need to be taken to get firm evidence whether or not hRGD is the direct reason for improved cell attachment. If so, this could be the first time finding a substitution for RGD sequence.

4.6 References

1. Zhou, M.; Smith, A. M.; Das, A. K.; Hodson, N. W.; Collins, R. F.; Ulijn, R. V.; Gough, J. E., Self-assembled peptide-based hydrogels as scaffolds for anchorage-dependent cells. *Biomaterials* **2009**, 30, 2523-2530.
2. Ginsberg, M.; Pierschbacher, M. D.; Ruoslahti, E., Inhibition of fibronectin binding to platelets by proteolytic fragments and synthetic peptides which support fibroblast adhesion.

Journal of Biological Chemistry **1985**, 260, (7), 3931-3936.

3. Mackintosh, F. C.; Kas, J.; Janmey, P. A., Elasticity of semiflexible biopolymer networks. *Physical Review Letters* **1995**, 75, (24), 4425-4428.
4. Boothroyd, S.; Saiani, A.; Miller, A. F., Formation of mixed Ionic complementary peptide fibrils. *Macromolecular Symposia* **2008**, 273, 139-145.
5. Cebe, P.; Hu, X.; Kaplan, D., Determining beta-sheet crystallinity in fibrous proteins by thermal analysis and infrared spectroscopy. *Macromolecules* **2006**, 39, (18), 6161-6170.
6. Saiani, A.; Mohammed, A.; Frielinghaus, H.; Collins, R.; Hodson, N.; Kielty, C. M.; Sherratt, M. J.; Miller, A. F., Self-assembly and gelation properties of alpha-helix versus beta-sheet forming peptides. *Soft Matter* **2009**, 5, (1), 193-202.
7. Hadjipanayi, E.; Mudera, V.; Brown, R. A., Close dependence of fibroblast proliferation on collagen scaffold matrix stiffness. *Journal of Tissue Engineering and Regenerative Medicine* **2009**, 3, 77-83.
8. Kantlehner, M.; Schaffner, P.; Finsinger, D.; Meyer, J.; Jonczyk, A.; Diefenbach, B.; Nies, B.; Hözemann, G.; Goodman, S. L.; Kessler, H., Surface coating with cyclic RGD peptides stimulates osteoblast adhesion and proliferation as well as bone formation. *ChemBioChem* **2000**, 1, (2), 107-114.
9. Gasiorowski, J. Z.; Collier, J. H., Directed Intermixing in Multicomponent Self-Assembling Biomaterials. *Biomacromolecules* **2011**, 12, (10), 3549-3558.
10. Stevenson, M. D.; Pirstine, H.; Hoglebe, N. J.; Nocera, T. M.; Boehm, M. W.; Reen, R. K.; Koelling, K. W.; Agarwal, G.; Sarang-Sieminski, A. L.; Gooch, K. J., A self-assembling peptide matrix used to control stiffness and binding site density supports the formation of microvascular networks in three dimensions. *Acta Biomaterialia* **2013**, 10.1016/j.actbio.2013.04.002.
11. Jung, J. P.; Nagaraj, A. K.; Fox, E. K.; Rudra, J. S.; Devgun, J. M.; Collier, J. H., Co-assembling peptides as defined matrices for endothelial cells. *biomaterials* **2009**, 30, (12), 2400-2410.
12. Genove, E.; Shen, C.; Zhang, S.; Semino, C. E., The effect of functionalized self-assembling peptide scaffolds on human aortic endothelial cell function. *Biomaterials* **2005**, 26, (16), 3341-3351.
13. Lim, Y.-b.; Kwon, O.-J.; Lee, E.; Kim, P.-H.; Yun, C.-O.; Lee, M., A cyclic RGD-coated peptide nanoribbon as a selective intracellular nanocarrier. *Organic & Biomolecular Chemistry* **2008**, 6, 1944-1948.
14. Kessler, H.; Hersel, U.; Dahmen, C., RGD modified polymers: biomaterials for stimulated cell adhesion and beyond. *Biomaterials* **2003**, 24, (24), 4385-4415.
15. King, W. J.; Murphy, W. L., Bioinspired conformational changes: an adaptable mechanism for bio-responsive protein delivery. *Polymer Chemistry* **2010**, 2, 476-491.
16. Sieminski, A. L.; Semino, C. E.; Gong, H.; Kamm, R. D., Primary sequence of ionic self-

assembling peptide gels affects endothelial cell adhesion and capillary morphogenesis. *Journal of Biomedical Materials Research Part A* **2008**, 87A, (2), 494-504.

17. Abcam Product datasheet - anti-fibronectin antibody [F1] ab32419.
<http://www.abcam.com/fibronectin-antibody-f1-ab32419.html> (25 06 2013),

Chapter 5 Conclusion and future work

The peptide FEFEFKFK used in this project has been reported to self-assemble in solution, forming hydrogels with a 3D fibrous network structure above a critical gelation concentration. The self-assembly process has been well studied and it fitted into the self-assembly model which has been proposed by Zhang *et al.* for another ionic complementary octapeptide FKFEFKFE. Although peptide FEFEFKFK hydrogel shows potential to be used as a mimic of the ECM, little work has been done on the study of the gelation properties and to explore the possibility of this hydrogel to be used for biomedical applications. This project started by focusing on the mechanical properties of FEFEFKFK peptide followed by studying the effects of pH and ionic strength on the self-assembly and gelation properties were examined. Finally the FEFEFKFK hydrogels were functionalised and assessed the possibility to be used as a tissue culture scaffold.

In Chapter 3, it was confirmed that FEFEFKFK peptide formed nanofibres with an anti-parallel β -sheet structure in aqueous solution. When increasing the concentration of peptide solution, a fibrillar network with the mesh size around 30 nm was observed before the gelation occurred. It was noticed that the fibre density increased with increasing hydrogel concentration, but the mesh size of the network decreased with increasing hydrogel concentration. A solid-like behaviour was observed for FEFEFKFK hydrogels at all concentrations during the rheology studies. For the first time, the Guenet's fibrillar model and Ferry's study of the power law relationship were applied to the FEFEFKFK hydrogel system. The rheology data fitted in the models very well, which indicated a lightly cross-linked or entangled network structure in hydrogels. Jones and Marques theory was used to study the relation between the gel strength and gel concentration. However, in this project, the gel concentration was pushed to as high as 60 mg ml^{-1} . A dramatic increase in gel strength caused a second slope too high to fit into the Jones and Marques theory anymore. This pointed out the network structure of the gels at concentrations over 45 mg ml^{-1} arranged differently than the gels at lower concentrations. The gel network at lower concentration could be damaged by increasing temperature or applying shear stress. The damage was confirmed in the rheology tests. However, the recovery of hydrogels was also observed after removing the source of the damage. It was noticed in the previous studies

that the self-assembly and gelation properties of FEFKFK peptide were strongly influenced by the variation of pH. In this project, a new technology SANS was introduced to provide a new prospect of view on the effect of pH. The self-assembly and gelation properties were affected by altering the charges of peptide molecules. Peptide molecules were positively charged in acidic solutions. Increasing pH resulted in the decreasing of repulsion forces between fibres, which then caused the increasing of the mechanical strength of hydrogels. Peptide molecules were negatively charged in basic solutions. Increasing pH resulted in an opposite observation. By using SANS, it was possible to examine the scattering intensity at high q value. More data containing structural information at high q value were observed and analysed. A two radii model was proposed for the formation of the gel network. It was postulated before that the ionic strength would have an influence on the self-assembly and gelation properties. This influence was studied in the second section. The ionic strength effect was demonstrated by the effect of NaCl. Increasing salt concentration in hydrogels decreased the solubility of peptide molecule in aqueous solution which promoted the formation of peptide fibres, caused more entangled network structure and lowered the critical gelation concentration. Although the fibres size did not change with increasing salt concentration, the screening effect may cause the increase of rigidity of fibres which lead to an increased mechanical strength. However, the gels were more brittle at salt concentrations over 500 mM which could also be the effect of more rigid peptide fibres. Both pH and salt can be used to trigger the transition from peptide solution to peptide hydrogel, thus it was postulated that cell culture medium which is a pH 7 buffer solution can be used to trigger the gelation process. However, when studying the effect of pH and ionic strength, the condition was simplified by varying one variable at a time. So the results could be easily compared with the original state of the FEFKFK hydrogel, which helps the understanding of the mechanism of the self-assembly of fibres as well as the formation of network structures. The original FEFKFK hydrogels have a pH of 2.8 and no salt in the system. Thus when studying the pH effect, no salt was added; while when studying the ionic strength effect, only NaCl was used to adjust the ionic strength effect at pH 2.8. However, cell culture medium is a more complicated pH 7 solution with the presence of all kinds of salts. Thus the conclusions drawn from Section 3.2 were only used as references but not direct guides for cell culture studies. Since no previous cell culture work had been done on the hydrogels of FEFKFK when the project started, the protocols of gel preparation were developed for both 2 dimensional (2D) and 3

dimensional (3D) cell culture. Two different hydrogel preparation methods were developed to meet the basic requirements for a tissue culture scaffold. The preliminary tests were done on chondrocyte cells. The cells stay alive on the gels prepared by either method. However, distinct morphologies of chondrocytes were observed. Chondrocytes remained round shape on the gels with NaOH in the system; whilst chondrocytes changed to a fibroblast-like shape on the gels without NaOH in the system. HDF cells were also cultured on these gels for up to 7 days. It was promising to observe the good cell viability 7 days post cell culture. However, HDF cells were all remain round on both gel surfaces. HDF takes spindle-like shapes in 3D environment and more elongated shapes in 2D. The round shape of HDF on both gel surfaces suggested lack of cell attachment sites. The preliminary cell culture tests proved the biocompatibility of FEFEFKFK hydrogels and revealed the requirement of further surface modification to promote cell adhesion.

In Chapter 4, a short peptide sequence homoarginine-glycine-aspartate (hRGD) has been introduced onto the amide end of the self-assembly peptide instead of bioactive ligand arginine-glycine-aspartate (RGD), creating hydrogels with a fibrous network with the functionalised groups at the fibre surface. This is the first time hRGD was introduced to FEFEFKFK sequence and to be used as a replacement of RGD in cell culture studies. The modified peptide could also self-assemble into fibres with an anti-parallel β sheet structure in distilled water, which then form transparent and self-supporting hydrogels with fibrous network structure. The self-assembly process and gel properties were characterised using various techniques. And then both the FEFEFKFK gels and the ``hRGD`` gels were applied to the 2D and 3D HDF cell culture studies. Both gels were proven to be biocompatible, and can sustain cell growth up to 14 days in 2D and 7 days in 3D cell culture studies. The functionalised peptide hydrogels enhanced cell adhesion on gel surface, with cell interaction assessed using various imaging and spectroscopic techniques. A preliminary 3D cell culture study also showed the potential of these peptide gels to be used for encapsulated HDF cell studies.

In the future, quantitative assays on the synthesis of ECM should be utilised. Serum free medium could be used in the gel preparation process to eliminate the effect of protein absorption on cell culture studies. More detailed and systematic analysis should be taken in 3D cell culture studies to qualify the octapeptide and its derivatives to be used as tissue culture scaffolds. The RGD sequence could also be introduced into the octapeptide

backbone to be compared with the hRGD sequence which may help understanding the role of hRGD in promoting cell adhesion. It would also be interesting to investigate the injectability of these peptide hydrogels for biomedical applications.